INNOVATIVE NUCLEIC ACID BASED STRATEGIES FOR FIBER OPTIC SURFACE PLASMON RESONANCE BIOSENSOR DESIGN

Bernd Peeters

Supervisors:
Prof. J. Lammertyn
Dr. D. Daems

Dissertation presented in partial fulfilment of the requirements for the degree of Doctor of Bioscience Engineering (PhD)

Members of the Examination Committee:
Prof. B. Sels, chair
Prof. J. Lammertyn, promotor
Dr. D. Daems, co-promotor
Prof. S. De Feyter
Prof. P. H. Wagner
Prof. I. Pividori (UAB, Spain)
Dr. Ir. F. Delport (FOx Biosystems, CTO)

May 2020

Doctoraatsproefschrift nr. 1647 aan de faculteit Bio-ingenieurswetenschappen van de KU Leuven

© 2020 KU Leuven, Science, Engineering & Technology
Uitgegeven in eigen beheer, Bernd Peeters, Tiensestraat 201 box 0202, 3000 Leuven, Belgium

Alle rechten voorbehouden. Niets uit deze uitgave mag worden vermenigvuldigd en/of openbaar gemaakt worden door middel van druk, fotokopie, microfilm, elektronisch of op welke andere wijze ook zonder voorafgaandelijke schriftelijke toestemming van de uitgever.

All rights reserved. No part of the publication may be reproduced in any form by print, photoprint, microfilm, electronic or any other means without written permission from the publisher.

Acknowledgements

Here I am, at the end of one phase in life and at the start of another one. Time to look back, reflect and pay gratitude to those who made it possible.

In particular, I would like to express my gratitude to my promotor Prof. Jeroen Lammertyn, who convinced me to start this PhD journey about four and a half year ago. Many thanks for the opportunity you gave me and the valuable confidence whenever I doubted my own skills. I truly appreciate all your effort and patience during the course of this PhD and the final support to make it all to the end. Thank you!

My appreciation goes also to my co-promotor, Dr. Devin Daems, on whose expertise I could always rely to tackle many of the daily challenges along the road. Despite your early leave out of the group, I was still able to count on you for revising the manuscript and for some final input to reach all the necessary milestones. I might not have been the easiest PhD student, but I have enjoyed working together with you.

Further, I would like to thank all the members of the jury for reading my PhD dissertation and for their valuable comments and remarks, which helped to improve and fine-tune this dissertation into its final shape. In particular, I would like to acknowledge Filip Delport for the support and consultancy concerning both conceptual and technical aspects, which were eventually realized in this work. Along these years I have admired your persistence for launching your own spin-off project.

Some parts of this research would not have been possible without the expertise and support across the borders of divisions and faculties. My gratitude goes to Tom Van der Donck (Department of Materials Engineering, KU Leuven), with whom I managed to visualize some of the research by means of high-resolution SEM imaging. Thanks for sharing some of your work, insights and the conversations while waiting for some successful results. Many thanks to Prof. Peter Goos (Department of Biosystems, Biostatistics group, KU Leuven) for the proofreading of my latest paper manuscript and your guidance in the field of design of experiments (DOE). I would also like to thank all my colleagues of the Biosystems II building for sharing their equipment, knowledge, tips and tricks, which made me a better scientist.

On top of that, I was fortunate to spend my days in the marvelous Biosensors group with a great atmosphere and nice colleagues. Thanks Dragana for your guidance in lots of my writing and your interest in the progress of both my research and personal life from time-to-time. I would also like to thank my office buddies Elena, Karen, Henry, Aida, Saba, Jiahuan and Julie for the moments of laughter and chats in between all the work. A special thanks to Karen, who from the start was there to listen and give advice, always with a positive mindset. Thanks to Karen and Iene, who started this journey with me after surviving our masters and with whom I got to discover parts of the USA. Thanks to Dries and Jolien for our few nights out; I had a great time and may the future bring some more opportunities. Thanks to Wouter for your deep understanding of so many things, the highly philosophical and weirdly funny conversations, which made us lose track of time over lunch. Thanks to Tadej, Iulia, Phalguni, Pelin, Deborah, Jiadi, Lisa, Suresh, Jaroslav, Francesco, Bert, Elfie, Bram, Sara, Annelies, Lorenz, Ruben, Seppe, Louanne, Arno, Yagmur, Yura, Victor, Matthias, Caroline and Hans for the help in the lab and the fun moments during the several group activities.

Graag zou ik ook mijn familie en vrienden willen bedanken, die ondanks het feit dat ze misschien niet altijd begrepen waarmee ik juist bezig was, er toch altijd zijn geweest om me te steunen en aan te moedigen wanneer dit nodig was. In het bijzonder wil ik mijn ouders bedanken die een onevenaarbare drijfkracht hebben en altijd paraat staan voor hun kinderen. Aan mijn zussen, broer, Joris en Bert, merci om jullie ervaringen te delen, te luisteren en raad te geven van tijd tot tijd. En Leon, het gelukkigste petekind dat automatisch een lach naar boven doet komen.

Finalmente, eu gostaria de agradecer à pessoa que entrou na minha vida, neste momento, há quase dois anos. Isabel, tem sido uma montanha-russa de mudanças, decisões e emoções, mas aqui estamos ☺ juntos. Muito obrigado por estares sempre presente e me apoiares durante esta fase final! Mal posso esperar pelo nosso futuro e novas aventuras!

Abstract

The diverse information embedded in the specific sequence of DNA molecules has been feeding our understanding and insights in disease heritage, spreading and evolution. Ultrasensitive detection of the DNA molecules themselves is crucial for the early-stage detection of several diseases, as it facilitates the minimization of actual disease burden. Gold standard technologies, such as the polymerase chain reaction (PCR), are mainly restricted to sophisticated laboratory settings, relying on trained personal, bulky equipment and large batches of samples. In order to improve the accessibility of nucleic acid (NA) analysis and provide its valuable information outside these sophisticated settings, alternative biosensors are being developed. These biosensors can offer more user-friendly, robust, fast and cost-effective devices, thereby focusing on the needs of the end-user. In addition, biosensors do not limit themselves to the use of DNA as target molecule. Instead, the unique structure of DNA is also exploited as a building block for smart biosensor design.

Fiber optic surface plasmon resonance (FO-SPR) is a mass-sensitive biosensing technique with some advantageous characteristics, such as its real-time aspect, user-friendliness and fast analysis. While these FO-SPR characteristics match several of the features mentioned above, DNA-based FO-SPR assays are mainly restricted to classical hybridization strategies, limiting the sensitivity to the lower nM range. Ultrasensitive detection of NAs continues to be challenging and alternative FO-SPR designs to generate and amplify this signal have not been fully explored.

Upcoming fields like DNA nanotechnology drive these innovative designs by discovering new functional molecules, such as DNAzymes. These enzyme-like molecules are of great interest in biosensor development due to their easy coupling to existing signal generation systems and their inherent amplification. Because of their NA-based structure, they are more stable, cost-effective, and show superior flexibility compared to their protein counterparts in their design towards different target molecules. However, DNA nanotechnology is not yet mature and surface-based DNAzyme strategies have been concentrating mainly on metal ion detection. NA and protein applications are rare and demand more advanced design and implementation of current DNAzyme-based strategies.

In this framework, the main objective of this dissertation was to design innovative NA-based strategies using a FO-SPR platform for the sensitive and specific detection of NAs. To do so, three different NA-based strategies were presented: (i) a FO-PCR melting assay, (ii) a FO-SPR sensor design sensitive to catalytic DNAzyme activity and (iii) a DNAzyme-based FO-PCR assay.

The first design was based on PCR amplification of the target sequences, which subsequently hybridized to the FO sensor surface and DNA-functionalized gold nanoparticles (AuNPs) for amplification. As a proof-of-concept, the assay was explored for the detection of celery DNA, one of the most important provokers of food allergic reactions. Different concentrations of celery DNA (1 pM – 0.1 fM) were detected and inclusion of a following melting step enabled distinction from closely related sequences, such as carrot DNA. The concept was validated in cleaning water samples and benchmarked against a reference qPCR followed by high resolution melting, which showed excellent agreement ($R^2 = 0.96$). This way the FO-PCR melting assay provided a rapid and simple detection method, suitable for one-step quantification and discrimination of single stranded DNA (ssDNA) with great potential in fields such as food quality and safety assurance.

For the second design, first a robust ligation strategy was developed to functionalize the FO-SPR sensing surface with ssDNA, which in turn was labelled with AuNPs, to serve as the DNAzyme substrate. Next, we studied the relation between the change in FO-SPR shift and the DNAzyme cleavage activity, which showed faster cleavage kinetics for higher DNAzyme concentrations. Finally, we translated this real-time cleavage activity into a generic biosensing concept for the detection of ssDNA targets. A DNAzyme-inhibitor complex was designed to release active DNAzymes in a controlled way as function of the target concentration. Reproducible target detection was demonstrated with a theoretical LOD of 1.4 nM. In summary, an innovative DNAzyme-based FO-SPR biosensor was established with great potential to act as universal sensor for promising applications in the medical and agrofood sector.

The final design in this dissertation combined insights from both the first and the second design by boosting the catalytic cleavage activity through PCR-amplification of the DNAzymes. Based on the readout system of the

second design, the surface cleavage efficiency of the DNAzyme-extended amplicons (DNAzyme-amps) was first evaluated and confirmed. Next, the PCR and cleavage reaction conditions were fine-tuned to assure compatibility with the FO-SPR system and establish a one-step assay. As a proof-of-concept, the primer pair with the built-in DNAzyme complement was tested for the detection of the antimicrobial resistance gene MCR-2. PCR-amplified DNAzyme-amps generated in the presence of the MCR-2 gene were monitored in real-time, resulting in an experimental LOD of 4×10^5 copy numbers or 6.6 fM. In addition, the DNAzyme-based FO-PCR assay was able to discriminate between the MCR-1 and MCR-2 genes, further proving the specificity of this assay. In short, this DNAzyme-based FO-PCR assay provides a universally applicable, real-time system for the detection of virtually any NA target, in a specific and sensitive manner.

Samenvatting

De diverse informatie die vervat ligt in de specifieke sequentie van DNA-moleculen is een belangrijke drijfveer in onze kennis en inzichten in de erfelijkheid van ziekten, hun verspreiding en evolutie. Ultragevoelige detectie van deze DNA-moleculen is cruciaal voor de vroegtijdige detectie van verschillende ziekten, vermits dit de minimalisatie van de werkelijke ziektelast vergemakkelijkt. Standaardreferentietechnieken, zoals de polymerase kettingreactie (*PCR*), zijn hoofdzakelijk beperkt tot geavanceerde laboratoria, die afhankelijk zijn van getraind personeel, omvangrijke toestellen en een groot aantal stalen. Om de toegankelijkheid van nucleïnezuur (NZ) -analyses te verbeteren en zijn waardevolle informatie buiten deze geavanceerde instellingen te kunnen aanbieden, worden er biosensoren ontwikkeld. Deze biosensoren kunnen gebruiksvriendelijkere, robuustere, snellere en kostenefficiëntere apparaten leveren en richten zich daarbij op de behoeften van de eindgebruiker. Bovendien beperken biosensoren zich niet tot het gebruik van DNA als doelwitmolecule. In plaats daarvan wordt de unieke structuur van DNA ook gebruikt als bouwsteen voor het slimme ontwerp van biosensoren.

Fiber optic surface plasmon resonance (FO-SPR) is een massagevoelige biosensingtechniek met enkele voordelige kenmerken, zoals zijn real-time aspect, gebruiksvriendelijkheid en snelle analyse. Hoewel deze *FO-SPR*-kenmerken overeenkomen met verschillende van de hierboven genoemde behoeften, zijn NZ-gebaseerde *FO-SPR*-tests voornamelijk beperkt tot klassieke hybridisatiestrategieën. Dit beperkt hun gevoeligheid tot het lagere nM-concentratiebereik. Ultragevoelige detectie van NZ blijft een uitdaging en alternatieve ontwerpen om het signaal te genereren en versterken zijn nog te weinig onderzocht.

Opkomende onderzoeksgebieden, zoals DNA-nanotechnologie, stimuleren dergelijke innovatieve ontwerpen door de ontdekking van nieuwe functionele moleculen, zoals *DNAzymes*. Deze enzymachtige moleculen zijn van groot belang voor de ontwikkeling van biosensoren vanwege hun gemakkelijke koppeling aan bestaande signaal genererende systemen en inherente amplificatie. Vanwege hun NZ-gebaseerde structuur zijn ze stabieler, kostenefficiënter en vertonen ze een superieure flexibiliteit, in vergelijking met hun eiwittegenhangers, in hun herontwerp naar andere

doelmoleculen. DNA-nanotechnologie is echter verre van volledig ontwikkeld en oppervlakte-gebaseerde *DNAzyme*-strategieën hebben zich geconcentreerd op metaaliondetectie. NZ- en eiwittoepassingen zijn schaars en vereisen een geavanceerder ontwerp en implementatie van de huidige *DNAzyme*-gebaseerde strategieën.

In dit kader was het hoofddoel van dit proefschrift het ontwerp van innovatieve, NZ-gebaseerde strategieën met behulp van een *FO-SPR*-platform voor de gevoelige en specifieke detectie van NZ. Om dit te doen, werden drie verschillende NZ-gebaseerde strategieën gepresenteerd: (i) een *FO-PCR* smelttest, ii) een *FO-SPR*-sensorontwerp, gevoelig voor katalytische *DNAzyme*-activiteit en (iii) een *DNAzyme*-gebaseerde *FO-PCR* test.

Het eerste ontwerp was gebaseerd op *PCR*-amplificatie van de doelsequenties, die vervolgens hybridiseerden aan het *FO*-sensoroppervlak en met DNA-gefunctionaliseerde gouden nanodeeltjes (*AuNP*'s) voor amplificatie. Als proof-of-concept werd de test onderzocht voor de detectie van selderij-DNA, een van de belangrijkste oorzaken van voedingsallergieën. Verschillende concentraties selderij-DNA (1 pM – 0,1 fM) werden gedetecteerd en een aansluitende smeltstap maakte het mogelijk om een onderscheid te maken tussen nauw verwante sequenties, zoals wortel-DNA. Het concept werd gevalideerd in reinigingswaterstalen en vergeleken met een referentie *qPCR* gevolgd door smeltstap met hoge resolutie. Deze vergelijking vertoonde een uitstekende overeenstemming (R^2 = 0,96). Op deze manier bood de *FO-PCR* smelttest een snelle en eenvoudige detectiemethode, geschikt voor éénstapskwantificatie en discriminatie van enkelstrengig DNA (*ssDNA*) met een groot potentieel in toepassingsgebieden zoals voedselkwaliteit en -veiligheid.

Voor het tweede ontwerp werd er eerst een robuuste ligatiestrategie ontwikkeld om het *FO-SPR*-detectieoppervlak te functionaliseren met *ssDNA*. Dit *ssDNA* was op zijn beurt gelabeld met *AuNP*'s om als *DNAzyme*-substraat te fungeren. Vervolgens onderzochten we de relatie tussen de verandering in *FO-SPR-shift* en de *DNAzyme*-splitsingsactiviteit, wat een snellere splitsingskinetiek vertoonde voor hogere *DNAzyme*-concentraties. Ten slotte hebben we deze real-time splitsingsactiviteit vertaald naar een generiek biosensingconcept voor de detectie van *ssDNA*-doelwitmoleculen. Een DNA-inhibitiecomplex werd ontworpen om actieve *DNAzymes* vrij te geven op een

gecontroleerde manier en in functie van de concentratie van de doelwitsequentie. Reproduceerbare detectie van de doelwitsequentie werd aangetoond met een theoretische detectielimiet (*LOD*) van 1,4 nM. Kortom, een innovatieve, *DNAzyme*-gebaseerde *FO-SPR*-biosensor werd verwezenlijkt met groot potentieel om te fungeren als universele sensor in veelbelovende toepassingen in de medische en agrofoodsector.

Het laatste ontwerp in dit proefschrift combineerde inzichten uit zowel het eerste als het tweede ontwerp door de katalytische splitsingsactiviteit te versterken via *PCR*-amplificatie van de *DNAzymes*. Gebaseerd op het uitleessysteem van het tweede design, werd de splitsingsefficiëntie van met *DNAzyme*-verlengde *amplicons* (*DNAzyme-amp's*) aan het sensoroppervlak eerst geëvalueerd en bevestigd. Vervolgens werden de PCR- en splitsingsreactieomstandigheden verfijnd om compatibiliteit met het *FO-SPR*-systeem te verzekeren en een éénstapsreactie te bekomen. Als proof-of-concept werd het primerpaar met ingebouwd *DNAzyme*-complement getest voor de detectie van het antimicrobiële resistentiegen MCR-2. *PCR*-geamplificeerde *DNAzyme-amp's*, die gegenereerd werden in aanwezigheid van het MCR-2-gen, werden in real-time gevolgd, wat resulteerde in een experimentele *LOD* van 4 x 10^5 kopieën van het gen of 6,6 fM. Bovendien was de *DNAzyme*-gebaseerde *FO-PCR*-test in staat om onderscheid te maken tussen het MCR-1- en MCR-2-gen, wat de specificiteit van deze test verder illustreert. Kortom, deze *DNAzyme*-gebaseerde *FO-PCR*-test bood een universeel toepasbaar, real-time systeem voor de detectie van vrijwel elk NZ-doelwit, op een specifieke en gevoelige manier.

List of abbreviations

Ab	Antibody
ABTS	2,2'-azinobis(3-ethylbenzo-thiozoline)-6-sulfonic acid
ANOVA	Analysis of variance
Api g	Apium graveolens
ASSURED	Affordable, Sensitive, Specific, User-friendly, Rapid and robust, Equipment-free and Delivered
ATP	Adenosine triphosphate
Au	Gold
AuNP	Gold nanoparticle
BRCA	Breast cancer gene
CBS	Concentric backscatter detector
CDT	Circular DNA template
CEM	Crude extracellular matrix
CHA	Catalytic hairpin assembly
-COOH	Carboxyl-group
Cq	Cycle of quantification
DCFI	Drift corrected frame integration
DE	Distal end
DNA	Deoxyribonucleic acid
DNAzyme	DNA enzyme
DNAzyme-amp	DNAzyme amplicon
DOE	Design of experiments
DP	DNA primer
dsDNA	Double stranded DNA
DTT	Dithiothreitol
E. coli	Escherichia coli
ECL	Electrochemiluminescence

EDC	1-ethyl-3-(-3-dimethylaminopropyl) carbodiimide hydrochloride
EDTA	Ethylenediaminetetraacetic acid
ELISA	Enzyme-linked immunosorbent assay
Eqn	Equation
EW	Evanescent wave
FO-PCR-MA	Fiber optic polymerase chain melting assay
FO-SPR	Fiber optic surface plasmon resonance
FP	Forward primer
F-Q	Fluorophore-quencher
HCR	Hybridization chain reaction
HIV	Human immunodeficiency virus
HRM	High-resolution melting
HRP	Horseradish peroxidase
ICC	Intraclass correlation coefficient
LAMP	Loop mediated isothermal amplification
LCR	Ligation chain reaction
LOD	Limit of detection
LS	Lateral surface
M. bovis	Mycobacterium bovis
MAP	Mycobacterium Avium Paratuberculosis
MCH	6-mercapto-1-hexanol
MCR-2	Mobile colistin resistance type 2
Mtd	Mannitol dehydrogenase
NA	Nucleic acid
NAzymes	Nucleic acid enzyme
NGS	Next generation sequencing
-NH	Amine-group
NHS	N-hydroxysuccinimide
Nt	Nucleotide

NTC	Non-target control
OD	Optical density
PB	Phosphate buffer
PCR	Polymerase chain reaction
POCT	Point-of-care testing
QCM	Quartz crystal microbalance
qPCR	Quantitative polymerase chain reaction
RCA	Rolling circle amplification
RCD	RNA-cleaving DNAzyme
RDS	RNA containing substrate
RI	Refractive index
RMSE	Root mean squared error
RNA	Ribonucleic acid
RP	Reverse primer
RPA	Recombinase polymerase amplification
SAM	Self-assembling monolayer
SD	Standard deviation
SDS	Sodium dodecyl sulfate
SELEX	Systematic evolution of ligands by exponential enrichment
SEM	Scanning electron microscopy
-SH	Thiol-group
SNP	Single nucleotide polymorphism
SP	Surface plasmon
SPR	Surface plasmon resonance
SPRi	Surface plasmon resonance imaging
SPW	Surface plasmon wave
ssDNA	Single stranded DNA
ST-AP	Streptavidin-alkaline phosphatases
TE	Tris- ethylenediaminetetraacetic acid

Th	Threshold
TIR	Total internal reflection
TMB	Tetramethylbenzidine
T-profile	Temperature profile
WHO	World health organization
α-NP	α-naphthyl phosphate

List of symbols

c	Speed of light in vacuum
E	Electric field
h	Planck constant 6.626×10^{-34}J.s
k	Wave vector
m	Integer representing the diffraction order
n	Refractive index
S	Slope
T_m	Melting temperature
Δ	Penetration depth
ΔG	Gibbs free energy
E	Permittivity
Θ	Angle of incident/reflected/transmitted light
Λ	Groove period of the grating
Λ_0	Wavelength in vacuum
π	Pi
σ	Standard deviation
ω	Angular frequency

Table of content

Acknowledgements ..... *i*
Abstract ..... *iii*
Samenvatting ..... *vi*
List of abbreviations ..... *ix*
List of symbols ..... *xiii*
Table of content ..... *xiv*

CHAPTER 1 ..... **1**

1.1. DNA – FROM MOLECULAR STRUCTURE TO BIOSENSOR TOOL 2
1.2. THE POLYMERASE CHAIN REACTION 4
1.3. BIOSENSORS 7
1.4. DNA NANOTECHNOLOGY FOR BIOSENSOR DESIGN 9
1.5. OBJECTIVES AND OUTLINE OF THE THESIS 12
1.6. REFERENCES 16

CHAPTER 2 ..... **21**

2.1. INTRODUCTION 22
2.2. FUNCTIONAL NUCLEIC ACIDS 22
2.2.1. DNAzyme functions and reactions *23*
2.2.1.1. RNA-cleaving DNAzymes 23
2.2.1.2. Peroxiding DNAzymes 24
2.2.1.3. Other DNAzyme catalytic reactions 25
2.2.2. RNA-cleaving DNAzyme selection *26*
2.2.3. Solution-based DNAzyme biosensors *28*
2.2.3.1. DNAzyme-based biorecognition and signal generation 28
2.2.3.2. DNAzyme-coupled and –triggered signal amplification 29
2.2.4. Solid-phase DNAzyme biosensors *31*
2.2.4.1. DNAzyme-based biorecognition and signal generation 32
2.2.4.2. DNAzyme-coupled and –triggered signal amplification 34
2.2.5. Other applications *36*
2.3. SURFACE PLASMON RESONANCE 37
2.3.1. Principle of surface plasmon resonance *37*
2.3.1.1. Surface plasmons 37
2.3.1.2. Principle of surface plasmon resonance 38
2.3.2. Surface plasmon excitation methods *42*
2.3.2.1. Grating-enhanced surface plasmon resonance 42
2.3.2.2. Prism-enhanced surface plasmon resonance 43
2.3.2.3. Fiber-optic surface plasmon resonance 45
2.3.3. Surface functionalization *46*
2.3.4. DNA-based signal amplification strategies *48*
2.3.5. Miniaturized SPR devices *52*

2.4. CONCLUSIONS 54
2.5. REFERENCES 56

CHAPTER 3 65

3.1. INTRODUCTION 66
3.2. EXPERIMENTAL SECTION 67
3.2.1. Materials and reagents 67
3.2.2. qPCR/HRM 69
3.2.3. Surface functionalization of FO-SPR sensors and AuNPs 69
3.2.4. FO-PCR-MA in solution 70
3.2.5. Biological sample preparation 70
3.2.6. Data processing 70
3.3. RESULTS AND DISCUSSION 71
3.3.1. Selection of celery target sequence using qPCR/HRM 71
3.3.2. Establishing FO-PCR-MA for celery DNA detection 72
3.3.3. Validation of established FO-PCR-MA with biological samples 76
3.4. CONCLUSIONS 78
3.5. SUPPLEMENTARY INFORMATION 79
3.6. REFERENCES 83

CHAPTER 4 85

4.1. INTRODUCTION 86
4.2. EXPERIMENTAL SECTION 88
4.2.1. Materials and reagents 88
4.2.2. FO-SPR sensor fabrication and gold surface functionalization 89
4.2.3. AuNP-ligation to the FO-SPR sensor surface 89
4.2.4. SEM images and data analysis 90
4.3. RESULTS AND DISCUSSION 91
4.3.1. Ligation-based functionalization of FO-SPR sensor surface 91
4.3.2. Screening of an optimal ligation temperature 92
4.3.3. Screening of an optimal template concentration 94
4.4. CONCLUSIONS 96
4.5. SUPPLEMENTARY INFORMATION 97
4.5.1. Material and methods 97
4.5.1.1. FO-SPR experimental setup 97
4.5.1.2. FO-SPR high resolution melting 98
4.5.2. Results and discussion 99
4.5.2.1. Determination lower melting temperature ligation complex 99
4.5.2.2. SEM images and AuNP count 100
4.6. REFERENCES 103

CHAPTER 5 105

5.1. INTRODUCTION 106
5.2. EXPERIMENTAL SECTION 108
5.2.1. Materials and reagents 108
5.2.2. Real-time FO-SPR monitoring of DNAzyme activity 109
5.2.3. DNAzyme blocking with inhibitor strand 109
5.2.4. DNAzyme-based target detection 109
5.2.5. SEM images and data analysis 110
5.3. RESULTS AND DISCUSSION 111
5.3.1. Concept of DNAzyme based FO-SPR biosensing 111
5.3.2. Characterization of DNAzyme activity with FO-SPR 112
5.3.3. Screening of inhibitor concentration for DNAzyme blocking 114
5.3.4. DNAzyme-based detection of a synthetic DNA target 116
5.4. CONCLUSIONS 118
5.5. SUPPLEMENTARY INFORMATION 120
5.5.1. Material and methods 120
5.5.1.1. Gel electrophoresis 120
5.5.2. Results and discussion 121
5.5.2.1. SEM visualization of negative control 121
5.5.2.2. SEM visualization of FO-SPR DNAzyme activity 122
5.5.2.3. FO-SPR characterization of DNAzyme activity 124
5.5.2.4. Inhibitor-DNAzyme complex illustration 125
5.5.2.5. Visualization of blocked DNAzyme activity by gel electrophoresis 126
5.5.2.6. Visualization of target recognition and DNAzyme release by gel electrophoresis 127
5.5.2.7. Proof-of-concept detection of a synthetic DNA strand 128
5.6. REFERENCES 130

CHAPTER 6 133

6.1. INTRODUCTION 134
6.2. EXPERIMENTAL SECTION 136
6.2.1. Materials and reagents 136
6.2.2. FO-SPR sensor preparation and surface functionalization 136
6.2.3. AuNP functionalization and covalent surface immobilization 137
6.2.4. DNAzyme-amplicon surface cleavage activity and optimal reaction conditions 137
6.2.5. PCR-amplified DNAzyme-amplicon activity and qPCR calibration curve 138
6.2.6. Upscaling PCR reaction volume and DNAzyme-based FO-PCR measurements 139
6.3. RESULTS AND DISCUSSION 140
6.3.1. Concept of DNAzyme based FO-PCR biosensing 140

6.3.2. Evaluating DNAzyme-amp cleavage activity on the FO-SPR surface 141
6.3.3. Screening reaction conditions towards combining PCR amplification with FO-SPR activity of DNAzyme-amplicons 143
6.3.4. PCR specificity improvement and establishment of MCR-2 calibration curve with qPCR 146
6.3.5. DNAzyme-based FO-PCR assay for MCR-2 detection 148
6.4. CONCLUSIONS 150
6.5. SUPPLEMENTARY INFORMATION 152
6.5.1. Materials and methods 152
6.5.1.1. Nucleic acid sequences 152
6.5.1.2. Experimental design and data analysis 153
6.5.2. Results and discussion 154
6.5.2.1. Influence of the substrate arms on surface DNAzyme cleavage activity 154
6.5.2.2. Design of experiment for screening DNAzyme-amplicon activity and PCR reaction conditions 155
6.5.2.3. Prediction of FO-SPR DNAzyme-amplicon cleavage activity 156
6.5.2.4. Prediction of PCR-based DNAzyme-amplicon amplification 158
6.5.2.5. Joint optimization of FO-SPR DNAzyme-amp activity and the PCR amplification with qPCR 160
6.5.2.6. PCR specificity improvement and selection annealing temperature primer pair 2 with qPCR 161
6.6. REFERENCES 163

CHAPTER 7 167

7.1. GENERAL CONCLUSIONS 168
7.2. FUTURE PERSPECTIVES 172
7.2.1. Expanding the range of target molecules 172
7.2.2. Improving surface functionalization 176
7.2.3. Biosensors for point-of-care applications 178
7.2.3.1. Isothermal signal amplification 179
7.2.3.2. Portable FO-SPR sensors 180
7.3. REFERENCES 182

PUBLICATIONS 185

ARTICLES IN INTERNATIONAL REVIEWED JOURNALS 185
PAPERS AT INTERNATIONAL SCIENTIFIC CONFERENCES 185
PATENTS 185

Chapter 1

General introduction

1.1. DNA – from molecular structure to biosensor tool

The discovery of deoxyribonucleotide acids (DNA) dates back to 1869[1], when Friedrich Miescher isolated DNA molecules for the first time. As he found the substance in the nuclei of human white blood cells, he named the substance 'nuclein'. Following 84 years, further insights led to the redefinition of this nuclein to nucleic acid[1] and to the demonstration that probably DNA is the carrier of genetic information[2]. A better understanding of the individual DNA components resulted in the description of its double helix structure by Watson and Crick in 1953[3]. This **unique structure of DNA** makes it a very attractive molecule from the perspective of diagnostics, both as a target and as a building block for smart biosensor design (Figure 1.1)[4].

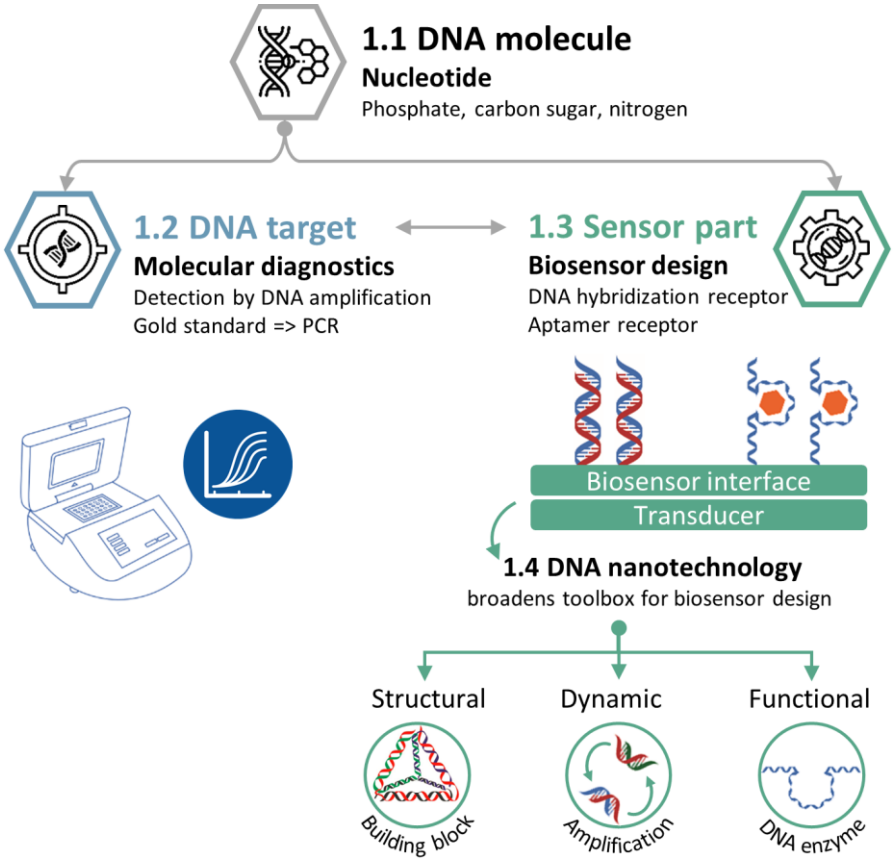

Figure 1.1: *Overview of the different roles of DNA. Chapter 1 follows the outlined structure, creating the framework for the work presented in this dissertation. Adapted with permission of Royal Society of Chemistry, from Wang et al. © (2015); permission conveyed through Copyright Clearance Center, Inc. Icons from www.flaticon.com.*

DNA molecules consist of smaller units known as nucleotides (Figure 1.2)[5]. Each nucleotide contains a phosphate group, a sugar and a base. The phosphate group and sugar make up the backbone of single stranded DNA (ssDNA), while the bases are responsible for pairing of the ssDNA and formation of the double helix, which looks like a twisted ladder. Two groups of bases are distinguished: (i) the purines, containing adenine (A) and guanine (G) and (ii) the pyrimidines, containing cytosine (C) and thymine (T). Pairing of the bases follows a fixed rule in which C-G and A-T couple through hydrogen bonds[5].

Unraveling the DNA structure together with insights in how these molecules are produced in nature stimulated the formulation of the 'central dogma', which postulates that the information contained in DNA is

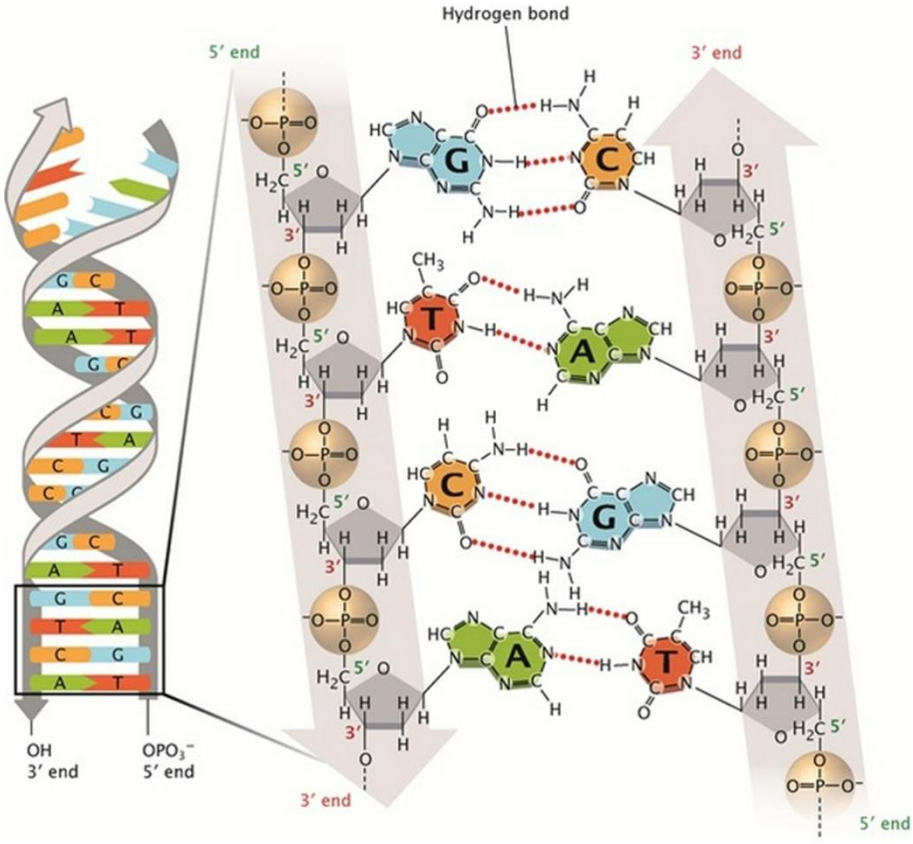

Figure 1.2: *Schematic and chemical structure of the DNA double helix. Each nucleotide consists of a phosphate-group, a five-carbon sugar and a nitrogenous base, either a purine (A and G) or a pyrimidine (C and T). Hydrogen bonds between the fixed base pairs A-T and C-G forms the basis of the duplex structure through hybridization. Adapted from Pray (2008).*

translated to proteins by the use of ribonucleic acids (RNA)[6]. Eventually, the genetic code was solved in 1965[7], enabling scientists to read and extract its relevant information. Sequencing of the complete human genome was established by 2003[8] and created a wealth of knowledge with great value in our healthcare system[9], such as insights in disease heritage[10], disease mechanisms[11], the identification of pathogens[12] and more[13].

Based on this knowledge and next to their expertise, physicians nowadays are supported by diagnostic tests to assure proper disease diagnosis and treatment. These diagnostic tests facilitate the determination of diseases or conditions responsible for a patient's symptoms. A milestone in this context and currently still a gold standard in the field is the polymerase chain reaction (PCR, see Section 1.2)[14], using **DNA as target** for disease diagnosis (Figure 1.1, left side). Early examples of diagnosis based on PCR were the detection of the human immunodeficiency virus (HIV)[15,16], DNA gag sequences and the breast cancer genes BRCA1 and 2[17–19].

Next to molecular diagnostics such as PCR, controlling the characteristics of DNA and the know-how to synthesize them ourselves enabled the use of **DNA as sensor part** (Figure 1.1, right side) in the development of groundbreaking diagnostic devices or DNA-based biosensors[20,21] (see Section 1.3). Initially, DNA has been used mainly as receptor for different targets, such as proteins[22,23], DNA[24] and small molecules[25]. Nowadays, DNA nanotechnology[26,27] (see Section 1.4) forms a separate innovative research field, providing: (i) structural building blocks, (ii) dynamic amplification cascades and (iii) functional enzymatic units. This way, DNA-based biosensors play a crucial role in the development of future diagnostics to overcome many challenges, such as the rising appearance of cancers[28,29], the worldwide spread of infectious diseases[12,30] and antimicrobial resistance[31,32]. Other non-medical applications include the detection of foodborne pathogens[33,34] and environmental monitoring[35].

1.2. The polymerase chain reaction

With the development of PCR[14], researchers went beyond the double helix structure of DNA and showed how DNA can be more than only the carrier of genetic information. PCR enables the detection of a ssDNA sequence of interest from a pool of ssDNA or dsDNA molecules by enzymatic amplification of that specific sequence[36]. The strength of PCR is that it only

requires trace amounts of the ssDNA sequence of interest to result into an exponential amplification and detection of the sequence (Figure 1.3A)[37]. Next to the ssDNA sequence of interest, serving as a template, every PCR reaction makes use of a primer pair, nucleotides and a DNA polymerase[36]. The primers are short ssDNA sequences, which are complementary to the DNA template of interest. As described in previous section, nucleotides make up the main four building blocks of DNA and are put together by the DNA polymerase. The first DNA polymerase to turn PCR in a successful technique was the *Taq* polymerase, a thermostable polymerase found in the bacterium *Thermus aquaticus*[38]. The DNA amplification cycles start with an initial dehybridization step to unwind all dsDNA molecules by increasing the temperature (95 °C). Once the melting temperature (T_m) of the dsDNA molecules is reached, the ssDNA templates become available for

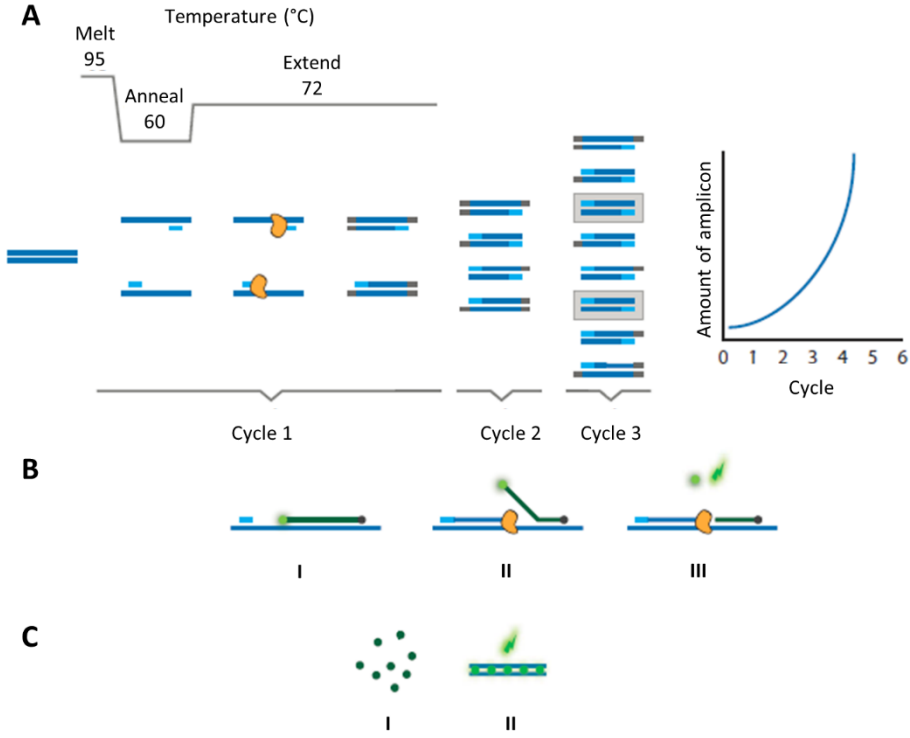

Figure 1.3: *Schematic of the polymerase chain reaction (PCR).* ***A)*** *Temperature profile of one single cycle and illustration of the exponential amplification of amplicons;* ***B)*** *Illustration of the Taqman probe principle. Only when the Taqman probe is degraded, signal is generated.* ***C)*** *Illustration of a high-affinity fluorescent dye. Only in presence of dsDNA, the fluorescent dye starts emitting. Adapted from Janssen (2013).*

amplification. In a next step known as annealing, the temperature is lowered (50 - 60 °C) to enable primer recognition of their complementary DNA template and hybridization to the matching part. Finally, the temperature is increased again (72 °C), optimal for the DNA polymerase to be active. This step is known as the extension step, in which the DNA polymerase builds further on the 3' terminal hydroxyl of the primers to make a copy of the DNA template, referred to as the amplicon. Once copied, the dehybridization, annealing and extension steps are repeated as a cycle, in which every amplicon act as an additional template in the next cycle, resulting into an exponential amplification.

As the genetic code of any organism is unique, DNA molecules can reveal disease related causes, such as the presence of pathogens and the malfunctioning of a gene. Since its development, PCR contributed to a more early diagnosis of several diseases, which were difficult to detect due to their low sample concentrations[39]. PCR evolved from a more preparatory technique with post-PCR analysis to a highly sensitive and real-time technique with the development of quantitative PCR (qPCR) in 1992[40]. The real-time readout mainly relies on hybridization of Taqman probes[41] to the ssDNA templates or on the high affinity of fluorescent dyes for the dsDNA templates. Labeled with a fluorophore-quencher pair (Figure 1.3B), Taqman probes bind downstream of the primers. The 5' to 3' exonuclease activity of the polymerase degrades the Taqman probe during primer extension, resulting in a fluorescent signal. On the other hand, fluorescent dyes such as SYBR Green show high affinity for dsDNA and reveal fluorescence under UV-light upon binding to the dsDNA (Figure 1.3C)[42]. PCR became the technique of choice for molecular diagnostics and has been adopted by clinical laboratories[43,44], making up the laboratory diagnostic toolbox next to cell culture methods (histopathology/cytology), enzyme-linked immunosorbent assays (ELISA) and next generation sequencing (NGS)[45].

On the one hand, these techniques provide highly sensitive and specific results and are designed to reach optimal efficiency when processing relatively large batches of samples. On the other hand, they require multiple steps and rather complex sample protocols. Therefore, diagnostic analysis remains often labor-intensive and time-consuming (up to days for NGS[45], multiple hours for ELISA and few hours for PCR[45]), while sample volumes up

to a mL are not unusual[46]. Furthermore, potential causes of error such as sample contamination ask for caution towards misleading results. Consequently, these conventional techniques are still confined to sophisticated laboratory environments with trained personnel, increasing time-to-result and reducing the cost-effectiveness. Expanding the accessibility or providing the valuable information of these techniques outside their sophisticated environment requires alternative and innovative assay formats. This goal has been the focus of biosensor technology, a field driven by the needs of the end-user[47].

1.3. Biosensors

Biosensors are analytical devices which convert a biological or chemical reaction into a detectable signal, proportional to the concentration of an analyte such as proteins, nucleic acids, and small molecules[48,49]. In order to generate signals, biosensors make use of several components illustrated in Figure 1.4[48,50] Bioreceptors are responsible for the specific recognition of the analyte and mainly evolved from enzymes[51] to antibodies (Abs) and NAs. The transducer element translates this event into an electronic signal, which is further processed into meaningful information for the end-user. Promising

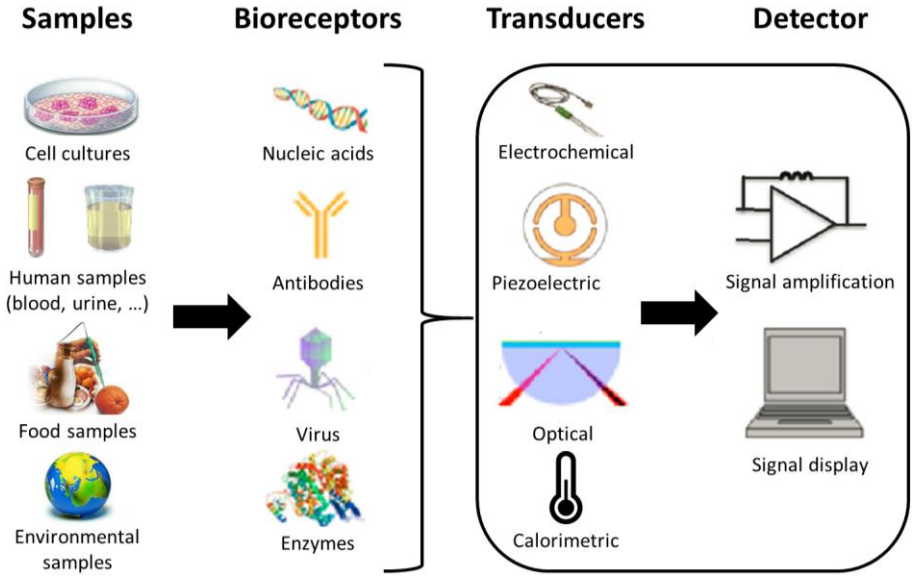

Figure 1.4: *Biosensor concept and components. Adapted from Grieshaber et al. (2008) and Zhou et al. (2019).*

transducer elements have been defined and are distinguished based on the generated signal: (i) electrochemical signals, translating the analyte-receptor interaction into a voltage or a current, (ii) optical signals, looking at the changes in e.g. absorption, color, fluorescence and surface plasmon resonance (SPR), (iii) piezoelectric signals, relating mass change to the resonance frequency of a quartz crystal and (iv) thermal signals, measuring the temperature change (i.e. calorimetry) or the change in thermal conductivity (i.e. heat-transfer method) upon interaction of the analyte and receptor[48,50,52]. With their unique concept, biosensors aim to bridge the gap between conventional, advanced laboratory diagnostics and the end-users needs, such as more user-friendly, time-efficient and affordable devices. This goes hand-in-hand with the challenge of assuring the robustness, specificity and sensitivity of such devices.

As a subfield, DNA biosensors exploit synthetic DNA for target detection, using ssDNA sequences mainly as capture probes. DNA probes are more than suitable for biosensor design, based on some interesting features. DNA molecules are relatively stable and can be synthesized with great accuracy, lacking any batch-to-batch variations as often observed for Abs[53]. Moreover, due to the complete *in vitro* synthesis of DNA, mass production can be realized with minimal contamination and under good manufacturing practice in a cost-effective way[53]. During this synthesis, diverse modifications can be built in, enabling simple DNA-labelling and -immobilization. Once immobilized on the biosensor surface, DNA target molecules from e.g., pathogen strains and metabolic disorders, can be detected based on simple hybridization.

Surface plasmon resonance (SPR) is a very interesting transducer element for designing DNA-based biosensors. SPR is a mass-based technique, enabling real-time monitoring of molecular binding events[54]. In order to meet the requirement of a more affordable and user-friendly device, an in-house fiber optic SPR (FO-SPR) platform has been reported and was further developed in this dissertation[55]. The FO-SPR platform can be fully automated and has the potential to be miniaturized. Moreover, the platform demonstrated its competence for the detection of different target molecules[56–58], where in this dissertation the focus will be on its NA-based applications. Many of these applications have been relying on the gold

nanoparticle (AuNP) compatibility of the FO-SPR platform as a label, increasing the mass of the target and therefore the sensitivity of the device[59]. Despite these promising prospects and compatibility with AuNPs, ultrasensitive (low pM – fM range) and robust target detection remains challenging. These challenges are related to the limited control of surface functionalization protocols and scarcity of robust amplification strategies, enabling low enough sensitivity levels in a decent timeframe. Moreover, all assay components and steps are mostly optimized in function of a certain group of target molecules or even in function of one particular target. Once optimized, it is very rare that an assay concept can be adapted towards another target or extended to a different group of molecules without re-starting the entire assay development, which makes this a very timely and costly process. Moving away from traditional target hybridization and labelling as done so far could be explored with DNA nanotechnology, which expanded as a new and remarkable field[27]. Instead, this field has been working on innovative target-induced systems with autonomous and more universal signal generation, opening up some opportunities for DNA-based FO-SPR design.

1.4. DNA nanotechnology for biosensor design

Over the last three decades, DNA technology evolved into an independent research field with promising features for the design of biosensing platforms[27]. Next to the general advantages of DNA in biosensor design as mentioned in previous section, DNA nanotechnology expands this by taking DNA beyond its regular linear hybridization. It turned DNA into a smart self-assembling nanomaterial and revealed a diverse repertoire of new DNA functionalities[60]. Furthermore, DNA nanotechnology developed interesting ways to provide DNA with controlled motion and reconfiguration. Based on these different aspects, DNA nanotechnology can be subdivided into three main categories: structural, dynamic and functional DNA nanotechnology[60].

Structural DNA nanotechnology uses DNA molecules as building blocks on the micro- and nanoscale. Initially, basic DNA structures were formed, relying on simple hybridization of sticky ends and structures, such as the Holliday junction[61]. Two- and three-dimensional structures were developed later and reached a milestone with the design of DNA origami (Figure 1.5)[62–64]. Starting from a long ssDNA scaffold, DNA origami

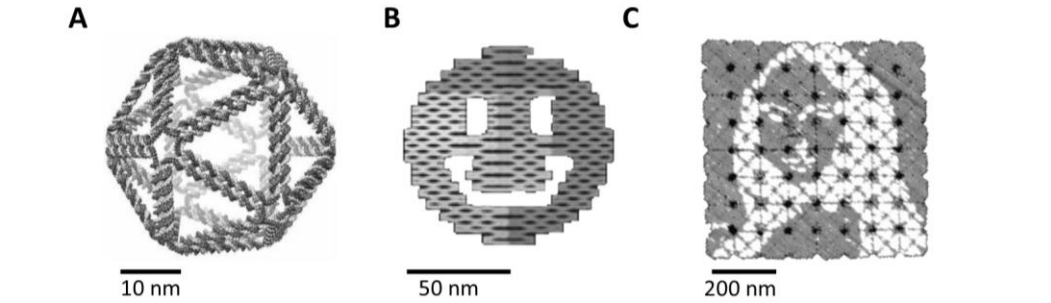

Figure 1.5: *Illustrations of structural DNA nanotechnology.* ***A)*** *3D polyhedron,* ***B)*** *DNA origami smiley and* ***C)*** *AFM image of origami arrays with an example pattern (Mona Lisa). Adapted from Veneziano et al. (2016) and reprinted with permission from AAAS; Adapted by permission from Springer Nature: Rothemund (2006); Adapted by permission from Springer Nature: Tikhomirov et al. (2017).*

nanostructures are built by folding the scaffold into the desired shape with the aid of multiple ssDNA staples. In terms of biosensing, structural DNA nanotechnology offers quite some flexibility, biocompatibility and controlled spacing of bioreceptors with nanoscale precision. Accessibility and orientation can therefore potentially be improved[65], while innovative structures have led to mutation detection and drug delivery[66].

Where structural DNA nanotechnology results in a final static structure, **dynamic DNA nanotechnology** exploits DNA molecules to create nanomachines and cascade reactions[60]. Strand displacement [67,68] and branch migration are the driving forces behind the concept, which can be controlled by a toehold structure. The toehold is a short DNA domain, typically 5 – 8 bases in length, with which a ssDNA sequence is able to bind a partially hybridized dsDNA complex. Once the toehold has bound, the ssDNA sequence can replace the original complementary DNA strand by branch migration. In combination with structural DNA nanotechnology, advanced nanomachines such as DNA motors[69], DNA walkers[68] and DNA computing systems[70] have been described (Figure 1.6A and B). DNA switches and walkers have been shown to be responsive to target triggers, such as pH and miRNA, opening opportunities for innovative biosensor design[27]. Furthermore, the toehold-based cascade reactions announced a new direction in signal amplification. Initial progress was made in creating isothermal, DNA-based amplification similar to PCR but without the need of any protein-enzyme, which is promising for stability improvement and cost reduction of current amplification systems.

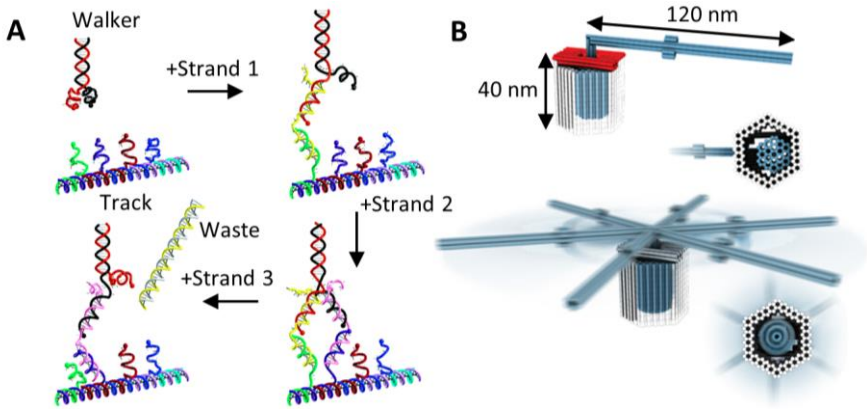

Figure 1.6: *Illustrations of dynamic DNA nanotechnology.* ***A)*** *DNA walker for molecular transport. Based on strand displacement the walker moves along the track; and* ***B)*** *DNA origami mobile rotor. Based on the solution conditions the rotor remains in the docking sites or performs a random rotary movement around the central axis. Adapted with permission of from Shin et al. © (2004) American Chemical Society; Adapted with permission from Ketterer et al. © (2016), with permission from AAAS.*

Most recently, **functional DNA nanotechnology** was added as subcategory, introducing DNA-based interactions going beyond the formation of the double helix. Multiple DNA molecules showing high affinity and specificity towards other molecules than DNA have been selected and are known as aptamers[53]. Aptamers bind a broad range of molecules, such as small molecules, proteins and viral particles, turning them into an interesting alternative to their protein counterparts, such as Abs (Figure 1.7A)[71]. On the other hand, several enzymatic functions can be reproduced with so-called nucleic acid enzymes (NAzymes). With signal amplification a key aspect for early diagnosis, NAzymes found their way into the biosensor field and proved to be compatible with existing transducer mechanisms(Figure 1.7B).

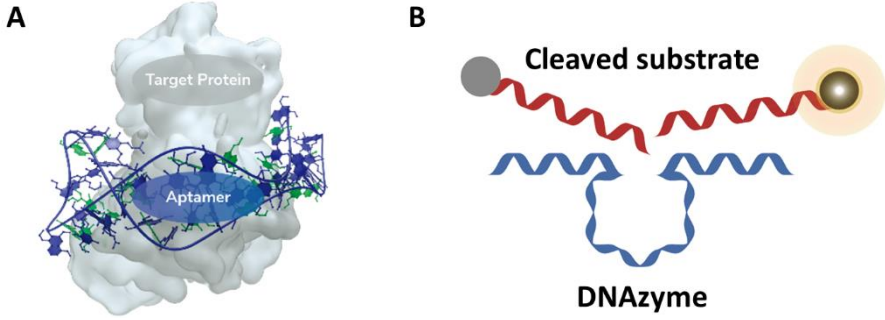

Figure 1.7: *Illustrations of functional DNA nanotechnology.* ***A)*** *Interaction between an aptamer and protein target molecule and* ***B)*** *Cleavage of a fluorescent substrate by a DNAzyme. Adapted from © 2011-2019 Aptamer Sciences, Inc. All right reserved.*

1.5. Objectives and outline of the thesis

As discussed above, classical PCR remains the gold standard in NA-based analysis, restricting its main use to laboratory settings. Expanding the accessibility or providing the valuable information of NA-based analysis outside this sophisticated environment could improve early diagnosis and minimize future disease burden. To do so, alternative and innovative DNA biosensor devices are being developed, focusing on the needs of the end-user, such as more user-friendliness, robustness, rapidity and cost-effectiveness. Among DNA biosensors, SPR is a transducer element of interest due to some advantageous features such as its real-time characteristic. More specific, our in-house developed FO-SPR platform has proven its competence for diverse applications. However, for NA-analysis FO-SPR assays are restricted to classical hybridization strategies, relying on immobilized capture probes and labeled detection probes. Assay sensitivities down to the lower nanomolar range can be reached[55], but ultrasensitive (low pM – fM range) detection remains challenging. These challenges are linked to the target-bioreceptor interaction and alternative ways of signal generation and amplification have not been fully explored. Within this regard, DNA nanotechnology has become a hot topic with alternative discoveries such as DNAzymes, driving the next generation of DNA biosensors by going beyond the classical hybridization assays. Despite, being still in its infancy, DNAzyme-based technologies designed at the solid-liquid interface have been focusing on metal ion detection and are not fully exploited for the detection of proteins and NAs.

In this framework, **the main objective of this dissertation is to design innovative NA-based biosensing strategies using a FO-SPR platform for the sensitive and specific detection of NAs.** This main objective is translated in following sub-objectives:

- **The design of a FO-PCR melting assay** with the aim of quantifying and differentiating DNA molecules with closely related sequences. The assay is explored for the detection of celery DNA as a proof-of-concept for the food industry and evaluated in cleaning water samples, spiked with known concentrations of celery DNA

- **The design of a FO-SPR biosensing concept sensitive to surface-based catalytic cleavage activity of DNAzymes** with the aim of evaluating the feasibility of this cleavage activity in future universal solid-phase diagnostics.
- **The design of a DNAzyme-based FO-PCR assay** with the aim of real-time and ultrasensitive DNA detection by combining NA amplification strategies and DNAzymes. The assay is explored for the detection of an antimicrobial resistance gene in *E. Coli* as a proof-of-concept for health care and livestock applications.

The results generated to realize the aforementioned objectives are presented in the following seven chapters (Figure 1.8):

In **Chapter 2**, the reader will be introduced into the field of DNA nanotechnology through a more detailed description of functional NAs, with the focus on RNA-cleaving DNAzymes (RCDs) and their selection. Further, the potential of RCDs in the development of (DNA-)biosensors is elucidated and some challenges are pinpointed. With SPR showing up at the forefront of DNA-based diagnostics, its physical principles, different formats and surface functionalization methods are explained. Most recent advancements in DNA-based signal amplification strategies are discussed, linking both the RCD and SPR technology.

As described in Section 1.2, PCR remains limited to clinical laboratories and can benefit from alternative implementations and their associated characteristics. In **Chapter 3,** the amplification strength of PCR is combined with an in-house developed, user-friendly FO-SPR platform in a one-step assay. Fiber-optic DNA capture and detection probes were designed to bind and label the PCR products. Subsequently, an increasing temperature gradient was used to differentiate among them, exploiting the melting temperature of the products. As-proof-of-concept, the fiber-optic PCR melting assay (FO-PCR-MA) is evaluated for the quantification of celery DNA and differentiation from potential false positives such as carrot DNA, limiting current ELISAs.

DNA technology has been introduced as an exciting field with some promising perspectives regarding biosensing, such as target recognition, surface patterning and signal amplification (Section 1.4). As premature field, several opportunities remain unexplored and require further research.

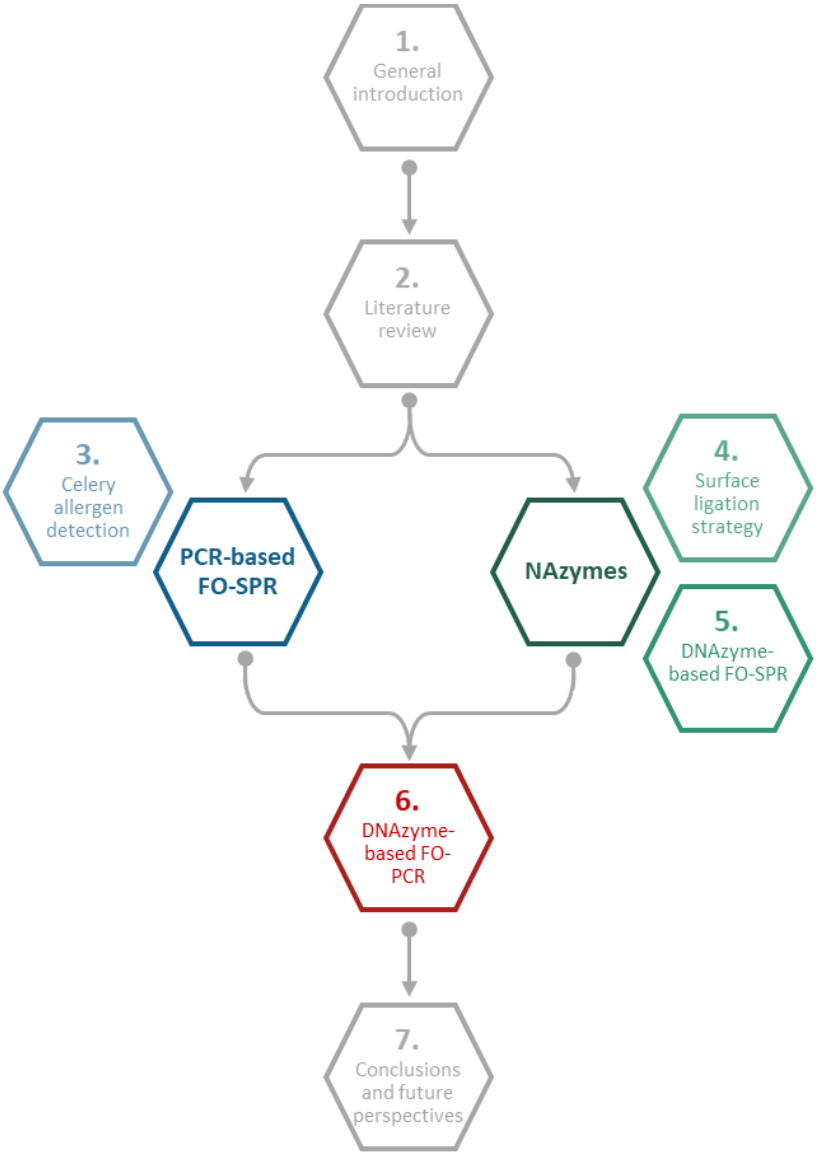

Figure 1.8: *Schematic overview of the different chapters in the dissertation.*

Therefore, **Chapter 4** focusses on an innovative surface functionalization strategy towards exploring the cleavage activity of DNAzymes in solid-phase biosensing. The AuNP-based functionalization strategy is implemented on the surface of a FO-SPR biosensor, optimized, and characterized in terms of maximal signal readout.

Building further on the previous chapter, **Chapter 5** exploits a new functionalization strategy for the real-time detection of DNAzyme cleavage activity. A NA target detection system is designed, while aiming for a universal readout system based on FO-SPR surface cleavage activity. An additional DNA strand is introduced and optimized as temporary inhibitor for the DNAzymes. Finally, target-triggered activation of the inhibited DNAzymes is evaluated with the FO-SPR platform.

Ultrasensitive detection of NAs plays a key role in screening and early diagnosis (Section 1.1). In this context, PCR is mainly used for target amplification. In **Chapter 6** a biosensing concept based on target-triggered PCR-amplification of DNAzymes is developed. Therefore, PCR primers are designed with an overhang, consisting of a DNAzyme complementary sequence. FO-SPR sensors as designed in Chapter 4 are used for one-step signal generation, requiring selection of reaction conditions which both enable PCR amplification and surface cleavage activity. As-proof-of-concept, the final assay is evaluated for the detection of an antimicrobial resistance gene.

Finally, **Chapter 7** gives an overview of the different FO-SPR sensor designs, realized in this dissertation, and the most important findings concerning their performance such as sensitivity and specificity. Furthermore, remaining challenges and suggestions for future applications are discussed in more detail.

1.6. References

1. Dahm, R. Friedrich Miescher and the discovery of DNA. *Dev. Biol.* **278**, 274–288 (2005).
2. Avery, O. T., MacLeod, C. M. & McCarty, M. STUDIES ON THE CHEMICAL NATURE OF THE SUBSTANCE INDUCING TRANSFORMATION OF PNEUMOCOCCAL TYPES. *J. Exp. Med.* **79**, 137–158 (1944).
3. Watson, J. D. & Crick, F. H. C. Molecular structure of nucleic acids: A structure for deoxyribose nucleic acid. *Nature* **171**, 737–738 (1953).
4. Freepik & Smashicons. Icons. Available at: www.flaticon.com.
5. Pray, L. A. Discovery of DNA Double Helix: Watson and Crick | Learn Science at Scitable. *Nature Education* 1(1):100 (2008). Available at: https://www.nature.com/scitable/topicpage/discovery-of-dna-structure-and-function-watson-397/. (Accessed: 3rd January 2020)
6. Crick, F. Central Dogma of Molecular Biology. *Nature* **227**, 561–563 (1970).
7. Nirenberg, M. *et al.* RNA codewords and protein synthesis, VII. On the general nature of the RNA code. *Proc. Natl. Acad. Sci.* **53**, 1161–1168 (1965).
8. Institute, N. H. G. Human Genome Project Timeline of Events. Available at: https://www.genome.gov/human-genome-project/Timeline-of-Events. (Accessed: 3rd January 2020)
9. Dwivedi, S. *et al.* Diseases and Molecular Diagnostics: A Step Closer to Precision Medicine. *Indian J. Clin. Biochem.* **32**, 374–398 (2017).
10. Brunham, L. R. & Hayden, M. R. Hunting human disease genes: lessons from the past, challenges for the future. *Hum. Genet.* **132**, 603–617 (2013).
11. Cutting, G. R. Cystic fibrosis genetics: from molecular understanding to clinical application. *Nat. Rev. Genet.* **16**, 45–56 (2015).
12. Singh, R. *et al.* Biosensors for pathogen detection: A smart approach towards clinical diagnosis. *Sensors Actuators B Chem.* **197**, 385–404 (2014).
13. Linacre, A. & Graham, D. Role of molecular diagnostics in forensic science. *Expert Rev. Mol. Diagn.* **2**, 346–353 (2002).
14. Mullis, K. *et al.* Specific Enzymatic Amplification of DNA In Vitro: The Polymerase Chain Reaction. *Cold Spring Harb. Symp. Quant. Biol.* **51**, 263–273 (1986).
15. Jackson, J. B. *et al.* Establishment of a quality assurance program for human immunodeficiency virus type 1 DNA polymerase chain reaction assays by the AIDS Clinical Trials Group. ACTG PCR Working Group, and the ACTG PCR Virology Laboratories. *J. Clin. Microbiol.* **31**, 3123–3128 (1993).
16. Busch, M. P. & Satten, G. A. Time course of viremia and antibody seroconversion following human immunodeficiency virus exposure. *Am. J. Med.* **102**, 117–124 (1997).
17. Hall, J. *et al.* Linkage of early-onset familial breast cancer to chromosome 17q21. *Science (80-.).* **250**, 1684–1689 (1990).
18. Wooster, R. *et al.* Localization of a breast cancer susceptibility gene, BRCA2, to chromosome 13q12-13. *Science (80-.).* **265**, 2088–2090 (1994).
19. Chan, P. C. R., Wong, B. Y. L., Ozcelik, H. & Cole, D. E. C. Simple and Rapid Detection of BRCA1 and BRCA2 Mutations by Multiplex Mutagenically Separated PCR. *Clin. Chem.* **45**, 1285–1287 (1999).
20. Asal, M., Özen, Ö., Şahinler, M. & Polatoğlu, İ. Recent Developments in Enzyme, DNA and Immuno-Based Biosensors. *Sensors* **18**, 1924 (2018).
21. Du, Y. & Dong, S. Nucleic Acid Biosensors: Recent Advances and Perspectives. *Anal. Chem.* **89**, 189–215 (2017).

22. Wang, J., Shan, Y., Zhao, W.-W., Xu, J.-J. & Chen, H.-Y. Gold Nanoparticle Enhanced Electrochemiluminescence of CdS Thin Films for Ultrasensitive Thrombin Detection. *Anal. Chem.* **83**, 4004–4011 (2011).
23. Tran, D. T. *et al.* Selection of aptamers against Ara h 1 protein for FO-SPR biosensing of peanut allergens in food matrices. *Biosens. Bioelectron.* **43**, 245–251 (2013).
24. Mandli, J., Mohammadi, H. & Amine, A. Electrochemical DNA sandwich biosensor based on enzyme amplified microRNA-21 detection and gold nanoparticles. *Bioelectrochemistry* **116**, 17–23 (2017).
25. Contreras Jiménez, G. *et al.* Aptamer-Based Label-Free Impedimetric Biosensor for Detection of Progesterone. *Anal. Chem.* **87**, 1075–1082 (2015).
26. Chao, J., Zhu, D., Zhang, Y., Wang, L. & Fan, C. DNA nanotechnology-enabled biosensors. *Biosens. Bioelectron.* **76**, 68–79 (2016).
27. Ebrahimi, A., Ravan, H. & Khajouei, S. DNA nanotechnology and bioassay development. *TrAC Trends Anal. Chem.* **114**, 126–142 (2019).
28. Graybill, R. M. & Bailey, R. C. Emerging Biosensing Approaches for microRNA Analysis. *Anal. Chem.* **88**, 431–450 (2016).
29. Senel, M., Dervisevic, M. & Kokkokoğlu, F. Electrochemical DNA biosensors for label-free breast cancer gene marker detection. *Anal. Bioanal. Chem.* **411**, 2925–2935 (2019).
30. Campuzano, S., Yáñez-Sedeño, P. & Pingarrón, J. Molecular Biosensors for Electrochemical Detection of Infectious Pathogens in Liquid Biopsies: Current Trends and Challenges. *Sensors* **17**, 2533 (2017).
31. Reder-Christ, K. & Bendas, G. Biosensor Applications in the Field of Antibiotic Research—A Review of Recent Developments. *Sensors* **11**, 9450–9466 (2011).
32. Anjum, M. F., Zankari, E. & Hasman, H. Molecular Methods for Detection of Antimicrobial Resistance. *Microbiol. Spectr.* **5**, (2017).
33. Baraketi, A., Salmieri, S. & Lacroix, M. Foodborne Pathogens Detection: Persevering Worldwide Challenge. in *Biosensing Technologies for the Detection of Pathogens - A Prospective Way for Rapid Analysis* 20 (InTech, 2018). doi:10.5772/intechopen.74421
34. Wu, Q., Zhang, Y., Yang, Q., Yuan, N. & Zhang, W. Review of Electrochemical DNA Biosensors for Detecting Food Borne Pathogens. *Sensors* **19**, 4916 (2019).
35. Justino, C., Duarte, A. & Rocha-Santos, T. Recent Progress in Biosensors for Environmental Monitoring: A Review. *Sensors* **17**, 2918 (2017).
36. Garibyan, L. & Avashia, N. Polymerase Chain Reaction. *J. Invest. Dermatol.* **133**, 1–4 (2013).
37. Janssen, K. P. F. *Aptamer based strategies for ultrasensitive protein detection*. (2013).
38. Chien, A., Edgar, D. B. & Trela, J. M. Deoxyribonucleic acid polymerase from the extreme thermophile Thermus aquaticus. *J. Bacteriol.* **127**, 1550–1557 (1976).
39. Heilek, G. Nucleic Acids — The Use of Nucleic Acid Testing in Molecular Diagnostics. in *Nucleic Acids - From Basic Aspects to Laboratory Tools* **i**, 13 (InTech, 2016).
40. Higuchi, R., Dollinger, G., Walsh, P. S. & Griffith, R. Simultaneous Amplification and Detection of Specific DNA Sequences. *Bio/Technology* **10**, 413–417 (1992).
41. Holland, P. M., Abramson, R. D., Watson, R. & Gelfand, D. H. Detection of specific polymerase chain reaction product by utilizing the 5'----3' exonuclease activity of Thermus aquaticus DNA polymerase. *Proc. Natl. Acad. Sci.* **88**, 7276–7280 (1991).
42. Ponchel, F. *et al.* Real-time PCR based on SYBR-Green I fluorescence: An alternative to the TaqMan assay for a relative quantification of gene rearrangements, gene amplifications and micro gene deletions. *BMC Biotechnol.* **3**, 18 (2003).
43. Sohrabi, N., Valizadeh, A., Farkhani, S. M. & Akbarzadeh, A. Basics of DNA biosensors and cancer diagnosis. *Artif. Cells, Nanomedicine, Biotechnol.* **44**, 654–663 (2016).

44. Tsongalis, G. J. & Silverman, L. M. Molecular diagnostics: A historical perspective. *Clin. Chim. Acta* **369**, 188–192 (2006).
45. Bellassai, N., D'Agata, R., Jungbluth, V. & Spoto, G. Surface Plasmon Resonance for Biomarker Detection: Advances in Non-invasive Cancer Diagnosis. *Front. Chem.* **7**, (2019).
46. Petralia, S. & Conoci, S. PCR Technologies for Point of Care Testing: Progress and Perspectives. *ACS Sensors* **2**, 876–891 (2017).
47. Hahn, S., Mergenthaler, S., Zimmermann, B. & Holzgreve, W. Nucleic acid based biosensors: The desires of the user. *Bioelectrochemistry* **67**, 151–154 (2005).
48. Grieshaber, D., MacKenzie, R., Vörös, J. & Reimhult, E. Electrochemical Biosensors - Sensor Principles and Architectures. *Sensors* **8**, 1400–1458 (2008).
49. Bhalla, N., Jolly, P., Formisano, N. & Estrela, P. Introduction to biosensors. *Essays Biochem.* **60**, 1–8 (2016).
50. Zhou, Y., Fang, Y. & Ramasamy, R. Non-Covalent Functionalization of Carbon Nanotubes for Electrochemical Biosensor Development. *Sensors* **19**, 392 (2019).
51. Clark, L. C. & Lyons, C. Electrode systems for continuous monitoring in cardiovascular surgery. *Ann. N. Y. Acad. Sci.* **102**, 29–45 (1962).
52. Khorshid, M. *et al.* Searching for a common origin of heat-transfer effects in bio- and chemosensors: A study on thiols as a model system. *Sensors Actuators B Chem.* **310**, 127627 (2020).
53. Zhou, J. & Rossi, J. Aptamers as targeted therapeutics: current potential and challenges. *Nat. Rev. Drug Discov.* **16**, 181–202 (2017).
54. Homola, J. Surface Plasmon Resonance Sensors for Detection of Chemical and Biological Species. *Chem. Rev.* **108**, 462–493 (2008).
55. Pollet, J. *et al.* Fiber optic SPR biosensing of DNA hybridization and DNA–protein interactions. *Biosens. Bioelectron.* **25**, 864–869 (2009).
56. Janssen, K. P. F. *et al.* Enabling fiber optic serotyping of pathogenic bacteria through improved anti-fouling functional surfaces. *Nanotechnology* **23**, 235503 (2012).
57. Lu, J. *et al.* Fiber optic-SPR platform for fast and sensitive infliximab detection in serum of inflammatory bowel disease patients. *Biosens. Bioelectron.* **79**, 173–179 (2016).
58. Daems, D. *et al.* Competitive inhibition assay for the detection of progesterone in dairy milk using a fiber optic SPR biosensor. *Anal. Chim. Acta* **950**, 1–6 (2017).
59. Bedford, E. E., Spadavecchia, J., Pradier, C.-M. & Gu, F. X. Surface Plasmon Resonance Biosensors Incorporating Gold Nanoparticles. *Macromol. Biosci.* **12**, 724–739 (2012).
60. Wang, W. *et al.* Bioapplications of DNA nanotechnology at the solid–liquid interface. *Chem. Soc. Rev.* **48**, 4892–4920 (2019).
61. Kallenbach, N. R., Ma, R.-I. & Seeman, N. C. An immobile nucleic acid junction constructed from oligonucleotides. *Nature* **305**, 829–831 (1983).
62. Rothemund, P. W. K. Folding DNA to create nanoscale shapes and patterns. *Nature* **440**, 297–302 (2006).
63. Veneziano, R. *et al.* Designer nanoscale DNA assemblies programmed from the top down. *Science (80-.).* **352**, 1534–1534 (2016).
64. Tikhomirov, G., Petersen, P. & Qian, L. Fractal assembly of micrometre-scale DNA origami arrays with arbitrary patterns. *Nature* **552**, 67–71 (2017).
65. Daems, D. *et al.* Three-Dimensional DNA Origami as Programmable Anchoring Points for Bioreceptors in Fiber Optic Surface Plasmon Resonance Biosensing. *ACS Appl. Mater. Interfaces* **10**, 23539–23547 (2018).
66. Chandrasekaran, A. R., Anderson, N., Kizer, M., Halvorsen, K. & Wang, X. Beyond the Fold: Emerging Biological Applications of DNA Origami. *ChemBioChem* **17**, 1081–1089

(2016).
67. DeLuca, M., Shi, Z., Castro, C. E. & Arya, G. Dynamic DNA nanotechnology: toward functional nanoscale devices. *Nanoscale Horizons* **5**, 182–201 (2020).
68. Shin, J.-S. & Pierce, N. A. A Synthetic DNA Walker for Molecular Transport. *J. Am. Chem. Soc.* **126**, 10834–10835 (2004).
69. Ketterer, P., Willner, E. M. & Dietz, H. Nanoscale rotary apparatus formed from tight-fitting 3D DNA components. *Sci. Adv.* **2**, e1501209 (2016).
70. Li, F. *et al.* A DNAzyme-mediated logic gate for programming molecular capture and release on DNA origami. *Chem. Commun.* **52**, 8369–8372 (2016).
71. Sciences, A. About Aptamer –Aptamer Sciences. Available at: http://aptsci.com/en/aptamer/aptamer/. (Accessed: 4th January 2020)

Chapter 2

State-of-the-art of functional nucleic acid DNA nanotechnology and DNA-based FO-SPR bioassays

2.1. Introduction

In Chapter 1 the field of DNA nanotechnology was briefly introduced, showing that the current role of DNA goes far beyond the storage and transmission of genetic information. In this chapter, first the subdomain of functional DNA nanotechnology is described in more detail, while focusing on the catalytic sequences or NAzymes. Their potential role in biosensor development is illustrated and some current challenges are highlighted. Being still in its infancy, NAzyme-based technologies designed at the solid-liquid interface are not fully exploited yet for the detection of different target molecules such as NAs. Therefore, the second main section in this chapter is devoted to SPR technology, providing real-time information at the solid-liquid interface. The concept is explained and its compatibility with DNA biosensor design is illustrated.

2.2. Functional nucleic acids

Functional DNA nanotechnology comprises two main groups of sequences with new physical and chemical functionalities[1]: (i) aptamers[2,3] and (ii) NAzymes[4]. Aptamers are short RNA or ssDNA sequences with specific affinity towards different targets of interest, such as proteins and small molecules[5,6]. The target-specific affinity of the aptamers is based on hydrophobic, electrostatic and alternative hydrogen interactions (e.g. Hoogsteen hydrogen bonds between two guanines) rather than classical Watson-Crick hybridization. As such, aptamers have been used successfully as bioreceptors[5], enabling regeneration of the biosensor surfaces, even after multiple cycles of de- and renaturation. In contrast to aptamers, NAzymes are characterized by their catalytic activity similar to protein enzymes and can consist fully of ssDNA, referred to as DNAzymes[7]. Their catalytic activity originates from the specific interaction with a cofactor, enabling the formation of a catalytic core. Due to their catalytic activity, DNAzymes are used extensively in biosensing for signal generation and signal amplification[8,9]. Different types of DNAzymes have been reported in the literature, each of them catalyzing different reactions. They can be divided in the following subgroups: (i) RNA-cleaving DNAzymes, (ii) peroxidase mimicking DNAzymes and (iii) DNAzymes catalyzing other reactions.

2.2.1. DNAzyme functions and reactions

2.2.1.1. RNA-cleaving DNAzymes

The first RNA-cleaving DNAzyme (RCD) was reported in 1994 by Breaker and Joyce, using an *in vitro* selection technique[10]. Pb^{2+} was considered as the first cofactor to target cleavage of a DNA substrate, containing a single ribonucleotide. Once established, multiple *in vitro* selection experiments followed each other and the exploration of these new molecules began. In 1997, Santoro and Joyce described two additional RCDs[4], which currently are still the two most intensively studied RCDs (Figure 2.1). The 8-17 and the 10-23 RCDs both consist of a catalytic core flanked by two substrate-binding arms. Their catalytic cores rely on divalent metal ions as cofactor and have proven to be very robust in obtaining reproducible cleavage activity. This robustness enables great flexibility in the choice of the binding arm sequences, which currently still results in diverse applications of the enzymes[11]. Commonly, the **8-17 DNAzyme** is used as a Pb^{2+}-dependent DNAzyme and, although initially believed to be restricted to any N-G

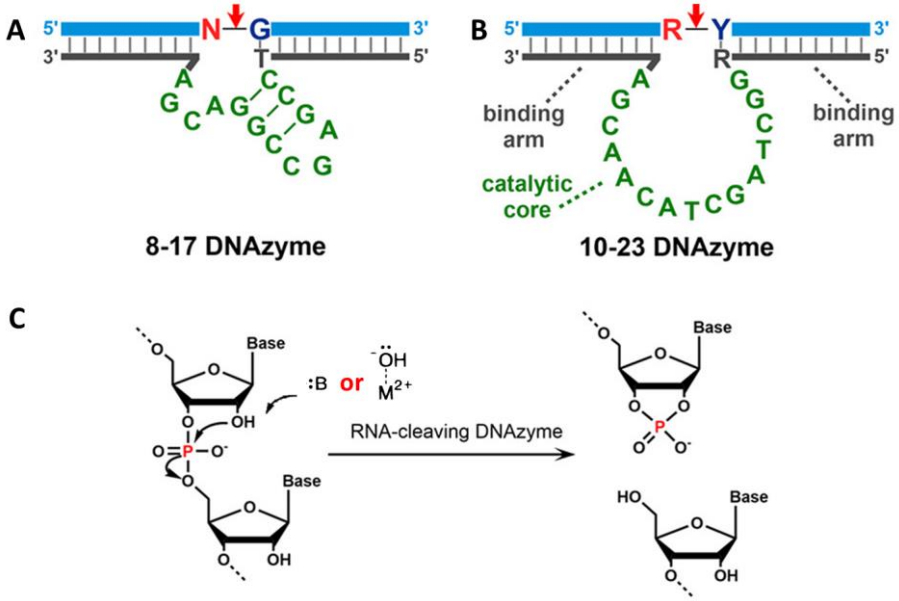

Figure 2.1: *Main RNA-cleaving DNAzymes.* ***A)*** *Illustration of the 8-17 DNAzyme, N can be any nucleotide;* ***B)*** *Illustration of the 10-23 DNAzyme, R = A or G and Y = U or C;* ***C)*** *Proposed reaction scheme of RNA-cleaving DNAzymes, deprotonation by: (i) a metal hydroxide(M-OH) or (ii) a Lewis base (B). Adapted with permission from Peng et al. © (2018) American Chemical Society.*

combination, able to cleave all 16 dinucleotide combinations (Figure 2.1A)[9,12]. The small catalytic core consists of four unpaired nucleotides, a three base pair stem, a constant AGC-loop and a G-T wobble structure. On the other hand, the **10-23 DNAzyme** is Mg^{2+}-dependent and able to cleave all purine-pyrimidine combinations (Figure 2.1B)[13]. Its small catalytic core counts 15 nts and based on a more limited insight in the structure of the DNAzyme, the core nucleotides are always represented as unpaired. Although less is known about its structure, the 10-23 DNAzyme does possess some high conserved nucleotides similar to the 8-17 DNAzyme, making it a potential structural variant of the 8-17 DNAzyme upon pairing with its divalent metal ion cofactor[14].

In combination with stable base pairing between the substrate-binding arms and the substrate, RNA-cleavage is initiated by attack of the 2'-hydroxyl group near the scissile phosphodiester bond (Figure 2.1C)[13]. This deprotonation is hypothesized to be caused by: (i) a metal hydroxide or (ii) a Lewis base, while the metal cofactor stabilizes the generated nucleophile[15]. The nucleophilic attack of the phosphor backbone results into the 2', 3'-cyclic phosphate and the 5'-hydroxyl groups. This mechanism is similar to the one found in nature for the hammerhead ribozyme[16]. In physiological conditions, catalytic efficiencies of 4×10^5 and 3.2×10^8 M^{-1} min^{-1} were obtained for the 8-17 and 10-23 DNAzyme, respectively[17]. These values are similar to the catalytic efficiency of the diffusion limited enzyme horseradish peroxidase (HRP)[18], which is regularly used in biosensing and has an efficiency in the order of ~10^8 M^{-1} min^{-1}. Depending on the type of divalent metal ion and the used concentration as cofactor, catalytic efficiencies have been improved. In case of the 10-23 DNAzyme, improved catalytic efficiencies are achieved at higher Mg^{2+} concentrations (10 – 100 mM) up to 4.9×10^9 M^{-1} min^{-1}, making it one of the faster RCDs[16,17].

2.2.1.2. Peroxiding DNAzymes

Next to the RCDs, **peroxidase-mimicking G-quadruplexes** form a second group of DNAzymes, widely studied and developed into biosensing applications[9,19]. G-quadruplexes originate from the association between guanine-rich sequence domains, based on Hoogsteen hydrogen bonds[18,19]. Alternative to the Watson-Crick pairing, four guanines align into a square plane, forming a G-quartet which in turn can stack on top of other G-quartets

and result into a final G-quadruplex (Figure 2.2A). In general, the G-quadruplex structure has been stabilized by monovalent ions, such as K^+ and Na^+, aligning themselves in the core of the G-quartets. However, depending on the specific metal ions and the interaction between them, the G-quadruplex structure shows a slightly altered configuration. The G-quadruplex structure can be formed by a single (PS2.M), two separate (Agro 100) or four different (T4G4) sequences as illustrated in Figure 2.2A. The PS2.M DNAzyme was the first G-quadruplex sequence to show specific affinity for hemin and enable oxidation of 2,2'-azinobis(3-ethylbenzo-thiozoline)-6-sulfonic acid (ABTS) in presence of H_2O_2 into a cationic radical $ABTS^{\bullet+}$ (Figure 2.2B). Similar to HRP, a color reaction takes place during oxidation, which made the G-quadruplex an interesting label for sensing purposes, such as on-site applications[9]. Other substrates such as tetramethylbenzidine (TMB) and luminol are also converted by the G-quadruplex complex, allowing to fine-tune and improve the sensitivity depending on the application.

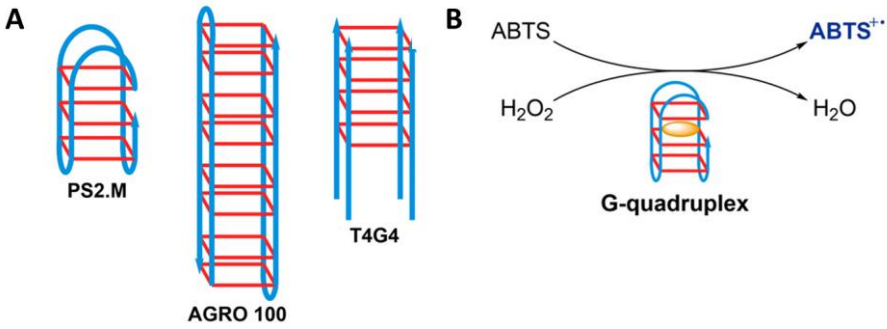

Figure 2.2: *Peroxidase-mimicking DNAzymes.* ***A)*** *G-quadruplex DNAzymes can be formed by one, two or four DNA strands and* ***B)*** *G-quadruplex DNAzyme mediated color reaction. Adapted with permission from Peng et al. © (2018) American Chemical Society.*

2.2.1.3. Other DNAzyme catalytic reactions

Through *in vitro* selection and the relatively ease of modification, the diversity in DNAzymes has expanded a lot over the last three decades. In addition to the RNA-cleavage and peroxidase activity[13,14] other functionalities are gaining importance. Among the DNAzymes acting on NA substrates, DNA-cleaving DNAzymes have been selected in order to use as artificial restriction enzymes. Further, DNAzymes have been selected able to cleave **other NA substrates**, composed of ester bonds, anilides and

monophosphoester linkages. More challenging in terms of selection was the search for DNAzymes creating new chemical bonds, such as ligation reactions. DNA- and RNA-ligating NAzymes have been an interesting alternative for the use of the T4 ligase, synthesis of branched DNA, labeling of RNA molecules and solid-phase synthesis of NAs.

In turn, incorporation of **non-NA substrates** into the *in vitro* selection process has led to different DNAzymes, enabling the formation of C-C bonds by facilitating the Diels-Alder reaction and Friedel-Crafts alkylation[13,14]. Eventually, also modified nucleotides and sugar backbones have been introduced as DNAzyme building blocks. Inclusion of modified nucleotides enabled NAzymes independent of (divalent) metal ions, while xeno-nucleotide based DNAzymes or XNAzymes were more robust towards nuclease degeneration. Although more complex and less cost-effective, these modifications significantly broadened the chemical space available in the DNAzyme selection process, which will be discussed in the next section.

2.2.2. RNA-cleaving DNAzyme selection

Since the discovery of aptamers shortly preceded the one of DNAzymes, several insights and techniques, such as the *in vitro* selection, were translated to the field of DNAzymes[14]. **Systematic evolution of ligands by exponential enrichment (SELEX)** is an iterative process, which was designed to select NA sequences with new potential functionalities. The technique starts with building a library of oligonucleotides, which consist of a typically 40 – 80 nucleotides long random region, flanked by two constant regions at both ends (Figure 2.3A). These constant regions act as primer recognition sites in the subsequent PCR step. Additional functional groups are introduced to immobilize the library and obtain the functionalities of interest. In case of RCDs, RNA nucleotides have been built-in by including them into the DNA primers.

Once the random library is established (around 10^{15} molecules), the different oligonucleotides are incubated under desired reactions conditions, based on the considered application (Figure 2.3B). Important parameters are the reaction temperature, monovalent metal ion concentration, the incubation time and the concentration of the specific cofactors, such as divalent metal ions or small molecules. All these parameters will affect the different configurations of the library sequences and only some of them will

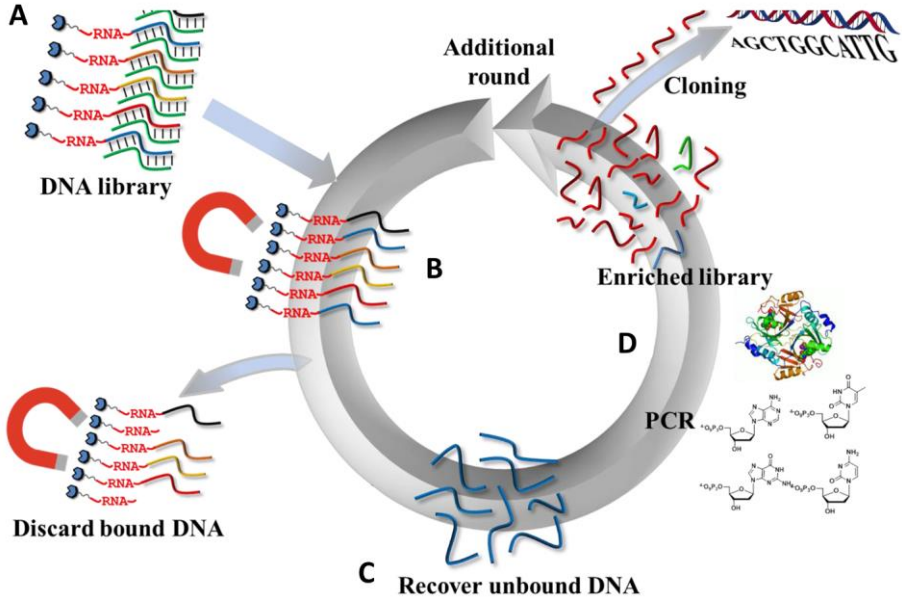

Figure 2.3: *Systematic evolution of ligands by exponential enrichment. Adapted from Hollenstein (2015).*

fulfill the required functionalities. For RCDs, the sequences of interest can be distinguished relatively simple by labelling the RNA-containing primer with biotin or coupling it to magnetic particles. By running the complete library through a streptavidin column or using a magnet, the sequences of interest can be recovered at a high yield, while non-active sequences are retained and discarded (Figure 2.3C). After separation, another PCR round amplifies the sequences of interest and the whole selection process starts over (Figure 2.3D). Typically, 5 – 15 iterations are performed to enrich the library enough to obtain reproducible catalytic activity. In addition, the selection pressure can be increased during the iterations to further steer the selection to a successful outcome. Eventually, individual DNAzymes are then cloned and sequenced to identify the most promising candidates. Using SELEX, multiple functionalities and DNAzyme variants have been discovered (Section 2.2.1), of which a major group belongs to the RCDs because of the initial interest of their use in gene silencing by targeting mRNA. After more than two decades of selection and design, the NAzyme repertoire evolved to an extensive toolbox with diverse applications, of which RCD applications will be illustrated in following sections.

2.2.3. Solution-based DNAzyme biosensors

Although DNAzymes were initially selected for gene silencing purposes, their use in the development of innovative biosensors started shortly after their discovery and increased during the last three decades[8,9]. Based on insights in their nature and selected characteristics, DNAzymes are exploited as alternative and innovative bioreceptors, signal generators and signal amplifiers. Following sections give an overview of the main strategies used to develop DNAzyme-based biosensors, focusing on the RCDs as one of the major DNAzyme groups of interest as described above. Initial DNAzyme biosensors were solution-based, meaning that both DNAzyme and substrate are free in solution and therefore the associated catalytic activity too.

2.2.3.1. DNAzyme-based biorecognition and signal generation

Among the first DNAzyme-based biosensors, the activity of RCDs was used to separate fluorophore-quencher (F-Q) pairs at the sequence ends of the DNAzyme/substrate in order to generate a target specific signal (Figure 2.4A)[20]. As target, the detection of metal ions such as Pb^{2+}, Cu^{2+}, Mg^{2+}, Mn^{2+} and UO_2^{2+} (uranyl ion), was most convenient since for the majority of RCDs they act as a cofactor[21,22]. The F-Q pair position has been varied from the substrate endings to internal sequence positions, completed with extra quenchers or replaced by molecular beacon-like complexes to further reduce the background[8,21]. While some researchers focused on optimizing the fluorescent readout, in parallel others broadened the field for NA and protein targets[8,9]. Based on the flexibility of the substrate-binding arms, this was mainly obtained by inactivation of the DNAzymes. Different approaches have been proposed: (i) allosteric inhibitors, additional sequences or loop–structures which (partially) block the RCDs (Figure 2.4B[23–25]) and can be aptamers (e.g. aptazymes), or (ii) allosteric activators, which are required to enable activity (Figure 2.4C), and (iii) binary DNAzymes[26] or MNAzymes[27,28], of which the catalytic core is split up and only reforms when both parts bind the target (Figure 2.4D). Next to biorecognition and signal generation, RCDs intrinsically cause signal amplification in multiple turnover conditions (e.g. RCDs can perform their activity more than once). Although their intrinsic amplification capacity, ultrasensitivity in the lower pM – fM range is often not reached. Ultrasensitivity is crucial for the early-stage detection of several

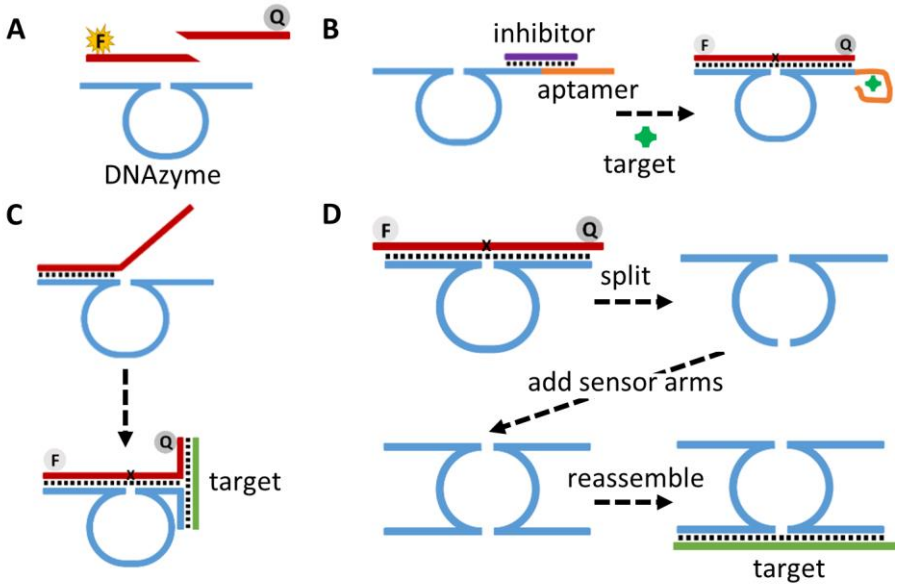

Figure 2.4: *DNAzyme signaling and control.* ***A)*** *Fluorescent RCD readout,* ***B)*** *DNAzyme inactivation by inhibitor sequence and illustration of aptazyme,* ***C)*** *allosteric DNAzymes, cleavage activity is controlled by modifying the enzyme-substrate interaction and* ***D)*** *MNAzymes splitting up the catalytic core enabled control over the cleavage activity. Adapted with permission from Mokany et al. © (2010) American Chemical Society; Adapted from Zhou et al. (2017).*

disease-related NAs and proteins, requiring an additional form of amplification.

DNAzyme-coupled and –triggered signal amplification

Due to their DNA nature, RCDs have been coupled with existing NA-amplifying techniques[29], such as PCR[30] and rolling circle amplification (RCA)[31]. In case of classical PCR, RCDs have been introduced into the PCR cycles by primer overhangs, containing the RCD complement of interest[30]. Every time the primer with overhang is copied, an additional RCD is being generated. This approach enabled successful detection of a human K-ras oncogene, as few as 10 copy numbers or 0.3 aM. Alternatively, isothermal amplification of RCDs was realized, for instance, by making use of RCA. RCA is a technique that uses the circular DNA as template for NA extension, similar to classic PCR. In contrast, the circular DNA template (CDT) can be copied continuously at a constant temperature without denaturation and as long reagents are available. Liu *et al.* reported a DNAzyme feedback system, using two CDT

complexes: (i) complex 1 forms itself in presence of the target (DP) and (ii) complex 2 drives the feedback loop (Figure 2.5)[32]. In presence of the target and by including the RCD antisense in the CDT, multiple RCDs were generated in serie. The RNA containing substrate (RDS) could then be cleaved and provide additional complex 1 CDTs. Detection was realized with a ssDNA-binding fluorescent dye and enabled miRNA detection down to 0.1 fM. However, some of these techniques require thermocycling or sophisticated sequence design, which increases complexity. Further, all of them rely on protein enzymes, which make up a significant part of the cost and are less stable compared to the NA templates and primers[9,33].

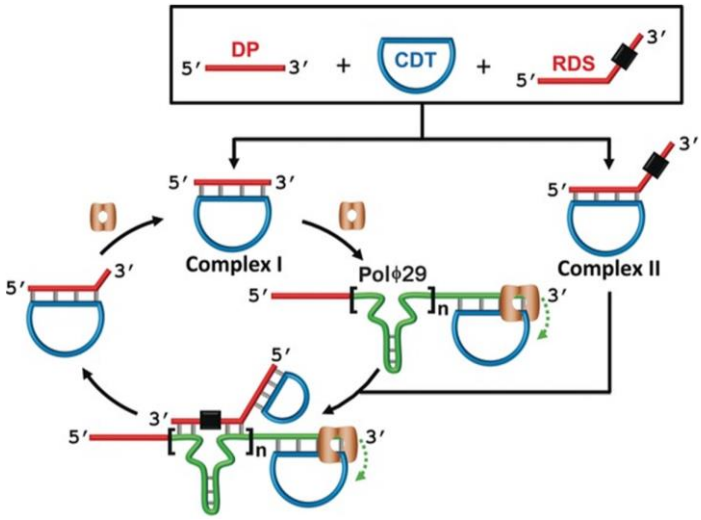

Figure 2.5: *DNAzyme-based RCA amplification feedback loop. DP = DNA primer or target, CDT = circular DNA template, RDS = RNA-containing substrate and Polφ29 = φ29 DNA polymerase. The RNA-cleaving DNAzymes getting copied are indicated in green and the black square indicates the RNA-cleaving site in the substrate. Adapted with permission from Liu et al. © (2017) Wiley-VCH Verlag GmbH & Co. KGaA, Weinheim.*

Alternatively, **enzyme-free (e.g. no protein enzymes) amplification cascades** have been developed, preserving the isothermal characteristic like RCA. The hybridization chain reaction (HCR)[34], for example, is a technique which exploits a triggering sequence and a set of hairpin structures (usually 2) to form long DNA nanowires after sequential hybridization. Providing some of the hairpins with overhangs supporting the formation of active DNAzymes resulted into catalytic active DNA nanowires upon target triggering (Figure 2.6). Wang *et al.* reported such a system where neighboring

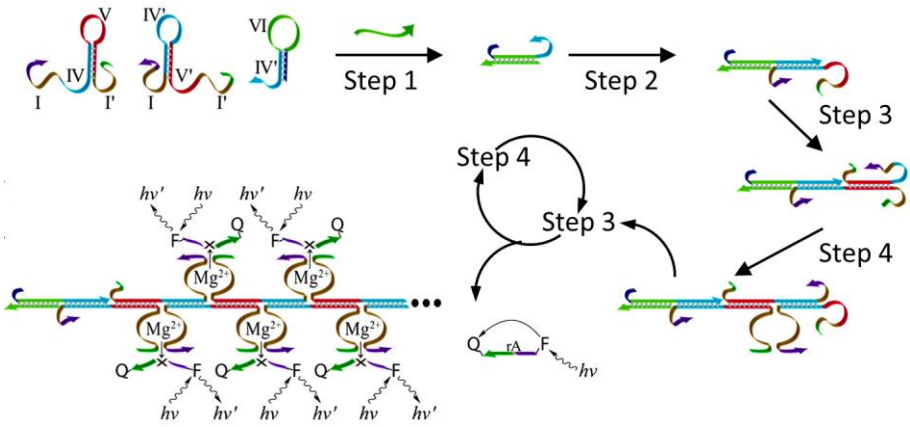

Figure 2.6: *DNAzyme-based hybridization chain reaction (HCR). Classical HCR is based on hairpin structures, which remain folded in the absence of a specific target. In presence of the target, a first hairpin unfolds in favor of a more stable hybridization complex with the target. Unfolding of the first hairpin triggers a sequential unfolding of the other hairpins, driven by the formation of more stable hybridization complexes or DNA nanowires. In contrast with classical HCR, providing the hairpins with overhangs to form active DNAzymes enabled amplified signal generation, using F-Q labelled DNAzyme substrates. Adapted with permission from Wang et al. © (2011) American Chemical Society.*

overhang structures formed active MNAzymes[35]. Another approach also making use of a triggering sequence and a set of hairpins is called catalytic hairpin assembly (CHA)[36]. Instead of forming DNA nanowires, also individual dsDNA structures can be formed. Moreover, the triggering sequence gets recycled and drives the continuous assembly of the dsDNA structures, which can be MNAzymes[33]. A more detailed illustration of CHA can be found in the next section. Both HCR and CHA showed to be relevant for cancer diagnosis, by identifying oncogenes and quantification of miRNA, with LODs of 10 fM and 1 pM, respectively[33,35]. While not using any enzyme is an asset in terms of stability and cost, assay times increased to several hours and sensitivities are not always improved.

2.2.4. Solid-phase DNAzyme biosensors

Next to the solution-based concepts, introducing solid interfaces provided new design strategies and broadened the potential readout systems. Moreover, surface immobilization brought some practical advantages[21,37]: (i) surfaces are better compatible with washing steps, which facilitates the reduction of any potential background signals, (ii) bioreceptor immobilization enables them to switch between the un- and bound states,

making the sensors potentially reusable, and (iii) immobilized bioreceptors have shown improved stabilities, increasing their potential for long-term storage. Therefore, the combination of both DNAzymes and/or (non-)intact substrates with surface immobilization strategies has led to the development of innovative biosensing concepts.

2.2.4.1. DNAzyme-based biorecognition and signal generation

Similar to the solution-based sensors, initial concepts used the RCDs as bioreceptors and subsequent signal generators, based on their catalytic activity. A first main approach has been characterized by **confining the RCD activity to the solid surface enabling direct surface cleavage**. In case of fluorescence, both RCDs and their fluorophore-labelled substrates as introduced in previous section have been immobilized on nanoparticles[38] and flat surfaces[39] to replace or support the function of the quenchers. A 10-fold improvement in sensitivity compared to the solution-based system and nearly 100% quenching were reported, both for the detection of Pb^{2+}[38,39]. Other metal ions such as uranyl were also detected this way, based on nanoparticle immobilized DNAzymes (Figure 2.7A)[40]. Further, the diversity of DNA modifications facilitated the development of alternative solid-phase

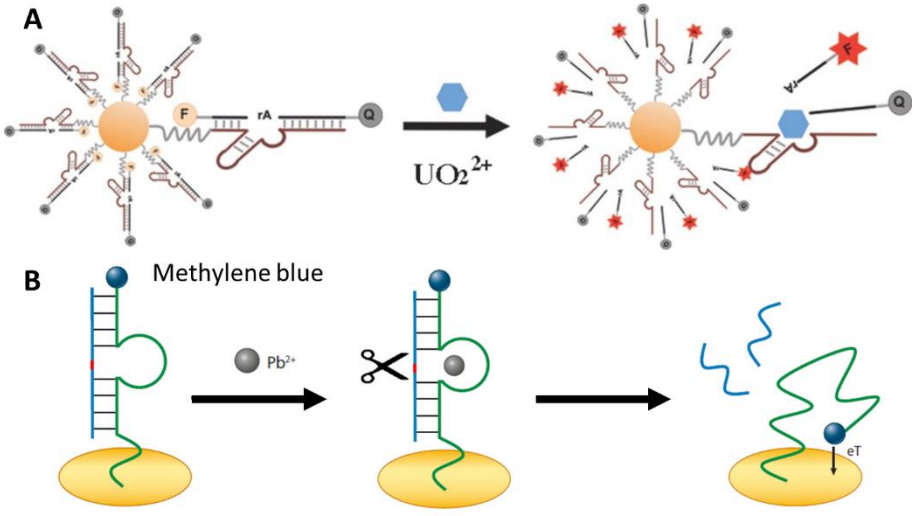

Figure 2.7: *Direct surface cleavage activity.* ***A)*** *Nanoparticle-based fluorescent readout and* ***B)*** *DNAzyme-based electrochemical readout. Adapted with permission from Wu et al. © (2013) American Chemical Society; Adapted with permission of Annual Reviews, Inc., from Zhang et al. © (2011), permission conveyed through Copyright Clearance Center, Inc.*

readout systems. The RCD activity was kept on the surface by exchanging fluorophores with electrochemical[41–44], electrochemiluminescence (ECL)[45], or quartz crystal microbalance (QCM) labels[46]. Figure 2.7B illustrates how the RCD activity has enabled the electron transfer from a redox active label to the electrode. However, the main applications of direct surface cleavage have been restricted to the detection of metal ions down to lower nM concentrations[21]. Moreover, for some types of RCDs the orientation (5' or 3') when being immobilized can affect the catalytic activity[47].

In a second main approach, the **RCD activity takes place in solution, but is indirectly coupled to solid-phase readout systems**, exploiting the (non-) intact substrates. Liu *et al.* proposed a colorimetric sensor based on gold nanoparticle (AuNP) aggregation for the detection of Pb^{2+} (Figure 2.8A)[48]. RCD substrates were designed to hybridize to the functionalized AuNPs and initiate aggregation, which results in an absorption peak at higher wavelengths (blue color). In the presence of Pb^{2+}, cleavage took place and prevented the subsequent hybridization, causing the absorption peak to occur at lower wavelengths (red color). Using different RCDs, other metal ions like UO^{2+} were detected down to a LOD of 50 nM[49]. Further, due to the solution-based RCD activity, the use of aptazymes and MNAzymes was readily translated to this indirect solid-phase approach. Small molecules and NAs, like ATP and infection pathogens were detected down to LODs of 100

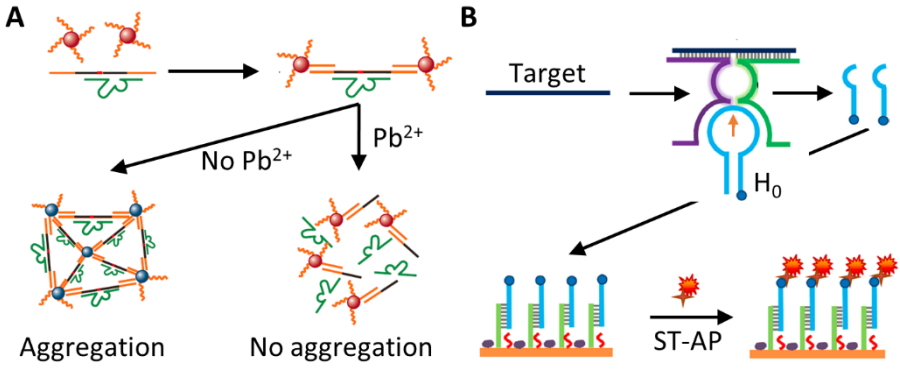

Figure 2.8: *Indirect coupled surface readout.* ***A)*** *AuNP-based colorimetry and* ***B)*** *electrochemically labelled cleavage products. Upon target binding, the MNAzyme cleaved the substrate, generating biotin detection probes which bind the surface to be labelled with ST-AP. Adapted with permission of Annual Reviews, Inc., from Zhang et al. © (2011), permission conveyed through Copyright Clearance Center, Inc.; Adapted by permission from Springer Nature: Diao et al. © (2016).*

µM and 50 pM, respectively[48,50]. Colorimetry simplifies the required readout equipment and is extremely user-friendly, which makes it interesting for on-site detection. However, their practical application suffers from background interference and LODs remain at lower nM concentrations, unless intensive optimizations were performed[51,52].

Next to colorimetry, also electrochemical sensors[53–55] became of interest, because they have good sensitivity, are suitable for miniaturization and are more cost-effective compared to the fluorescence equipment[37]. Usually, cleavage products have been bound to the electrodes by pre-immobilized capture probes and tagged by an additional label or a labelled detection probe. Xia *et al.* used quantum dot coated AuNPs as ECL label[54], while Diao *et al.* used streptavidin-alkaline phosphatases (ST-AP) to convert α-naphthyl phosphate (α-NP) substrates into their electrochemical active counterparts (Figure 2.8B)[55]. Sensitive detection was achieved with LODs of 0.28 fM thrombin and 79 pM target DNA, respectively. Particular combination of the labels and transducer elements improved the sensitivity compared to colorimetry[37]. However, overall the indirect signal generation as described above often required additional washing and labeling steps, increasing the assay times up to several hours.

2.2.4.2. DNAzyme-coupled and –triggered signal amplification

Extending the applications of the direct surface cleavage approach to targets different than metal ions also required concepts such as MNAzymes. Moreover, reaching more sensitive LODs for both the direct and indirect approaches was enabled by more complex assays and additional amplification steps. Here, **protein enzymes** have been used for the NA amplification of cleavage products rather than creating DNAzymes[56,57]. Chen *et al* described a surface plasmon resonance imaging (SPRi) platform, a variant of the classical SPR platforms. Both are mass-based techniques, however in case of SPRi the Au surface is patterned with a DNA array of which each individual spot can be monitored. In presence of the thrombin target, the direct surface cleavage activity was blocked, as the substrate was part of the aptamer binding the target (Figure 2.9). Therefore, the aptamer overhang remained bound to the surface and could be amplified by a RNA polymerase. These amplified reporter sequences were bound to a second sensor surface and labelled with AuNPs in a typical sandwich assay format.

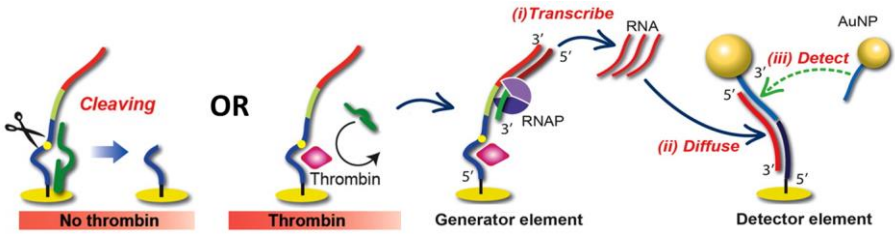

Figure 2.9: *RNAse transcription as additional amplification. Adapted with permission from Chen & Corn © (2013) American Chemical Society.*

Although a LOD of 100 fM was obtained, the assay took more than a day, and multiple sensor elements and amplification steps were required. For the indirect surface coupled cleavage approach, a variant on the MNAzyme-based assay in Figure 2.8B was reported[57]. Instead of ST-AP, the streptavidin molecules bound detection probes, which were used as primer-input for RCA amplification. Additionally, the RCA extended strands were labelled with multiple ST-AP per strand.

Like for the solution-based systems, **enzyme-free assays** have been appealing for RCD-based solid-phase sensors, with the additional argument that NAs tend to stick less to the sensor surface. Qian *et al.* reported RCD-triggered solid-phase HCR, based on surface-immobilized hairpin substrates[58]. In presence of the target, the first hairpin turned into an activated RCDs and could cleave the surface hairpins, revealing capture probes which triggered the DNA nanowire formation on the surface. Electrochemical labelling of the nanowire enabled NA detection down to 4.3 aM. Alternatively, Figure 2.10 illustrates a MNAzyme-initiated CHA, in which the cleavage product formed the CHA trigger to be recycled[59]. Combination with the two hairpins resulted in biotinylated dsDNA structures, which were able to hybridize to the surface capture probes. Binding of streptavidin further increased the mass of the dsDNA and was detected with SPR down to 1 pM.

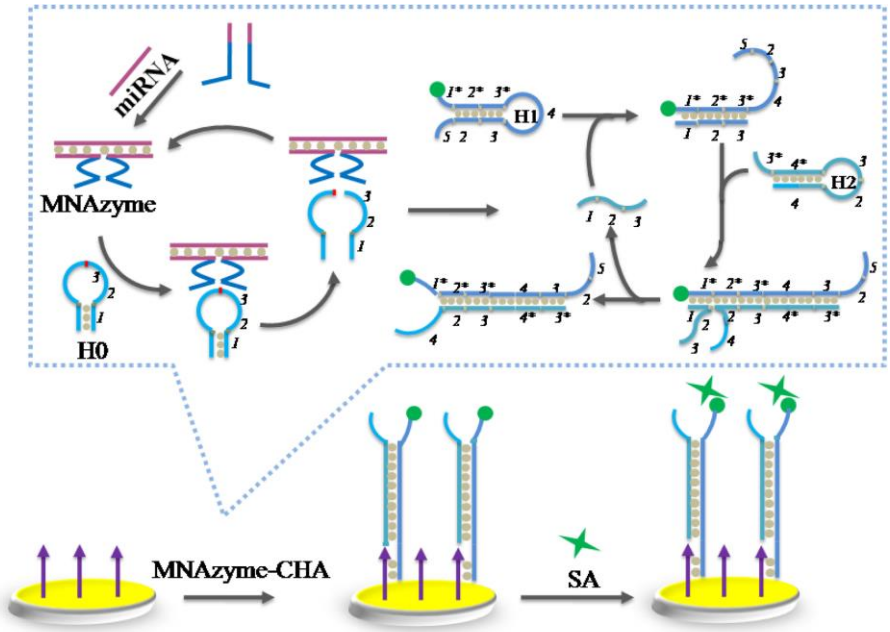

Figure 2.10: *MNAzyme-based solid-phase CHA. Adapted from Li et al. © (2016), with permission from Elsevier.*

2.2.5. Other applications

Next to biosensing, the flexibility and characteristics of RCDs have been explored for several different applications. RCDs were initially developed as **therapeutic agents** by modulating downstream signaling pathways or by targeting regulatory regions in the genome[60]. Interesting research has been reported on potential cancer[61] and HIV[62] treatments. Furthermore, RCDs have been implemented as **nanodevices**, varying from logic gates to RCD switches and nanowalkers[8,63]. A DNAzyme motor, consisting of AuNPs loaded with DNAzyme substrates and a swing arm containing a temporary blocked RCD, realized *in vivo* imaging. Finally, RCDs have shown their potential in **target drug delivery**[64]. Using RCDs as stimulus-responsive gates that block the pores of nanocarriers enabled specific and controlled release of the embedded cargo, such as anti-cancer drug molecules.

2.3. Surface plasmon resonance

In Chapter 1, the biosensor concept showed the importance of bioreceptors and highlighted that the interaction between the bioreceptors and target molecules is a key aspect for a successful biosensor. In this framework, surface plasmon resonance (SPR) evolved from demonstrating its capacity of studying processes at metal surfaces and gas sensing to becoming a golden standard for characterizing biomolecular interactions[65]. Further development of the technology facilitated other applications like the detection of chemical and biological molecules, making it appealing for food quality control[66,67], clinical diagnostics[68,69] and environmental monitoring[70,71]. Following sections provide a detailed insight into the physics underlying the SPR phenomena and the different configurations to obtain the SPR effect. Further discussion will highlight the main surface functionalization strategies to create relevant SPR biosensors and the state-of-the-art concerning miniaturized SPR biosensors.

2.3.1. Principle of surface plasmon resonance

2.3.1.1. Surface plasmons

The existence of the SPR phenomenon is based on the charge characteristics of conductors[72,73]. Conductors such as metals have been described as a rigid positive ion lattice in which a high density of electrons, also called plasma[74], is balanced, while maintaining an overall neutral charge of the metal. Locally, this balance can be disturbed by an external electrical field, which causes the electrons to start moving and getting attracted to the ions due to a much lower mass of the electrons. The electrons accumulate into the more positive regions, reaching higher densities than required to balance the positive charge. At this instance, a repulsion amongst the electrons builds up and is translated into a force in the opposite direction. This force moves the electrons in the other direction, reducing the repulsion until the attraction takes over again. This interaction between attraction and repulsion creates oscillations of the electrons, known as plasma oscillations. A plasmon is defined as a quantum of this oscillation[72]. In case of surface plasmons (SPs), the charge density oscillations are confined to the interface between the metal and a dielectric, and can be excited by the electric field of a light wave[73,75].

2.3.1.2. Principle of surface plasmon resonance

In 1902, Wood initially observed SPs at a metallic grating, when exposing it to polarized light[76]. However, only in 1957 a first theory was formulated by Ritchie *et al.*, showing that SPs can exist near a metal surface[77]. Figure 2.11A gives a schematic overview of the metal-dielectric interface with the incident light, travelling through a dielectric, and the transmitted light, penetrating

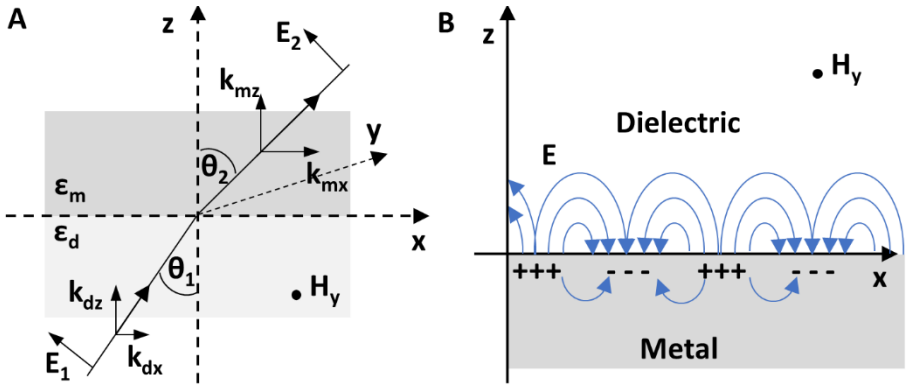

Figure 2.11: *Schematic overview of metal dielectric interface and surface plasmons.* ***A)*** *Illustration of the incident and refracted light with corresponding wavevectors and angles in the dielectric (k_d, θ_1) and the metal (k_m, θ_2), while H_y represents the magnetic field.* ***B)*** *Illustration of the surface plasmons and their electric field at the interface, together resulting in a surface plasmon wave (SPW). Adapted with permission from Zhang et al. © (2012) IOP Publishing. Reproduced with permission. All rights reserved*

the metal. The photons of the incident light have a momentum hk_d, with k_d the corresponding wavevector and h the reduced Planck constant. The wavevector k_d is defined by the equation (eqn):

$$k_d = \sqrt{k_{dx}^2 + k_{dy}^2 + k_{dz}^2} = \frac{2\pi n_d}{\lambda_0} = \frac{n_d \omega}{c} \qquad (2.1)$$

where n_d is the refractive index (RI) of the dielectric, ω the angular frequency of the incident light, and λ_0 and c are the wavelength and the speed of light in vacuum. Assuming the light is only propagating in the x-z plane (e.g. the plane of incidence), the electric field $\vec{E}$ of the light can be described mathematically based on the wavevector as following[73]:

$$\vec{E} = E_0 \exp\left[i\left(\vec{k_d}\vec{r} - \omega t\right)\right] = E_0 \exp[i(k_{dx}x \pm k_{dz}z - \omega t)] \qquad (2.2)$$

where E_0 is the amplitude of the electric field, k_{dx} and k_{dz} the wavevectors in the associated directions, while $k_{dy} = 0$. To indicate the direction of the electric field components a '±' symbol was used: '+' indicates an electric field in the dielectric layer, while '-' indicates an electric field in the metal layer with an opposite direction. For now, the '+' is used for the incident light wave.

When light reaches the surface, part of it will reflect on the surface and part of it will propagate into the metal[72,73]. Snell's law determines the propagation direction of the refracted wave as following:

$$n_d \sin\theta_1 = n_m \sin\theta_2 \tag{2.3}$$

where n_m is the RI of the metal. Equivalently to the dielectric, the momentum in the metal equals hk_m with $k_m = \frac{2\pi n_m}{\lambda_0}$. Therefore, the electric wave propagating into the metal can be described with eqn (2.2), when filling in the corresponding metal wavevector k_m, k_{mx} and k_{mz}. In case of the metal the vector component along the z-axis is opposite and therefore '-' is used. Moreover, by combining eqns (2.1) and (2.3), following relation holds for the propagation of photons along the x-axis in the dielectric and metal:

$$k_{dx} = k_{mx} = k_x \tag{2.4}$$

which means that the propagation along the x-direction remains constant. Based on eqns (2.1) and (2.4), an expression can be found for the wavevector perpendicular to the interface as following:

$$k_{mz}^2 = n_d^2 \left(\frac{2\pi}{\lambda_0}\right)^2 \left(\frac{n_m^2}{n_d^2} - \sin^2\theta_1\right) \tag{2.5}$$

Commonly, $n_m < n_d$ for visible wavelengths, so that for $\sin\theta_1 > \frac{n_m}{n_d}$ the right part becomes negative and therefore k_{mz} is purely imaginary. Combining this with eqn (2.2), only a wave parallel to the interface, known as evanescent wave (EW), is observed and no more propagation into the metal is possible[73,75]. However, this EW has more momentum along the surface interface than can be supported by the metal[73]. Consequently, the oscillating electric field will result into oscillating surface charges at the metal-dielectric interface (Figure 2.11B), previously described as SPs and collectively known

as SP wave (SPW). Based on eqn (2.1), the Maxwell's equations[73,75] and the infinite boundary conditions, the wavevectors of the SPW can be written as:

$$k_{SP,x} = k_x = \frac{2\pi}{\lambda_0}\sqrt{\frac{\varepsilon_d \varepsilon_m}{\varepsilon_d + \varepsilon_m}} \tag{2.6}$$

$$k_{SP,zd} = \frac{2\pi}{\lambda_0}\sqrt{\frac{\varepsilon_d^2}{\varepsilon_d + \varepsilon_m}}\ and\ k_{SP,zm} = \frac{2\pi}{\lambda_0}\sqrt{\frac{\varepsilon_m^2}{\varepsilon_d + \varepsilon_m}} \tag{2.7}$$

where ε_d and ε_m are the permittivity's of the dielectric and metal respectively. As a metal contains many free electrons, its ε_m is negative while ε_d is positive[75]. Based on eqns (2.1) and (2.6), this means that for a given ω or λ, there exists a momentum mismatch between the SPW and the light in vacuum, as $k_x = \frac{\omega}{\lambda_0}$ is always smaller than $k_{SP,x}$. Therefore, SPs remain unexcited when directly shining light on a metal. As discussed above, an EW is suitable to excite SPs, based on total internal reflection (TIR), which is discussed together with other methods in Section 2.3.2 to increase k_x.

In summary, the equations above elucidate two important requirements for excitation of the SPs or the SPW: (i) the use of p-polarized light (i.e. the electric field is parallel to the plane of incidence) also known as transverse-magnetic (TM) mode, based on eqn (2.2) and (ii) the wavevectors for both the incident light and SPW along the x-axis should match, based on eqns (2.4) and (2.6). When both requirements are met and SPs are being excited, this condition is referred to as SPR. Rewriting eqn (2.6) illustrates how the resonance conditions depend on a small change in RI, which results in the change of the SP wavevector $k_{SP,x}$:

$$\frac{2\pi}{\lambda_0}\sqrt{\frac{n_d^2 \varepsilon_m}{n_d^2 + \varepsilon_m}} = \frac{2\pi}{\lambda_0}\sqrt{\varepsilon_d}\sin\theta_1 = \frac{\omega}{c}\sqrt{\varepsilon_d}\sin\theta_1 \tag{2.8}$$

Therefore, to keep eqn (2.4) fulfilled, the incident wavelength or angle have to be changed accordingly to preserve the resonance conditions (e.g. wavelength or angle interrogation). The angle or wavelength at which SP excitation occurs are called the resonant angle or wavelength.

Since energy is transferred from the incident light to the SPs, an intensity drop or dip can be observed in the corresponding angular and wavelength spectrum[72]. By monitoring the resonant angle or wavelength, **SPR biosensors** enable the monitoring of local RI changes, caused by the binding of target molecules (n_d in eqn (2.8) then becomes the RI of the sample n_s, Figure 2.12A and B). As the monitoring of the RI change is based on the electric field of the SPW, the penetration depth of the field into the sample will be particularly important. The SPW has associated electric fields, penetrating both into the dielectric and into the metal (Figure 2.12C). For both media the electric field decays exponentially away from the interface and has its maximum close to the interface. The penetration depth of the field in the dielectric is defined as $\delta_d = \frac{1}{k_{zd}}$, which combined with eqn (2.7) gives:

$$\delta_d = \frac{1}{k_{SP,zd}} = \frac{\lambda_0}{2\pi}\sqrt{\frac{\varepsilon_d + \varepsilon_m}{\varepsilon_d^2}} \qquad (2.9)$$

In case of an incident wavelength of 600 nm, the penetration depth in water is approximately 149 nm, with ε_{Au} -9.39 and ε_{water} 1.77[78].

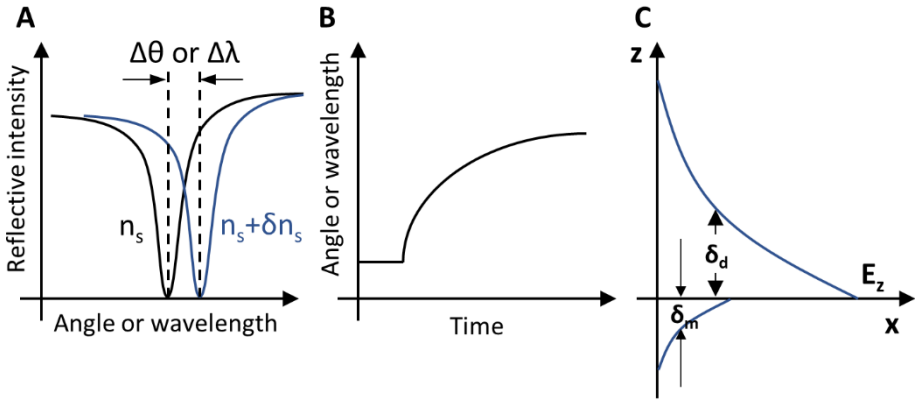

Figure 2.12: *Real-time monitoring and penetration depths.* ***A)*** *As part of the incident light energy is translated into SP oscillations, this will be reflected as a dip in the intensity spectrum. The angle or wavelength at which the dip is minimal is the resonance angle or wavelength. When the RI changes at the metal-dielectric interface, the resonance angle or wavelength will change and* ***B)*** *can be observed as a shift in time;* ***C)*** *Illustration of the exponential decaying electric field associated with the SPW. Adapted with permission from Zhang et al. © (2012) IOP Publishing. Reproduced with permission. All rights reserved.*

2.3.2. Surface plasmon excitation methods

After being observed and theoretically described, further advancements towards potential applications were made by the development of optical systems for the excitation of the SPs[65,73]. Over the years, two main techniques have been used: (i) incident light diffraction on a metal grating, interfacing the dielectric and (ii) EW excitation, using TIR. Both techniques have been realized in different formats, of which the main ones and their theory behind it are described in this section.

2.3.2.1. Grating-enhanced surface plasmon resonance

A first method to excite SPs efficiently was realized by interaction of the incident light with a metallic grating, resulting into several diffracted waves as observed by Wood[65,76]. Figure 2.13 presents a schematic illustration of the diffraction phenomenon[79] with m an integer representing the diffraction order and Λ the groove period of the grating. By diffraction, a series of diffracted waves is generated, so that the incident momentum is changed into an increased diffracted momentum with following relation:

$$k_{diff} = k_d + m \times \frac{2\pi}{\Lambda} \qquad (m = \pm 1, \pm 2, \dots) \qquad (2.10)$$

Substitution with $k_{diff,x}$ and rewriting with eqns (2.1 and 2.3), the diffracted waves can couple with the SPs when matching the SPW vector eqn (2.6):

$$\sin\theta + m\frac{\lambda}{\Lambda} = \sqrt{\frac{n_s^2 \varepsilon_m}{n_s^2 + \varepsilon_m}} \qquad (2.11)$$

with n_s the RI of the sample. In case of a constant grating period, eqn (2.11) shows that both angle or wavelength interrogation can be used to excite the SPs and result in resonance conditions. This configuration was used as biosensor for the first time in 1987[80], illustrating the real-time monitoring of specific molecular binding events at the metal-dielectric interface. Other applications have been reported[81], but the lower sensitivities of this configuration compared to the prism-enhanced systems (next paragraph) made its use rather limited[82]. On the other hand, different methods for

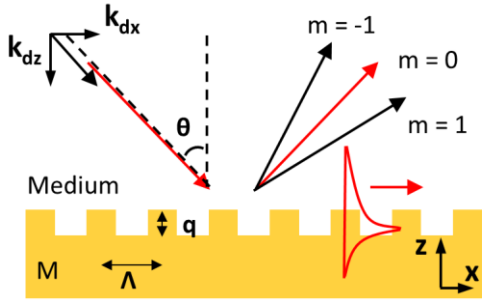

Figure 2.13: *Grating enhanced surface plasmons. An incident light wave gets diffracted and generates a series of diffraction waves, which enables SP excitations. With a constant grating period Λ and grating depth q, resonance conditions can be finetuned by angle or wavelength interrogation. Adadpted from Prabowo (2018).*

increasing the sensitivity are being studied[83–85], as the grating-enhanced systems have much greater miniaturization and integration potential compared to their prism-based equivalents[86–88].

2.3.2.2. Prism-enhanced surface plasmon resonance

A second method to excite SPs is realized by passing the incident light through a high RI prism, which among the different SPR configurations is the most common one[65]. If the incident light exceeds a certain critical angle, TIR will occur and generate an EW at the metal-prism interface, which can be used for SP excitations. For excitation to take place, the EW vector along the metal-prism interface should match the SPW vector, as described in eqn (2.6):

$$\frac{\omega}{c}\sin\theta\sqrt{\varepsilon_{pr}} = \frac{\omega}{c}\sqrt{\frac{n_s^2\varepsilon_m}{n_s^2+\varepsilon_m}} \qquad (2.12)$$

with θ the incident angle at the metal-prism interface and ε_{pr} the permittivity of the prism ($\varepsilon_{pr} > \varepsilon_s$). Both angular and wavelength interrogation have been used with prism-enhanced systems and two variants of this configuration were described in the same year (Figure 2.14)[89–91]. The Otto configuration generates the EW at the prism-air interface, in proximity of the metal surface supporting the SPW. By loading a sample in the gap between prism and metal surface, local RI changes caused by the sample can be picked up. However, based on eqn (2.9) this gap has to be chosen carefully

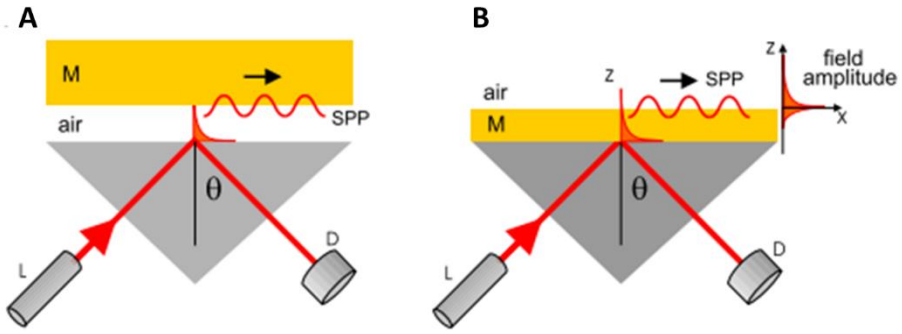

Figure 2.14: *Prism-enhanced surface plasmons.* ***A)*** *In the Otto configuration, an EW at the prism-dielectric interface can excite SPs at the metal-dielectric interface across the air gap and* ***B)*** *In case of the Kretschmann configuration the air gap was removed and SPs were excited at the outer metal-dielectric interface. Adapted with permission from Novotny et al. © (2012) Cambridge university press. Reproduced with permission of The Licensor through PLSclear.*

in order to avoid unsuccessful SPW excitation (gap too big) or radiation damping of the SPW (gap too small). Due to the small gap size, both the prism-metal surface alignment and loading of the sample are challenging, which limited the use of the Otto configuration in biosensing.

On the other hand, the gap in the Otto configuration is not present in the Kretschmann configuration, whereas the metal is deposited as a thin layer on top of the prism. When the metal layer is thin enough (< 100 nm for the visible part of the spectrum), the EW at the prism-metal interface can tunnel through the metal layer and cause SPW excitation at the outer metal-dielectric interface[65]. In order to obtain SPW excitation, the thickness of the metal layer has to be controlled and optimally varies from 44 – 50 nm Au for wavelengths between 600 - 1000 nm[65]. Other metals such as silver and aluminum have been used, however, in terms of biosensing are less suitable due to fast oxidation[92–94]. The Kretschmann configuration paved the way for the development of sensitive and label-free SPR-based biosensors with applications in different fields, such as environmental monitoring[70,71], food industry[66,67] and medical diagnosis[68,69]. This was also facilitated by the successful commercialization of the SPR systems, such as the Biacore (since 1990 Pharmacia Biosensor AB, today Biacore Life Sciences, GE Healthcare). The prism in the Biacore is fixed and interchangeable chips, hosting the metal layer, enable custom surface functionalization (Section 2.3.3) and target selection. Moreover, the combination with microfluidics automated several processing steps and up to 16 parallel reactions can be monitored. Although

their superior sensitivity and label-free characteristic, these prism-based systems are rather bulky and therefore mainly restricted to lab environments. Moreover, the costs of the chips increases rapidly and potential regeneration requires optimization, depending on the used reagents[95].

2.3.2.3. Fiber-optic surface plasmon resonance

A third and final method to excite SPs is based on the use of optical fibers[96,97]. Optical fibers are characterized by the ability to guide light through their glass core, exploiting the mechanism of TIR (Figure 2.15). Like the prism-based systems, fiber optic (FO)-based systems rely on TIR to generate an EW. Partial removal of the outer jacket and the low RI polymer surrounding the core (cladding) enables coating of the core with a thin metal film, where the excitation of the SPW can take place. Figure 2.15A illustrates an initial design[98,99], where the incident light along its way through the fiber interacted with a metal-coated region and was analyzed at the end (e.g. forward

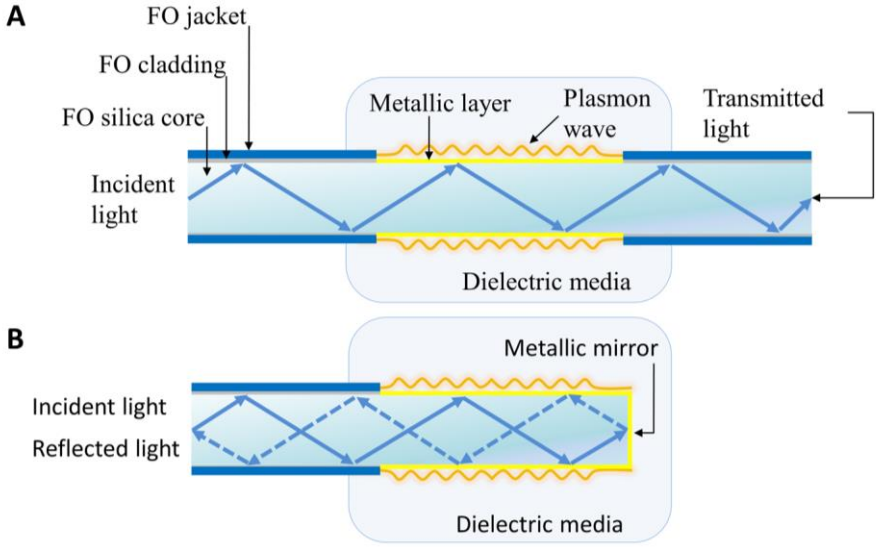

Figure 2.15: *Surface plasmon enhancement with optical fibers.* ***A)*** *In forward scattering mode, the jacket and cladding are partly removed in a central region of the optical fiber and coated with Au. Light is send into the fiber at one end and analyzed by a spectrometer at the other end, and* ***B)*** *In backward scattering mode, the jacket and cladding of the optical fiber at one end is completely removed and coated with Au. Light is sended into the fiber to interacts with the Au layer, reflects back at the end of the fiber acting as a mirror and finally gets analyzed with a spectrometer. Adapted from Arghir et al. © (2015), with permission from Elsevier.*

scattering or transmission mode). In contrast to the prism-based systems, FO-SPR mainly uses wavelength interrogation since polychromatic light is sent into the fiber under variable angles. A second design is known as the backward scattering or reflection mode (Figure 2.15B), where one end of the fiber is completely stripped and coated by a metal film[98,100,101]. The metallic mirror at the fiber end reflects the incident light back to a spectrometer by using a bifurcated fiber. A similar design was used in this dissertation, which simply dips the FO-sensor tip into a sample while exciting the SPs in the 50 nm thick Au-coating. FO-SPR became of interest due to its simple and flexible design, remote sensing capability, miniaturized sensing system and cost-effectiveness, compared to the bulkier designs described above. On the other hand, theoretical analysis showed that the propagation through optical fibers affects the quality of the intensity dip and reduces the sensitivity about 10 times[98]. Therefore, other FO-based designs have been developed, such as D-shaped fibers, U-shaped fibers, grating-assisted fibers and microstructured fibers. However, these designs introduce additional polishing, etching, heating or challenging metal deposition steps, increasing the complexity of the designs significantly. More in debt description of these systems can be found in specialized reviews[72,96,97].

2.3.3. Surface functionalization

As mentioned in previous section, SPR biosensors enable the monitoring of local RI changes, caused by the binding of target molecules. Accurate detection is possible if only the targets of interest bind, which is determined by a sensor's specificity. Therefore, different strategies have been developed to functionalize the Au-surface of the SPR sensors, previously highlighted as the main metal of use in SPR biosensing. Different bioreceptors such as antibodies, cells and DNA have been immobilized to broaden the fields of application[102]. In framework of this dissertation, the focus was directed to DNA-immobilization strategies.

The most straightforward strategy for DNA-immobilization is **adsorption** (Figure 2.16A), which does not require any chemical activation or modification of the DNA. However, due to the electrostatic-based interactions, DNA-molecules easily detach again during washing steps. The immobilization occurs randomly, which hampers the DNA availability, and

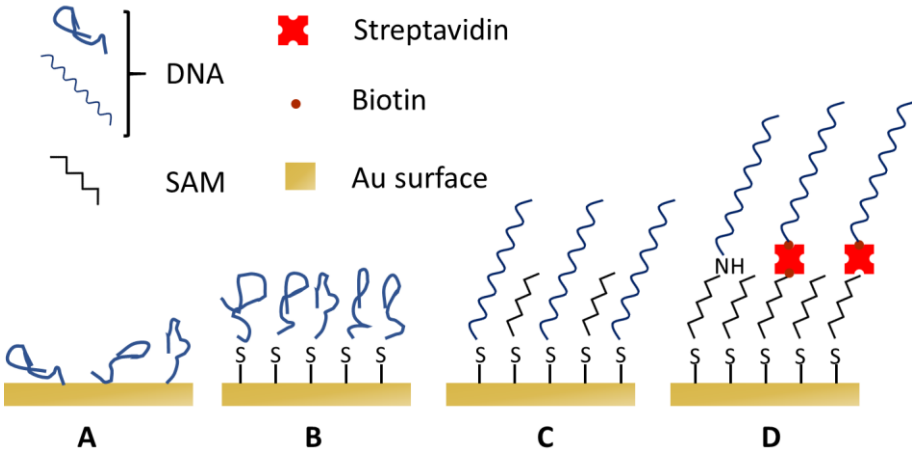

Figure 2.16: *DNA surface immobilization.* ***A)*** *Adsorption;* ***B)*** *Thiol-chemistry;* ***C)*** *Thiol-chemistry with self-assembling monolayer (SAM) backfilling; and* ***D)*** *Carboxylic- or biotin-SAM for peptide, affinity bond or combination of both.*

the DNA surface density affects further binding efficiency[49,103]. Moreover, upon DNA hybridization, the dsDNA prefers to detach from the surface[104].

Alternative approaches were developed based on the variety of available synthetic DNA-modifications at the 3' or 5' end[105]. The most popular immobilization chemistry links the DNA-molecules to the Au-surface by **functional thiol (-SH) groups or chemisorption** (Figure 2.16B). Based on the high affinity between Au and sulfur, thiol-modified DNA arranges into a self-assembling monolayer (SAM) formation, providing good stability, flexibility, and high binding strengths. Potential weakly bound thiol-groups can be replaced by incubation with small and longer alkanethiols, such as 6-mercapto-1-hexanol (MCH) or oligoethyleneglycols, also referred to as backfilling (Figure 2.16C)[106–108]. In addition, these molecules favor the upwards orientation of the DNA, enable tuning of the DNA density and reduce the non-specific adsorption of other sample molecules significantly[108,109]. Other covalent immobilization methods have been introduced, based on **functional SAMs** with maleimide, aldehyde, carboxyl (-COOH) or amine ($-NH_2$) groups (Figure 2.16D)[110–113]. Subsequent binding with modified DNA molecules is realized by activation of the functional groups with for example 1-ethyl-3-(-3-dimethylaminopropyl) carbodiimide hydrochloride (EDC) and N-hydroxysuccinimide (NHS) chemistry to form a peptide link[114]. In case of these functionalized SAMs, tuning of the DNA-

density is based on mixed SAMs, containing different ratios of functional and inactive groups.

Biotinylated DNA allows affinity-based immobilization, using the strong **biotin-streptavidin (avidin) interaction** (K_a 1 × 10^{15} M^{-1})[115]. Since streptavidin is a tetrameric protein, surface immobilization is typically realized with functional SAMs, which are modified with another biotin molecule[115,116]. Further, also carboxylic SAMs have been used to immobilize the streptavidin through maleimide or (EDC-) NHS chemistry[101,117]. In general, the affinity-based immobilization results in lower DNA-surface densities compared to the thiol-based strategy, promoting the accessibility[118]. However, in terms of stability the affinity-based bond gets more affected by subsequent washing, regeneration or increased temperature steps due to disintegration of the proteins[119]. Moreover, use of a protein linkage increases the risk of nonspecific adsorption of other molecules.

Next to these different SAMs, functional groups can also be introduced by **three-dimensional matrices and hydrogels**[119–122]. The 3D aspect increases the available active sites to immobilize the DNA-molecules of interest. However, the more dense packing of the DNA and presence of the matrix can interfere with efficient and selective hybridization, and can slow down diffusion of target molecules[123]. In addition, **different strategies** are being developed to further improve the control over the surface immobilization. Conducting polymers like polpyrrole are of interest because of their uniformity, controlled thickness and antifouling properties[124–126]. Also molecular imprinted polymers (MIPs) are being studied for their higher stability, generality and potential improved cost effectiveness[127]. However, their main challenge remains a lower binding performance, which might be improved by the combination with functional NAs[128]. On the other hand, 'click' chemistry is being considered as alternative for SAM-functionalization due to its high yields and selectivity[129–131].

2.3.4. DNA-based signal amplification strategies

Previous section presented different immobilization strategies for the functionalization of SPR sensors with specific bioreceptors, focusing on NAs. This section illustrates how these DNA-functionalized SPR sensors have been exploited for target detection, going from simple hybridization assays to

more complex amplification systems to reach ultrasensitive detection and quantification of NAs[132,133].

Initial assays have been using **simple DNA hybridization** to the surface-immobilized DNA molecules or capture probes, illustrating the label-free characteristic of SPR. Depending on the target and its size, the hybridization conditions and the SPR configuration of choice, LODs in the lower nanomolar and high subnanomolar range have been obtained[101,132]. However, ultrasensitive detection (lower pM – fM range) was not possible without alternative assay concepts, introducing additional signal amplification steps.

The use of **AuNPs** is the most common amplification strategy for SPR sensors[134] and was introduced in 1998 for immunosensing[135]. With similar immobilization strategies as described above, AuNPs have been functionalized with DNA detection probes to result into 'sandwich' assay formats. This assay format was reported to increase the SPR sensitivity up to a 100-fold[136]. Due to their relatively large mass compared to biomolecular labels, AuNPs cause a large change in RI. Moreover, it has been hypothesized that mainly their high coverage with detection probes and coupling of their local SPR field with the SPR field of the sensors are responsible for an improved SPR sensitivity[137,138]. In the meantime, the influence of other AuNP characteristics such as size and shape are being studied as well[137,139]. Due to the complex microfluidics integrated with the prism-based systems, potential clogging of the AuNPs remains a risk here. In contrast, the use of AuNPs was especially an improvement for the FO-SPR systems, because it made them competitive towards the superior sensitivity of the prism-based systems[140,141]. However, depending on the target, the AuNP size and platform used, signal amplification with merely AuNPs does not meet ultrasensitivity.

Next to and in combination with AuNPs, **enzymatic amplification strategies** can facilitate SPR-based ultrasensitive NA detection. PCR-based SPR sensors were initially implemented by post-PCR hybridization of the products to the functionalized sensor surface. Label-free hybridization using the prism-based systems enabled ssDNA and dsDNA detection down to 500 pM and 150 nM, respectively[142,143]. On the other hand, by the combination with AuNP labels, real-time FO-SPR quantification of DNA was established down to 10 pM but not further explored. Here, the AuNPs boosted the

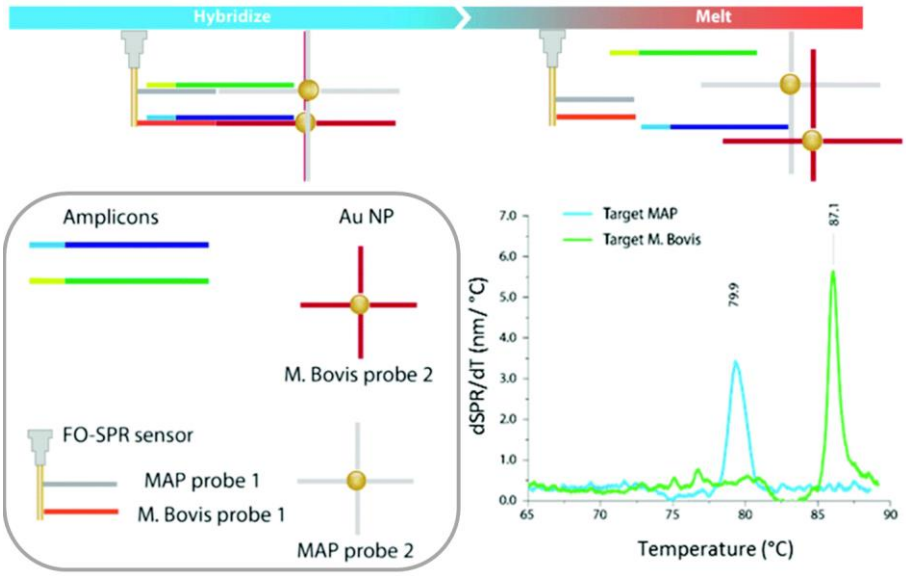

Figure 2.17: *PCR-based FO-SPR with high resolution melting. Specific amplification of both* Mycobacterium Avium Paratuberculosis (MAP) *and* Mycobacterium bovis (M. bovis) *was enabled. After every PCR cycle, the amplicons hybridize to the FO-SPR capture probes and with the AuNP labels. During the PCR denaturation step, both AuNP-labelled targets dehybridize at a specific T_m, which was monitored in real-time and enabled discrimination between the targets. Adapted with permission of Royal Society of Chemistry, from Daems et al. © (2016); permission conveyed through Copyright Clearance Center, Inc.*

response during the PCR annealing and extension steps[144,145]. In addition, integrating a gradual temperature increase or 'melting' phase into the denaturation step extended the applications towards single nucleotide polymorphism (SNP) detection and multiplexing (Figure 2.17)[145–147]. Depending on the location and the specific nucleotide forming the mismatch, SNPs differ in melting temperatures (T_m). This was reflected in the temperature at which the FO-SPR shift suddenly dropped, corresponding to the release of AuNP-labels. Similarly, DNA targets also differ in T_m's, which enabled to distinguish them from each other with improved resolution versus qPCR-based high resolution melting.

Further sensitivity improvements were obtained with **LCR and RCA**. Knez *et al.* exploited solution-based ligation, triggered by the target, to generate multiple hybridization probes (Figure 2.18)[148]. Subsequent hybridization with the FO-SPR sensor surface and AuNP labels resulted in a LOD of 13.75 fM. Since the target itself is not being amplified, response

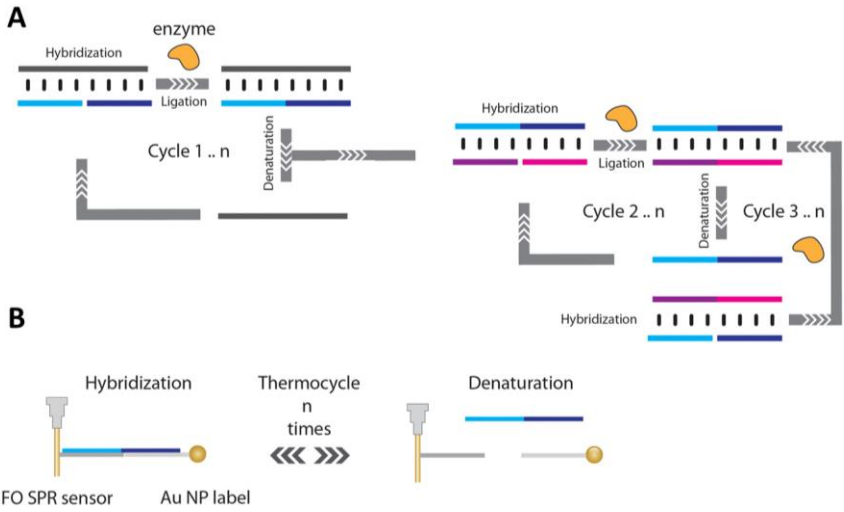

Figure 2.18: *Ligation chain reaction with FO-SPR.* ***A)*** *Forward probes (light and dark blue) were able to hybridize with the target (grey) and triggered the ligation reaction. After denaturation, the forward LCR product triggered ligation of the reverse probes (purple and pink), resulting in an exponential amplification.* ***B)*** *Real-time monitoring of the reaction was established by forward LCR product hybridizing to the FO-SPR sensor and with AuNP labels. Adapted from Knez et al., © (2015), with permission from Elsevier.*

signals were more specific and including a melting phase also here enabled SNP detection. On the other hand, RCA introduced isothermal amplification of the signal with ligation-based specificity. Target recognition by a padlock probe and subsequent circularization could take place in solution, while solid-phase RCA enhanced the final response. Circularized padlock probes hybridized to the prism-based SPR sensors' capture probes and were extended by a polymerase, using the circular DNA as template. Labelling the extended probes with AuNPs resulted into a LOD of 5 pM[149]. Multiplexing was enabled by coating the eight-channel tandem detection well with different capture probes. The same group further increased the LOD 10× by first coating the sensor surface with AuNPs, functionalized with capture probes[150]. Therefore, the sensor surface area increased and improved accessibility for RCA-amplification and AuNP-labelling.

More recently, developments in DNA nanotechnology have led to **enzyme-free assays** as potential alternatives to the restricted cost-effectiveness, stability and higher reaction temperatures of the enzyme-based approaches. Also in case of SPR, HCR (Section 2.2.3) has been a method of interest, based on the mass-sensitive characteristic of SPR. By

target triggering, binding of the hairpins to immobilized capture probes is enabled, accumulating linear DNA nanowires along the SPR sensor surface[151]. Highly sensitive DNA detection down to 0.3 fM was obtained. Furthermore, non-linear branching of the DNA-nanowire can improve and speed up the mass accumulation by creating more connection points. Therefore, non-linear HCR is expected to outperform current LODs and reaction times[152]. Another approach that has proven its worth in terms of solid-phase sensing is CHA (Section 2.2.4). Recycling of the DNA target in combination with the hairpins resulted in small dsDNA duplex structures with two overhangs[153]. Hybridization to the SPR sensor with one end and streptavidin labelling at the other end resulted into accurate detection down to 5 pM. Both HCR and CHA simplify the type of reagents, which reduces potential background while good sensitivities are maintained. However, often these simplified and enzyme-free characteristics go at the cost of the reaction time. Introduction of NAzymes during the last couple of years has been considered as potential improvement and alternative for this need. For other DNA-coupled amplification strategies, such as different nanomaterials, digestion enzymes and redox reactions, the reader is referred to some recent reviews[1,133].

2.3.5. Miniaturized SPR devices

Next to laboratory SPR equipment, the interest in SPR technology has grown further based on its huge potential to be miniaturized, which would broaden its accessibility and applicability. Moreover, miniaturization could reduce the cost of the devices and the time-to-result by on-site measurements and data analysis. A first effort to broaden the SPR applicability appeared at the end of the nineties with the development and commercialization of the Spreeta™, a portable prism-based device[154]. Figure 2.19A illustrates the device, which consisted of a LED light source, plastic prism and mirror to direct the reflected light to the photodiode for analysis. All components were integrated into a plastic casing and mounted on top of a printed circuit board. The device was successfully used for the detection of cancer-related mutations[155] and further extended to a lunchbox-sized high throughput device SPIRIT (Seattle sensing systems), by assembling eight Spreeta™ devices in series[156]. Other devices did follow and were also commercialized, such as SPRmicro (KMAC), Smart SPR SS-1001 (Mebius advance technology) and Biosuplar 6 (Analytical µ-systems/Mivitec)[157]. All optical elements in

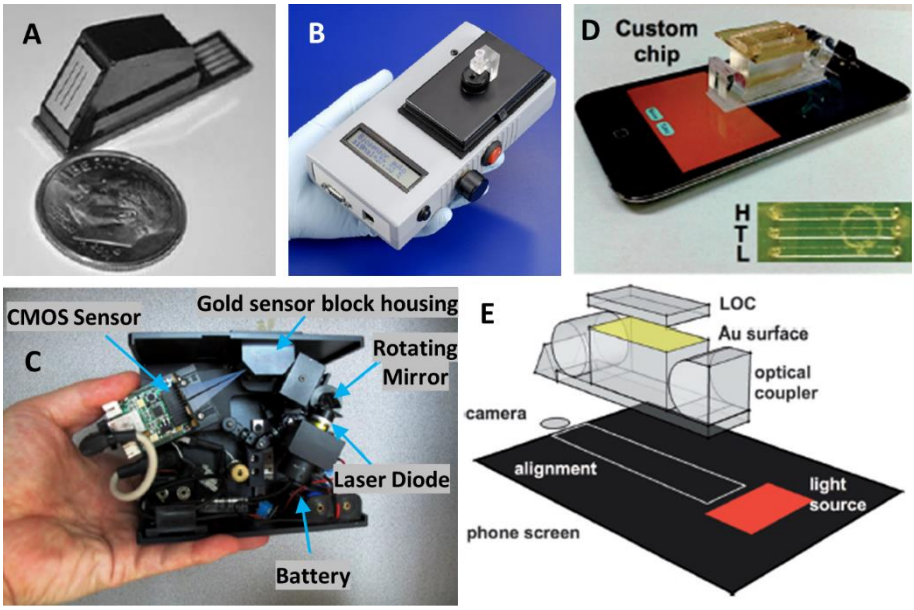

Figure 2.19: *Miniaturized prism-based SPR systems.* ***A)*** *Spreeta™ device compared to a US dime (18 mm);* ***B)*** *First handheld SPR device with a weight of 600g, powered by a 9 V battery and sample injection from the plastic cylinder on top;* ***C)*** *Palm-sized SPR device with angle interrogation, based on rotating mirror);* ***D)*** *Smartphone based SPR device, using screen illumination for SPR excitation and camera as intensity readout; and* ***E)*** *schematic of the smartphone system, where all components are PDMS-based, a 45 nm Au-layer for SPR excitation and a lab-on-chip (LOC) element for sample introduction. Adapted by permission from Springer Nature: Soelberg et al. © (2005); Adapted from Feltis et al. © (2008) and Shin et al. © (2010), with permission from Elsevier. Adapted with permission from Preechaburana et al. © (2012) Wiley-VCH Verlag GmbH & Co. KGaA, Weinheim.*

these devices have been organized in a fixed unit where only the SPR chip is interchangeable. The majority relies on a microfluidic flow cell with corresponding pumps, providing two or more channels for referencing and multiplexing.

Further miniaturization has led to a first series of handheld devices as introduced by Feltis *et al.* (Figure 2.19B)[158]. A fully self-contained device was developed with a similar sensitivity compared to many commercial ELISA tests. Moreover, the device was powered by a 9 V battery, completely avoiding the need of any external connection to be operational. Assay times took maximally 20 min as illustrated by detection of the toxin ricin down to 200 ng/mL. Another palm-sized device is illustrated in Figure 2.19C, integrating a rotating mirror to enable angle interrogation[159]. Angle interrogation is usually more sensitive, however integrating moving parts

makes device design more complex and increase in size. Currently, a second series of handheld devices based on smartphone coupled SPR equipment found its way into the field of sensing. Simple fixation of a miniaturized SPR device to the phone, illumination by the screen and alignment with the camera enabled β_2 microglobulin detection, a marker for cancer, inflammatory disorders and kidney disease. Detection was established in a clinical relevant range down to 0.1 µg/mL (Figure 2.19D and E)[160].

2.4. Conclusions

In this chapter, both the biological components and technology making up the biosensor design in this dissertation were positioned within their field. The origin and catalytic mechanism of RCDs were discussed in detail and it was illustrated how the selection process resulted in the extensive DNAzyme toolbox of today. Furthermore, the RCD characteristics and advantages were described and illustrated in both solution- and solid-based assay formats. The solid-phase technique of SPR was reviewed in more debt and its physical principles were explained. An in-house developed FO-SPR platform was highlighted and how proper surface functionalization led to NA-based applications. Finally, some miniaturized devices were presented, which combined with innovative assay design hold great potential for the future.

In general, DNAzymes are regarded as an interesting alternative and extension of the existing pool of catalytic molecules. They are characterized by several advantages, such as ease of production and modification, robust activity and thermal stability. RCDs make up one of the main groups of DNAzymes due to the high design flexibility of their substrate binding arms. Based on this flexibility, RCDs can be easily modified towards different applications without affecting the catalytic activity. Two RCDs in particular, the 8-17 and 10-23 DNAzymes, distinguished themselves from other DNAzymes based on their higher catalytic activity. On the other hand, G-quadruplex DNAzymes have shown to process similar substrates as the well-known HRP, generating color signals which are of interest for on-site applications. Other DNAzymes have been identified, but so far have not been studied as extensively and are mainly limited to more fundamental studies. Based on their catalytic activity, DNAzymes can intrinsically be used for signal generation and signal amplification in biosensing, similar to their protein counterparts. Several solution- and solid-based readout formats using RCDs

were reported, such as fluorescence, colorimetry, electrochemistry and chemiluminescence. Solution-based assays suffered from higher background, which was improved by some of the solid-phase approaches, but often at the cost of sensitivity. Therefore, RCDs have been combined with NA amplification techniques such as PCR, RCA, HCR and CHA. This way, ultrasensitive assays have been developed, but assay complexity and longer assay times remain a challenge.

Among the RCD readout formats, SPR-based assays so far have been rather limited, but will be the key technology throughout this dissertation. Prism-enhanced SPR formats have been the standard due to their superior sensitivity, but are still rather bulky and not cost-effective. On the other hand, grating-enhanced and FO-SPR are less complex, more cost-effective and user-friendly alternatives. Gratings benefit from a simplified production process, but have restricted sensitivity mainly due to the incident light that first needs to cross the sample before interacting with the grating. In turn, FO-SPR is well suited for remote sensing and its biosensing applications have been increasing over the years, mainly using the transmission and reflection mode. Alternatively, other FO-SPR designs with adapted structures and characteristics of the optical fibers have been implemented, but increase the complexity of the FO fabrication process. Next to the technological aspects, surface functionalization is a key component for an operational SPR sensor. More specific, surface immobilized NA capture probes have formed the basis for protein and NA detection. Orientation and density of the capture probes directly affects specificity and sensitivity. The most practical and extensive strategy remains thiolated NA captures probes with SAMs to reduce nonspecific adsorption. To cope with restricted SPR sensitivities, AuNP labels and DNA-based amplification strategies have been successful, but strategies involving DNAzymes are rather limited. Finally, the overview of miniaturized SPR devices indicates the future potential accessibility of the technology. Among these, FO-SPR requires a minimum of optical components, no separate chips and can be produced in an affordable way.

2.5. References

1. Wang, W. *et al.* Bioapplications of DNA nanotechnology at the solid–liquid interface. *Chem. Soc. Rev.* **48**, 4892–4920 (2019).
2. Ellington, A. D. & Szostak, J. W. In vitro selection of RNA molecules that bind specific ligands. *Nature* **346**, 818–822 (1990).
3. Tuerk, C. & Gold, L. Systematic evolution of ligands by exponential enrichment: RNA ligands to bacteriophage T4 DNA polymerase. *Science (80-.).* **249**, 505–510 (1990).
4. Santoro, S. W. & Joyce, G. F. A general purpose RNA-cleaving DNA enzyme. *Proc. Natl. Acad. Sci.* **94**, 4262–4266 (1997).
5. Song, K.-M., Lee, S. & Ban, C. Aptamers and Their Biological Applications. *Sensors* **12**, 612–631 (2012).
6. Citartan, M., Gopinath, S. C. B., Tominaga, J., Tan, S. C. & Tang, T. H. Assays for aptamer-based platforms. *Biosens. Bioelectron.* **34**, 1–11 (2012).
7. Silverman, S. K. Catalytic DNA: Scope, Applications, and Biochemistry of Deoxyribozymes. *Trends Biochem. Sci.* **41**, 595–609 (2016).
8. Gong, L. *et al.* DNAzyme-based biosensors and nanodevices. *Chem. Commun.* **51**, 979–995 (2015).
9. Peng, H. *et al.* DNAzyme-Mediated Assays for Amplified Detection of Nucleic Acids and Proteins. *Anal. Chem.* **90**, 190–207 (2018).
10. Breaker, R. R. & Joyce, G. F. A DNA enzyme that cleaves RNA. *Chem. Biol.* **1**, 223–229 (1994).
11. Hasick, N. J., Ramadas, R. & Todd, A. V. Subzymes: Regulating DNAzymes for point of care nucleic acid sensing. *Sensors Actuators B Chem.* **297**, 126704 (2019).
12. Schlosser, K. & Li, Y. A Versatile Endoribonuclease Mimic Made of DNA: Characteristics and Applications of the 8-17 RNA-Cleaving DNAzyme. *ChemBioChem* **11**, 866–879 (2010).
13. Silverman, S. K. Catalytic DNA (deoxyribozymes) for synthetic applications—current abilities and future prospects. *Chem. Commun.* 3467 (2008). doi:10.1039/b807292m
14. Hollenstein, M. DNA catalysis: The chemical repertoire of DNAzymes. *Molecules* **20**, 20777–20804 (2015).
15. Santoro, S. W. & Joyce, G. F. Mechanism and Utility of an RNA-Cleaving DNA Enzyme †. *Biochemistry* **37**, 13330–13342 (1998).
16. Baum, D. A. & Silverman, S. K. Deoxyribozymes: useful DNA catalysts in vitro and in vivo. *Cell. Mol. Life Sci.* **65**, 2156–2174 (2008).
17. Schlosser, K. & Li, Y. Biologically Inspired Synthetic Enzymes Made from DNA. *Chem. Biol.* **16**, 311–322 (2009).
18. Travascio, P., Li, Y. & Sen, D. DNA-enhanced peroxidase activity of a DNA aptamer-hemin complex. *Chem. Biol.* **5**, 505–517 (1998).
19. Ida, J. *et al.* G-Quadruplexes as An Alternative Recognition Element in Disease-Related Target Sensing. *Molecules* **24**, 1079 (2019).
20. Li, J. & Lu, Y. A Highly Sensitive and Selective Catalytic DNA Biosensor for Lead Ions. *J. Am. Chem. Soc.* **122**, 10466–10467 (2000).
21. Zhang, X.-B., Kong, R.-M. & Lu, Y. Metal Ion Sensors Based on DNAzymes and Related DNA Molecules. *Annu. Rev. Anal. Chem.* **4**, 105–128 (2011).
22. Lake, R. J., Yang, Z., Zhang, J. & Lu, Y. DNAzymes as Activity-Based Sensors for Metal Ions: Recent Applications, Demonstrated Advantages, Current Challenges, and Future Directions. *Acc. Chem. Res.* **52**, 3275–3286 (2019).
23. Stojanovic, M. N., de Prada, P. & Landry, D. W. Catalytic Molecular Beacons. *ChemBioChem* **2**, 411–415 (2001).

24. Tian, Y. & Mao, C. DNAzyme amplification of molecular beacon signal. *Talanta* **67**, 532–537 (2005).
25. Navani, N. K. & Li, Y. Nucleic acid aptamers and enzymes as sensors. *Curr. Opin. Chem. Biol.* **10**, 272–281 (2006).
26. Kolpashchikov, D. M. A Binary Deoxyribozyme for Nucleic Acid Analysis. *ChemBioChem* **8**, 2039–2042 (2007).
27. Mokany, E., Bone, S. M., Young, P. E., Doan, T. B. & Todd, A. V. MNAzymes, a Versatile New Class of Nucleic Acid Enzymes That Can Function as Biosensors and Molecular Switches. *J. Am. Chem. Soc.* **132**, 1051–1059 (2010).
28. Wang, F., Elbaz, J., Teller, C. & Willner, I. Amplified Detection of DNA through an Autocatalytic and Catabolic DNAzyme-Mediated Process. *Angew. Chemie Int. Ed.* **50**, 295–299 (2011).
29. Wang, F., Lu, C.-H. & Willner, I. From Cascaded Catalytic Nucleic Acids to Enzyme–DNA Nanostructures: Controlling Reactivity, Sensing, Logic Operations, and Assembly of Complex Structures. *Chem. Rev.* **114**, 2881–2941 (2014).
30. Todd, A. V, Fuery, C. J., Impey, H. L., Applegate, T. L. & Haughton, M. A. DzyNA-PCR: use of DNAzymes to detect and quantify nucleic acid sequences in a real-time fluorescent format. *Clin. Chem.* **46**, 625–30 (2000).
31. Tian, Y., He, Y. & Mao, C. Cascade Signal Amplification for DNA Detection. *ChemBioChem* **7**, 1862–1864 (2006).
32. Liu, M. *et al.* A DNAzyme Feedback Amplification Strategy for Biosensing. *Angew. Chemie* **129**, 6238–6242 (2017).
33. Chen, J. *et al.* Enzyme-free amplified detection of microRNA using target-catalyzed hairpin assembly and magnesium ion-dependent deoxyribozyme. *Sci. China Chem.* **58**, 1906–1911 (2015).
34. Dirks, R. M. & Pierce, N. A. Triggered amplification by hybridization chain reaction. *Proc. Natl. Acad. Sci.* **101**, 15275–15278 (2004).
35. Wang, F., Elbaz, J., Orbach, R., Magen, N. & Willner, I. Amplified Analysis of DNA by the Autonomous Assembly of Polymers Consisting of DNAzyme Wires. *J. Am. Chem. Soc.* **133**, 17149–17151 (2011).
36. Turberfield, A. J. *et al.* DNA Fuel for Free-Running Nanomachines. *Phys. Rev. Lett.* **90**, 118102 (2003).
37. Liu, J., Cao, Z. & Lu, Y. Functional Nucleic Acid Sensors. *Chem. Rev.* **109**, 1948–1998 (2009).
38. Kim, J. H., Han, S. H. & Chung, B. H. Improving Pb2+ detection using DNAzyme-based fluorescence sensors by pairing fluorescence donors with gold nanoparticles. *Biosens. Bioelectron.* **26**, 2125–2129 (2011).
39. Swearingen, C. B. *et al.* Immobilization of a Catalytic DNA Molecular Beacon on Au for Pb(II) Detection. *Anal. Chem.* **77**, 442–448 (2005).
40. Wu, P., Hwang, K., Lan, T. & Lu, Y. A DNAzyme-gold nanoparticle probe for uranyl ion in living cells. *J. Am. Chem. Soc.* **135**, 5254–5257 (2013).
41. Xiao, Y., Rowe, A. A. & Plaxco, K. W. Electrochemical Detection of Parts-Per-Billion Lead via an Electrode-Bound DNAzyme Assembly. *J. Am. Chem. Soc.* **129**, 262–263 (2007).
42. Shen, L. *et al.* Electrochemical DNAzyme Sensor for Lead Based on Amplification of DNA−Au Bio-Bar Codes. *Anal. Chem.* **80**, 6323–6328 (2008).
43. Yang, X., Xu, J., Tang, X., Liu, H. & Tian, D. A novel electrochemical DNAzyme sensor for the amplified detection of Pb2+ ions. *Chem. Commun.* **46**, 3107 (2010).
44. Lu, L. *et al.* Highly selective and sensitive electrochemical biosensor for ATP based on the dual strategy integrating the cofactor-dependent enzymatic ligation reaction with

self-cleaving DNAzyme-amplified electrochemical detection. *Biosens. Bioelectron.* **63**, 14–20 (2015).

45. Zhang, M. *et al.* Three-dimensional paper-based electrochemiluminescence device for simultaneous detection of Pb2+ and Hg2+ based on potential-control technique. *Biosens. Bioelectron.* **41**, 544–550 (2013).
46. Teh, H. B., Li, H. & Yau Li, S. F. Highly sensitive and selective detection of Pb 2+ ions using a novel and simple DNAzyme-based quartz crystal microbalance with dissipation biosensor. *Analyst* **139**, 5170–5175 (2014).
47. Yehl, K. *et al.* Catalytic Deoxyribozyme-Modified Nanoparticles for RNAi-Independent Gene Regulation. *ACS Nano* **6**, 9150–9157 (2012).
48. Liu, J. & Lu, Y. Accelerated Color Change of Gold Nanoparticles Assembled by DNAzymes for Simple and Fast Colorimetric Pb 2+ Detection. *J. Am. Chem. Soc.* **126**, 12298–12305 (2004).
49. Lee, J. H., Wang, Z., Liu, J. & Lu, Y. Highly Sensitive and Selective Colorimetric Sensors for Uranyl (UO 2 2+): Development and Comparison of Labeled and Label-Free DNAzyme-Gold Nanoparticle Systems. *J. Am. Chem. Soc.* **130**, 14217–14226 (2008).
50. Zagorovsky, K. & Chan, W. C. W. A Plasmonic DNAzyme Strategy for Point-of-Care Genetic Detection of Infectious Pathogens. *Angew. Chemie Int. Ed.* **52**, 3168–3171 (2013).
51. Liu, J. & Lu, Y. Optimization of a Pb 2+ -Directed Gold Nanoparticle/DNAzyme Assembly and Its Application as a Colorimetric Biosensor for Pb 2+. *Chem. Mater.* **16**, 3231–3238 (2004).
52. Chang, C.-C. *et al.* Gold Nanoparticle-Based Colorimetric Strategies for Chemical and Biological Sensing Applications. *Nanomaterials* **9**, 861 (2019).
53. Sun, C., Zhang, L., Jiang, J., Shen, G. & Yu, R. Electrochemical DNA biosensor based on proximity-dependent DNA ligation assays with DNAzyme amplification of hairpin substrate signal. *Biosens. Bioelectron.* **25**, 2483–2489 (2010).
54. Xia, H., Li, L., Yin, Z., Hou, X. & Zhu, J.-J. Biobar-Coded Gold Nanoparticles and DNAzyme-Based Dual Signal Amplification Strategy for Ultrasensitive Detection of Protein by Electrochemiluminescence. *ACS Appl. Mater. Interfaces* **7**, 696–703 (2015).
55. Diao, W. *et al.* Electrochemical DNA biosensor based on MNAzyme-mediated signal amplification. *Microchim. Acta* **183**, 2563–2569 (2016).
56. Chen, Y. & Corn, R. M. DNAzyme Footprinting: Detecting Protein–Aptamer Complexation on Surfaces by Blocking DNAzyme Cleavage Activity. *J. Am. Chem. Soc.* **135**, 2072–2075 (2013).
57. Yang, J. *et al.* Electrochemical strategy for ultrasensitive detection of microRNA based on MNAzyme-mediated rolling circle amplification on a gold electrode. *Microchim. Acta* **183**, 3061–3067 (2016).
58. Qian, Y., Wang, C. & Gao, F. Ultrasensitive electrochemical detection of DNA based on Zn 2+ assistant DNA recycling followed with hybridization chain reaction dual amplification. *Biosens. Bioelectron.* **63**, 425–431 (2015).
59. Li, X. *et al.* A novel surface plasmon resonance biosensor for enzyme-free and highly sensitive detection of microRNA based on multi component nucleic acid enzyme (MNAzyme)-mediated catalyzed hairpin assembly. *Biosens. Bioelectron.* **80**, 98–104 (2016).
60. Zhou, W., Ding, J. & Liu, J. Theranostic DNAzymes. *Theranostics* **7**, 1010–1025 (2017).
61. Wu, Y. *et al.* Inhibition of bcr-abl Oncogene Expression by Novel Deoxyribozymes (DNAzymes). *Hum. Gene Ther.* **10**, 2847–2857 (1999).
62. Singh, N., Ranjan, A., Sur, S., Chandra, R. & Tandon, V. Inhibition of HIV-1 Integrase

gene expression by 10-23 DNAzyme. *J. Biosci.* **37**, 493–502 (2012).
63. Willner, I., Shlyahovsky, B., Zayats, M. & Willner, B. DNAzymes for sensing, nanobiotechnology and logic gate applications. *Chem. Soc. Rev.* **37**, 1153 (2008).
64. Lu, C.-H. & Willner, I. Stimuli-Responsive DNA-Functionalized Nano-/Microcontainers for Switchable and Controlled Release. *Angew. Chemie Int. Ed.* **54**, 12212–12235 (2015).
65. Homola, J. *Surface Plasmon Resonance Based Sensors*. *Springer Series on Chemical Sensors and Biosensors* **4**, (2006).
66. Hodnik, V. & Anderluh, G. Toxin Detection by Surface Plasmon Resonance. *Sensors* **9**, 1339–1354 (2009).
67. Zhou, J. *et al.* Surface plasmon resonance (SPR) biosensors for food allergen detection in food matrices. *Biosens. Bioelectron.* **142**, 111449 (2019).
68. Mariani, S. & Minunni, M. Surface plasmon resonance applications in clinical analysis. *Anal. Bioanal. Chem.* **406**, 2303–2323 (2014).
69. Masson, J.-F. Surface Plasmon Resonance Clinical Biosensors for Medical Diagnostics. *ACS Sensors* **2**, 16–30 (2017).
70. Rebe Raz, S., Leontaridou, M., Bremer, M. G. E. G., Peters, R. & Weigel, S. Development of surface plasmon resonance-based sensor for detection of silver nanoparticles in food and the environment. *Anal. Bioanal. Chem.* **403**, 2843–2850 (2012).
71. Justino, C., Duarte, A. & Rocha-Santos, T. Recent Progress in Biosensors for Environmental Monitoring: A Review. *Sensors* **17**, 2918 (2017).
72. Sharma, A. K., Jha, R. & Gupta, B. D. Fiber-Optic Sensors Based on Surface Plasmon Resonance: A Comprehensive Review. *IEEE Sens. J.* **7**, 1118–1129 (2007).
73. Zhang, J., Zhang, L. & Xu, W. Surface plasmon polaritons: physics and applications. *J. Phys. D. Appl. Phys.* **45**, 113001 (2012).
74. Pines, D. Collective Energy Losses in Solids. *Rev. Mod. Phys.* **28**, 184–198 (1956).
75. Schasfoort, R. B. M. & Tudos, A. J. *Handbook of Surface Plasmon Resonance*. (Royal Society of Chemistry, 2008). doi:10.1039/9781847558220
76. Wood, R. W. On a Remarkable Case of Uneven Distribution of Light in a Diffraction Grating Spectrum. *Proc. Phys. Soc. London* **18**, 269–275 (1902).
77. Ritchie, R. H. Plasma Losses by Fast Electrons in Thin Films. *Phys. Rev.* **106**, 874–881 (1957).
78. Polyanskiy, M. N. Refractive index database. (2008). Available at: https://refractiveindex.info/?shelf=main&book=Au&page=Johnson. (Accessed: 19th November 2019)
79. Prabowo, B., Purwidyantri, A. & Liu, K.-C. Surface Plasmon Resonance Optical Sensor: A Review on Light Source Technology. *Biosensors* **8**, 80 (2018).
80. Cullen, D. C., Brown, R. G. W. & Lowe, C. R. Detection of immuno-complex formation via surface plasmon resonance on gold-coated diffraction gratings. *Biosensors* **3**, 211–225 (1987).
81. Wang, Y., Dostalek, J. & Knoll, W. Magnetic Nanoparticle-Enhanced Biosensor Based on Grating-Coupled Surface Plasmon Resonance. *Anal. Chem.* **83**, 6202–6207 (2011).
82. Homola, J., Koudela, I. & Yee, S. S. Surface plasmon resonance sensors based on diffraction gratings and prism couplers: sensitivity comparison. *Sensors Actuators B Chem.* **54**, 16–24 (1999).
83. Ruffato, G., Zacco, G. & Romanato, F. Innovative Exploitation of Grating-Coupled Surface Plasmon Resonance for Sensing. in *Plasmonics - Principles and Applications* 444 (InTech, 2012). doi:10.5772/51044
84. Perino, M., Pasqualotto, E., Scaramuzza, M., De Toni, A. & Paccagnella, A.

Enhancement and control of surface plasmon resonance sensitivity using grating in conical mounting configuration. *Opt. Lett.* **40**, 221 (2015).

85. Rossi, S., Gazzola, E., Capaldo, P., Borile, G. & Romanato, F. Grating-Coupled Surface Plasmon Resonance (GC-SPR) Optimization for Phase-Interrogation Biosensing in a Microfluidic Chamber. *Sensors* **18**, 1621 (2018).
86. Dostálek, J., Homola, J. & Miler, M. Rich information format surface plasmon resonance biosensor based on array of diffraction gratings. *Sensors Actuators B Chem.* **107**, 154–161 (2005).
87. Yoon, K. H., Shuler, M. L. & Kim, S. J. Design optimization of nano-grating surface plasmon resonance sensors. *Opt. Express* **14**, 4842 (2006).
88. Piliarik, M., Vala, M., Tichý, I. & Homola, J. Compact and low-cost biosensor based on novel approach to spectroscopy of surface plasmons. *Biosens. Bioelectron.* **24**, 3430–3435 (2009).
89. Otto, A. Excitation of nonradiative surface plasma waves in silver by the method of frustrated total reflection. *Zeitschrift für Phys. A Hadron. Nucl.* **216**, 398–410 (1968).
90. Kretschmann, E. & Raether, H. Notizen: Radiative Decay of Non Radiative Surface Plasmons Excited by Light. *Zeitschrift für Naturforsch. A* **23**, 2135–2136 (1968).
91. Novotny, L. & Hecht, B. Surface plasmons. in *Principles of Nano-Optics* 369–413 (Cambridge University Press, 2006). doi:10.1017/CBO9780511794193.014
92. Abdelghani, A., Veillas, C., Chovelon, J. M., Jaffrezic-Renault, N. & Gagnaire, H. Stabilization of a surface plasmon resonance (SPR) optical fibre sensor with an ultra-thin organic film: application to the detection of chloro-fluoro-carbon (CFC). *Synth. Met.* **90**, 193–198 (1997).
93. Sahm, H., Charton, C. & Thielsch, R. Oxidation behaviour of thin silver films deposited on plastic web characterized by spectroscopic ellipsometry (SE). *Thin Solid Films* **455–456**, 819–823 (2004).
94. Evertsson, J. *et al.* The thickness of native oxides on aluminum alloys and single crystals. *Appl. Surf. Sci.* **349**, 826–832 (2015).
95. Knoglinger, C. *et al.* Regenerative biosensor for use with biotinylated bait molecules. *Biosens. Bioelectron.* **99**, 684–690 (2018).
96. Caucheteur, C., Guo, T. & Albert, J. Review of plasmonic fiber optic biochemical sensors: improving the limit of detection. *Anal. Bioanal. Chem.* **407**, 3883–3897 (2015).
97. Gupta, B. D. & Kant, R. [INVITED] Recent advances in surface plasmon resonance based fiber optic chemical and biosensors utilizing bulk and nanostructures. *Opt. Laser Technol.* **101**, 144–161 (2018).
98. Jorgenson, R. C. & Yee, S. S. A fiber-optic chemical sensor based on surface plasmon resonance. *Sensors Actuators B Chem.* **12**, 213–220 (1993).
99. Arghir, I., Delport, F., Spasic, D. & Lammertyn, J. Smart design of fiber optic surfaces for improved plasmonic biosensing. *N. Biotechnol.* **32**, 473–484 (2015).
100. Zeng, J. & Liang, D. Application of Fiber Optic Surface Plasmon Resonance Sensor for Measuring Liquid Refractive Index. *J. Intell. Mater. Syst. Struct.* **17**, 787–791 (2006).
101. Pollet, J. *et al.* Fiber optic SPR biosensing of DNA hybridization and DNA–protein interactions. *Biosens. Bioelectron.* **25**, 864–869 (2009).
102. Chambers, J. P., Arulanandam, B. P., Matta, L. L., Weis, A. & Valdes, J. J. Biosensor Recognition Elements. *Curr. Issues Mol. Biol.* **10**, 1–12 (2008).
103. Zhang, X., Servos, M. R. & Liu, J. Surface Science of DNA Adsorption onto Citrate-Capped Gold Nanoparticles. *Langmuir* **28**, 3896–3902 (2012).
104. Wang, Z., Lee, J. H. & Lu, Y. Label-Free Colorimetric Detection of Lead Ions with a Nanomolar Detection Limit and Tunable Dynamic Range by using Gold Nanoparticles

and DNAzyme. *Adv. Mater.* **20**, 3263–3267 (2008).
105. Integrated DNA Technologies. Strategies for Attaching Oligonucleotides to Solid Supports. (2014).
106. Lee, C.-Y., Gamble, L. J., Grainger, D. W. & Castner, D. G. Mixed DNA/oligo (ethylene glycol) functionalized gold surfaces improve DNA hybridization in complex media. *Biointerphases* **1**, 82–92 (2006).
107. Jans, H. *et al.* Increased stability of mercapto alkane functionalized Au nanoparticles towards DNA sensing. *Nanotechnology* **21**, 285608 (2010).
108. Liu, B. *et al.* Design and mechanisms of antifouling materials for surface plasmon resonance sensors. *Acta Biomater.* **40**, 100–118 (2016).
109. Boozer, C., Chen, S. & Jiang, S. Controlling DNA orientation on mixed ssDNA/OEG SAMs. *Langmuir* **22**, 4694–4698 (2006).
110. Lee, C.-Y., Nguyen, P.-C. T., Grainger, D. W., Gamble, L. J. & Castner, D. G. Structure and DNA Hybridization Properties of Mixed Nucleic Acid/Maleimide−Ethylene Glycol Monolayers. *Anal. Chem.* **79**, 4390–4400 (2007).
111. Peelen, D. & Smith, L. M. Immobilization of Amine-Modified Oligonucleotides on Aldehyde-Terminated Alkanethiol Monolayers on Gold. *Langmuir* **21**, 266–271 (2005).
112. Samanta, D. & Sarkar, A. Immobilization of bio-macromolecules on self-assembled monolayers: methods and sensor applications. *Chem. Soc. Rev.* **40**, 2567 (2011).
113. Brockman, J. M., Frutos, A. G. & Corn, R. M. A Multistep Chemical Modification Procedure To Create DNA Arrays on Gold Surfaces for the Study of Protein−DNA Interactions with Surface Plasmon Resonance Imaging. *J. Am. Chem. Soc.* **121**, 8044–8051 (1999).
114. Solanki, P. R., Prabhakar, N., Pandey, M. K. & Malhotra, B. D. Self-assembled monolayer for toxicant detection using nucleic acid sensor based on surface plasmon resonance technique. *Biomed. Microdevices* **10**, 757–767 (2008).
115. Jung, L. S. *et al.* Surface plasmon resonance measurement of binding and dissociation of wild-type and mutant streptavidin on mixed biotin-containing alkylthiolate monolayers. *Sensors Actuators B Chem.* **54**, 137–144 (1999).
116. Ladd, J. *et al.* DNA-Directed Protein Immobilization on Mixed Self-Assembled Monolayers via a Streptavidin Bridge. *Langmuir* **20**, 8090–8095 (2004).
117. Vaisocherová, H. *et al.* Investigating oligonucleotide hybridization at subnanomolar level by surface plasmon resonance biosensor method. *Biopolymers* **82**, 394–398 (2006).
118. Mir, M., Álvarez, M., Azzaroni, O. & Knoll, W. Comparison of Different Supramolecular Architectures for Oligonucleotide Biosensing. *Langmuir* **24**, 13001–13006 (2008).
119. Wang, R., Tombelli, S., Minunni, M., Spiriti, M. M. & Mascini, M. Immobilisation of DNA probes for the development of SPR-based sensing. *Biosens. Bioelectron.* **20**, 967–974 (2004).
120. Li, Y.-J. *et al.* Reversible immobilization of proteins with streptavidin affinity tags on a surface plasmon resonance biosensor chip. *Anal. Bioanal. Chem.* **386**, 1321–1326 (2006).
121. Liu, Y. & Wilson, W. D. Quantitative Analysis of Small Molecule–Nucleic Acid Interactions with a Biosensor Surface and Surface Plasmon Resonance Detection. in *Methods in molecular biology (Clifton, N.J.)* **613**, 1–23 (2010).
122. Guo, B. *et al.* An enzyme-free and label-free surface plasmon resonance biosensor for ultrasensitive detection of fusion gene based on DNA self-assembly hydrogel with streptavidin encapsulation. *Biosens. Bioelectron.* **112**, 120–126 (2018).
123. Yang, N., Su, X., Tjong, V. & Knoll, W. Evaluation of two- and three-dimensional

streptavidin binding platforms for surface plasmon resonance spectroscopy studies of DNA hybridization and protein–DNA binding. *Biosens. Bioelectron.* **22**, 2700–2706 (2007).
124. Hu, W., Li, C. M. & Dong, H. Poly(pyrrole-co-pyrrole propylic acid) film and its application in label-free surface plasmon resonance immunosensors. *Anal. Chim. Acta* **630**, 67–74 (2008).
125. Wijaya, E. *et al.* Surface plasmon resonance-based biosensors: From the development of different SPR structures to novel surface functionalization strategies. *Curr. Opin. Solid State Mater. Sci.* **15**, 208–224 (2011).
126. Janmanee, R., Chuekachang, S., Sriwichai, S., Baba, A. & Phanichphant, S. Functional Conducting Polymers in the Application of SPR Biosensors. *J. Nanotechnol.* **2012**, 1–7 (2012).
127. Rico-Yuste, A. & Carrasco, S. Molecularly Imprinted Polymer-Based Hybrid Materials for the Development of Optical Sensors. *Polymers (Basel).* **11**, 1173 (2019).
128. Zhang, Z. & Liu, J. Molecular Imprinting with Functional DNA. *Small* **15**, 1805246 (2019).
129. El-Sagheer, A. H. & Brown, T. Click chemistry with DNA. *Chem. Soc. Rev.* **39**, 1388 (2010).
130. Yaakov, N. *et al.* Application of Surface Click Reactions to Localized Surface Plasmon Resonance (LSPR) Biosensing. *Chem. - A Eur. J.* **23**, 10148–10155 (2017).
131. Isozaki, K. *et al.* Robust Surface Plasmon Resonance Chips for Repetitive and Accurate Analysis of Lignin–Peptide Interactions. *ACS Omega* **3**, 7483–7493 (2018).
132. Šípová, H. & Homola, J. Surface plasmon resonance sensing of nucleic acids: A review. *Anal. Chim. Acta* **773**, 9–23 (2013).
133. Zhou, C. *et al.* Signal amplification strategies for DNA-based surface plasmon resonance biosensors. *Biosens. Bioelectron.* **117**, 678–689 (2018).
134. Bedford, E. E., Spadavecchia, J., Pradier, C.-M. & Gu, F. X. Surface Plasmon Resonance Biosensors Incorporating Gold Nanoparticles. *Macromol. Biosci.* **12**, 724–739 (2012).
135. Lyon, L. A., Musick, M. D. & Natan, M. J. Colloidal Au-Enhanced Surface Plasmon Resonance Immunosensing. *Anal. Chem.* **70**, 5177–5183 (1998).
136. He, L. *et al.* Colloidal Au-Enhanced Surface Plasmon Resonance for Ultrasensitive Detection of DNA Hybridization. *J. Am. Chem. Soc.* **122**, 9071–9077 (2000).
137. Mustafa, D. E. *et al.* Surface Plasmon Coupling Effect of Gold Nanoparticles with Different Shape and Size on Conventional Surface Plasmon Resonance Signal. *Plasmonics* **5**, 221–231 (2010).
138. Hong, X. & Hall, E. A. H. Contribution of gold nanoparticles to the signal amplification in surface plasmon resonance. *Analyst* **137**, 4712 (2012).
139. Špringer, T., Ermini, M. L., Špačková, B., Jabloňků, J. & Homola, J. Enhancing Sensitivity of Surface Plasmon Resonance Biosensors by Functionalized Gold Nanoparticles: Size Matters. *Anal. Chem.* **86**, 10350–10356 (2014).
140. Knez, K., Janssen, K. P. F., Pollet, J., Spasic, D. & Lammertyn, J. Fiber-Optic High-Resolution Genetic Screening Using Gold-Labeled Gene Probes. *Small* **8**, 868–872 (2012).
141. Qian, S. *et al.* Boronic Acid Functionalized Au Nanoparticles for Selective MicroRNA Signal Amplification in Fiber-Optic Surface Plasmon Resonance Sensing System. *ACS Sensors* **3**, 929–935 (2018).
142. Kai, E. *et al.* Detection of PCR Products in Solution Using Surface Plasmon Resonance. *Anal. Chem.* **71**, 796–800 (1999).
143. Zhang, D. *et al.* Label-free and high-sensitive detection of Salmonella using a surface plasmon resonance DNA-based biosensor. *J. Biotechnol.* **160**, 123–128 (2012).

144. Pollet, J., Janssen, K. P. F., Knez, K. & Lammertyn, J. Real-time monitoring of solid-phase PCR using fiber-optic SPR. *Small* **7**, 1003–1006 (2011).
145. Daems, D., Knez, K., Delport, F., Spasic, D. & Lammertyn, J. Real-time PCR melting analysis with fiber optic SPR enables multiplex DNA identification of bacteria. *Analyst* **141**, 1906–1911 (2016).
146. Janssen, K. P. F. *et al.* Enabling fiber optic serotyping of pathogenic bacteria through improved anti-fouling functional surfaces. *Nanotechnology* **23**, 235503 (2012).
147. Knez, K. *et al.* Spherical Nucleic Acid Enhanced FO-SPR DNA Melting for Detection of Mutations in Legionella pneumophila. *Anal. Chem.* **85**, 1734–1742 (2013).
148. Knez, K., Spasic, D., Delport, F. & Lammertyn, J. Real-time ligation chain reaction for DNA quantification and identification on the FO-SPR. *Biosens. Bioelectron.* **67**, 394–399 (2015).
149. Xiang, Y. *et al.* Isothermal detection of multiple point mutations by a surface plasmon resonance biosensor with Au nanoparticles enhanced surface-anchored rolling circle amplification. *Biosens. Bioelectron.* **49**, 442–449 (2013).
150. Shi, D. *et al.* Isothermal and rapid detection of pathogenic microorganisms using a nano-rolling circle amplification-surface plasmon resonance biosensor. *Biosens. Bioelectron.* **62**, 280–287 (2014).
151. Li, X., Wang, Y., Wang, L. & Wei, Q. A surface plasmon resonance assay coupled with a hybridization chain reaction for amplified detection of DNA and small molecules. *Chem. Commun.* **50**, 5049–5052 (2014).
152. Ding, X. *et al.* An enzyme-free surface plasmon resonance biosensing strategy for detection of DNA and small molecule based on nonlinear hybridization chain reaction. *Biosens. Bioelectron.* **87**, 345–351 (2017).
153. Li, J. *et al.* An enzyme-free surface plasmon resonance biosensor for real-time detecting microRNA based on allosteric effect of mismatched catalytic hairpin assembly. *Biosens. Bioelectron.* **77**, 435–441 (2016).
154. Soelberg, S. D. *et al.* A portable surface plasmon resonance sensor system for real-time monitoring of small to large analytes. *J. Ind. Microbiol. Biotechnol.* **32**, 669–674 (2005).
155. Jiang, T. *et al.* Detection of TP53 mutation using a portable surface plasmon resonance DNA-based biosensor. *Biosens. Bioelectron.* **20**, 1939–1945 (2005).
156. Chinowsky, T. M. *et al.* Portable 24-analyte surface plasmon resonance instruments for rapid, versatile biodetection. *Biosens. Bioelectron.* **22**, 2268–2275 (2007).
157. Couture, M., Zhao, S. S. & Masson, J.-F. Modern surface plasmon resonance for bioanalytics and biophysics. *Phys. Chem. Chem. Phys.* **15**, 11190 (2013).
158. Feltis, B. N. *et al.* A hand-held surface plasmon resonance biosensor for the detection of ricin and other biological agents. *Biosens. Bioelectron.* **23**, 1131–1136 (2008).
159. Shin, Y.-B., Kim, H. M., Jung, Y. & Chung, B. H. A new palm-sized surface plasmon resonance (SPR) biosensor based on modulation of a light source by a rotating mirror. *Sensors Actuators B Chem.* **150**, 1–6 (2010).
160. Preechaburana, P., Gonzalez, M. C., Suska, A. & Filippini, D. Surface Plasmon Resonance Chemical Sensing on Cell Phones. *Angew. Chemie Int. Ed.* **51**, 11585–11588 (2012).

Chapter 3

Identification and quantification of celery allergens using fiber optic surface plasmon resonance PCR

The work in this chapter was adapted from:

Daems, D., **Peeters, B.**, Delport, F., Remans, T., Lammertyn, J. and Spasic, D., Identification and Quantification of Celery Allergens Using Fiber Optic Surface Plasmon Resonance PCR. *Sensors* 17, 1754 (2017).

Contributions of Peeters B. to this manuscript:

Data processing, analysis, discussion of the results and editing of the manuscript.

3.1. Introduction

Celery (*Apium graveolens*) is one of the most common foods causing allergic reactions in European countries, particularly in France, Switzerland and Germany. Notably, in France, 30% of anaphylactic reactions are caused by the ingestion of the celery allergen protein Api g 1[1–3]. Although celery is consumed cooked or processed, compared to raw celery, food processing only lowers the allergenicity, but does not destroy the allergenic properties completely[2]. Therefore, celery was added to the list of fourteen groups of allergenic species with strict labelling legislation issued by the EU Commission (Directive 2003/89/EC and Directive 1169/2011) in order to ensure that consumers are adequately informed on the presence of allergenic ingredients in food[4,5].

The presence of food allergens, similar to food toxins and food pathogens, can have considerable consequences on food safety. Therefore, it is of the utmost importance to avoid and prevent accidental contaminations in the food industry. Accurate identification and quantification are key in this context. To achieve this, many food companies send a representative sample of their final products to a remote laboratory, since only a limited number of available tests can be performed on-site that are truly fast, affordable and easy-to-use.

The two main approaches to detect food allergens, including in celery, are antibody-based immunoassays and DNA-based PCR. At present, available ELISAs for the specific detection of celery show cross-reactivity with allergen proteins of closely related members of the *Apiaceae* family, such as carrots[2,6,7] or parsley[8]. Therefore, several real-time (i.e., quantitative) PCR (qPCR) assays have been developed as a more specific alternative[9–12], targeting sequences from the *Api g 1* or the mannitol dehydrogenase (*Mtd*) gene. Although *Api g 1* codes for the major allergenic protein of celery, *Mtd* is more widely recommended for use in these assays due to the lower risk of cross-reactivity with sequences of other (closely) related species[10,13]. Despite their high specificity, qPCR assays are considered laborious and require sophisticated, bulky equipment, as well as trained personnel. Furthermore, qPCR and post-amplification high-resolution melting (HRM) analysis rely on costly fluorescent reporters for labelling DNA. All these intrinsic features

make this method unsuitable for a simple on-site high-throughput detection of celery in food matrices[14].

Therefore, **the aim of this chapter is to develop an innovative, fast and highly sensitive proof-of-concept bioassay on a compact FO-SPR biosensor platform.** SPR is one of the most advanced label-free, real-time detection technologies that provides information not only for the quantification, but also on the kinetics, of the binding reaction[15,16]. Over the past years, a FO-SPR biosensor has been developed as a cost-effective and easy-to-use alternative for the more expensive and complex SPR systems[17], such as the well-known commercially available Biacore instrument (GE Healthcare, Uppsala, Sweden). The FO-SPR biosensor makes use of multimode optical fibers that facilitate SPR generation and enable implementation of bioassays[18–20]. As has already been demonstrated by our group, the FO-SPR biosensor developed in-house has the unique capacity to quantify a variety of different molecules, ranging from proteins and NAs to small molecules not only in buffer but also in the complex sample matrices, such as whole blood, serum, plasma or milk[14,21–24]. Moreover, the platform is compatible with AuNPs, which are used for signal amplification and improvement of the bioassay sensitivity[25,26]. In a previous publication, a FO-SPR PCR melting assay (FO-PCR-MA)[14] was established for one-step cycle-to-cycle identification of multiple DNA targets on the same FO-SPR sensor. Here, the concept is further elaborated to enable quantification of celery DNA targets both in buffer and in cleaning water samples.

3.2. Experimental section

3.2.1. Materials and reagents

All chemicals were of analytical reagent grade and were purchased from Sigma-Aldrich (Bornem, Belgium), unless stated otherwise. Citrate-stabilized AuNPs, with a mean diameter of 20 nm, were ordered from BBI international (Cardiff, UK). Celery (*Apium graveolens*) was bought from a local market. Two target regions were selected for celery detection (*Api* and *Mtd*). Target sequences reported in literature (*Api g 1*[27] and *Mtd*[10]), as well as target sequences selected in-house (*Mtd 2* and *Mtd 3*), sequences of the primers used for DNA amplification and sequences of the hybridization probes used in the FO-SPR bioassay are all presented in Table 3.1. The primers selected

Table 3.1: *Overview of used oligonucleotides for the qPCR and the FO-PCR-MA.*

Target sequences	**Length (nt)**	**Sequence 5' → 3'**
Api g 1	76	GGG CTT TGT CAT TGA TGT TGA CAC AGT CCT TCC CAA GGC TGC GCC TGG AGC TTA CAA GAG TGT CGA AAT CAA GGG A
Mtd	101	CGA TGA GCG TGT ACT GAG TCA GTG TTA TGT TTG GAT TAC GGT GTG ATG AGT CAG CGT TAT CTG TTT TTA TAT GTT TGG TAT GAT TAA TGT TAG TTC CTA TT
Mtd 2	101	CCT TGT TAG CGG AGT CTA AAT CGG AAT CTA AAT CTA AAT CAT TTT AAG CAT GTT AGC CCT TGT ATT TTG GCT TTT GGC TTT TAA CCA TTT TGT TC
Mtd 3	109	CCC GTA CGA GAT ATA TTT TTG TCT GGT TTG AGA TAT ATA TTA CAT GCT GAG TCA CGA TGA GCG TGT ACT GAG TCA GTG TTA TGT TTG GAT TAC GGT GTG ATG AGT CAG C
Primer sequences		**Sequence 5' → 3'**
Api g 1 forward	22	GGG CTT TGT CAT TGA TGT TGA C
Api g 1 reverse	24	TCC CTT GAT TTC GAC ACT CTT GTA
Mtd forward	20	CGA TGA GCG TGT ACT GAG TC
Mtd reverse	29	AAT AGG AAC TAA CAT TAA TCA TAC CAA AC
Mtd 2 forward	24	CCT TGT TAG CGG AGT CTA AAT CGG
Mtd 2 reverse	20	GAA CAA AAT GGT TAA AAG CC
Mtd 3 forward	26	CCC GTA CGA GAT ATA TTT TTG TCT GG
Mtd 3 reverse	23	GCT GAC TCA TCA CAC CGT AAT CC
Hybridization probes		**Sequence 5' → 3'**
Mtd 3 probe 1	66	GTG ACT CAG CAT GTA ATA TAT ATC TCA AAC CAG ACA AAA ATA TAT CTC GTA CGG GTT TTT TTT TT
Mtd 3 probe 2	64	TTT TTT TTT TGC TGA CTC ATC ACA CCG TAA TCC AAA CAT AAC ACT GAC TCA GTA CAC GCT CAT C

in-house were checked for the absence of homology with DNA sequences of other plants using the BLAST software (National Center for Biotechnology Information, Bethesda, MD, USA). The hybridization probes were modified with a 3' C3 (probe 1) or 5' C6 thiol-modifier (-SH) (probe 2) for their immobilization on the FO-SPR sensor and the AuNPs surfaces, respectively. All the hybridization probes were equipped with a poly-T spacer in order to improve the hybridization efficiency of the DNA[28]. The free 3' end of the hybridization probe 2 was blocked from extension by the polymerase enzyme using a 3' phosphate modification. The primers and hybridization probes were chemically synthesized by Integrated DNA Technologies (IDT, Haasrode, Belgium).

3.2.2. qPCR/HRM

A qPCR master mix (PerfeCTa Sybr Green Fastmix, QuantaBio, Beverly, CA, USA) was used, containing all necessary components for the qPCR reaction except for the primers. The reaction mixture consisted of 6.50 µL PCR master mix, 0.87 µL of each primer (333 nM final concentration), 3.89 µL distilled H_2O and 0.87 µL target DNA. The qPCR (using a Rotor-gene Q HRM from Qiagen, Venlo, The Netherlands) was optimized for standard cycling conditions with an initial 240 s enzyme activation step at 95 °C, followed by 30 cycles of 30 s annealing and extension at 60 °C and 5 s denaturation at 95 °C. Afterwards a HRM was conducted by increasing the temperature from 60 °C to 95 °C (ramp speed = 0.5 °C/s).

3.2.3. Surface functionalization of FO-SPR sensors and AuNPs

The FO-SPR instrument and accompanying sensors were manufactured as described by Knez *et al.*[14,21]. Hybridization probes, modified with a 5' or 3' thiol-group, were first activated with dithiothreitol (DTT, 0.1 M in Phosphate Buffer (PB) 0.18 mM, pH 8.3). DTT was used to split thiol dimers which could prevent the surface functionalization process and it was removed from the solution by DNA purification with a NAP-5 Sephadex column (GE Healthcare, Oslo, Norway). Those 5' or 3' thiol modified hybridization probes were immobilized on the AuNPs or FO-SPR sensors by adding 1 µM of probes. In case of the AuNPs, a gradual salt maturation protocol was used to maximize the DNA density[29]. The AuNPs were then washed three times in PB with 0.01% SDS and stored in the same buffer at 4 °C until further use. Both the

FO-SPR sensors and AuNPs were backfilled to enable the PCR assay by incubating them in a 50 µM alkane thiol PEG (Polypure, Oslo, Norway) dissolved in pure ethanol for 2 h. Finally, both surfaces were washed three times with a 0.01% SDS PB buffer and stored afterwards at 4 °C in H_2O until further use.

3.2.4. FO-PCR-MA in solution

A PCR master mix (DimerEraser, Takara, Shiga, Japan) containing all needed components for the PCR reaction except for the primers was used. The reaction mixture consisted of 50 µL PCR master mix, 3 µL of every primer (300 nM final concentration), 20 µL of the functionalized AuNPs (1 nmol/L in distilled nuclease free H_2O), 4 µL $MgCl_2$ (50 mM), 4 µL NaCl (400 mM), 6 µL distilled H_2O and 10 µL target DNA, unless stated otherwise. The reaction mixture was covered by a layer of mineral oil (Immobiline DryStrip Cover Fluid, GE healthcare, Diegem, Belgium) to protect it from evaporation during thermocycling. The FO-PCR-MA was optimized for standard cycling conditions, first with an enzyme activation step at 95 °C (30 s), followed by 40 cycles of 30 s annealing at 53 °C (ramp speed = 5.0 °C/s), 30 s elongation at 72 °C (ramp speed = 5.0 °C/s), and finally 5 s denaturation at 90 °C (ramp speed = 1.0 °C/s).

3.2.5. Biological sample preparation

Three cleaning water samples (referred to as DNA 1–3) were spiked with 200 mg of celery (in 2 mL sample) from stem and leaf tissues, corresponding to the low pM range for stem tissue and the high fM range for leaf tissue. DNA was extracted from these samples using the commercial Qiagen DNeasy plant mini kit (Venlo, The Netherlands). The total DNA amount was measured by Qubit dsDNA HS Assay Kit (Thermo Fisher Scientific, Gent, Belgium). These spiked DNA 1–3 samples were evaluated both with qPCR and FO-PCR-MA for the presence of celery.

3.2.6. Data processing

The qPCR/HRM assay was recorded with the supplied program of Rotor-gene Q HRM and analyzed with the supplied Rotor-gene Q series Software version 2.3.1 (Qiagen, Venlo, The Netherlands). The data analysis (first derivative dF/dT and the threshold) was automatically calculated by this program.

FO-PCR-MA data acquisition was done with the in-house developed LabView program (National Instruments, Austin, TX, USA) to control two spectrometers and the NiDaq coupled thermocouples. By combining the SPR and thermocouple data, a first order derivative could be calculated for each PCR melting cycle. The resulting melting peak was fitted in Matlab (MathWorks, Natick, MA, USA) using a Gaussian fit to determine the T_m and evaluate the melting peak shape for each PCR cycle. The threshold was calculated as $x_{NTC} + 3\ \sigma_{noise}$, where x_{NTC} is the average value of the non-template control (n = 40 cycles) and σ_{noise} equals one standard deviation. The intraclass correlation coefficient (ICC)[30], which assesses the reliability of ratings by comparing the variability of different ratings of the same object, was calculated with the statistical package R (version 2.11.1, R foundation for Statistical Computing, Vienna, Austria).

3.3. Results and discussion

3.3.1. Selection of celery target sequence using qPCR/HRM

A qPCR reaction followed by HRM analysis is commonly the most used method for detection of celery[9–12]. In general, HRM analysis is performed on double-stranded PCR-amplified DNA samples by heating the DNA between 60 °C and 95 °C. At the point known to be the melting temperature (T_m) of the DNA target, two strands of DNA are separated, which is accompanied by a drop in fluorescent signal. This change in signal is due to the release of intercalating fluorescent dyes that have the unique properties to selectively bind only to dsDNA and brightly fluoresce in this bound state. Because the T_m is highly dependent on the DNA sequence, even two sequences of the same length, differing in only one nucleotide, will have different T_m values. Therefore, HRM is used for detecting mutations, polymorphisms and epigenetic differences, but also for target identification, the latter being of relevance for this study (Figure S3.1). qPCR/HRM was, for these reasons, selected here as a reference technology.

The qPCR/HRM assay was performed first to select the most appropriate region from the celery genome, suitable for its detection (Figure S3.2). Synthetic DNA targets were designed based on four different sequences from the two celery genes of interest, namely *Api g 1* and *Mtd* (Table 3.1) and used as targets in the qPCR/HRM analysis. One sequence,

here referred to as *Mtd 3*, was identified as the optimal one due to the absence of signal in the non-template control (NTC). *Mtd 3* corresponds to a 109 bp region of the celery sequence in the *Mtd* gene. Using *Mtd 3* synthetic DNA at various concentrations, ranging from 1 pM to 1 fM, a calibration curve was obtained as depicted in Figure 3.1A. This calibration curve will be further used to benchmark the sensitivity of the established FO-PCR-MA, as well as to determine the celery concentration in biological samples. The T_m of the selected target (77.1 °C with a standard deviation (SD) of 0.2) was determined based on the HRM profile following the qPCR reaction (Figure 3.1B) (n = 8, 2 repetitions of 4 different concentrations). The assessed T_m will give information concerning the identification of the amplified target sequence.

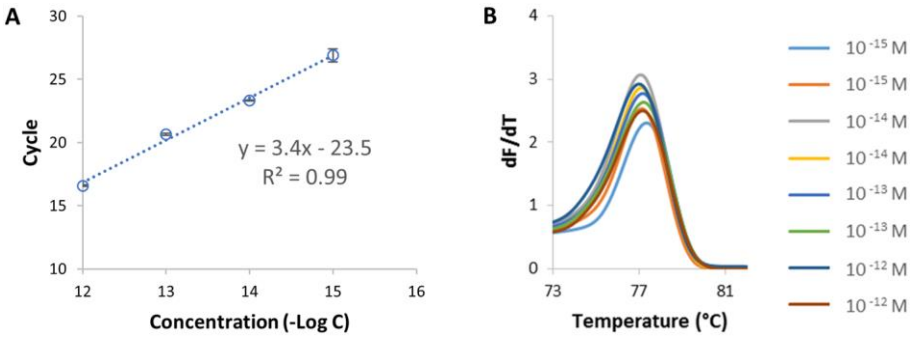

Figure 3.1: *qPCR followed by HRM analysis, using the Mtd 3 sequence.* ***A)*** *Calibration curve obtained by plotting the amount of cycles needed to reach the detection threshold in function of the concentrations (semi-log plot). Error bars represent one standard deviation (n = 2);* ***B)*** *Melting analysis of the Mtd 3 target after 30 qPCR cycles at concentrations ranging from 1 pM to 1 fM.*

3.3.2. Establishing FO-PCR-MA for celery DNA detection

In order to develop a proof-of-concept, fast and highly sensitive FO-SPR bioassay for celery DNA detection, we started from the FO-PCR-MA concept previously established in the group for bacterial detection[14]. The FO-PCR-MA concept is schematically illustrated in Figure 3.2. Briefly, DNA probe 1 for celery DNA detection is immobilized on the FO-SPR sensor surface, and DNA probe 2 is immobilized on the AuNPs, each of them designed to be complementary to the first and second half of the target celery sequence, respectively. In the presence of the target DNA, these two probes hybridize to the target, thereby bringing the AuNPs very close to the sensor surface.

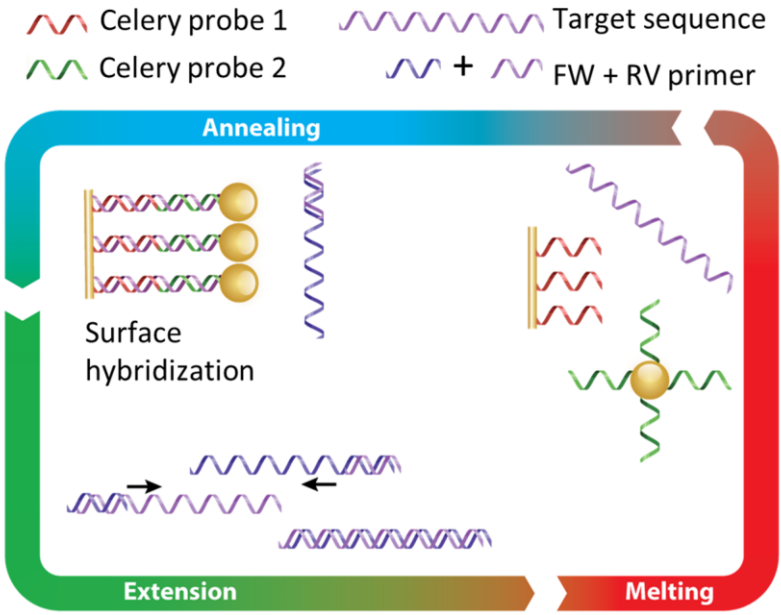

Figure 3.2: *Conceptual overview of the FO-PCR-MA. The PCR primers specific for celery targets are used to amplify a target region during a standard PCR reaction. The amplicons hybridize during the PCR reaction to complementary DNA probes on the FO-SPR sensor and those on AuNPs. During the normal PCR thermocycling, used to denature the amplicons, the FO-SPR sensor registers a change in mass (i.e., change in refractive index), which can be used for determining characteristic T_m of the target sequence and thus its identification.*

During the PCR, the target DNA is amplified, resulting in an increasing amount of DNA binding to the sensor (indicated as surface hybridization on the scheme). During the heating phase (indicated as melting on the scheme), the target DNA strands disconnect from the probes on the FO-SPR and AuNPs, releasing AuNPs from the FO-SPR surface. This causes a change in mass on the sensor and consequently a change in RI, which can be used for determining the characteristic T_m of the target sequence and thus its identification.

Although the established FO-PCR-MA its multiplexing capacity, real-time measurement of the amplification reaction and detection of multiple mutations in the target sequence[14] were demonstrated, the real sensitivity of this assay and its LOD have not been explored. Therefore, starting from the known concept, a new FO-PCR-MA was developed here for the celery detection. A synthetic celery target, indicated as *Mtd 3*, was used together with specific DNA probes 1 and 2, as well as specific primers, as depicted in

Table 3.1. The cycle-to-cycle amplification of celery DNA in the solution was studied in real-time in the presence of the FO-SPR sensor. Initially, the FO-SPR signal of the FO-PCR-MA reaction, which was continuously monitored with a thermocouple (Figure 3.3A), shows to be the inverse of the temperature change. However, from the moment the DNA target is amplified above the FO-PCR-MA signal detection threshold of the FO-SPR, the melting signal of the amplified DNA target will superimpose on the RI shift of the temperature (Figure 3.3B)[14]. A calibration curve was obtained with concentrations of synthetic DNA ranging from 1 pM to 0.1 fM (Figure 3.4A),

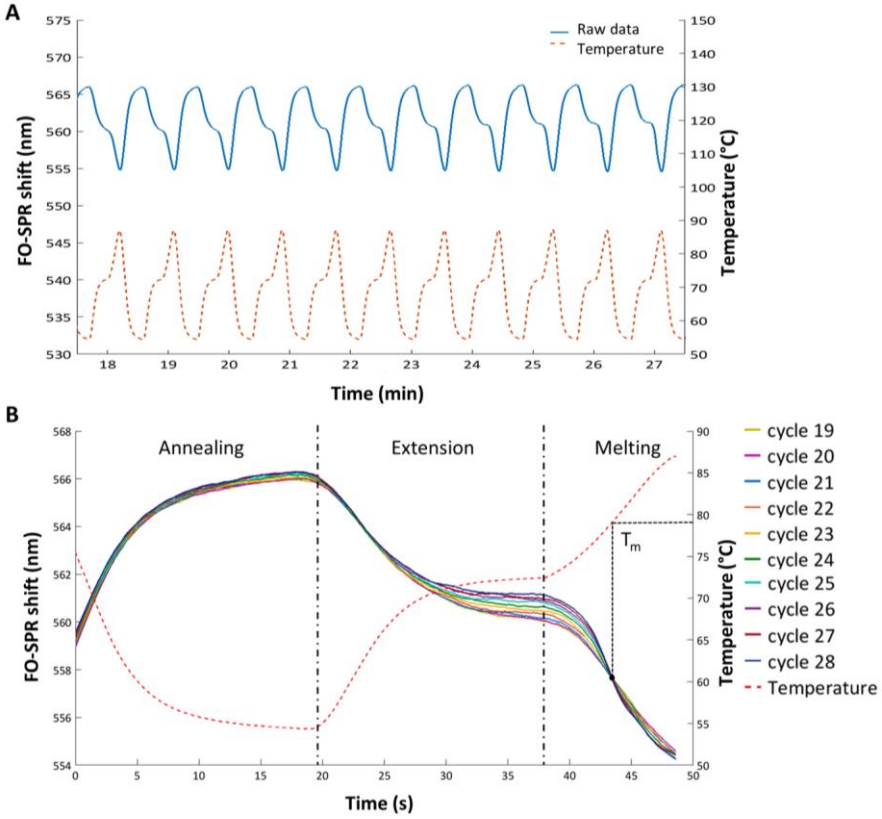

Figure 3.3: *Illustration of the FO-SPR signals and temperature data.* ***A)*** *Raw data of an FO-SPR PCR measurement. One measurement channel measures the change in RI due to the thermocycling. The FO-SPR signal is the inverse of the temperature measured with a thermocouple;* ***B)*** *FO-SPR signal for 10 PCR cycles containing 100 fM celery DNA. Initially the FO-SPR signal is the exact inverse of the temperature signal; however, as the DNA concentration reaches the detection threshold of the FO-SPR biosensor, a melting point is visible around 44 s.*

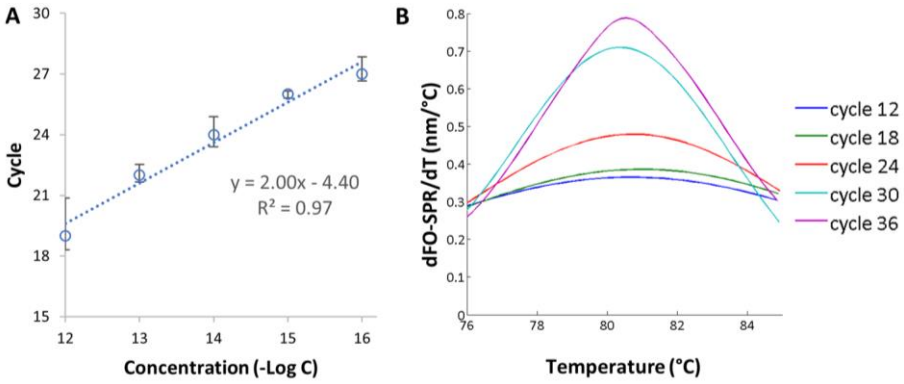

Figure 3.4: *Quantification of celery Mtd 3 target using FO-PCR-MA.* ***A)*** *Calibration curve obtained by plotting the number of cycles, needed to reach the detection threshold, as a function of the target concentration (semi-log plot). Error bars represent the standard error on the last 5 melting peak signals of FO-PCR-MA cycles needed to reach the detection threshold (Supplementary Information);* ***B)*** *First order derivative of the FO-SPR signal to the temperature, which allows resolving the melting point of 100 fM target DNA (Mtd 3) amplified with the PCR on the FO-SPR device. Once the cycle-to-cycle amplification of the DNA target during the FO-PCR-MA reaction has reached the detection threshold of the FO-SPR sensor, the dSPR/dT signal increases every PCR round.*

which was one order of magnitude lower than the qPCR calibration curve. Moreover, melting analysis performed simultaneously during the PCR reaction on the FO-SPR revealed a T_m of 79.4 °C with a SD of 0.5 for the *Mtd 3* target (Figure 3.4B). The determined T_m is essential for the specific identification of amplified sequences in order to distinguish them from the non-specific amplification that can occur. The FO-PCR-MA signal threshold of 0.095 nm/°C was calculated as described in Section 3.2.6 and used to determine the exceeding cycle for each concentration (Figure S3.3). By taking the first order derivative of the FO-SPR signal with respect to the temperature, the T_m of the celery DNA target was resolved very precisely and corresponded well to the T_m value determined using the reference qPCR/HRM technology (Figure 3.1). The small difference in T_m values can be attributed to the different PCR reaction mixtures used in two assays as it has been shown previously that buffer ionic strengths can have a strong influence on the T_m[14].

In conclusion, the performance of the FO-PCR-MA was slightly better than the qPCR concerning the detection range, but in accordance with the HRM in terms of its variability and the estimation of the T_m. The obtained FO-

PCR-MA calibration curve will be used further to determine the celery DNA concentration in biological samples, while the assessed T_m will be used to confirm the identification of the amplified target sequence. Moreover, the newly developed FO-PCR-MA combines PCR and HRM in one step, which reduces the overall assay time for at least 25 min, whereas the time needed to perform sample preparation is the same for both approaches. Here, the exact difference in time-to-result was 1460 s, or 24.3 min, as the qPCR (30 cycles) followed by HRM took 4810 s while the FO-PCR-MA (40 cycles) had a time-to-result of 3350 s. Furthermore, as the FO-PCR-MA provides cycle-to-cycle information during the melting assay in real-time, the reaction can be stopped earlier. This means that, from the moment the signal reaches the threshold, all the information concerning identification and quantification of the sample will be present, which can significantly reduce the assay time.

3.3.3. Validation of established FO-PCR-MA with biological samples

The developed FO-PCR-MA biosensor for the quantification of celery DNA was further benchmarked with qPCR/HRM using three cleaning water samples spiked with celery. These samples were prepared as mentioned in Section 3.2.5. Sample DNA 1 and DNA 2 were spiked with celery derived from stem tissue, while DNA 3 contained celery leaf tissue. The celery DNA concentrations were determined in these samples with the FO-PCR-MA methodology (Figure 3.5A), using the calibration curve shown in Figure 3.4A and with the qPCR/HRM technology (Figure 3.5B), using the calibration curve shown in Figure 3.1A. The same FO-PCR-MA signal threshold of 0.095 nm/°C was applied on the spiked celery samples as it was for the samples in the calibration curve (Figure S3.4, Supplementary Information). Based on the qPCR/HRM and the FO-PCR-MA, the T_m of the three samples was estimated at 76.9 °C with a SD of 0.3 and 80.8 °C with a SD of 0.07, respectively (n = 3 for both analysis). The obtained values were in perfect accordance with the T_m determined in Figure 3.1B and Figure 3.4B, proving the correct identification of the amplified *Mtd* 3 target sequence in the cleaning water samples. As shown in Figure 3.5C, the celery concentrations quantified with the FO-PCR-MA biosensor correlated linearly with the corresponding qPCR/HRM results (R^2 = 0.96). Moreover, the ICC was calculated to be 0.94 (n = 3).

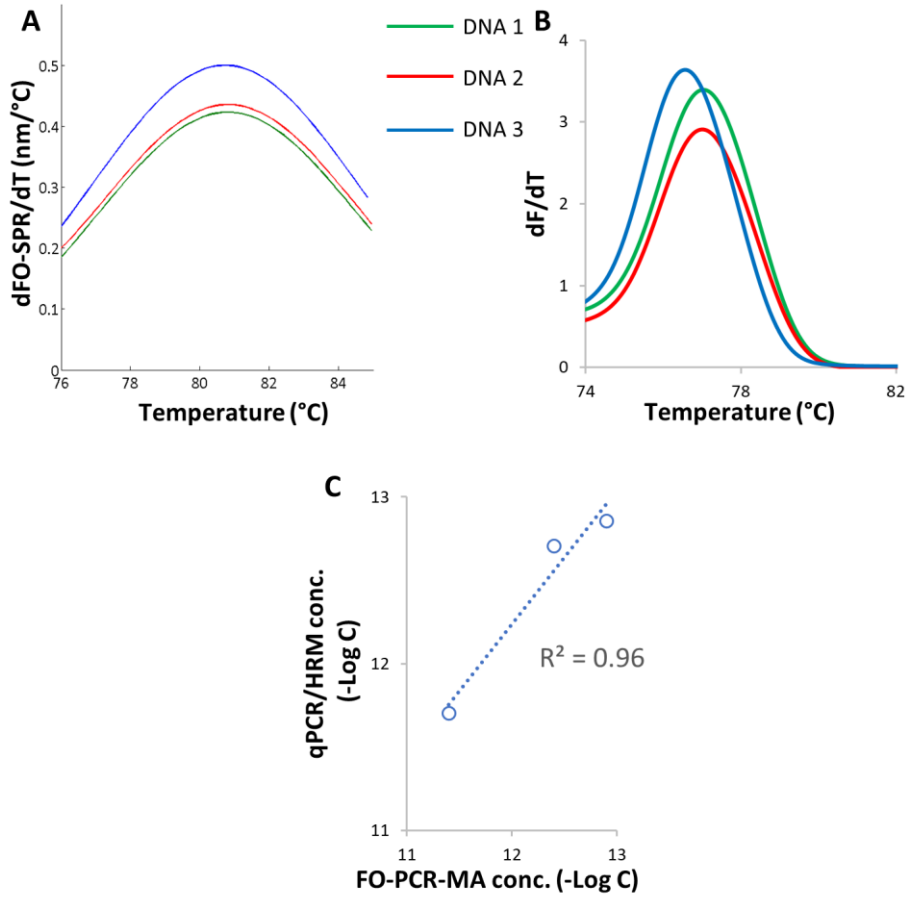

Figure 3.5: *Detection of celery in biological samples.* ***A)*** *FO-PCR-MA of the Mtd 3 target sequence in sample DNA 1, DNA 2 and DNA 3, cycle 35;* ***B)*** *HRM results of sample DNA 1, DNA 2 and DNA 3 after qPCR;* ***C)*** *Comparison of the Mtd 3 levels determined with the in-house developed FO-PCR-MA biosensor (40 cycles) and the qPCR/HRM test (30 cycles).*

3.4. Conclusions

For some hypersensitive patients, even traces of celery in food can often elicit life-threatening allergic reactions. Therefore, accurate identification and quantification of this common allergen is key in healthcare, biotechnology, and food quality and safety. The specificity issues when detecting celery DNA have been partially resolved by the introduction of qPCR/HRM. In search of new techniques to quantify celery, an in-house developed FO-SPR biosensor was explored in this proof-of-concept paper. Here, a real-time FO-PCR-MA approach was established based on the *Mtd* gene of celery and used to quantify this target between 1 pM and 0.1 fM. The developed concept was comparable with the qPCR/HRM analysis in terms of the linear range and the determination of the melting peaks. Finally, the FO-PCR-MA was benchmarked with a reference qPCR/HRM technique using cleaning water samples spiked with celery. This showed excellent agreement, as confirmed with the ICC of 0.94. In conclusion, this non-fluorescence-based technology platform holds great potential for the real-time detection and quantification of celery allergens. Furthermore, as this platform is fast, cost-effective and automated, it fulfils the requirements for the next generation of diagnostic tests.

3.5. Supplementary information

The specificity of a FO-SPR melting assay, as described by Knez *et al.*[21,22], was tested by performing multiplex analysis of a celery DNA sequence (originating from the *Api g 1* celery gene) and a carrot DNA sequence (originating from the *dau c1* carrot gene). The carrot DNA sequence was included as exogenous positive control to demonstrate the specificity of our assay because it is well known from literature that carrots show high cross reactivity with celery[2,6,7]. Sample mixtures consisted of 15 µL of the DNA targets (10 nM final concentration), added to 42 µL PBS with 300 mM NaCl, and 43 µL functionalized AuNPs. Before each measurement, the samples were heated to 94 °C for 5 s. Subsequently, the temperature was lowered to allow hybridization. After 15 min, the temperature was slowly raised (0.1 °C/s) till 94 °C. The results of the FO-SPR melting analysis experiments revealed 15 °C difference in melting temperature between the carrot and the celery DNA (Figure S3.1), confirming indeed that the designed FO-SPR melting assay is specific. The bump in the melting peak of celery DNA was hypothesized to result from the bulk process used to immobilize the DNA strands. The uncontrolled number of potential hybridizations per AuNP could lead to a significant group of AuNPs with multiple hybridizations, melting off with a slightly delay and causing the bump in the curve.

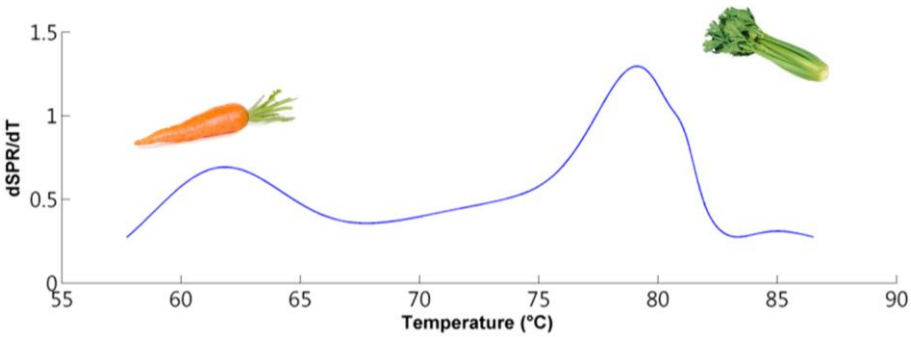

Figure S3.1: *A multiplex FO-SPR melting analysis performed for carrot DNA and celery DNA target sequences on the same FO-SPR sensor.*

Nevertheless, when the same celery sequence from the *Api g 1* gene (Figure S3.2A) was tested using qPCR/HRM together with 3 other sequences from *Mtd* celery gene (*Mtd*, *Mtd 2* and *Mtd 3*), Mtd (Figure S3.2B) and *Mtd 3* (Figure S3.2D), were identified as more optimal compared to *Api g 1* due to

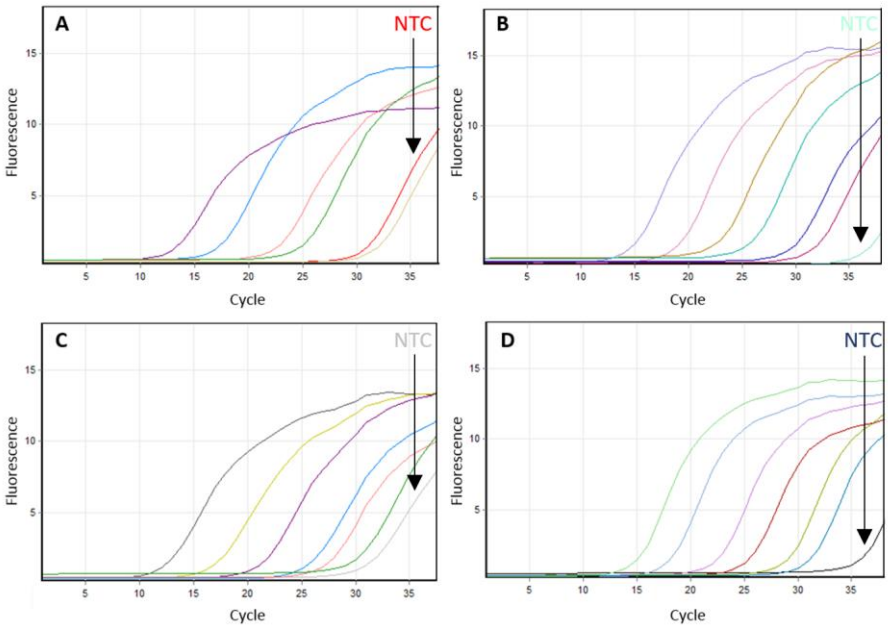

Figure S3.2: *qPCR signal for different concentrations of different synthetic targets (1 nM–10 fM):* ***A)*** *Api g 1,* ***B)*** *Mtd,* ***C)*** *Mtd 2 and* ***D)*** *Mtd 3 region. Non-template controls (NTC) have been included.*

the reproducible absence of signal in the NTC after 30 cycles. Because the specificity of *Mtd 3* sequence was confirmed through the BLAST report, this sequence was finally selected for all experiments as presented in this chapter.

The amplification of DNA in solution, by heating up and cooling down the PCR mixture, was studied in the presence of the FO-SPR sensor. The FO-SPR signal was continuously monitored with a thermocouple, which is the inverse of the temperature change. However, from the moment DNA target is amplified through the FO-PCR-MA above the detection threshold of the FO-SPR, the melting signal of the amplified DNA target will superimpose on the RI shift of the temperature measured with the FO-SPR sensor[14]. By taking the first order derivative of the SPR signal with respect to the temperature, the T_m of the *Mtd 3* target was resolved very precisely. When the FO-SPR melting peak height is plotted versus the PCR cycle number for different *Mtd 3* concentrations (Figure S3.3), it can be seen that melting peaks increase cycle-to-cycle. In Figure S3.4, the melting peak signals of the three spiked samples are visualized in function of the number of PCR cycles.

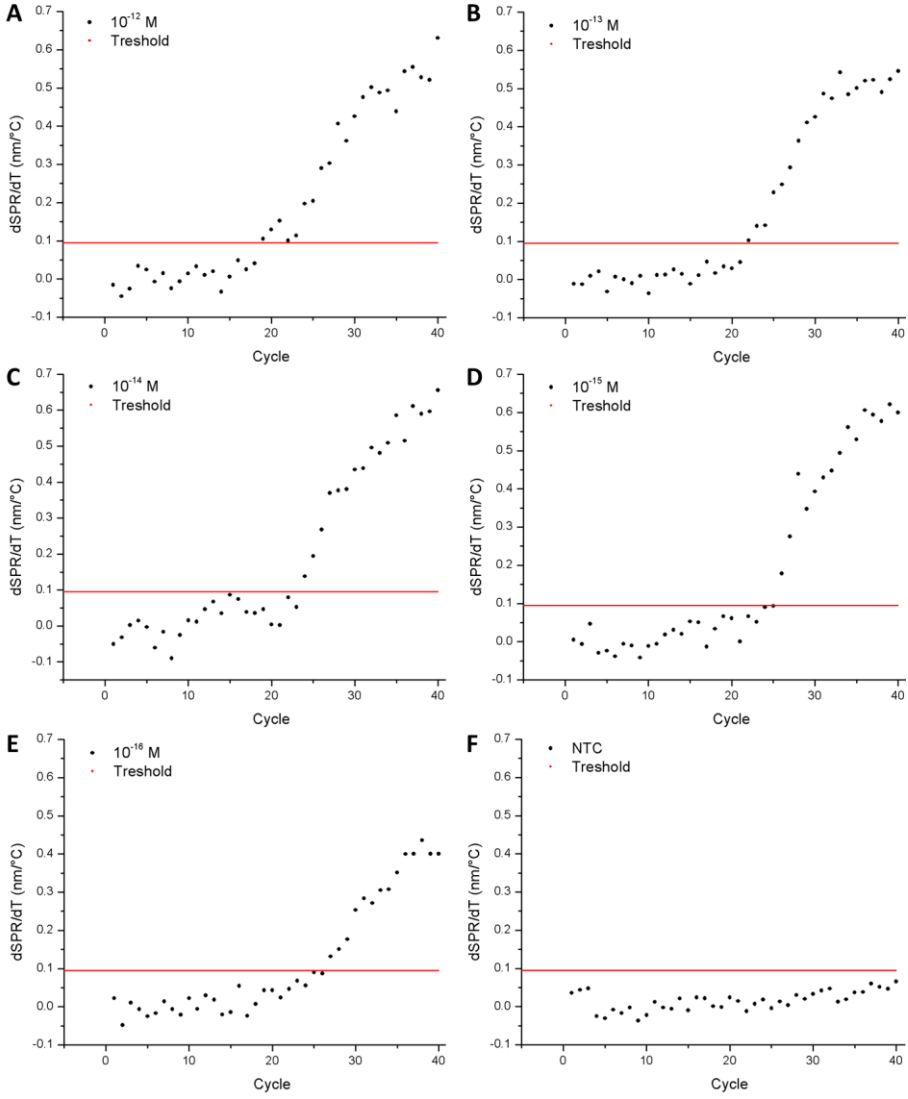

Figure S3.3: *Presentation of the melting peak signals in function of the number of PCR cycles. The FO-PCR-MA signal threshold of 0.095 nm/°C is depicted with the red line on the figures. Analysis of the signal height for different DNA concentrations (10^{-12} – 10^{-16} M) is shown for the Mtd 3 target sequence. Furthermore, the non-template control (NTC) analysis of the signal height is presented in the bottom right corner of the figure.*

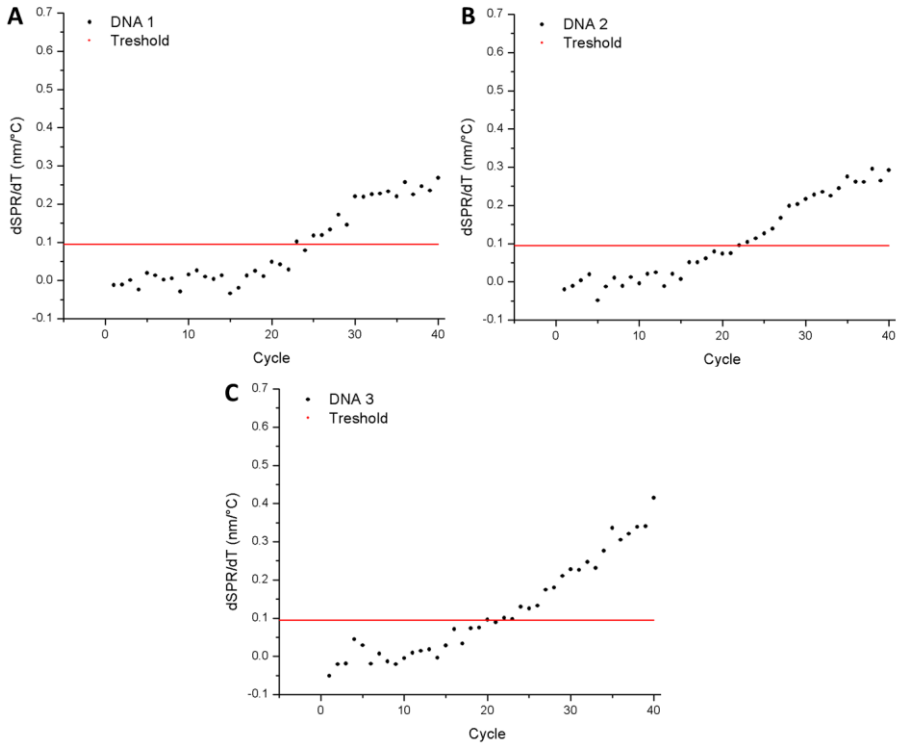

Figure S3.4: *Presentation of the melting peak signals in function of the number of PCR cycles. The FO-PCR-MA signal threshold of 0.095 nm/°C is shown on the figures. Analysis of the signal height of different spiked biological samples (**A)** DNA 1, **B)** DNA 2 and **C)** DNA 3) are shown for the Mtd 3 target sequence.*

To determine the error bars in Figure 3.4A, the following procedure was followed. First, the standard deviation on the FO-SPR signal of the last 5 cycles (here: cycles 36 till 40), where saturation occurs, was calculated. Assuming that the standard deviation is constant and independent of the cycle number, this value was transferred to the FO-PCR-MA signal threshold value (Th). The FO-PCR-MA signal threshold value plus one standard deviation (Th + 1 sigma) and minus one standard deviation (Th – 1 sigma) were calculated. The variability on the cycle number was then determined by taking the highest cycle number for which the FO-SPR signal was equal to Th – 1 sigma and by taking the lowest cycle number for which the FO-SPR value was equal to Th + 1 sigma. As this conversion is a non-linear transformation, the error bars in Figure 3.4A are typically asymmetric.

3.6. References

1. Wang, H., Li, G., Yuan, F., Wu, Y. & Chen, Y. Detection of the allergenic celery protein component (Api g 1.01) in foods by immunoassay. *Eur. Food Res. Technol.* **233**, 1023–1028 (2011).
2. Fuchs, M., Cichna-Markl, M. & Hochegger, R. Development and validation of a duplex real-time PCR method for the simultaneous detection of celery and white mustard in food. *Food Chem.* **141**, 229–235 (2013).
3. Palle-Reisch, M., Hochegger, R. & Cichna-Markl, M. Development and validation of a triplex real-time PCR assay for the simultaneous detection of three mustard species and three celery varieties in food. *Food Chem.* **184**, 46–56 (2015).
4. Commission, E. Directive 2003/89/EC of 10 November 2003 amending Directive 2000/13/EC as regards indications of the ingredients present in foodstuffs. *Off. J. Eur. Union* 15–18 (2003).
5. Commission, E. Directive 1169/2011 of the European Parliament and of the Council on the provision of food information to consumers, amending Regulations (EC) No 1924/2006 and (EC) No 1925/2006 of the European Parliament and of the Council, and repealing Commission Direc. *Off. J. Eur. Union* 18 (2011).
6. Faeste, C. K. *et al.* Differentiating cross-reacting allergens in the immunological analysis of celery (apium graveolens) by mass spectrometry. *J. AOAC Int.* **93**, 451–461 (2010).
7. Sun, M. *et al.* A novel loop-mediated isothermal amplification method for detection of the carrot materials in foods. *Eur. Food Res. Technol.* **241**, 295–302 (2015).
8. Demmel, A. & Hahn, A. Analytik von Lebensmittelallergenen. in *Molekularbiologische Methoden in der Lebensmittelanalytik* 169–192 (Springer Berlin Heidelberg, 2010). doi:10.1007/978-3-642-10716-0_11
9. Dovicovicova, L., Olexova, L., Pangallo, D., Siekel, P. & Kuchta, T. Polymerase chain reaction (PCR) for the detection of celery (Apium graveolens) in food. *Eur. Food Res. Technol.* **218**, 493–495 (2004).
10. Hupfer, C., Waiblinger, H.-U. & Busch, U. Development and validation of a real-time PCR detection method for celery in food. *Eur. Food Res. Technol.* **225**, 329–335 (2007).
11. Mustorp, S., Engdahl-Axelsson, C., Svensson, U. & Holck, A. Detection of celery (Apium graveolens), mustard (Sinapis alba, Brassica juncea, Brassica nigra) and sesame (Sesamum indicum) in food by real-time PCR. *Eur. Food Res. Technol.* **226**, 771–778 (2008).
12. Luber, F., Demmel, A., Pankofer, K., Busch, U. & Engel, K.-H. Simultaneous quantification of the food allergens soy bean, celery, white mustard and brown mustard via combination of tetraplex real-time PCR and standard addition. *Food Control* **47**, 246–253 (2015).
13. Stephan, O. *et al.* Protein Quantification, Sandwich ELISA, and Real-Time PCR Used to Monitor Industrial Cleaning Procedures for Contamination with Peanut and Celery Allergens. *J. AOAC Int.* **87**, 1448–1457 (2004).
14. Daems, D., Knez, K., Delport, F., Spasic, D. & Lammertyn, J. Real-time PCR melting analysis with fiber optic SPR enables multiplex DNA identification of bacteria. *Analyst* **141**, 1906–1911 (2016).
15. Schasfoort, R. B. M. & Tudos, A. J. *Handbook of Surface Plasmon Resonance*. (Royal Society of Chemistry, 2008). doi:10.1039/9781847558220
16. Homola, J. Surface Plasmon Resonance Sensors for Detection of Chemical and Biological Species. *Chem. Rev.* **108**, 462–493 (2008).

17. Pollet, J., Janssen, K. P. F., Knez, K. & Lammertyn, J. Real-time monitoring of solid-phase PCR using fiber-optic SPR. *Small* **7**, 1003–1006 (2011).
18. Aray, A. *et al.* SPR-based plastic optical fibre biosensor for the detection of C-reactive protein in serum. *J. Biophotonics* **9**, 1077–1084 (2016).
19. Caucheteur, C., Guo, T. & Albert, J. Review of plasmonic fiber optic biochemical sensors: improving the limit of detection. *Anal. Bioanal. Chem.* **407**, 3883–3897 (2015).
20. Ribaut, C. *et al.* Cancer biomarker sensing using packaged plasmonic optical fiber gratings: Towards in vivo diagnosis. *Biosens. Bioelectron.* **92**, 449–456 (2017).
21. Knez, K., Janssen, K. P. F., Pollet, J., Spasic, D. & Lammertyn, J. Fiber-Optic High-Resolution Genetic Screening Using Gold-Labeled Gene Probes. *Small* **8**, 868–872 (2012).
22. Knez, K. *et al.* Spherical Nucleic Acid Enhanced FO-SPR DNA Melting for Detection of Mutations in Legionella pneumophila. *Anal. Chem.* **85**, 1734–1742 (2013).
23. Tran, D. T. *et al.* Selection of aptamers against Ara h 1 protein for FO-SPR biosensing of peanut allergens in food matrices. *Biosens. Bioelectron.* **43**, 245–251 (2013).
24. Lu, J. *et al.* Fiber optic-SPR platform for fast and sensitive infliximab detection in serum of inflammatory bowel disease patients. *Biosens. Bioelectron.* **79**, 173–179 (2016).
25. Pollet, J. *et al.* Fast and accurate peanut allergen detection with nanobead enhanced optical fiber SPR biosensor. *Talanta* **83**, 1436–1441 (2011).
26. Pollet, J. *et al.* Fiber optic SPR biosensing of DNA hybridization and DNA–protein interactions. *Biosens. Bioelectron.* **25**, 864–869 (2009).
27. Pafundo, S., Gullì, M. & Marmiroli, N. Comparison of DNA Extraction Methods and Development of Duplex PCR and Real-Time PCR To Detect Tomato, Carrot, and Celery in Food. *J. Agric. Food Chem.* **59**, 10414–10424 (2011).
28. Malanoski, A. P., Lin, B., Wang, Z., Schnur, J. M. & Stenger, D. A. Automated identification of multiple micro-organisms from resequencing DNA microarrays. *Nucleic Acids Res.* **34**, 5300–5311 (2006).
29. Hurst, S. J., Lytton-Jean, A. K. R. & Mirkin, C. A. Maximizing DNA Loading on a Range of Gold Nanoparticle Sizes. *Anal. Chem.* **78**, 8313–8318 (2006).
30. Koch, G. G. Intraclass Correlation Coefficient. in *Encyclopedia of Statistical Sciences* (John Wiley & Sons, Inc., 2006). doi:10.1002/0471667196.ess1275.pub2

Chapter 4

Innovative ligation strategy for FO-SPR surface functionalization

---

The work in this chapter was adapted from:

Daems, D., Delport, F., Lammertyn, J. and **Peeters, B.**, NUCLEIC ACID ENZYME SENSOR, WO/2019/030383, https://patentscope.wipo.int/search/en/detail.jsf?docId=WO2019030383

Peeters, B., Daems, D., Van der Donck, T., Delport, F. & Lammertyn, J. Real-Time FO-SPR Monitoring of Solid-Phase DNAzyme Cleavage Activity for Cutting-Edge Biosensing. *ACS Appl. Mater. Interfaces* 11, 6759–6768 (2019).

Contributions of Peeters B. to this manuscript:

Planning and performing of the experiments, data processing and analysis, writing and editing of the manuscript.

4.1. Introduction

Previous chapter showed how innovative FO-SPR implementation of NA-based strategies such as PCR and HRM can further improve the melting peak resolution and illustrate potential applicability in more complex matrices. Next to that, Chapter 1 and 2 revealed that over the last three decades NA research has been expanding the repertoire of DNA characteristics and functionalities significantly[1]. While the field of functional NAs is still immature, DNA nanotechnology in general has illustrated its many applications in different areas[2]. In biosensing, DNA molecules and structures are mainly used for nanostructuring of sensor surfaces[3], target recognition[4] and signal amplification[5]. In particular, functional NAs such as aptamers show high affinity for specific target molecules[6], while DNAzymes are of great interest in isothermal signal generation and amplification[5,7]. Among the broad variety of DNAzymes, RCDs are being explored for the detection of proteins and NAs[8]. RCDs are characterized by a small catalytic core accompanied by two binding arms, showing stable activity in the presence of their metal ion cofactors[9,10]. Their enzymatic activity is mainly determined by the catalytic core, enabling substantial freedom in redesigning the binding arms for any RNA or DNA/RNA chimeric substrates of interest (Chapter 2).

New functional DNA molecules and their potential applications ask for innovative ways of implementation. SPR-based biosensing mainly makes use of binding-assays, relying on the immobilized bioreceptor and a secondary labelling step if needed[11]. For DNA-based SPR assays, the bioreceptor and labelling of choice are ssDNA capture and detection probes as described in Chapter 2. Initial RCD-based SPR sensors have been restricted to this binding strategy for the detection of cleaved DNAzyme products[12,13]. Due to the small size of the DNAzyme substrate sequences (< 40 nt), labeling of their products is required and usually done with ssDNA functionalized AuNPs[14]. Other readout systems have explored the immobilization of the DNAzymes themselves, combined with prehybridization of labelled DNAzyme substrates[15,16]. This enabled direct monitoring of the DNAzyme cleavage activity, triggered by the metal ion cofactors of interest. However, multiple turnover activity of the DNAzymes in this format is not fully exploited, limiting the maximal signal amplification by these DNAzymes. Immobilization of labelled DNAzyme substrates in excess would enable

multiple turnover activity but is more challenging in getting specific and efficient signal generation, if based on simple hybridization protocols. In this type of protocol, the DNAzyme substrate would be immobilized as a DNA capture or detection probe, using a bulk process such as thiol chemistry (Chapter 2). Assuring that every immobilized DNAzyme substrate sequence gets labelled and that every label is bound by a single substrate sequence can therefore not be controlled. Moreover, relying on hybridization protocols limits the sensors stability in terms of pH, temperature and ionic strength because of the non-covalent nature of hybridization bonds.

One way to obtain more specific and stable surface functionalization is the use of enzyme-mediated coupling strategies[17–19]. In case of proteins, site-directed immobilization has been reported by means of *Staphylococcus aureus* sortase A[19]. Recombinant proteins, each labelled with a sortase A recognition motif, were immobilized via sortase A mediated transpeptidation to pre-functionalized Biacore chips with glycine-linker peptides. Main advantages were the site-specific covalent coupling of the ligand to the surface, enabling improved orientation, uniformity and stability of the immobilized proteins. For DNA, enzymatic ligation reactions have been used mainly in context of single nucleotide polymorphism detection because of the high specificity of the reaction[20], but also few reports apply ligation for surface functionalization[18], DNA computing[21] and the creation of nanostructures[22]. Lee *et al.* described surface ligation with the T4 DNA ligase to create RNA-DNA microarrays[18]. Prefunctionalized chips with DNA capture probes enabled immobilization of ssRNA sequences in a rapid and biocompatible format, minimizing potential damage and handling of the surface RNA probe molecules. Bioactivity of the array was proved by subsequent hybridization of complementary DNA to the RNA probes and hydrolysis of the surface-bound RNA by ribonucleases.

Based on the previously reported characteristics of ligation, **the objective of this chapter is the design of a ligation strategy to functionalize Au-surfaces in a one-step assay with labelled DNA-RNA hybrid sequences, able to act as robust DNAzyme substrates.** Compared to the classical hybridization approach, ligation and proper sequence design can assure that complete DNAzyme substrates are only formed if ligation takes place. Therefore, formation of unlabeled DNAzyme substrates, which are very

challenging to detect due to their size, can be avoided. To do so, we present for the first time the design of a covalently, AuNP-labelled FO-SPR sensor towards the detection of DNAzyme cleavage activity. The FO-SPR platform is selected based on several features, such as its AuNP compatibility, dip probe format and real-time analysis capacity of molecular binding events. AuNP-labelling of DNAzyme substrate sequences is integrated into the ligation reaction and several ligation parameters are optimized to obtain maximal signal generation.

4.2. Experimental section

4.2.1. Materials and reagents

All DNA sequences were synthesized and purified by Integrated DNA Technologies (IDT, Leuven, Belgium). Full sequence information is provided in Table S4.1 of the Supplementary Information. Trizma®base, sodium dodecyl sulfate (SDS) and DNA/RNAse-free water were purchased from The Merck group - Sigma-Aldrich (Bornem, Belgium). Potassium dihydrogen phosphate and sodium chloride were obtained from The Thermo Fisher Scientific group - Fisher Scientific (Merelbeke, Belgium) and dipotassium hydrogen phosphate and 1,4-dithiothreitol (DTT) from AppliChem GmbH (Darmstadt, Germany). Ethylenediaminetetraacetic acid (EDTA) was purchased from Acros Organics (Geel, Belgium), sodium hydroxide from Chemlab (Zedelgem, Belgium) and ethanol absolute from VWR Chemicals (Haasrode, Belgium). Both Illustra NAP-5 columns and Immobiline 9854DryStrip Cover Fluid were obtained from GE Healthcare Life Sciences (Diegem, Belgium). AuNPs (Ø 20 nm) were provided by BBI Solutions (Cardiff, UK) and PEG-molecules ($C_{27}H_{55}NO_9S$), used as a backfilling molecule, by Polypure AS (Oslo, Norway). The Ampligase® Thermostable DNA Ligase (5U/µL) with accompanying 10× reaction buffer was purchased from Epicentre® (Madison, USA).

Sensor preparation and reaction buffers were the following: PB buffer (180 mM phosphate, pH 8), PB-SDS buffer (10 mM phosphate, 0.01 % (w/v) SDS, pH 8.0), TE buffer (10 mM Tris, 1 mM EDTA, pH 8) and Tris-SDS buffer (20 mM Tris buffer, 0.01 % (w/v) SDS, pH 8.3).

4.2.2. FO-SPR sensor fabrication and gold surface functionalization

An overview of the FO-SPR experimental setup is presented in the Supplementary Information (Figure S4.1). Production of the FO-SPR sensors was based on the design described by Lu *et al.*[23]. Briefly, an optical fiber (Thorlabs, Newton, USA) (Ø 400 µm) was cut to a final length of 4.3 cm. Both endings were stripped and cleaned to remove the jacket and cladding respectively. The FO-SPR sensor was coated with a 50 nm gold layer, after which the FO-SPR sensor was ready for functionalization. The gold surfaces were functionalized based on the work of Hurst *et al.* and Daems *et al.*[24,25]. Both the FO-SPR sensors and the AuNPs were incubated with 1 µM thiolated DNA strands (Table S4.1), reduced in 0.05 M DTT in PB buffer prior to use. After an overnight incubation, the FO-SPR sensors and AuNPs were washed with Tris-SDS (dipped 5× in 2 mL) and PB-SDS (3× centrifuging at 16,200 g for 15 min and resuspended in a final volume of 1 mL). Next, backfilling of the FO-SPR sensors and AuNPs was done with 50 µM PEG-molecules for 1 h. The FO-SPR sensors were then washed with and stored in Tris-SDS at 4 °C until further use. The AuNPs were washed two times with PB-SDS and finally resuspended in DNA/RNAse-free water to a final concentration of 4.65 nM by measuring the maximal optical density (OD) at 530 nm with a microplate reader SpectraMax® M2/M2e (Molecular devices, San Jose, USA).

4.2.3. AuNP-ligation to the FO-SPR sensor surface

Creating a AuNP-labelled DNAzyme substrate coupled to the FO-SPR sensors was realized by means of ligation. A ligation reaction mix was prepared containing 1× Ampligase buffer, 0, 10, 100 or 1000 nM of ligation template, Ampligase (0.05 U/µL) and 2.32 nM functionalized AuNPs in a final volume of 100 µL. Prior to ligation, a baseline signal was established for 5 min in 20 mM Tris (pH 8.3), followed by incubation of the FO-SPR sensors in the ligation mixture for 20 min. Next, the FO-SPR sensors were washed for 4 min in 20 mM Tris (pH 8.3), two times 30 s in 10 mM NaOH and afterwards a second baseline was recorded in Tris buffer. All reaction vials were heated simultaneously to 50, 55 or 60 °C, and covered with 50 µL mineral oil (to avoid evaporation). The FO-SPR signals were monitored in real-time on an in-house developed FO-SPR system described by Lu *et al.*[23]. Finally, the AuNP-labelled

FO-SPR sensors were stored in Tris-SDS at 4 °C until further use in the DNAzyme-based experiments.

4.2.4. SEM images and data analysis

High-resolution scanning electron microscopy (SEM) images were made with a FEI Nova Nanosem 450 (The Thermo Fisher Scientific group – FEI, Hillsboro, USA). Visualization of the 20 nm AuNPs was established with a backscatter detector (CBS, concentric backscatter detector) using an acceleration voltage of 4.5 kV in the column and a magnification of 100,000. Applying a bias of 4 kV on the stage enabled beam deceleration, resulting in a landing energy of 500 V. To obtain stable imaging, drift corrected frame integration (DCFI) was used. The difference in contrast of the images could be explained by small differences in the sample preparation and different position of the image on the FO-SPR sensor surface. Quantification of the AuNPs was done by using ImageJ 1.48v (National Institutes of Health, Bethesda, USA)[26], a Java-based image-processing program. For every condition with images with a surface area of 7.5 μm^2 were sharpened if needed and after setting the proper noise tolerance, the AuNPs could be counted using the 'Find Maxima' tool in ImageJ. For every condition, the AuNP-density was determined for three images at different locations on the same fiber.

FO-SPR data were recorded with LabView (National Instruments, Austin, USA) and further processed using Matlab 2015b (The MathWorks Inc., Natick, USA). The FO-SPR signals were normalized by subtraction of the initial average baseline and different steps were distinguished within both the ligation and DNAzyme activity sensorgrams. Different parameters were defined to enable statistical analysis with JMP®13 (SAS Institute Inc., Cary, USA): (i) ligation shift and ligation efficiency. Significant differences were analyzed by performing one-way ANOVA followed by Tukey multiple comparison with an α-level of 0.05.

4.3. Results and discussion

4.3.1. Ligation-based functionalization of FO-SPR sensor surface

The ligation strategy to functionalize the FO-SPR sensor with AuNP-labelled substrates is depicted in Figure 4.1. Three DNA oligos are used to perform the ligation: (i) a 5'-thiolated FO-SPR oligo immobilized on the FO-SPR sensor surface, (ii) a 3'-thiolated AuNP oligo immobilized on the AuNP surface and (iii) a ligation template partially complementary to both the FO-SPR and AuNP oligo. Upon hybridization of the FO-SPR and AuNP oligo with the ligation template, the ligase recognizes the nick in the double DNA strand and links the 5'-phosporylated AuNP oligo with the FO-SPR oligo by a NAD-dependent ligation. As a result, AuNP-labelled DNAzyme substrates are formed. AuNP labels are well-known to significantly amplify the FO-SPR response signals[27] and are introduced here towards real-time direct monitoring of the DNAzyme cleavage activity. Furthermore, the FO-SPR and AuNP oligos are designed in such a way that both DNA oligos contain a part of the DNAzyme substrate, eliminating DNAzyme cleavage of unlabeled substrates. In order to realize the proposed ligation-based functionalization of the FO-SPR sensor surface, a first set of experiments is devoted to finding an optimal ligation temperature for AuNP-labelling of the FO-SPR oligos. A second set of experiments focused on optimizing the ligation template concentration to obtain maximal signal generation.

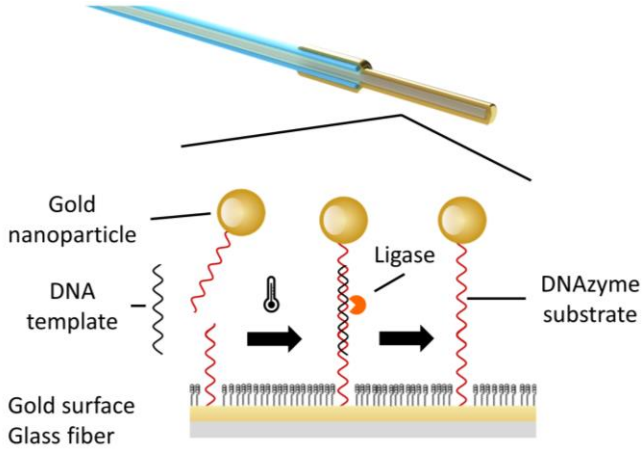

Figure 4.1: *Illustration of the ligation strategy.*

4.3.2. Screening of an optimal ligation temperature

RCDs are characterized by a cleave and release process, requiring labelled substrates to monitor the surface catalytic activity. Therefore, a ligation strategy was used, having important advantages such as: (i) the covalent linkage of AuNP labels to the DNAzyme substrate, stabilizing and creating a robust sensor surface and (ii) the elimination of non-labelled DNAzyme substrates. Cleavable substrates are only formed where ligation has taken place and minimizes the occurrence of DNAzyme cleavage without any signal generation. The AuNP-labelling of the immobilized FO-SPR oligos on the sensor surface depends on the ligation template concentration, the functionalized AuNP concentration, the amount of ligase, the incubation temperature and time. Both the ligation temperature and template concentration were studied in more detail in this chapter, while the other parameters were fixed based on previous work of Knez *et al.*[28,29] and the Ampligase product specifications.

While changing and studying the parameter of interest, the FO-SPR shift was monitored in real-time and consists of four different steps as illustrated in Figure 4.2A. Step 1 represents a first stabilization step, which enables the FO-SPR sensor to reach its baseline level. Initial signal drift is caused by a change in RI going from air to buffer and the increasing temperature, as the FO-SPR sensor is temperature sensitive. In step 2, binding of the AuNPs to the FO-SPR sensor surface through hybridization between the ligation template, FO-SPR and AuNP oligos causes the FO-SPR shift to increase. The nick in every hybridization complex, if recognized by the ligase, gets covalently coupled to form a AuNP-labelled DNAzyme substrate (Figure 4.1). In this step, also the non-ligated hybridization complexes contribute to the corresponding FO-SPR shift. Step 3 represents a washing step in Tris buffer and two times in NaOH, clearly distinguishable by the short RI changes in air when switching reaction vials. During this step, all hybridization complexes are dehybridized, removing all ligation templates and non-ligated AuNP labels to make the AuNP-labelled DNAzyme substrates available and avoid any nonspecific release of AuNPs during target detection. Finally, step 4 corresponds to a second stabilization step, which enables the FO-SPR sensor to reach a new baseline level in the identical conditions of step 1.

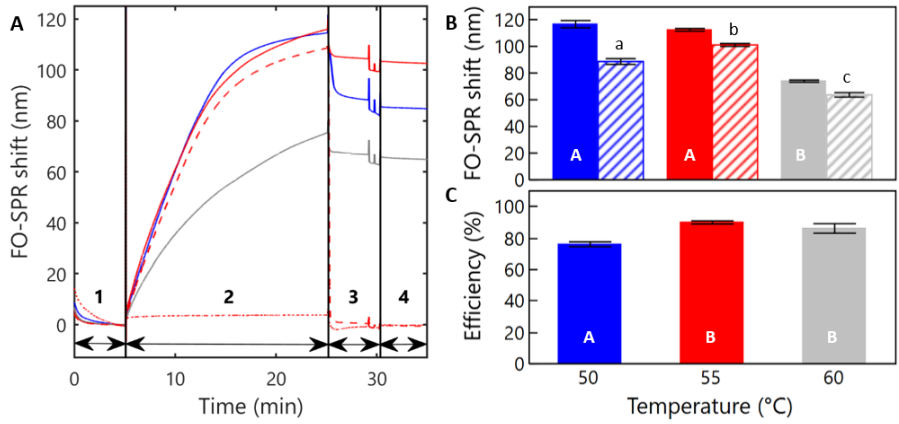

Figure 4.2: *Ligation temperature screening.* ***A)*** *Real-time FO-SPR shifts for ligation at 50 °C (blue), 55 °C (red) and 60 °C (grey). Controls containing no ligase (dashed line) or no template (dotted line) were included to evaluate nonspecific adsorption at 55 °C. Every measurement consists of 4 steps: 1) first baseline in buffer, 2) hybridization and ligation, 3) washing and 4) second baseline in buffer;* ***B)*** *FO-SPR shifts before washing (filled bars) and final ligation shifts after washing (shaded bars) and* ***C)*** *ligation efficiency. Error bars represent one standard deviation (n = 4). Upper- or lower-case letters group the factor levels between which Tukey multiple comparison was applied. Different letters indicate significant differences (P < 0.05).*

Optimal reaction conditions were defined as those resulting in a large FO-SPR shift at the end of step 4. This depends on the hybridization with the ligation template and actual ligation, both taking place in the same reaction vial in step 2. Therefore, the process is strongly dictated by a proper reaction temperature for both the hybridization complex formation and the ligase activity. The ligation process was first evaluated for three different temperatures, while keeping the ligation template concentration constant. As can be seen in step 2, the FO-SPR shifts increase significantly for all temperatures, except for both control experiments evaluating the FO-SPR shift in the absence of ligase or ligation template (Figure 4.2A). Moreover, the exact FO-SPR shifts determined as the difference between the start- and endpoint of step 2 are similar for 50 and 55 °C, but lower for 60 °C (Figure 4.2B). This depends on the sequence complementarity and T_m of the formed hybridization complex, being 65.1 °C with a SD of 0.3 (Figure S4.2). The decrease at 60 °C is explained by the fact that the reaction conditions are approaching the T_m of the hybridization complex. For the similar FO-SPR shifts at 50 and 55 °C, both well below the T_m, it is hypothesized that the change in hybridization equilibrium by the temperature difference of 5 °C is not significant to cause any change in the FO-SPR shift. Furthermore, final

ligation shifts were determined as the absolute difference between both baselines (step 1 and 4) after washing (step 3), because hybridization complexes where no ligation took place only release their non-covalent AuNP labels in step 3. This causes the FO-SPR shifts to decrease again for all temperatures in step 3. As the ligase's activity increases with temperature and has an optimum at 68 – 72 °C (see product specifications), an increasing ligation shift could be expected. As can be seen, the ligation shifts were found to indeed first increase significantly with temperature and decrease again at 60 °C (due to the lower FO-SPR shift at 60 °C in step 2 as explained earlier).

In addition to a large ligation shift, an optimal ligase activity is desired, meaning that all hybridized AuNPs are also ligated to the FO-SPR sensor surface. Ligation efficiencies were also determined as a function of temperature and defined as the ratio of the FO-SPR shift before the wash step and the final ligation shift (Figure 4.2C). Initially, the ligation efficiencies increased significantly, reaching a value of 90.0 % with a SD of 1.0 at 55 °C which did not improve further. Based on the maximal ligation shift of 101.5 nm with a SD of 2.1 and the ligation efficiency of 90.0 % with a SD of 1.0, 55 °C was regarded as the optimal temperature and selected for all further experiments. Compared to the typical range of FO-SPR shifts around 10 nm previously reported[23,30,31], the range of the obtained FO-SPR shifts is more than 10-fold higher. This can be explained by using relatively short DNA oligos, a higher AuNP concentration and the specific choice of incubation time and reaction temperature in order to improve and maximize FO-SPR parameters such as the FO-SPR shift, the dynamic range and the LOD.

4.3.3. Screening of an optimal template concentration

Furthermore, the screening of the ligation template concentration is visualized in Figure 4.3. The ligation shifts and ligation efficiencies were monitored in real-time (data not shown) and determined for 0, 10, 100 and 1000 nM ligation template. The ligation shift (Figure 4.3A) for 10 nM ligation template was significantly lower compared to the shift at higher ligation template concentrations. Further increase of the ligation template concentration enabled more AuNPs to bind the FO-SPR sensor and eventually for template concentrations ≥ 100 nM a saturation level on the FO-SPR sensor was reached. This saturation level is determined both by the geometry and steric interactions of the AuNPs under specified reaction

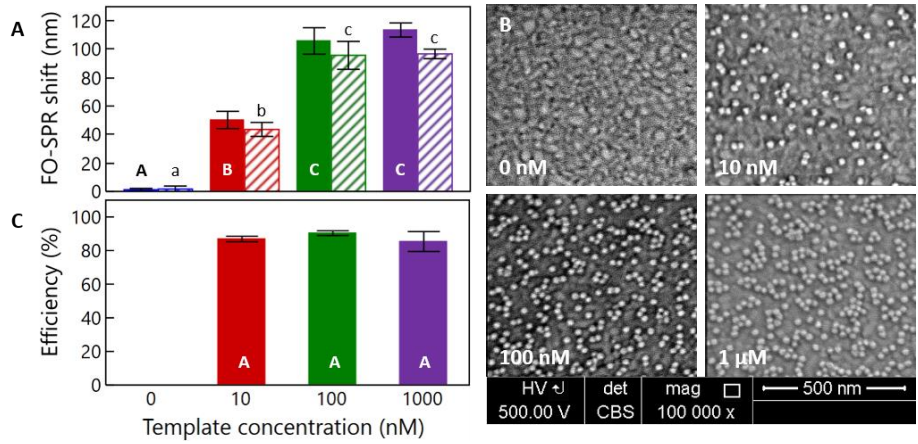

Figure 4.3: *Screening of the ligation template concentration.* ***A)*** *FO-SPR shifts before washing (filled bars) and final ligation shifts (shaded bars),* ***B)*** *SEM images of 4 different FO-SPR sensors after ligation with 0, 10, 100 and 1000 nM ligation template.* ***C)*** *Ligation efficiencies. Error bars represent one standard deviation (n = 4). Upper- or lower-case letters group the factor levels between which Tukey multiple comparison was applied. Different letters indicate significant differences (P < 0.05).*

conditions. In addition, the ligation of AuNPs to the FO-SPR sensor surface was evaluated with high resolution SEM images. Figure 4.3B shows part of the SEM images made for every ligation condition using a different ligation template concentration (full images, Figure S4.3). In case of 0 nM ligation template, nonspecific binding to the FO-SPR sensor surface caused few AuNPs to be observed, resulting in a AuNP density of 5 particles/µm² with a SD of 6 by counting the AuNPs in the SEM images. Furthermore, the SEM image at 0 nM ligation template shows the gold islands, which are formed during the sputtering process due to the initiation of gold deposition at different locations[32]. By increasing the ligation template concentration, an increasing amount of AuNPs was ligated to the FO-SPR sensor surface: the AuNP densities were 244 particles/µm^2 with a SD of 31, 666 particles/µm^2 with a SD of 56 and 678 particles/µm^2 with a SD of 95 for 10, 100 and 1000 nM ligation template, respectively. A saturation was obtained for 100 nM ligation template (Figure S4.4). Figure 4.3C depicts that the ligation efficiencies do not significantly depend on the template concentration. Based on the saturating ligation shifts at higher template concentrations (≥ 100 nM), 100 nM template with a ligation efficiency of 90.3 % with a SD of 1.4 was selected and will be used together with the optimal temperature of 55 °C in all further experiments, following in Chapters 5 and 6.

4.4. Conclusions

In this chapter we demonstrated for the first time a robust ligation strategy, linking DNA functionalized AuNPs covalently to the surface of a FO-SPR sensor in a controllable manner. Specific sequence design in combination with ligation enabled both formation and immobilization of AuNP-labelled DNAzyme substrates. Moreover, the ligation strategy eliminated the presence of non-labelled substrates, minimizing the interference with future DNAzyme-based signal generation. The AuNP surface density was controlled through the selection of the ligation temperature and ligation template concentration. Optimal values in order to maximize the signal generation were 55 °C and 100 nM of template concentration, establishing a 10-fold increase of the FO-SPR shifts usually measured. Furthermore, the quality of the designed ligation strategy is also reflected in the average ligation efficiency of 90.3 % with a SD of 1.4, which is similar than previously reported value of 80 % with a SD of 20 for the creation of RNA microarrays, but more reproducible[18].

Based on the successful ligation strategy developed in this chapter, Chapter 5 will use this FO-SPR design to evaluate its suitability for real-time detection of DNAzyme cleavage activity. In turn, this real-time DNAzyme activity sensor will be explored for biosensing applications. Once the suitability of the FO-SPR design is proven, future work could focus on functionalization strategies enabling every AuNP label to be bound by a single DNAzyme substrate sequence. Due to the size of the AuNP and the way of functionalization, the formation of more than one DNAzyme substrate per AuNP label could not fully be avoided by the proposed ligation strategy. Other approaches to further improve the sensor's performance is changing the AuNP size, shape and density to optimize the mass and coupling effect of the particles. Finally, redesigning the ligation template and associated FO-SPR and AuNP oligo could enable the use of different substrates, creating some interesting flexibility in the choice of the RCD of interest.

4.5. Supplementary information

Table S4.1: *DNA sequences*

Sequence name	Length (nt)	Sequence 5' -> 3'
FO-SPR oligo	33	HS-TTTTTTTTTTGAGGGATTATAGTAT**CAGCACAA**
AuNP oligo	23	Phos-**CCrGrUCACCAACCG**TTTTTTTTTT-SH
Template	24	TTGGTGACGGTTGTGCTGATACTA

Note

1. Bold region is bound by the DNAzyme
2. RNA-DNA hybrid substrate sequence is based on Bone *et al.* (2014)[33].

4.5.1. Material and methods

4.5.1.1. FO-SPR experimental setup

A picture of the in-house developed FO-SPR experimental setup is presented in Figure S4.1 and was based on Lu *et al.*[23]. All optics are integrated on a computer-controlled robot system to automate the movement of two FO-SPR sensors. Two tungsten halogen light sources (HL-2000, Ocean optics, Dunedin, USA) are used and sent light through a bifurcated fiber (Ocean optics, Dunedin, USA) into the FO-SPR sensor, which is in contact with the bifurcated fiber using a connector. Upon reaching the FO-SPR sensor's sensing tip, the SPR effect is created and reflected into the second part of the bifurcated fiber to a spectrometer (USB4000, Ocean Optics, Dunedin, USA). The resulting SPR signal is monitored by a LabVIEW program and the reaction temperatures were controlled by a T1 thermocycler (Biometra, Goettingen, Germany).

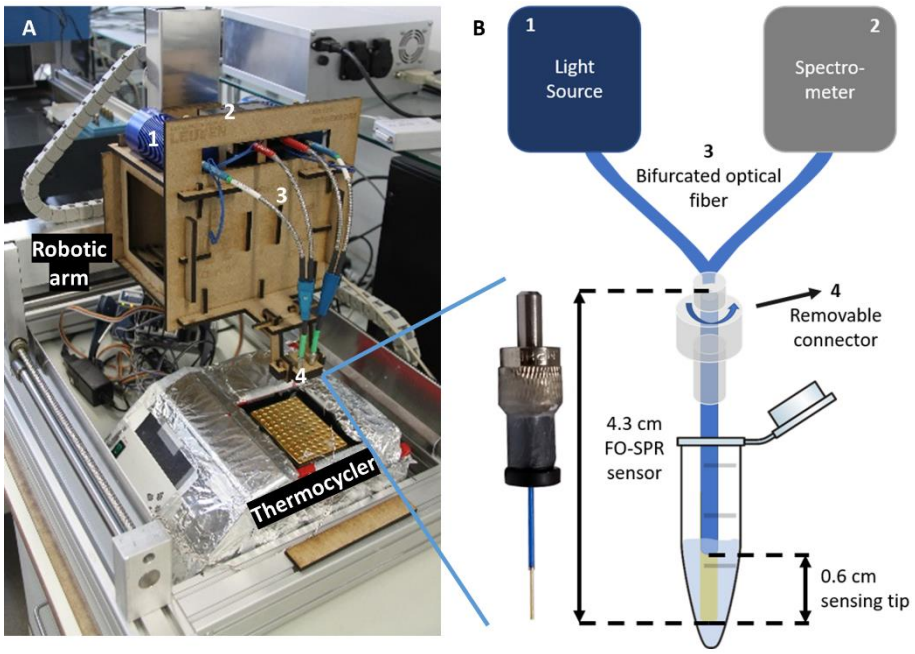

Figure S4.1: *Overview FO-SPR setup.* ***A)*** *Picture of the experimental setup and* ***B)*** *a schematic representation with 1) a light source, 2) a spectrometer, 3) a bifurcated fiber and 4) a connecting piece to mount the FO-SPR sensor. All components were integrated on a robotic arm and temperature was controlled with a thermocycler.*

4.5.1.2. FO-SPR high resolution melting

The HRM was performed by incubation of the functionalized FO-SPR sensor in a ligation mix containing 1× Ampligase buffer, 100 nM of ligation template, 2.32 nM functionalized AuNPs in a final volume of 100 µL, but without any Ampligase. Prior to melting, the ligation template, FO-SPR- and AuNP-probe were hybridized for 20 min at 50 °C. Thereafter, the temperature was increased up to 95 °C (ramp speed = 0.1 °C/s) and the T_m was determined as the maximal value of the temperature derivative of the FO-SPR sensogram. The melting peaks were fitted with a 1-term Gaussian function using Matlab 2015b.

4.5.2. Results and discussion

4.5.2.1. Determination lower melting temperature ligation complex

Since ligation is a temperature dependent process, this parameter was considered during the optimization of the ligation efficiency. The Ampligase requires a third DNA strand or template strand to line up the FO-SPR and AuNP oligo next to each other, enabling ligation by removing the nick and creating a phosphodiester bond. This alignment relies on simple hybridization with both the FO-SPR and AuNP oligo, which have a complementarity with the ligation template of 14 and 10 nucleotides, respectively. The optimal ligation temperature is therefore restricted by the lower T_m of the AuNP-probe and was determined by HRM on the FO-SPR sensor. This resulted in an average T_m of 65.05 °C with a SD of 0.25 (Figure S4.2).

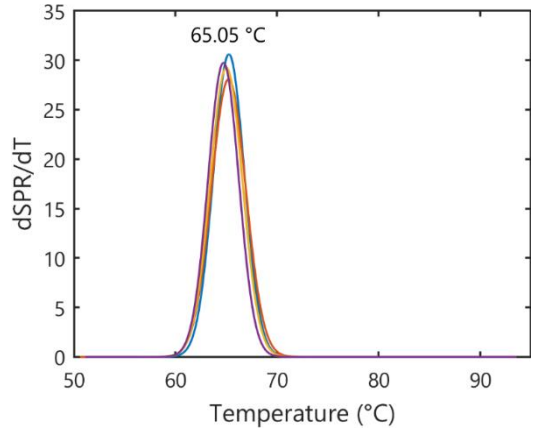

Figure S4.2: *FO-SPR high resolution melting. The lower T_m of the ligation complex was determined based on four experiments.*

4.5.2.2. SEM images and AuNP count

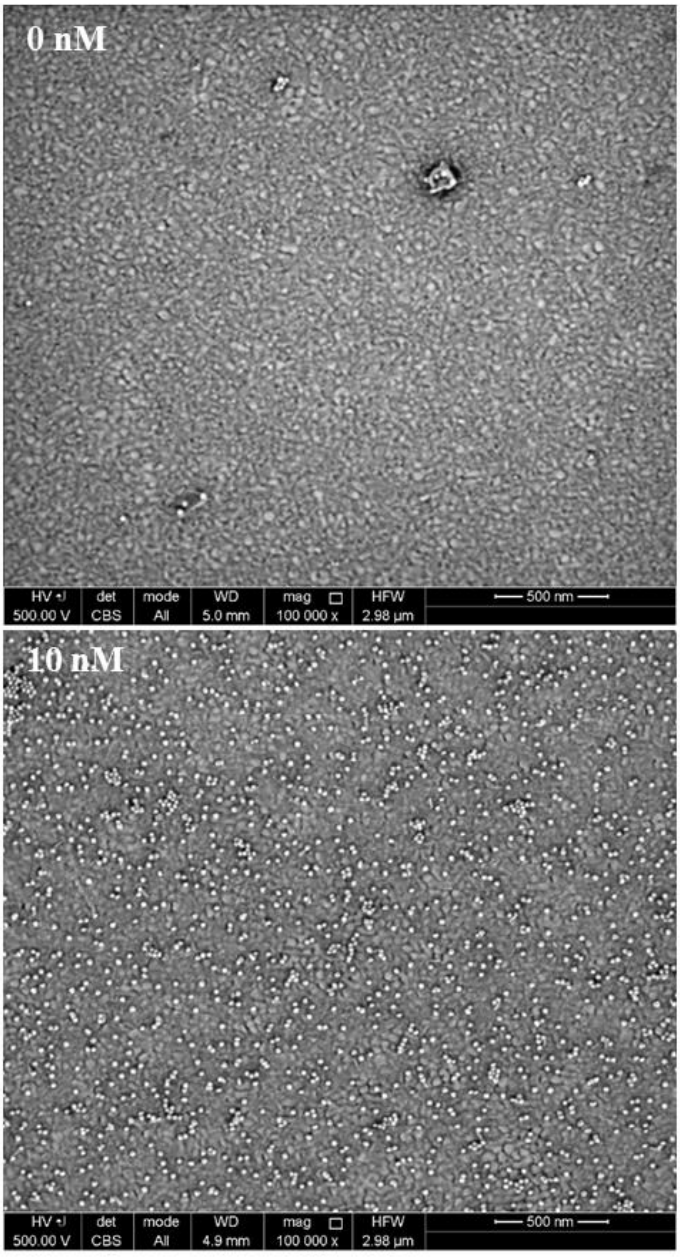

Figure S4.3: *High-resolution SEM images of four different FO-SPR sensors after ligation with 0, 10, 100 and 1000 nM ligation template.*

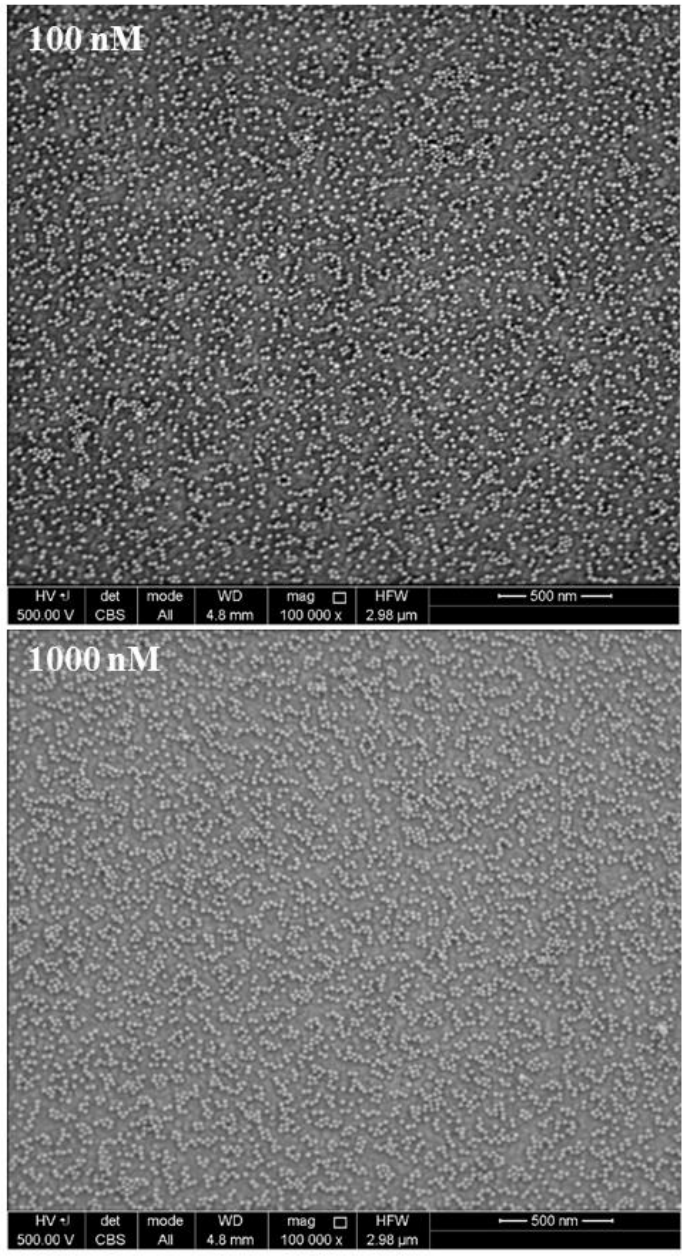

Figure S4.3: *Continued.*

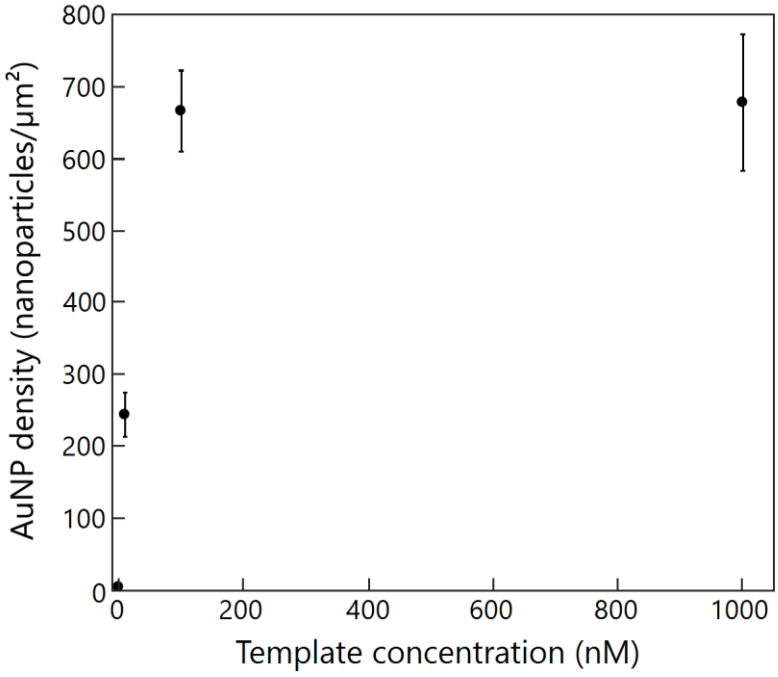

Figure S4.4: *AuNP density determined for 0, 10, 100 and 1000 nM template concentrations. For every concentration, three SEM images were obtained on the same optical fiber. Error bars represent the intrafiber variability of one standard deviation (n = 3).*

4.6. References

1. Wang, W. *et al.* Bioapplications of DNA nanotechnology at the solid–liquid interface. *Chem. Soc. Rev.* **48**, 4892–4920 (2019).
2. Zahid, M., Kim, B., Hussain, R., Amin, R. & Park, S. DNA nanotechnology: a future perspective. *Nanoscale Res. Lett.* **8**, 119 (2013).
3. Pei, H. *et al.* Scaffolded biosensors with designed DNA nanostructures. *NPG Asia Mater.* **5**, e51–e51 (2013).
4. Song, K.-M., Lee, S. & Ban, C. Aptamers and Their Biological Applications. *Sensors* **12**, 612–631 (2012).
5. Silverman, S. K. In vitro selection, characterization, and application of deoxyribozymes that cleave RNA. *Nucleic Acids Res.* **33**, 6151–6163 (2005).
6. Du, Y. & Dong, S. Nucleic Acid Biosensors: Recent Advances and Perspectives. *Anal. Chem.* **89**, 189–215 (2017).
7. Gong, L. *et al.* DNAzyme-based biosensors and nanodevices. *Chem. Commun.* **51**, 979–995 (2015).
8. Peng, H. *et al.* DNAzyme-Mediated Assays for Amplified Detection of Nucleic Acids and Proteins. *Anal. Chem.* **90**, 190–207 (2018).
9. Breaker, R. R. & Joyce, G. F. A DNA enzyme that cleaves RNA. *Chem. Biol.* **1**, 223–229 (1994).
10. Santoro, S. W. & Joyce, G. F. A general purpose RNA-cleaving DNA enzyme. *Proc. Natl. Acad. Sci.* **94**, 4262–4266 (1997).
11. Šípová, H. & Homola, J. Surface plasmon resonance sensing of nucleic acids: A review. *Anal. Chim. Acta* **773**, 9–23 (2013).
12. Chen, Y. & Corn, R. M. DNAzyme Footprinting: Detecting Protein–Aptamer Complexation on Surfaces by Blocking DNAzyme Cleavage Activity. *J. Am. Chem. Soc.* **135**, 2072–2075 (2013).
13. Li, X. *et al.* A novel surface plasmon resonance biosensor for enzyme-free and highly sensitive detection of microRNA based on multi component nucleic acid enzyme (MNAzyme)-mediated catalyzed hairpin assembly. *Biosens. Bioelectron.* **80**, 98–104 (2016).
14. Bedford, E. E., Spadavecchia, J., Pradier, C.-M. & Gu, F. X. Surface Plasmon Resonance Biosensors Incorporating Gold Nanoparticles. *Macromol. Biosci.* **12**, 724–739 (2012).
15. Shen, L. *et al.* Electrochemical DNAzyme Sensor for Lead Based on Amplification of DNA−Au Bio-Bar Codes. *Anal. Chem.* **80**, 6323–6328 (2008).
16. Teh, H. B., Li, H. & Yau Li, S. F. Highly sensitive and selective detection of Pb 2+ ions using a novel and simple DNAzyme-based quartz crystal microbalance with dissipation biosensor. *Analyst* **139**, 5170–5175 (2014).
17. Kufer, S. K. *et al.* Covalent immobilization of recombinant fusion proteins with hAGT for single molecule force spectroscopy. *Eur. Biophys. J.* **35**, 72–78 (2005).
18. Lee, H. J., Wark, A. W., Li, Y. & Corn, R. M. Fabricating RNA microarrays with RNA-DNA surface ligation chemistry. *Anal. Chem.* **77**, 7832–7837 (2005).
19. Clow, F., Fraser, J. D. & Proft, T. Immobilization of proteins to biacore sensor chips using Staphylococcus aureus sortase A. *Biotechnol. Lett.* **30**, 1603–1607 (2008).
20. Li, Y., Wark, A. W., Lee, H. J. & Corn, R. M. Single-Nucleotide Polymorphism Genotyping by Nanoparticle-Enhanced Surface Plasmon Resonance Imaging Measurements of Surface Ligation Reactions. *Anal. Chem.* **78**, 3158–3164 (2006).
21. Frutos, A. G., Smith, L. M. & Corn, R. M. Enzymatic Ligation Reactions of DNA "Words" on Surfaces for DNA Computing. *J. Am. Chem. Soc.* **120**, 10277–10282 (1998).
22. Matsuura, K., Yamashita, T., Igami, Y. & Kimizuka, N. 'Nucleo-nanocages': designed

ternary oligodeoxyribonucleotides spontaneously form nanosized DNA cagesElectronic supplementary information (ESI) available: a time course of absorbance increase of the ligated nucleo-nanocages 1–3, due to the enzymatic actio. *Chem. Commun.* 376–377 (2003). doi:10.1039/b210139d

23. Lu, J. *et al.* Fiber optic-SPR platform for fast and sensitive infliximab detection in serum of inflammatory bowel disease patients. *Biosens. Bioelectron.* **79**, 173–179 (2016).
24. Hurst, S. J., Lytton-Jean, A. K. R. & Mirkin, C. A. Maximizing DNA Loading on a Range of Gold Nanoparticle Sizes. *Anal. Chem.* **78**, 8313–8318 (2006).
25. Daems, D. *et al.* Identification and Quantification of Celery Allergens Using Fiber Optic Surface Plasmon Resonance PCR. *Sensors* **17**, 1754 (2017).
26. Schneider, C. A., Rasband, W. S. & Eliceiri, K. W. NIH Image to ImageJ: 25 years of image analysis. *Nat. Methods* **9**, 671–675 (2012).
27. Lyon, L. A., Musick, M. D. & Natan, M. J. Colloidal Au-Enhanced Surface Plasmon Resonance Immunosensing. *Anal. Chem.* **70**, 5177–5183 (1998).
28. Knez, K., Janssen, K. P. F., Pollet, J., Spasic, D. & Lammertyn, J. Fiber-Optic High-Resolution Genetic Screening Using Gold-Labeled Gene Probes. *Small* **8**, 868–872 (2012).
29. Knez, K., Spasic, D., Delport, F. & Lammertyn, J. Real-time ligation chain reaction for DNA quantification and identification on the FO-SPR. *Biosens. Bioelectron.* **67**, 394–399 (2015).
30. Daems, D. *et al.* Competitive inhibition assay for the detection of progesterone in dairy milk using a fiber optic SPR biosensor. *Anal. Chim. Acta* **950**, 1–6 (2017).
31. Pollet, J. *et al.* Fiber optic SPR biosensing of DNA hybridization and DNA–protein interactions. *Biosens. Bioelectron.* **25**, 864–869 (2009).
32. Malinský, P., Slepička, P., Hnatowicz, V. & Švorčík, V. Early stages of growth of gold layers sputter deposited on glass and silicon substrates. *Nanoscale Res. Lett.* **7**, 241 (2012).
33. Bone, S. M. *et al.* DNA-only Cascade: A Universal Tool for Signal Amplification, Enhancing the Detection of Target Analytes. *Anal. Chem.* **86**, 9106–9113 (2014).

Chapter 5

Real-Time FO-SPR monitoring of solid-phase DNAzyme cleavage activity for cutting-edge biosensing

---

The work in this chapter was adapted from:

Peeters, B., Daems, D., Van der Donck, T., Delport, F. & Lammertyn, J. Real-Time FO-SPR Monitoring of Solid-Phase DNAzyme Cleavage Activity for Cutting-Edge Biosensing. *ACS Appl. Mater. Interfaces* 11, 6759–6768 (2019).

Contributions of Peeters B. to this manuscript:

Planning and performing of the experiments, data processing and analysis, writing and editing of the manuscript.

5.1. Introduction

In Chapter 4, an alternative strategy was presented to immobilize and label DNAzyme substrates with AuNPs in an efficient and specific way, based on ligation. Commonly, DNAzyme substrates are labelled with a fluorophore and quencher, resulting in a solution-based, direct fluorescent readout upon substrate cleavage[1,2]. First applications restricted themselves to the detection of metal targets, based on the intrinsic DNAzyme characteristic of needing a metal cofactor for activity[1]. Extension of the non-metallic target repertoire is more challenging, yet possible using strategies in which the DNAzyme is blocked[3] in absence of the target or by splitting the catalytic core to form so-called binary deoxyribozymes[4] or MNAzymes (Chapter 2) [5–7]. Several efforts have been reported to improve the background signal of these fluorescent substrates with different configurations of organic quenchers[8–12]. However, another promising alternative is to move completely away from fluorescence and use the (non-) intact substrate or secondary DNA strands for the indirect signal generation with different readout systems. Electrochemical[13,14], colorimetric[15] and few SPR[16,17] strategies have been described, keeping the DNAzyme activity in solution, but still requiring an additional hybridization or labelling step for the indirect signal generation.

In a different approach the DNAzymes and/or their substrates are immobilized to a solid surface, confining the DNAzyme activity at this solid surface. Based on the various conjugation possibilities of NAs, different nanomaterials[18,19] and planar surfaces[20] can be functionalized and act as fluorescence quenchers. In addition, surface immobilization allows washing steps, minimizing potential background signals. Next to fluorescence, researchers have been developing DNAzyme-based solid-phase systems in combination with different labels such as nanoparticles[21] and electrochemically active components[22,23], avoiding complex and dual labelling of substrates with fluorophores and quenchers. So far, sensing applications of surface immobilized DNAzymes or their substrates are mainly restricted to the detection of their metal cofactors[24]. In contrast, direct solid-phase monitoring of DNAzyme activity on the surface has currently not been reported for the detection of NAs or proteins.

SPR is a solid-phase technology and known as the gold standard for molecular interaction analysis (Chapter 2). The technology uses an evanescent wave at the sensor's interface to measure changes in RI caused by the specific interaction between surface immobilized receptors and target molecules[25,26]. Starting from complex and bulky prism-based microfluidic systems, SPR technology has been developed into more user-friendly and cost-effective configurations, such as optical fibers[27,28]. An in-house developed FO-SPR device was previously reported by our group[29]. FO-SPR can compete in sensitivity and specificity with the prism-based systems, due to their compatibility with AuNPs for signal amplification[30]. However, not only binding of AuNPs labels, but also the release of AuNPs from the surface has been used to design sensitive bioassays, such as HRM assays (Chapter 3)[31]. In addition, the FO-SPR technology has proven its value in biosensing applications for the detection of DNA, proteins and small molecules[32–34]. Furthermore, compared to other standard techniques, the FO-SPR platform is capable of real-time monitoring, quantifying kinetic measurements and fast sample analysis.

Based on the limitations of the DNAzyme-based fluorescent sensors and restricted biosensing applications of surface immobilized DNAzymes and substrates, **the first objective of this chapter is to study surface-based catalytic cleavage activity of DNAzymes with the innovative, solid-phase FO-SPR biosensors**, developed in Chapter 4. Instead of secondary hybridization or labelling of DNAzyme products on the surface, the research focuses on the direct interaction between surface tethered substrates and DNAzymes to create an associated response signal. Direct solid-phase monitoring of DNAzyme activity has the advantage to enable integration of the signal transduction into DNAzyme cascades amplifying the amount of DNAzyme itself[6,35,36], enabling reduced assay times. These type of DNAzyme cascades are of great interest, as increasing the amount of DNAzymes intrinsically generates an additional amplification effect due to their catalytic activity. **The second aim of this work is to show the potential of the proposed solid-phase sensor concept towards biosensing applications.** This way, the interesting advantages of DNAzymes, such as their specificity, isothermal signal generation and amplification could be explored to create new DNAzyme-based bioassay concepts. Furthermore, in combination with

detection strategies only redesigning the initial step of the amplification cascade but keeping the DNAzyme binding arms and substrate strand constant, a universal solid-phase sensor could be developed for different targets such as proteins and NAs.

In order to do so, we present for the first time a generic DNAzyme-based bioassay concept for ssDNA detection, using a previously optimized AuNP-labelled FO-SPR sensor design. First, DNAzyme detection is established by monitoring the corresponding FO-SPR shifts for different DNAzyme concentrations in real-time. As a proof-of-concept, a second section focuses on the detection of a ssDNA target strand by temporary blocking the DNAzyme with an inhibitor strand. In combination with its real-time aspect, user-friendliness and fast response time, FO-SPR holds great potential in the study of surface-based DNAzyme cleavage activity and the development of innovative DNAzyme-based bioassay concepts for NA detection.

5.2. Experimental section

5.2.1. Materials and reagents

All DNA sequences were synthesized and purified by Integrated DNA Technologies (IDT, Leuven, Belgium). Full sequence information is provided in Table S5.1 of the Supplementary Information. Trizma®base, sodium dodecyl sulfate (SDS), magnesium chloride and DNA/RNAse-free water were purchased from The Merck group - Sigma-Aldrich (Bornem, Belgium). Potassium dihydrogen phosphate and sodium chloride were obtained from The Thermo Fisher Scientific group - Fisher Scientific (Merelbeke, Belgium) and dipotassium hydrogen phosphate and 1,4-dithiothreitol (DTT) from AppliChem GmbH (Darmstadt, Germany). Ethylenediaminetetraacetic acid (EDTA) was purchased from Acros Organics (Geel, Belgium), sodium hydroxide from Chemlab (Zedelgem, Belgium) and ethanol absolute from VWR Chemicals (Haasrode, Belgium). Both Illustra NAP-5 columns and Immobiline DryStrip Cover Fluid were obtained from GE Healthcare Life Sciences (Diegem, Belgium). AuNPs (Ø 20 nm) were provided by BBI Solutions (Cardiff, UK) and PEG-molecules ($C_{27}H_{55}NO_9S$), used as a backfilling molecule, by Polypure AS (Oslo, Norway). The Ampligase® Thermostable DNA Ligase (5U/µL) with accompanying 10× reaction buffer was purchased from Epicentre® (Madison, USA). Non-denaturing TBE gels (10 %) and 5× TBE

buffer were obtained from The Thermo Fisher Scientific group - Invitrogen (Merelbeke, Belgium) and 6× Orange DNA Loading Dye from The Thermo Fisher Scientific group - Thermo Scientific (Merelbeke, Belgium).

Sensor preparation and reaction buffers were the following: PB buffer (180 mM phosphate, pH 8), PB-SDS buffer (10 mM phosphate, 0.01 % (w/v) SDS, pH 8.0), TE buffer (10 mM Tris, 1 mM EDTA, pH 8), Tris-SDS buffer (20 mM Tris buffer, 0.01 % (w/v) SDS, pH 8.3) and DNAzyme reaction buffer (20 mM $MgCl_2$, 50 mM Tris, 150 mM NaCl, pH 9.4).

5.2.2. Real-time FO-SPR monitoring of DNAzyme activity

DNAzyme reaction mixtures contained DNAzyme reaction buffer and 0, 0.1, 1, 3.125, 6.250, 10, 12.5, 25, 50 or 100 nM DNAzyme in a final volume of 100 µL. A first baseline was established in DNAzyme reaction buffer for 7 min, followed by incubation of the FO-SPR sensors in one of the DNAzyme reaction mixtures for 30 min. The catalytic reaction was stopped by washing two times 30 s with 10 mM NaOH, one time 30 s with TE buffer and afterwards a second baseline was recorded in the DNAzyme reaction buffer. All reaction vials were heated simultaneously at 55 °C and were covered with mineral oil.

5.2.3. DNAzyme blocking with inhibitor strand

Different concentrations of 100, 140 or 180 nM inhibitor strand were mixed in DNAzyme reaction buffer with a fixed DNAzyme concentration of 100 nM. After 30 s heating at 95 °C and incubation at 55 °C for 30 min, the inhibitor-DNAzyme complex was cooled and stored at 4 °C. DNAzyme inhibition experiments were performed identically to the DNAzyme activity experiments, but instead of different DNAzyme concentrations, the FO-SPR sensors were incubated with a four-time dilution of the different inhibitor-DNAzyme mixtures in DNAzyme buffer.

5.2.4. DNAzyme-based target detection

Target concentrations of 0, 10, 12.5, 15, 20, 25 or 30 nM and 30 nM of non-matching ssDNA (Table S5.1) were incubated at 55 °C for 20 min in DNAzyme reaction buffer together with a 1.4:1 ratio of inhibitor-DNAzyme complex prepared as aforementioned, prior to starting the DNAzyme activity readout. Readout of the DNAzyme activity was performed identical as described

earlier, except for the first baseline. This baseline was prolonged to 10 min, making a total of 30 min incubation of the ssDNA target with the DNAzyme-inhibitor complex before starting the readout.

5.2.5. SEM images and data analysis

High resolution SEM images were made with a FEI Nova Nanosem 450 (The Thermo Fisher Scientific group – FEI, Hillsboro, USA). Visualization of the 20 nm AuNPs was established with a backscatter detector (CBS, concentric backscatter detector) using an acceleration voltage of 4.5 kV in the column and a magnification of 100,000. Applying a bias of 4 kV on the stage enabled beam deceleration, resulting in a landing energy of 500 V. To obtain stable imaging, drift corrected frame integration (DCFI) was used. The difference in contrast of the images could be explained by small differences in the sample preparation and different position of the image on the FO-SPR sensor surface. Quantification of the AuNPs was done by using ImageJ 1.48v (National Institutes of Health, Bethesda, USA)[37], a Java-based image-processing program. For every condition with images with a surface area of 7.5 μm^2 were sharpened if needed and after setting the proper noise tolerance, the AuNPs could be counted using the 'Find Maxima' tool in ImageJ. For every condition, the AuNP density was determined for three images at different locations on the same fiber.

FO-SPR data were recorded with LabView (National Instruments, Austin, USA) and further processed using Matlab 2015b (The MathWorks Inc., Natick, USA). The FO-SPR signals were normalized by subtraction of the initial average baseline and different steps were distinguished within both the ligation an DNAzyme activity sensorgrams. Different parameters were defined to enable statistical analysis with JMP®13 (SAS Institute Inc., Cary, USA): (i) DNAzyme shift, (ii) DNAzyme efficiency and (iii) half time value. Significant differences were analyzed by performing one-way ANOVA followed by Tukey multiple comparison with an α-level of 0.05. Calibration curves were linearly fitted by $y = a\,x + b$, with y the logarithmic half-life values, x the logarithmic concentration, a the slope and b the intercept. The LOD was based on the linear regression and calculated as $LOD = 3 \times \sigma / S$, with σ the standard deviation of the response, estimated by the root mean squared error (RMSE) and S the slope of the calibration curve[38].

5.3. Results and Discussion

5.3.1. Concept of DNAzyme based FO-SPR biosensing

The concept for a DNAzyme-based bioassay for NA detection is depicted in Figure 5.1. Based on the AuNP-labelled FO-SPR sensors designed in Chapter 4, a temporary DNAzyme-inhibiting system was designed in purpose of detecting target-triggered DNAzyme cleavage activity. The system includes three additional DNA oligos: (i) a synthetic, specific DNA target, (ii) a DNAzyme and (iii) a ssDNA inhibitor. The inhibitor is designed to block the DNAzyme by partial hybridization. It contains a loop of 22 nucleotides, which can be adapted to any target without changing the DNAzyme sequence. In presence of the target, the inhibitor preferentially binds the DNA target of interest due to higher complementarity and therefore resulting in a lower ΔG compared to the interaction with the DNAzyme. This way, the DNAzyme is activated and can start cleaving the AuNP-labelled substrate on the FO-SPR sensor surface.

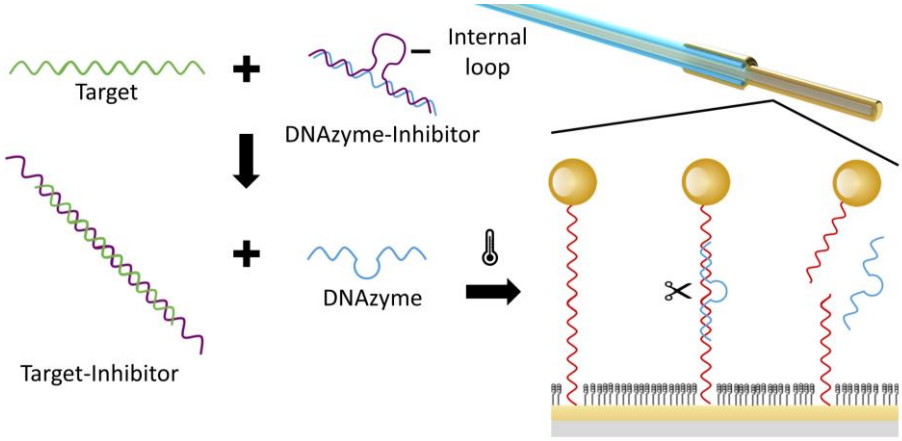

Figure 5.1: *Illustration of the DNAzyme-based target detection.*

In order to realize the proposed DNAzyme-based FO-SPR sensor, a first set of experiments is devoted to the real-time direct monitoring of the DNAzyme cleavage activity. Therefore, the activity of different DNAzyme concentrations is characterized and a calibration curve is established with the AuNP-labelled FO-SPR sensors. In a second set of experiments, blocking of the DNAzyme is evaluated for different inhibitor-DNAzyme ratios. Finally,

different synthetic DNA target concentrations are detected and a calibration curve is established.

5.3.2. Characterization of DNAzyme activity with FO-SPR

Based on the AuNP-labelled FO-SPR sensors produced under optimal ligation conditions defined in Chapter 4, here the DNAzyme cleavage activity is studied. The 10-23 DNAzyme was preferred, based on several of its characteristics as mentioned in Chapter 2[39,40]. Creating a FO-SPR sensor design, that is sensitive to the surface cleavage activity of DNAzymes, will make the FO-SPR platform more accessible to the increasing popularity and progress in the field of DNA nanotechnology. Interesting features of the DNAzyme technology are: (i) their intrinsic capacity of signal amplification and (ii) their superior *in vitro* synthesis, cost efficiency and stability compared to protein enzymes.

Figure 5.2A illustrates the corresponding DNAzyme activity sensorgrams with four steps similar to the ligation strategy. Step 1 represents a first stabilization step to reach a baseline level as discussed in Chapter 4. In step 2, the substrate cleavage and release of AuNPs were monitored in real-time. Reaction kinetics were studied by determining the half-life value of the FO-SPR sensor response. Step 3 represents a washing step, again clearly distinguishable by the short RI changes in air when switching reaction vials. Finally, step 4 corresponds to a second stabilization step, which enabled to

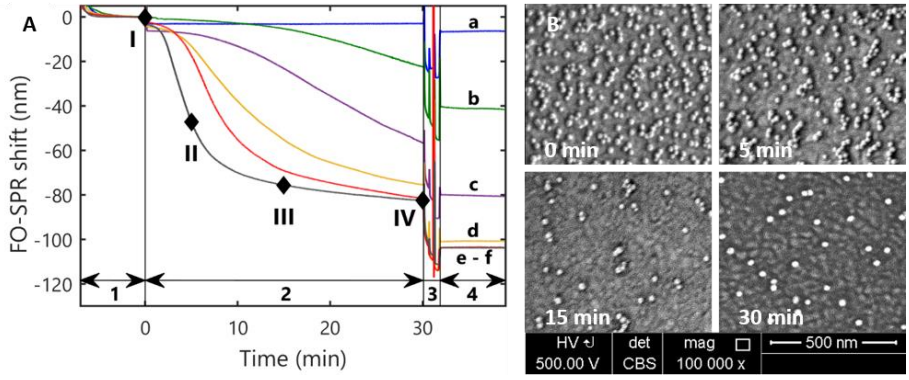

Figure 5.2: *DNAzyme response.* ***A)*** *Real-time FO-SPR shifts for a) 0 nM, b) 3.125 nM, c) 6.25 nM, d) 12.5 nM, e) 25 nM and f) 50 nM DNAzyme. Every measurement consisted of 4 steps: 1) first baseline, 2) DNAzyme incubation, 3) washing and 4) second baseline and* ***B)*** *Represents the SEM images taken after I) 0 min, II) 5 min, III) 15 min and IV) 30 min of incubation with 25 nM DNAzyme.*

quantify the corresponding FO-SPR shift. Moreover, in combination with the ligation shifts (Chapter 4), the DNAzyme efficiency was described.

FO-SPR sensors with AuNPs were incubated with DNAzyme concentrations between 0 - 100 nM. SEM images were made of four different FO-SPR sensors after 0, 5, 15 min and 30 min incubation with 25 nM DNAzyme (Figure 5.2B). The SEM images confirm the release of AuNPs by incubation with the DNAzyme over time. The starting AuNP density was 607 particles/µm² with a SD of 28, which decreased to 432 particles/µm² with a SD of 26 after 5 min, 87 particles/µm² with a SD of 4 after 15 min and 81 particles/µm² with a SD of 1 after 30 min (full images, Figure S5.2). For the negative control the AuNP density remained at 571 particles/µm² with a SD of 11, illustrating the specificity of the DNAzyme (Figure S5.1). DNAzyme shifts were defined as the difference between both baselines and DNAzyme efficiencies as the ratio of DNAzyme and ligation shifts (Figure S5.3). The ligation shifts obtained in Chapter 4 give the maximal shifts that can be expected after incubation with the DNAzyme. Both parameters showed an increasing, logarithmic trend with the DNAzyme concentration up to 12.5 nM DNAzyme, after which the DNAzyme shift saturated, giving a dynamic range of one decade. However, introducing the concept of the half-life values determined in step 2 (except for 0 nM DNAzyme, Figure S5.4) improved the dynamic range up to 100 nM DNAzyme and could make both baselines unnecessary. In Figure 5.3, a logarithmic transformation of the exponential part is plotted in function of the logarithmic DNAzyme concentrations and a linear calibration curve was obtained (R^2 of 0.95) with a RMSE of 0.07. The lowest detectable DNAzyme concentration was 3.125 nM and the theoretical LOD based on the linear regression was 2.3 nM.

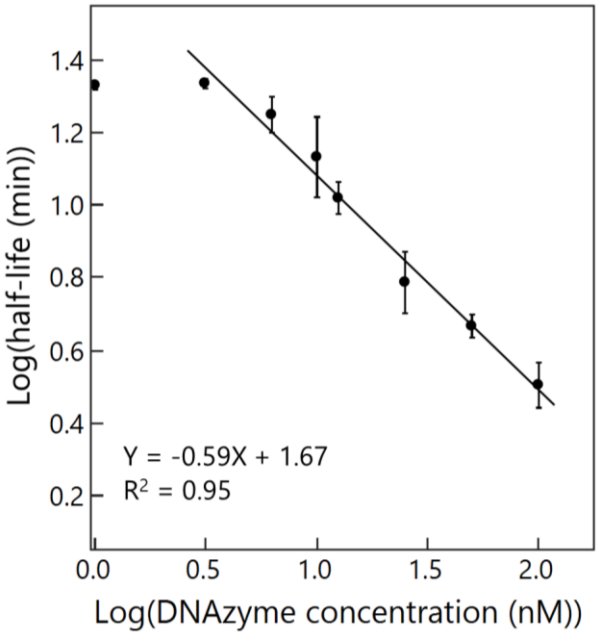

Figure 5.3: *DNAzyme calibration curve. A linear calibration curve was established by log-log transformation of the half-life and DNAzyme concentration. Error bars represent one standard deviation (n = 3).*

5.3.3. Screening of inhibitor concentration for DNAzyme blocking

To retain a controlled catalytic activity, DNAzyme blocking was established through partial DNA hybridization. The inhibitor strand was designed to be complementary to the DNAzyme's binding arms and part of the catalytic core, except for four nucleotides (Figure S5.5). In addition, one of the blocking regions lacked complementarity with the outer nucleotide of the binding arm and the other blocking region contained a G-T wobble structure[7]. This way, the inhibitor strand with internal loop was calculated to have a T_m enabling hybridization to the DNAzyme under DNAzyme reaction conditions and dehybridization only by a specific trigger (The DINAmelt Web Server[41,42]). Formation of the duplex between DNAzyme and inhibitor strand was confirmed qualitatively with gel electrophoresis prior to the FO-SPR experiments (Figure S5.6).

The degree of DNAzyme blocking is steered by the concentration ratio between the inhibitor strand and the DNAzyme. Moreover, there is a tradeoff between the background signal and the sensitivity of the assay. To

avoid significant background signal, an excess of inhibitor strand is required, while to obtain the lowest LOD, the inhibitor strand and the DNAzyme should be present in equimolar ratio. In the final biosensing concept it is only the DNAzyme bound fraction of the inhibitor that can trigger signal generation after interaction with the target of interest. Figure S5.6 illustrates this excess, which becomes visual from the 1.4:1 ratio onwards in case of the gel electrophoresis. In order to minimize the inhibitor excess and still reach a maximal DNAzyme shift, 25 nM DNAzyme was chosen as the concentration to study the FO-SPR shifts in function of different DNAzyme-inhibitor ratios. Figure 5.4 presents the FO-SPR shifts obtained for a 1:1, 1.4:1 and 1.8:1 ratio of inhibitor strands and DNAzyme. In comparison with the positive control, not containing any inhibitor, the presence of the inhibitor strand in a 1:1 ratio reduced the FO-SPR shift more than 50%. Further increase of the inhibitor-DNAzyme ratio resulted in FO-SPR shifts comparable to the negative control, only containing 200 nM inhibitor strand. Therefore, minimal background and inhibitor excess were realized with a ratio of 1.4:1 inhibitor strand and DNAzyme (used in further experiments).

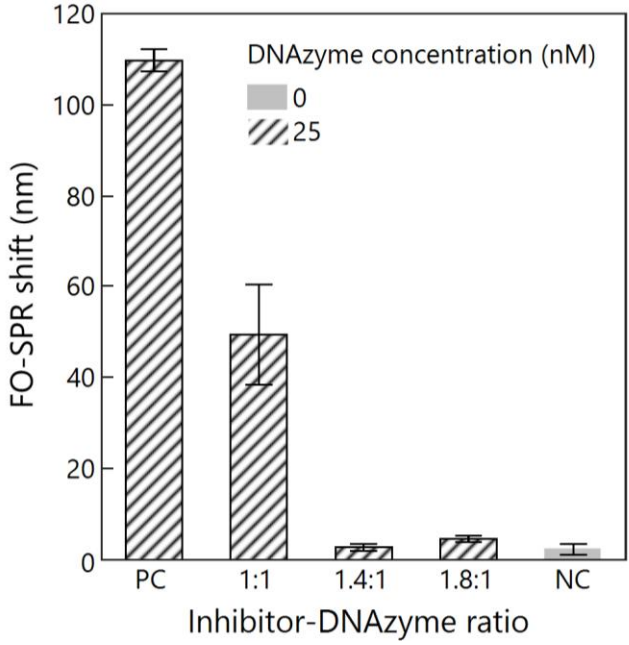

Figure 5.4: *Screening of the inhibitor-DNAzyme ratio for DNAzyme blocking. Positive (PC) and negative control (NC) contained only 25 nM DNAzyme and 200 nM inhibitor, respectively. Shaded bars contained 25 nM DNAzyme with increasing amount of inhibitor. Error bars represent one standard deviation (n = 3).*

5.3.4. DNAzyme-based detection of a synthetic DNA target

Strand displacement[43] was used as the mechanism for target specific signal generation. By establishing specific target detection, it is shown that the FO-SPR sensor has potential towards biosensing applications and that its sensitivity to surface cleavage activity is not restricted to DNAzyme monitoring. Hereto, the inhibitor strand with a built-in internal loop (Figure S5.5) was designed to enable preferential binding to the target in comparison with the DNAzyme. Higher complementarity of the inhibitor strand with the target sequence was provided by the internal loop, whereas the complementary regions were designed to assure blocking of the DNAzyme.

Initially, this target-triggered release of the DNAzyme was first confirmed qualitatively with gel electrophoresis (Figure S5.7). Next, specific target detection was explored using the same reaction conditions as applied for the real-time DNAzyme activity, however this time the DNAzyme was added as a blocked complex with the inhibitor strand as described in previous section. DNAzyme shifts and efficiencies, triggered by different target concentrations and a blank containing a non-matching ssDNA strand, were determined for all response signals as mentioned in Section 5.3.2 (Figure S5.8). FO-SPR shifts increased with target concentration, but no significant FO-SPR shifts were observed in absence of the target or in presence of scrambled ssDNA. Based on the half-life values obtained for 0, 10, 12.5, 15, 20, 25 and 30 nM of target DNA, a calibration curve was established. Both the DNAzyme shifts and DNAzyme efficiencies increased with elevated target concentrations. In contrast to the DNAzyme-only experiments, a sigmoidal trend was observed. We hypothesize that the inhibitor excess, needed to assure complete DNAzyme blocking, caused the initial lag in signal generation. Furthermore, the FO-SPR shifts saturated from 15 nM DNA target onwards. Therefore, half-life values of the FO-SPR response signals were determined (Figure S5.9) and a log-log transformation was performed like the DNAzyme-only results (Figure 5.3). Based on the log-log transformation of the half-life values, the kinetic information within the response signal was used to improve and increase the dynamic range compared to the use of the endpoint DNAzyme shifts. The logarithm of the half-life values was observed to decrease linearly (R^2 = 0.94) with the logarithmic target concentration

(Figure 5.5). An RMSE of 0.08 was obtained and the theoretical LOD was calculated to be 1.4 nM.

Based on these results, we demonstrated the potential of a user-friendly, innovative DNAzyme-based FO-SPR biosensor for the specific detection of DNA biomarkers. In comparison to our previous work focusing on the classical AuNP-amplified 'sandwich' approach for protein and NA detection, we extended the sensor's applicability to surface catalytic DNA-DNA/RNA interactions with prospects on a potential study tool for these catalytic molecules. In order to do so and to make a robust sensor design, the classical 'sandwich' approach in combination with ligation was applied for surface functionalization. Furthermore, we showed that the proposed FO-SPR sensor design can be developed towards biosensing applications by illustrating its capacity of ssDNA detection. The LOD was calculated to be 1.4 nM which is similar to previous reported 1 nM detection limit of our system for NA detection only using AuNP amplification[44]. Lower pM and sub-pM detection limits have been obtained[32,45], but required additional amplification of the target strand by PCR or LCR increasing the number of

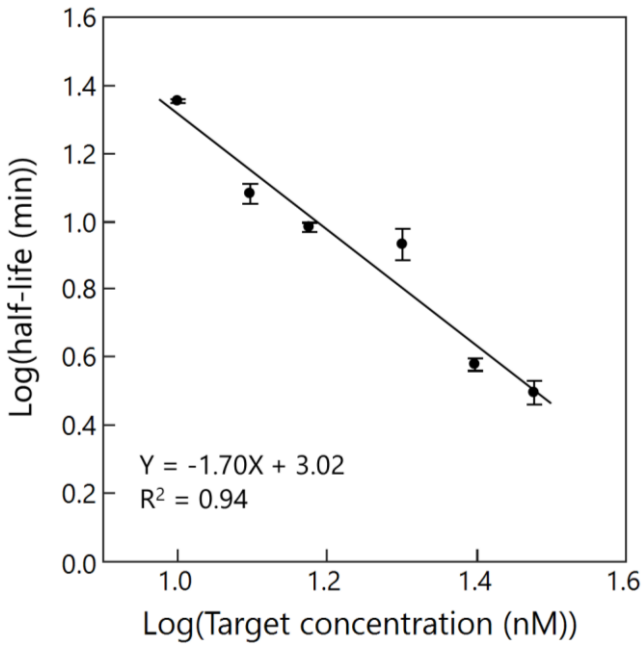

Figure 5.5: *Log-log linear calibration curve of the half-life values and target concentration from 10 – 30 nM. Error bars represent one standard deviation (n = 3).*

experimental steps and assay time to an hour or several hours depending on the target. By developing a DNAzyme-based FO-SPR sensor design, isothermal and protein-free DNAzyme amplification strategies[6] or the use of other RNA-cleaving DNAzymes can now be explored to improve specificity and reach pM - fM detection limits. Other SPR sensors using RNA-cleaving DNAzymes indirectly have reported lower pM[17] and high fM[16] detection limits for NAs and proteins respectively. However, also these systems apply additional indirect amplification strategies such as RNA transcription or catalyzed hairpin assembly with assay times ≥ hours and multiple incubation steps. So far, the proposed DNAzyme-based sensor in this work is the first to use FO-SPR, which typically requires smaller sample volume (< 100 µL) compared to the prism-based systems. However, since these systems mainly detect DNAzymes indirectly, their surface can be regenerated, whereas the proposed FO-SPR sensor is for one-time use only. Other optical biosensors using RNA-cleaving DNAzymes are those using AuNP aggregation depending on the intact substrates linking them together. Although cost-effective and user-friendly, most of these systems have been used for the detection of metal ions and few are reported on biological targets[15,46].

5.4. Conclusions

In this chapter, real-time detection of surface-based DNAzyme cleavage activity using FO-SPR was reported for the first time and a calibration curve for different DNAzyme concentrations was obtained. The dynamic range of the curve includes the lower nM range up to 100 nM and from 25 nM DNAzyme onwards signal generation efficiencies were > 95 %. Furthermore, the proposed FO-SPR sensor's potential in developing DNAzyme-based biosensing applications was proven. Using partial complementarity and the principle of strand displacement, DNAzymes were temporarily blocked with an inhibitor strand. Preferred complementarity between a ssDNA target and the inhibitor strand enabled specific, DNAzyme-based target detection. By exploiting the half-life values of the FO-SPR response signal, a calibration curve was obtained with a theoretical LOD of 1.4 nM.

In order to improve the current LOD further, Chapter 6 will evaluate the amplification of the DNAzyme itself by combining its activity with PCR amplification as presented in Chapter 3. In future work, the emphasis will be put on the integration of the designed FO-SPR sensor in isothermal

DNAzyme-based cascades. Moreover, the designed bioassay concept displays some interesting flexibility in choosing the target of interest. Redesigning the ligation template, the associated FO-SPR and AuNP oligo could enable the use of different substrates and therefore different targets. On the other hand, it is hypothesized that detection of different targets with the same DNAzyme and substrate used in this work could be obtained by modifying the internal loop of the inhibitor strand. The potential of the designed FO-SPR sensor to be integrated in other DNAzyme-based systems or to be modified towards different targets gives the sensor a universal character. Based on these characteristics, the FO-SPR design should be adapted towards a real target of interest and the compatibility in biological matrices should be validated. In these matrices, challenges such as nonspecific adsorption, potential degradation of DNA components by nucleases or interference with the assay mechanism can be encountered. As the FO-SPR platform is fully automated and able to perform four measurements at the same time, parallel detection of different targets based on one universal FO-SPR sensor would be feasible.

5.5. Supplementary information

Table S5.1: *DNA sequences*

Sequence name	Length (nt)	Sequence 5' → 3'
DNAzyme	35	CGGTTGGTGAGGCTAGCTACAACGAGGTTGTGCTG
Inhibitor	52	**CAGCGCAACCTCGTTG**ATCACGCCTCGTCTCCTCCCAG**TAG CCTCACCAACC**
Target	43	GGTGAGGCTACTGGGAGGAGACGAGGCGTGATCAACGAG GTTG
Non-matching ssDNA	44	CATTCTTGCCATCTAACATTACCTTCCTCCGCACACCCCCAG GT

Note

1. Bold region is bound by the DNAzyme
2. Underlined region forms the catalytic core. Regions left and right from the catalytic core are called the substrate arms.
3. DNAzyme and substrate sequences are based on Bone *et al.* (2014)[6].

5.5.1. Material and methods

5.5.1.1. Gel electrophoresis

All experiments were performed with a NovexTM XCell SureLock® Mini-Cell The Thermo Fisher Scientific group – Life Technologies (Merelbeke, Belgium), using precasted non-denaturating PAGE gels of 10%. While the Mini Cell was put on ice, the gels were run in 1x TBE buffer with 10 mM $MgCl_2$ for 100 min at 180 V. A first experiment studied different DNAzyme-inhibitor strand ratios, therefore containing a single stranded DNAzyme and inhibitor control (300 nM), followed by a 1:1, 1.2:1, 1.4:1, 1.6:1, 1.8:1 and 2:1 ratio of inhibitor-DNAzyme strand with a fixed 150 nM DNAzyme concentration. In a second experiment, potential target detection was considered based on a single stranded target, inhibitor and DNAzyme control (300 nM), followed by 0, 50, 100, 200 and 400nM ssDNA target concentrations and an inhibitor-target complex control (150 - 150 nM). Samples were prepared as described in the Sections 5.2.3 and 5.2.4 in 100 µL of which 15 µL was loaded onto the gels with 3 µL of loading dye.

5.5.2. Results and discussion

5.5.2.1. SEM visualization of negative control

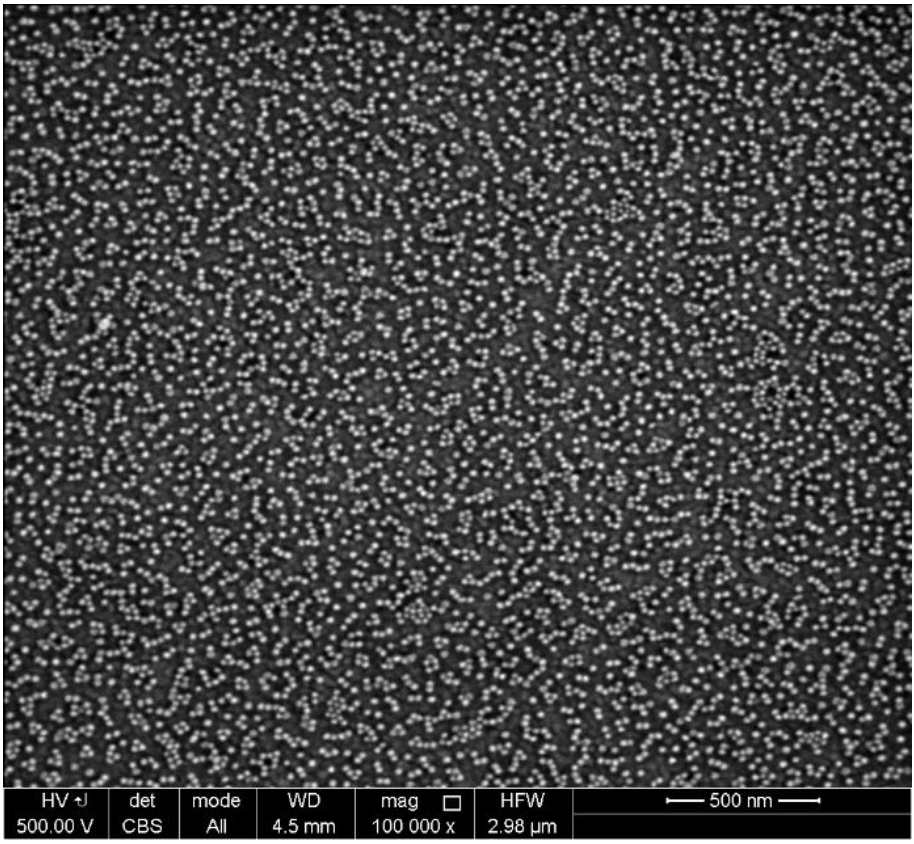

Figure S5.1: *High-resolution SEM image of a FO-SPR sensors after 30 min of incubation with the negative control: 0 nM DNAzyme.*

5.5.2.2. SEM visualization of FO-SPR DNAzyme activity

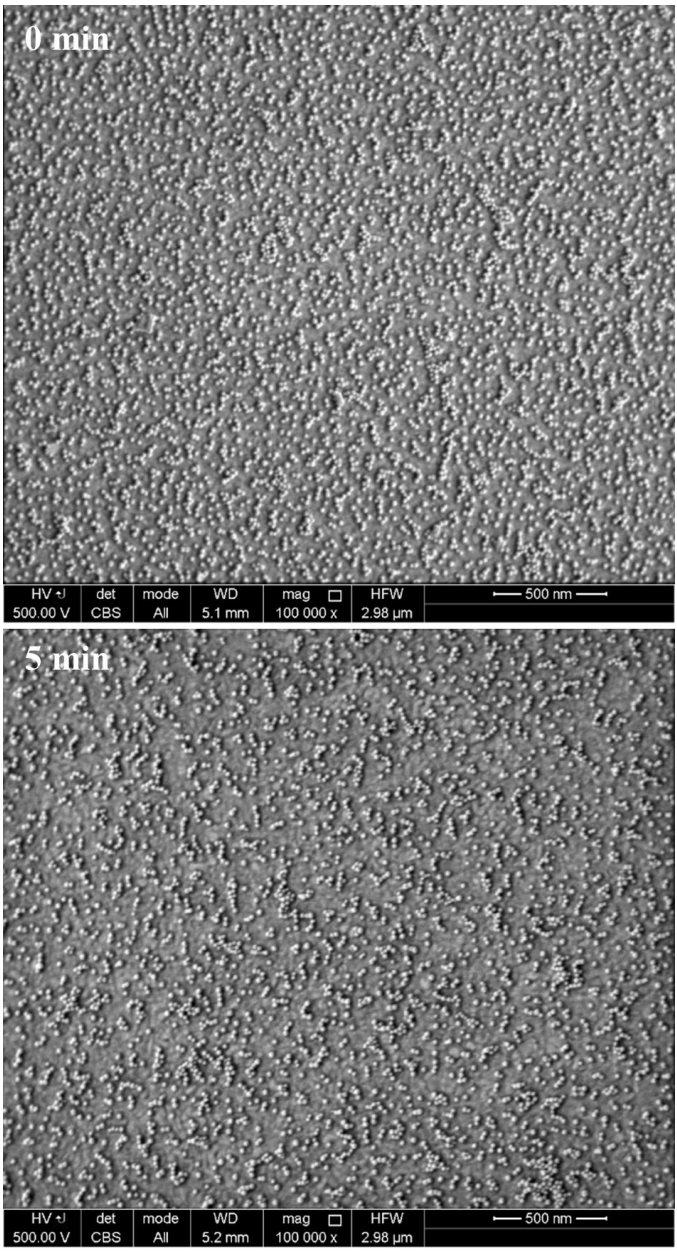

Figure S5.2: *High-resolution SEM images of 4 different FO-SPR sensors after 0, 5, 15 and 30 min of incubation with 25 nM DNAzyme.*

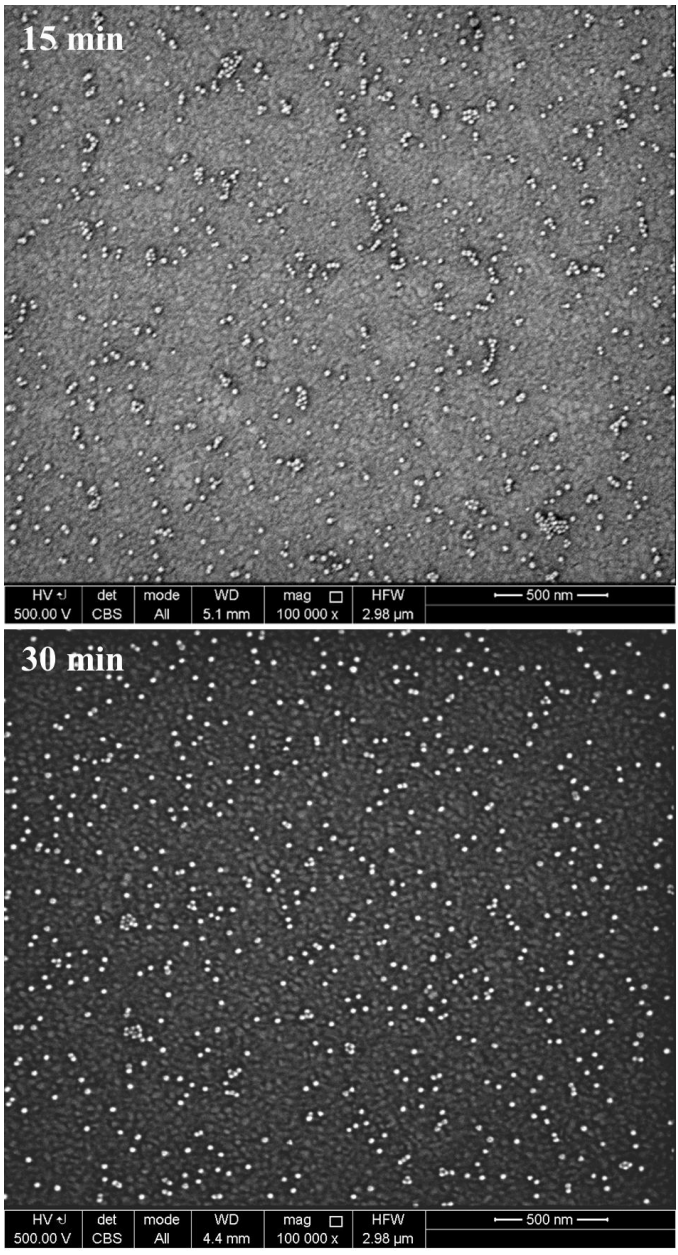

Figure S5.2: *Continued.*

5.5.2.3. FO-SPR characterization of DNAzyme activity

Cleavage of the AuNP-labelled substrate strands by the DNAzyme releases AuNPs into solution, causing the FO-SPR signal to shift towards lower wavelengths. This FO-SPR shift was monitored in real-time and determined as the difference between the baselines acquired before and after incubation of the FO-SPR sensor with different concentrations of DNAzyme (Figure S5.3A). In addition, DNAzyme efficiencies were expressed as the ratio of DNAzyme and ligation shifts, obtained for every DNAzyme concentration that was studied (Figure S5.3B). Taking advantage of the intrinsic real-time monitoring feature of the described FO-SPR sensor, half-life values were determined as kinetic parameter to evaluate the different DNAzyme concentrations (Figure S5.4).

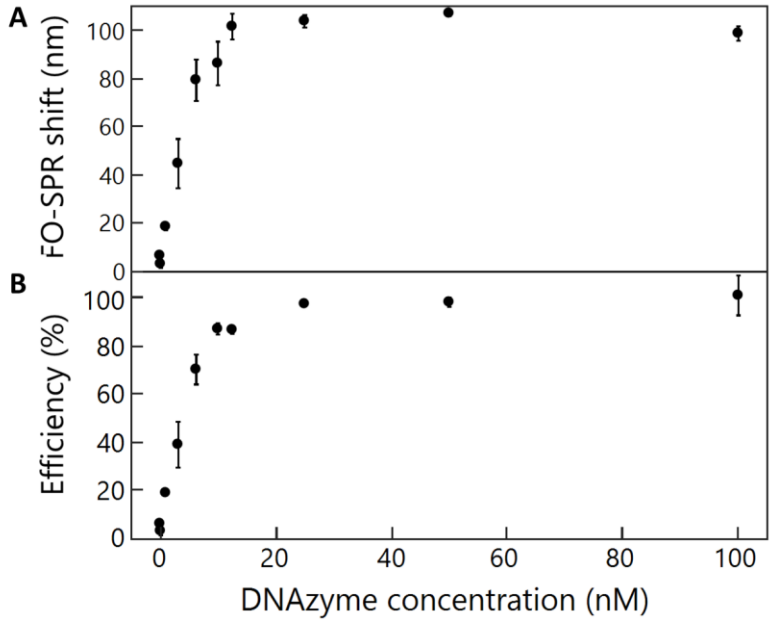

Figure S5.3: A) *DNAzyme shifts determined for 0, 0.1, 1, 3.125, 6.25, 12.5, 25, 50 and 100 nM DNAzyme.* ***B)*** *DNAzyme efficiencies determined as the ratio of DNAzyme and ligation shifts. Error bars represent one standard deviation (n = 3).*

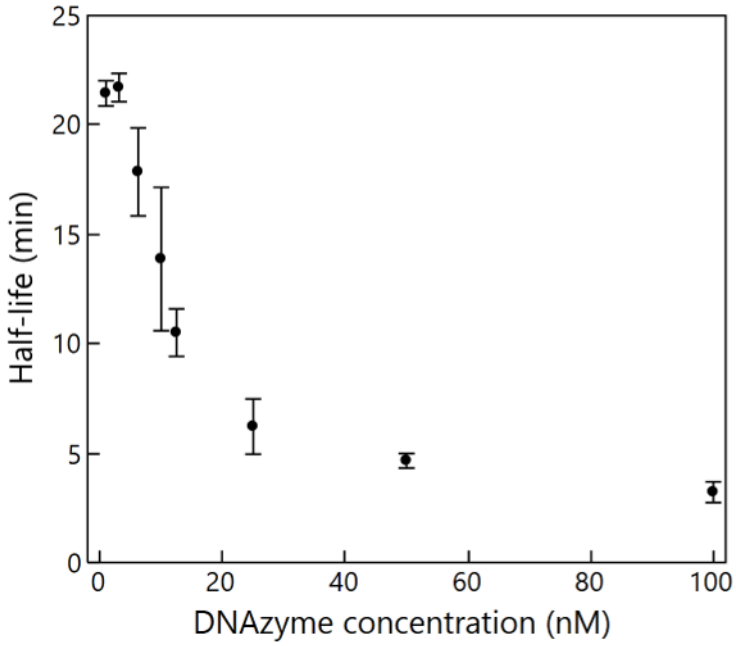

Figure S5.4: *Half-life values for 0, 1, 3.125, 6.25, 12.5, 25, 50 and 100 nM DNAzyme. Values were determined based on the DNAzyme incubation step. Error bars represent one standard deviation (n = 3).*

5.5.2.4. Inhibitor-DNAzyme complex illustration

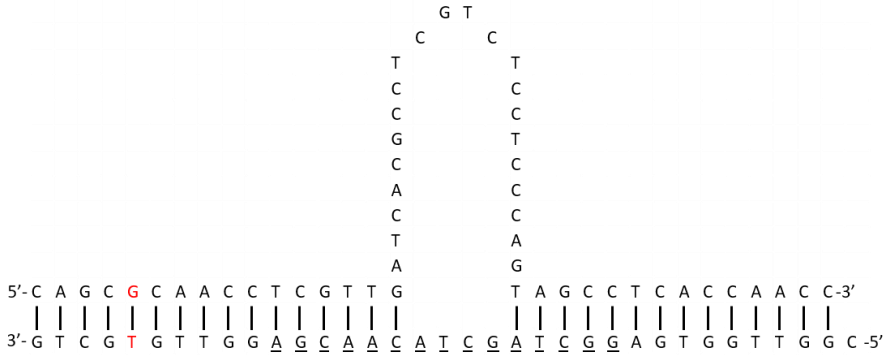

Figure S5.5: *Illustration of the inhibitor-DNAzyme complex. Top: inhibitor with internal loop and bottom: DNAzyme with the underlined core and the G-T wobble structure in red.*

5.5.2.5. Visualization of blocked DNAzyme activity by gel electrophoresis

Blocking of the DNAzyme was qualitatively confirmed by gel electrophoresis, comparing different ratios of inhibitor and DNAzyme with two controls. In Figure S5.6 the first two lanes of the gel contained single stranded control sequences of the DNAzyme and inhibitor respectively. In the following six lanes, different ratios of inhibitor and DNAzyme were loaded after a 30 min hybridization step at 55 °C with a fixed DNAzyme concentration of 150 nM. For the lower inhibitor-DNAzyme ratios 1:1 and 1.2:1, no bands were observed at the level of both controls, but a new band at higher position was observed. A higher band indicates a longer sequence or complex of sequences, which in this case could only be the inhibitor-DNAzyme complex. As the inhibitor-DNAzyme ratio was increased, a second band was observed at the level of the single stranded inhibitor control. This was expected, since the DNAzyme concentration was kept constant, creating an excess of the inhibitor from a 1.2:1 ratio onwards and reaching a visual concentration for all ratios ≥ 1.4.

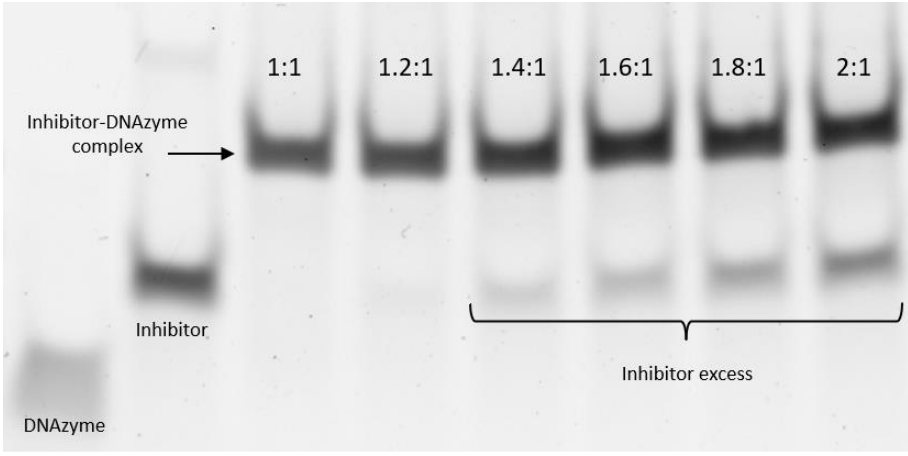

Figure S5.6: *Gel electrophoresis of different inhibitor and DNAzyme ratios. From left to right: a DNAzyme control (300 nM); an inhibitor control (300 nM); and increasing ratios of inhibitor and DNAzyme from 1:1 – 2:1 with fixed 150 nM DNAzyme concentration.*

5.5.2.6. Visualization of target recognition and DNAzyme release by gel electrophoresis

Once the DNAzyme could be blocked, target specific release was also evaluated qualitatively with gel electrophoresis. Figure S5.7 presents the obtained results, starting with three lanes containing single stranded controls of the target, inhibitor and DNAzyme respectively. Lane 4-9 contained a negative control followed by four different target concentrations and a positive control. As expected, the highest single stranded band was observed for the inhibitor (52 nt), followed by the target (43 nt) and the DNAzyme (35 nt). The band of the negative control was observed at a higher position than the single stranded controls as earlier, however also above the positive control, which has a higher total complementarity of 10 nt compared to the negative control. It was hypothesized that the internal loop of 22 nt in the DNAzyme-inhibitor complex caused slower migration through the gel than the linear hybridization between target and inhibitor. Once target was present (lane 5-8), a band appeared at the level of the positive control, illustrating the preferential binding of the target to the inhibitor and release of the blocked DNAzyme. This was confirmed by the fact that no bands appeared at the level of the single stranded inhibitor control. Furthermore, for the higher target concentrations the majority of blocked DNAzymes were released and a band was observed at the level of the single stranded

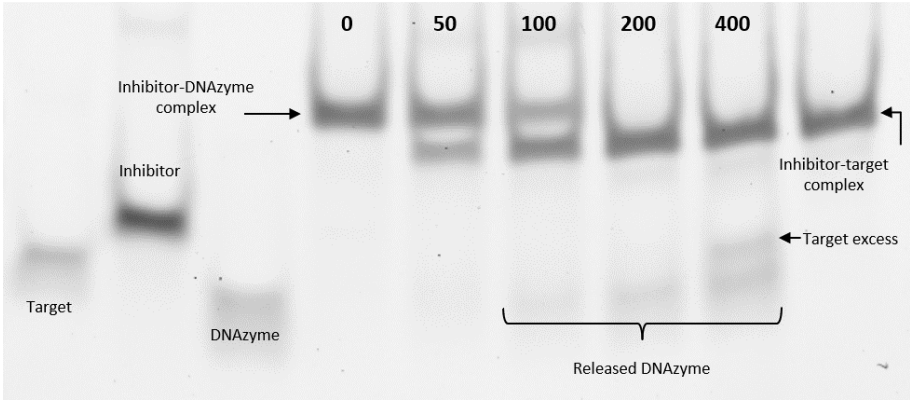

Figure S5.7: *Gel electrophoresis of different target concentrations. From left to right: a target control (300 nM); an inhibitor control (300 nM); a DNAzyme control (300 nM); increasing concentrations of target (nM), incubated with a 1.4:1 ratio of inhibitor (180 nM) and DNAzyme (150 nM); and a 1:1 inhibitor-target complex control (150 nM).*

DNAzyme control. For the highest target concentration of 400 nM a third band was observed at the position of the single stranded target control as there was a big excess of target compared to inhibitor strand.

5.5.2.7. Proof-of-concept detection of a synthetic DNA strand

Target detection with the FO-SPR sensor and specificity were established by first incubating the DNAzyme-inhibitor complex with the target or non-matching ssDNA for 30 min, releasing blocked DNAzyme molecules. Next, the FO-SPR sensor was used to detect the released DNAzymes, corresponding to a certain target concentration. FO-SPR shifts, DNAzyme efficiencies and half-life values were determined as described earlier but presented in function of the target concentration: 0, 10, 12.5, 20, 25 and 30 nM (Figure S5.8 and Figure S5.9).

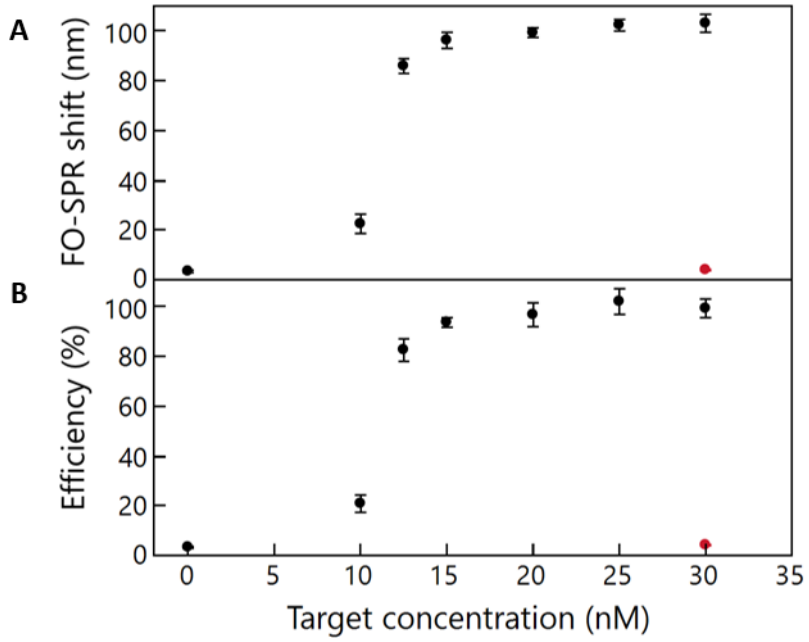

Figure S5.8: *Top panel: DNAzyme shifts determined for corresponding target concentrations of 0, 10, 12.5, 15, 20, 25, 30 nM and a blank containing 30 nM scrambled ssDNA (red); bottom panel: DNAzyme efficiencies determined as the ratio of DNAzyme and ligation shifts. Error bars represent one standard deviation (n = 3).*

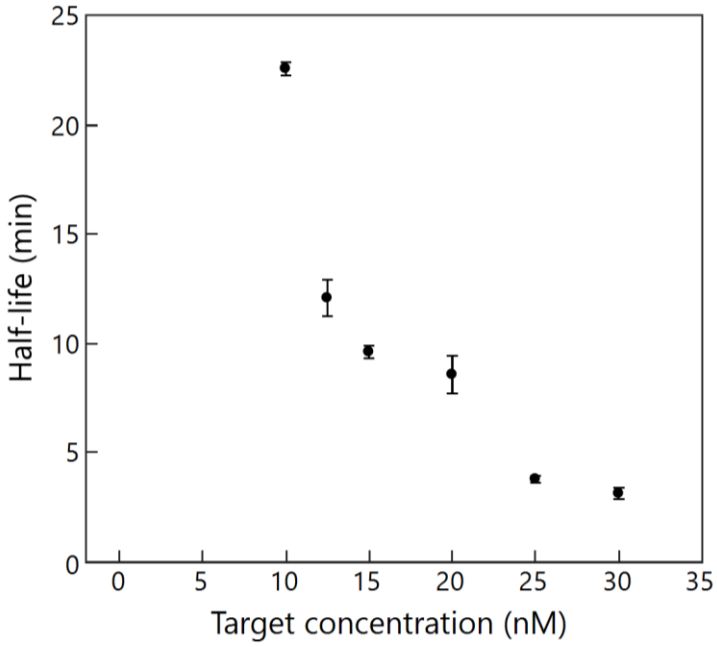

Figure S5.9: *Half-life values for corresponding target concentrations of 0, 10, 12.5, 20, 25 and 30 nM. Values were determined based on the DNAzyme incubation step. Error bars represent one standard deviation (n = 3).*

5.6. References

1. Gong, L. *et al.* DNAzyme-based biosensors and nanodevices. *Chem. Commun.* **51**, 979–995 (2015).
2. Peng, H. *et al.* DNAzyme-Mediated Assays for Amplified Detection of Nucleic Acids and Proteins. *Anal. Chem.* **90**, 190–207 (2018).
3. Navani, N. K. & Li, Y. Nucleic acid aptamers and enzymes as sensors. *Curr. Opin. Chem. Biol.* **10**, 272–281 (2006).
4. Kolpashchikov, D. M. A Binary Deoxyribozyme for Nucleic Acid Analysis. *ChemBioChem* **8**, 2039–2042 (2007).
5. Mokany, E., Bone, S. M., Young, P. E., Doan, T. B. & Todd, A. V. MNAzymes, a Versatile New Class of Nucleic Acid Enzymes That Can Function as Biosensors and Molecular Switches. *J. Am. Chem. Soc.* **132**, 1051–1059 (2010).
6. Bone, S. M. *et al.* DNA-only Cascade: A Universal Tool for Signal Amplification, Enhancing the Detection of Target Analytes. *Anal. Chem.* **86**, 9106–9113 (2014).
7. Bone, S. M., Lima, N. E. & Todd, A. V. DNAzyme switches for molecular computation and signal amplification. *Biosens. Bioelectron.* **70**, 330–337 (2015).
8. Li, J. & Lu, Y. A Highly Sensitive and Selective Catalytic DNA Biosensor for Lead Ions. *J. Am. Chem. Soc.* **122**, 10466–10467 (2000).
9. Stojanovic, M. N., de Prada, P. & Landry, D. W. Catalytic Molecular Beacons. *ChemBioChem* **2**, 411–415 (2001).
10. Mei, S. H. J., Liu, Z., Brennan, J. D. & Li, Y. An Efficient RNA-Cleaving DNA Enzyme that Synchronizes Catalysis with Fluorescence Signaling. *J. Am. Chem. Soc.* **125**, 412–420 (2003).
11. Liu, J. & Lu, Y. Improving Fluorescent DNAzyme Biosensors by Combining Inter- and Intramolecular Quenchers. *Anal. Chem.* **75**, 6666–6672 (2003).
12. Zhang, X.-B., Wang, Z., Xing, H., Xiang, Y. & Lu, Y. Catalytic and Molecular Beacons for Amplified Detection of Metal Ions and Organic Molecules with High Sensitivity. *Anal. Chem.* **82**, 5005–5011 (2010).
13. Sun, C., Zhang, L., Jiang, J., Shen, G. & Yu, R. Electrochemical DNA biosensor based on proximity-dependent DNA ligation assays with DNAzyme amplification of hairpin substrate signal. *Biosens. Bioelectron.* **25**, 2483–2489 (2010).
14. Diao, W. *et al.* Electrochemical DNA biosensor based on MNAzyme-mediated signal amplification. *Microchim. Acta* **183**, 2563–2569 (2016).
15. Zagorovsky, K. & Chan, W. C. W. A Plasmonic DNAzyme Strategy for Point-of-Care Genetic Detection of Infectious Pathogens. *Angew. Chemie Int. Ed.* **52**, 3168–3171 (2013).
16. Chen, Y. & Corn, R. M. DNAzyme Footprinting: Detecting Protein–Aptamer Complexation on Surfaces by Blocking DNAzyme Cleavage Activity. *J. Am. Chem. Soc.* **135**, 2072–2075 (2013).
17. Li, X. *et al.* A novel surface plasmon resonance biosensor for enzyme-free and highly sensitive detection of microRNA based on multi component nucleic acid enzyme (MNAzyme)-mediated catalyzed hairpin assembly. *Biosens. Bioelectron.* **80**, 98–104 (2016).
18. Kim, J. H., Han, S. H. & Chung, B. H. Improving Pb2+ detection using DNAzyme-based fluorescence sensors by pairing fluorescence donors with gold nanoparticles. *Biosens. Bioelectron.* **26**, 2125–2129 (2011).
19. Chen, J. *et al.* A Target-Triggered DNAzyme Motor Enabling Homogeneous, Amplified Detection of Proteins. *Anal. Chem.* **89**, 12888–12895 (2017).
20. Swearingen, C. B. *et al.* Immobilization of a Catalytic DNA Molecular Beacon on Au for

Pb(II) Detection. *Anal. Chem.* **77**, 442–448 (2005).
21. Teh, H. B., Li, H. & Yau Li, S. F. Highly sensitive and selective detection of Pb 2+ ions using a novel and simple DNAzyme-based quartz crystal microbalance with dissipation biosensor. *Analyst* **139**, 5170–5175 (2014).
22. Pelossof, G., Tel-Vered, R. & Willner, I. Amplified Surface Plasmon Resonance and Electrochemical Detection of Pb 2+ Ions Using the Pb 2+ -Dependent DNAzyme and Hemin/G-Quadruplex as a Label. *Anal. Chem.* **84**, 3703–3709 (2012).
23. Zhang, B., Liu, B., Zhou, J., Tang, J. & Tang, D. Additional Molecular Biological Amplification Strategy for Enhanced Sensitivity of Monitoring Low-Abundance Protein with Dual Nanotags. *ACS Appl. Mater. Interfaces* **5**, 4479–4485 (2013).
24. Zhang, X.-B., Kong, R.-M. & Lu, Y. Metal Ion Sensors Based on DNAzymes and Related DNA Molecules. *Annu. Rev. Anal. Chem.* **4**, 105–128 (2011).
25. Homola, J. Surface Plasmon Resonance Sensors for Detection of Chemical and Biological Species. *Chem. Rev.* **108**, 462–493 (2008).
26. Nguyen, H., Park, J., Kang, S. & Kim, M. Surface Plasmon Resonance: A Versatile Technique for Biosensor Applications. *Sensors* **15**, 10481–10510 (2015).
27. Caucheteur, C., Guo, T. & Albert, J. Review of plasmonic fiber optic biochemical sensors: improving the limit of detection. *Anal. Bioanal. Chem.* **407**, 3883–3897 (2015).
28. Gupta, B. D. & Kant, R. [INVITED] Recent advances in surface plasmon resonance based fiber optic chemical and biosensors utilizing bulk and nanostructures. *Opt. Laser Technol.* **101**, 144–161 (2018).
29. Pollet, J. *et al.* Fiber optic SPR biosensing of DNA hybridization and DNA–protein interactions. *Biosens. Bioelectron.* **25**, 864–869 (2009).
30. Bedford, E. E., Spadavecchia, J., Pradier, C.-M. & Gu, F. X. Surface Plasmon Resonance Biosensors Incorporating Gold Nanoparticles. *Macromol. Biosci.* **12**, 724–739 (2012).
31. Knez, K., Janssen, K. P. F., Pollet, J., Spasic, D. & Lammertyn, J. Fiber-Optic High-Resolution Genetic Screening Using Gold-Labeled Gene Probes. *Small* **8**, 868–872 (2012).
32. Daems, D. *et al.* Identification and Quantification of Celery Allergens Using Fiber Optic Surface Plasmon Resonance PCR. *Sensors* **17**, 1754 (2017).
33. Lu, J. *et al.* Fiber optic-SPR platform for fast and sensitive infliximab detection in serum of inflammatory bowel disease patients. *Biosens. Bioelectron.* **79**, 173–179 (2016).
34. Daems, D. *et al.* Competitive inhibition assay for the detection of progesterone in dairy milk using a fiber optic SPR biosensor. *Anal. Chim. Acta* **950**, 1–6 (2017).
35. Todd, A. V, Fuery, C. J., Impey, H. L., Applegate, T. L. & Haughton, M. A. DzyNA-PCR: use of DNAzymes to detect and quantify nucleic acid sequences in a real-time fluorescent format. *Clin. Chem.* **46**, 625–30 (2000).
36. Chen, J., Pan, J. & Chen, S. A naked-eye colorimetric sensor for Hg 2+ monitoring with cascade signal amplification based on target-induced conjunction of split DNAzyme fragments. *Chem. Commun.* **53**, 10224–10227 (2017).
37. Rasband, W. S. ImageJ.
38. European Medicines Agency. *ICH Topic Q 2 (R1) Validation of Analytical Procedures: Text and Methodology Step 5 Note for Guidance on Validation of Analytical Procedures: Text and Methodology*. (1995).
39. Breaker, R. R. & Joyce, G. F. A DNA enzyme that cleaves RNA. *Chem. Biol.* **1**, 223–229 (1994).
40. Santoro, S. W. & Joyce, G. F. A general purpose RNA-cleaving DNA enzyme. *Proc. Natl. Acad. Sci.* **94**, 4262–4266 (1997).

41. Markham, N. R. & Zuker, M. DINAMelt web server for nucleic acid melting prediction. *Nucleic Acids Res.* **33**, W577–W581 (2005).
42. Markham, N. R. & Zuker, M. UNAFold. in *Bioinformatics, Volume II. Structure, Function and Applications, number 453 in Methods in Molecular Biology* (ed. Keith, J. M.) 3–31 (Humana Press, 2008). doi:10.1007/978-1-60327-429-6_1
43. Yurke, B., Turberfield, A. J., Mills, A. P., Simmel, F. C. & Neumann, J. L. A DNA-fuelled molecular machine made of DNA. *Nature* **406**, 605–608 (2000).
44. Knez, K. *et al.* Spherical Nucleic Acid Enhanced FO-SPR DNA Melting for Detection of Mutations in Legionella pneumophila. *Anal. Chem.* **85**, 1734–1742 (2013).
45. Knez, K., Spasic, D., Delport, F. & Lammertyn, J. Real-time ligation chain reaction for DNA quantification and identification on the FO-SPR. *Biosens. Bioelectron.* **67**, 394–399 (2015).
46. Wei, L. *et al.* Proximity ligation-induced assembly of DNAzymes for simple and cost-effective colourimetric detection of proteins with high sensitivity. *Chem. Commun.* **52**, 5633–5636 (2016).

Chapter 6

Solid-phase PCR-amplified DNAzyme activity for real-time FO-SPR detection of the MCR-2 gene

---

The work in this chapter was adapted from:

Peeters, B.*, Safdar, S.*, Daems, D., Goos, P., Spasic, D. and Lammertyn, J., Solid-phase PCR-amplified DNAzyme activity for real-time FO-SPR detection of the MCR-2 gene. *Analytical Chemistry*, Submitted.

*Equal authorship

Contributions of Peeters B. to this manuscript:

Planning and performing of the experiments, data processing and analysis, writing and editing of the manuscript.

6.1. Introduction

Great advancements were realized in molecular diagnostics with the development of the PCR, which is still the gold standard for NA detection and quantification (Chapter 1)[1]. Alongside with its superior sensitivity and specificity, PCR technology has also seen multiple modulations and alternative formats over the years to realize different applications. For instance, real-time NA detection was enabled with quantitative PCR (qPCR)[2] whereas isothermal NA detection was accomplished using loop mediated isothermal amplification (LAMP)[3,4] and recombinase polymerase amplification (RPA)[5,6]. In addition to this, more recently, NA-based enzymes have been integrated with the PCR technology for enabling other appealing features[7]. NAzymes are short ssDNA sequences with enzymatic activities, similar to their protein counterparts but with superior stability and flexibility, which broadens their use[8,9]. G-quadruplex DNAzymes that form an oxidizing complex in combination with hemin[10,11] were used as fluorescent[12], electrochemical[13], luminescent[14,15] and colorimetric labels[16,17]; the latter has been of special interest to avoid the use of fluorescent labels and hence simplify the equipment for PCR monitoring[18–21]. Moreover, 10-23 or 8-17 core DNAzymes that cleave RNA-DNA hybrid substrates in a sequence dependent manner[22,23] were used to generate PCR templates, and were even combined with droplet digital PCR[24], illustrating the great flexibility for designing bioassays against different target molecules[7]. However, all these approaches, despite presented advantages, only allow end-point measurements[25], and even require post-PCR techniques such as gel electrophoresis[26] for product analysis. So far, real-time monitoring using DNAzyme-incorporated PCR was only obtained by designing fluorescent substrates[27] similar to Taqman probes[28]. Hence, the challenge still remains to develop a more feasible alternative for the fluorescent assays, that retains the real-time aspect of qPCR.

SPR is well known for its real-time monitoring aspect, enabling the visualization of molecular binding events and determination of the related kinetics[29]. The technology makes use of a multimode optical fiber, coated with a gold layer and promoting surface plasmon wave (SPW) generation along the surface. The SPW is sensitive to the surface-binding of target molecules, using target-specific receptors[30]. FO-SPR has been developed as a

more user-friendly and cost-effective alternative to the bulkier prism-based SPR systems[31]. The FO-SPR configuration, as previously described in Chapters 3-5, enables the automated handling of the sensors in a simple dip probe format[32]. FO-SPR sensitivities reached the µM - nM range using labels such as AuNPs[33], while ultrasensitive detection (pM – fM range) was enabled by incorporating additional amplification strategies such as the PCR[34] (Chapter 3) and the LCR[35] (Chapter 2). In Chapters 4 and 5, a streamlined protocol for functionalization of FO-SPR probes with the DNAzyme substrate has been reported, allowing real-time measurement of solid-phase DNAzyme cleavage activity[36]. However, to date the development of a DNAzyme-based PCR amplification strategy has not been explored utilizing the FO-SPR system, which promises retention of the real-time aspect of the fluorescent systems, while offering an alternative readout next to a potential improvement in sensitivity compared with amplification-free DNAzyme assays.

In this chapter, the objective is the development of a real-time, DNAzyme-based FO-PCR assay for the first time, obviating the use of expensive fluorescent labels whilst still preserving the user-friendly format. Based on the FO-SPR sensor developed in Chapter 5, an additional amplification step is introduced using PCR. Both concepts can be combined by integrating the complementary sequence of a 10-23 DNAzyme as an overhang structure into the forward primer (FP). During PCR amplification, amplicons harboring a catalytically active DNAzyme are generated (DNAzyme-amps), boosting the signal generation by multiplying the active DNAzyme-amps. Similar to the DNAzymes in Chapter 5, the DNAzyme-amps can cleave the surface immobilized substrate. This way, AuNP labels are released, which can be monitored in real-time with our in-house developed FO-SPR sensing platform[37,38]. As a proof-of-concept, the assay is designed to detect the mobile colistin resistance type 2 gene (MCR-2 gene), a gene prevalent in Gram negative bacteria, such as *Escherichia coli*[39]. In short, this work introduces a powerful, real-time, universal tool for specific and sensitive detection of NAs, opening doors for applications in medical diagnostics, food monitoring, environmental monitoring, and beyond.

6.2. Experimental section

6.2.1. Materials and reagents

Following buffer reagents were purchased from The Merck group - Sigma-Aldrich (Bornem, Belgium): DNA/RNAse-free water, Trizma®base, magnesium chloride and sodium dodecyl sulfate (SDS). Sodium chloride and potassium dihydrogen phosphate were obtained from The Thermo Fisher Scientific group - Fisher Scientific (Merelbeke, Belgium). AppliChem GmbH (Darmstadt, Germany) provided dipotassium hydrogen phosphate and 1,4-dithiothreitol (DTT). Chemlab (Zedelgem, Belgium) provided sodium hydroxide and ethylenediaminetetraacetic acid (EDTA) was purchased from Acros Organics (Geel, Belgium). Ethanol absolute was obtained from VWR Chemicals (Haasrode, Belgium), PEG-molecules ($C_{27}H_{55}NO_9S$) from Polypure AS (Oslo, Norway), and AuNPs (Ø 20 nm) from BBI Solutions (Cardiff, UK). Both Immobiline DryStrip Cover Fluid and Illustra NAP-5 columns were provided by GE Healthcare Life Sciences (Diegem, Belgium). In Table S6.1 a detailed overview of the used DNA sequences is presented, all of which were obtained through DNA synthesis and purification services of Integrated DNA Technologies (IDT, Leuven, Belgium). Ligations were performed using the Ampligase® Thermostable DNA Ligase (5 U/µL) from Epicentre® (Madison, WI, USA) with accompanying 10× reaction buffer, while PCR reactions were performed in premix Ex Taq™ DNA Polymerase Hot Start Version from Takara Bio Inc. (Shiga, Japan). MCR-1 and MCR-2 gene sequences were described by Liu *et al.*[40] and Xavier *et al.*[39], respectively. Plasmids containing MCR-1 and MCR-2 genes were provided by the Lab of Medical Microbiology, University of Antwerp, Belgium.

6.2.2. FO-SPR sensor preparation and surface functionalization

The FO-SPR setup described in this work is based on the research and protocols established in previous chapters[37,38]. The FO-SPR sensors were used in reflection mode and consisted of a 4.3 cm long optical fiber (Ø 400 µm). At one end, both jacket and cladding were removed over a length of 0.6 cm and a thin gold layer of 50 nm was deposited by sputtering, forming the FO sensor tip. Once coated, the gold layer was functionalized with thiolated ssDNA (Table S6.1). After DTT activation (50 µM FO oligos in 0.05 M DTT and 90 mM phosphate, pH 8), all FO sensor tips were incubated overnight (4 °C)

with 1 µM activated FO oligos in PB-SDS buffer (10 mM phosphate, 0.01 % (w/v) SDS, pH 8.0) with 1 M NaCl. On the next day, the FO sensor tips were washed in Tris-SDS buffer (20 mM Tris buffer, 0.01 % (w/v) SDS, pH 8.3) and backfilled with 50 µM of PEG-molecules to minimize any nonspecific binding. After 1 hour of backfilling, the FO sensor tips were both washed and stored (4 °C) in Tris-SDS buffer until further use.

6.2.3. AuNP functionalization and covalent surface immobilization

AuNP functionalization and surface immobilization protocols were also based on previous chapters[36]. Briefly, the AuNPs were up-concentrated by centrifuging 2 mL for 20 min (16 200 g) and redissolving them in 600 µL PB-SDS buffer. Once activated as described in Section 6.2.2, thiolated AuNP oligos (Table S6.1) were added to the AuNPs to reach a final concentration of 1 µM after gradually increasing the salt concentration to 1 M NaCl over 3.5 hours [41]. The beads were incubated overnight at room temperature on a rotator and washed 3 times by centrifugation (15 min, 16 200 g), followed by redissolving in 1 mL PB-SDS buffer. Backfilling was performed by mixing the AuNPs with 50 µM of PEG-molecules, similar as for the FO-SPR sensors. After backfilling, the AuNPs were washed again 3 times and finally redissolved in nuclease-free water to a concentration of 4.65 nM (optical density measured at 530 nm with a microplate reader SpectraMax® M2/M2e Molecular devices, San Jose, CA, USA).

Covalent coupling of the AuNPs to the FO-SPR sensor surface was established following a previously published ligation protocol[36]. Briefly, the FO sensor tips were incubated for 20 min in a 100 µL ligation mixture containing: (i) 1 × Ampligase buffer, (ii) 100 nM ligation template, (iii) 0.05 U Ampligase, and (iv) 2.32 nM of functionalized AuNPs. Subsequently, the FO sensor tips were washed once in Tris buffer for 4 min, and then twice for 30 s in 10 mM NaOH. Finally, the FO-SPR sensors were stored in Tris-SDS buffer at 4 °C until further use. All reaction vials were covered with 50 µL oil to avoid evaporation and monitored in real-time on the FO-SPR setup.

6.2.4. DNAzyme-amplicon surface cleavage activity and optimal reaction conditions

Before performing any PCR amplification, the surface cleavage activity of the synthetic DNAzyme-amps (Table S6.1) was tested separately and compared

with a standard 10-23 DNAzyme (Table S6.1) at a previously optimized temperature of 55 °C (Chapter 5)[36]. For every FO-SPR sensor, an initial reference baseline was established in 1× DNAzyme reaction buffer (20 mM $MgCl_2$, 50 mM Tris, 150 mM NaCl, pH 9.4) for 7 min. Next, the FO-SPR sensor was transferred to a 1× DNAzyme reaction mixture with 25 nM DNAzyme or synthetic DNAzyme-amps for 30 min. After the cleavage activity, the FO sensor tips were washed twice for 30 s in 10 mM NaOH and once for 30 s in TE buffer (10 mM Tris, 1 mM EDTA, pH 8). Finally, a second reference baseline was established in 1× DNAzyme reaction buffer. All measurements were performed using the FO-SPR setup in 100 µL sample volume, covered with 50 µL oil to avoid evaporation. Further optimization required additional measurements at 50 and 45 °C (Section 6.3.2) and a first design of experiments (DOE), set up with the JMP 14 statistical software (SAS Institute Inc., Cary, NC, USA), to combine and optimize the conditions for surface cleavage activity and PCR amplification of the DNAzyme-amps (Section 6.3.3 and Supplementary Information).

6.2.5. PCR-amplified DNAzyme-amplicon activity and qPCR calibration curve

A second DOE was performed in parallel with the first, using MCR-2 primer pair 1, to combine and optimize the PCR amplification step with the surface cleavage activity of the DNAzyme-amps. Measurements were performed on a qPCR system (CFX96 real-time qPCR detection system, Biorad (Hercules, CA, USA), using fluorophore-quencher (F-Q) labelled DNAzyme substrate sequences (Table S6.1) and a 3-step temperature profile (T-profile, Supplementary Information Section 6.5.2). In order to achieve increased specificity, we evaluated a PCR profile with two successive phases (referred to as phase 1 and 2) with each phase consisting of a 2-step T-profile. Next, this two-phase PCR profile, with 2-step T-profiles in each phase, was combined with primer pair 2. After activation of the Hot Start polymerase during 35 s at 95 °C, phase 1 consisted of 15 cycles, each remaining 30 s at elevated temperatures between 60 – 69 °C and 5 s at 95 °C (Section 6.3.4). In phase 2, the annealing/extension step was conducted at the lower temperature of 46 °C for 60 cycles. Fluorescent measurements were performed in this second phase at the end of the annealing/extension step. The ramp rates were 5 °C/s and the lid heating was fixed at 95 °C. The PCR

reactions were performed in a final volume of 25 µL containing: (i) 1× Takara PCR mix, (ii) 12 mM $MgCl_2$, (iii) 24 nM FP, (iv) 480 nM RP, and (v) 200 nM DNAzyme substrate. With the second primer pair a qPCR calibration curve was established, at the annealing/extension temperature of 63 °C in phase one (Supplementary Information Section 6.5.2) and monitoring the reactions of a non-target control (NTC) and an MCR-2 gene serial dilution of 10^0 - 10^7 copy numbers. Quantification cycle (Cq) values were calculated based on the second derivative maximum method[42] and PCR efficiencies were calculated as: $efficiency = 10^{\frac{-1}{slope}} - 1$[43]. The experimental LOD was determined as the lowest target concentration that falls within the 95 % interval of the calibration curve[44].

6.2.6. Upscaling PCR reaction volume and DNAzyme-based FO-PCR measurements

In case of the FO-SPR measurements (Section 6.2.3), the final reaction volume was 100 µL to assure complete immersion of the FO sensor tip. Therefore, PCR amplification reactions (Section 6.2.5) needed upscaling, which was initially evaluated with the qPCR device before testing with the FO-SPR setup. The same reaction mixture, concentrations, and T-profile as described above were used, with slight modification as following: phase 1 consisted of 15 cycles, each for 1 min at 63 °C and 15 s at 95 °C, while phase 2 consisted of 35 cycles, each for 1 min at 46 °C and 15 s at 95 °C. Fluorescence was measured in phase 2 at the end of the annealing/extension step. Heating rates were 5 °C/s and the lid heating was maintained at 95 °C.

Once validated with qPCR, the adapted T-profile described above was used with the FO-SPR setup and the F-Q labelled DNAzyme substrate was replaced by the surface-immobilized, AuNP-labelled substrate. A T1 thermocycler (Biometra, Goettingen, Germany) without lid was used to enable automated movement of the FO-SPR sensors to the samples. All samples were sealed during incubation to control thermal evaporation. A calibration was established for an MCR-2 gene serial dilution of 4×10^4 - 10^7 copy numbers and specificity was evaluated by measuring the readout for a NTC and MCR-1 gene sample of 5.7×10^7 copy numbers. Cq values and PCR efficiencies were calculated as described in Section 6.2.5.

6.3. Results and discussion

6.3.1. Concept of DNAzyme based FO-PCR biosensing

The DNAzyme-based FO-PCR assay is illustrated in Figure 6.1. In this concept, the complementary sequence of a DNAzyme is introduced as an overhang structure through the FP. During PCR amplification, amplicons harboring a catalytically active DNAzyme sequence (DNAzyme-amps) are generated, which cleave the surface immobilized substrate. This results in the release of the AuNP labels, which can be monitored in real-time with our in-house developed FO-SPR sensing platform[37,38]. In order to realize this DNAzyme-driven FO-PCR assay, we first study with FO-SPR the feasibility of surface cleavage by the DNAzyme-amps (Figure 6.1, bottom). Secondly, we select reaction conditions that enable both PCR amplification and cleavage activity of the DNAzyme-amps on the FO-SPR sensor surface (Figure 6.1, top). Thirdly, we validate the incorporation of the active DNAzyme sequence during qPCR

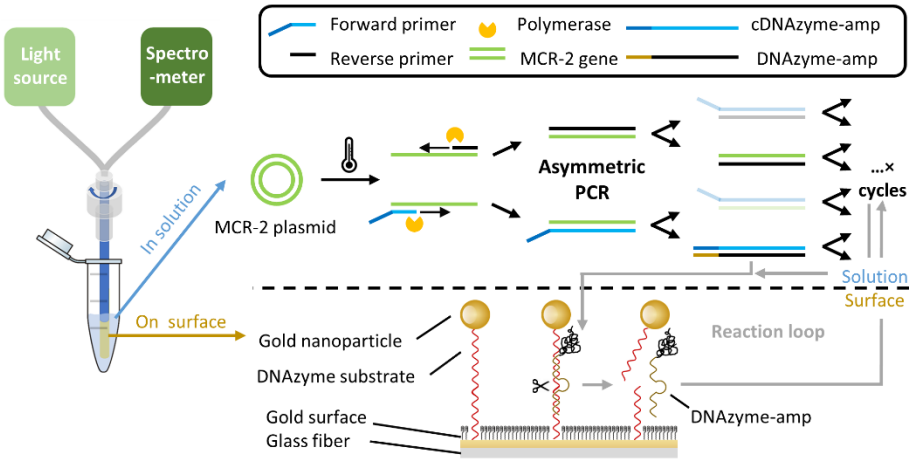

Figure 6.1: *Overview scheme of the DNAzyme-based FO-PCR detection system. The forward primer (FP) was designed to contain a target specific sequence and the complement of a DNAzyme sequence. After a first binding to the target (green) and extension of the FP, amplicons containing the DNAzyme complement (cDNAzyme-amps) are generated. In turn, binding and extension of the reverse primer (RP) to these cDNAzyme-amps during the next PCR cycles results into amplicons containing an active DNAzyme (DNAzyme-amps). Throughout the PCR reaction, the DNAzyme-amps are amplified and subsequently cleave AuNP-labelled DNAzyme substrates, immobilized on the surface of gold coated FO-SPR sensors as described in previous chapters[36]. The release of AuNPs from the surface changes the local refractive index, which can be monitored in real-time. The reaction loop indicates that after each denaturation step the DNAzyme-amps could reenter the PCR.*

in the presence of the MCR-2 gene and establish a reference qPCR calibration curve for different MCR-2 gene copy numbers. Finally, the optimal reaction conditions are combined with the FO-SPR sensing platform and detection of the MCR-2 gene is realized, using the final DNAzyme-based FO-PCR assay.

6.3.2. Evaluating DNAzyme-amp cleavage activity on the FO-SPR surface

DNAzyme-amps used in this work were based on a standard 10-23 DNAzyme (Table S6.1) because of: (i) its small catalytic core (15 nt) and high catalytic efficiency compared to other RCDs[23], (ii) its flexible substrate arms, (iii) its use of Mg^{2+} as cofactor, making it more compatible with physiological and PCR reaction conditions compared to other metal dependent DNAzymes, and (iv) its optimized FO-SPR surface cleavage activity as previously reported in Chapter 5[36]. However, contrary to the standard RCDs reported in literature, which mainly consist of relatively short DNA sequences (< 50 nt)[45], the DNAzyme-amps used here have an extended length of 149 nt, generated through PCR amplification (Figure 6.1). Because of this and the fact that the original DNAzyme sequence built into the DNAzyme-amps was reduced with one nucleotide, we first evaluated and compared the FO-SPR cleavage activity of the DNAzyme-amps with that of the standard DNAzyme. The shortening of the DNAzyme sequence was performed in order to minimize the difference in FP and RP length and as such match T_m's of the used primers, which was achieved by having maximal overlap between the complementary DNAzyme sequence and the FP.

All measurements were performed at this stage using synthetic DNAzyme-amps and the reactions were executed in previously described reference conditions (1× DNAzyme reaction buffer at 55 °C)[36]. A reaction without any DNAzyme was included as a negative control. The typical surface activity sensorgram measured with the FO-SPR setup is illustrated in Figure 6.2A and comprises four steps. In step 1, a reference baseline was established in 1× DNAzyme reaction buffer. Next, in step 2, cleavage by the DNAzyme resulted in a decrease in signal as AuNPs were released from the FO-SPR sensor surface. After incubation with the DNAzyme, the reaction was stopped in step 3 by washing the FO-SPR sensors shortly with NaOH and TE buffer. Finally, in step 4 a second baseline was established in identical conditions as in step 1 to determine the relative FO-SPR-shift due to the

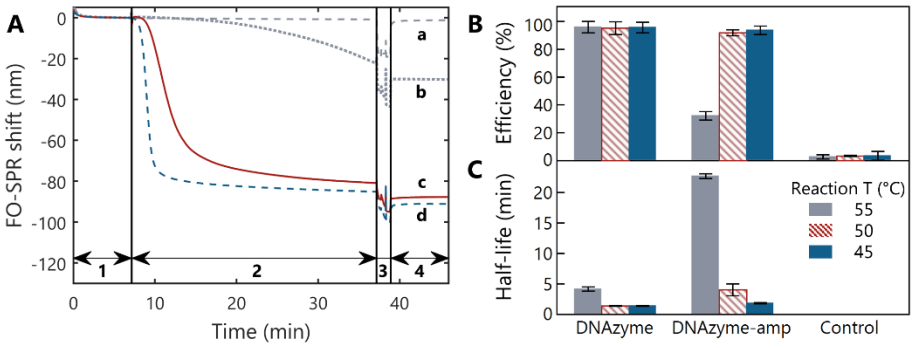

Figure 6.2: *Comparison of surface cleavage activity mediated by the DNAzyme-amps and standard DNAzymes.* ***A)*** *Real-time FO-SPR shifts for the DNAzyme-amp at 55 °C (curve b), 50 °C (curve c) and 45 °C (curve d), and the control at 55 °C (curve a). Standard DNAzyme curves and controls at 45 and 50 °C are not shown for clarity. Every measurement consisted of four steps: (1) reference baseline in buffer, (2) cleavage activity, (3) washing, and (4) second reference baseline in buffer. Since the FO-SPR sensor is sensitive to changes in RI and temperature, some initial drift and spikes in the signal can be observed when the sensors move from one vial to the other.* ***B)*** *Quantification of the reduced DNAzyme-amp activity and illustration of improved activity at lower temperatures by defining cleavage efficiency and* ***C)*** *half-life for both the standard DNAzyme and DNAzyme-amp. Error bars represent one standard deviation (n = 3).*

DNAzyme activity (e.g. the total DNAzyme shift = difference between both baselines). The observed activities were quantified as cleavage efficiencies (Figure 6.2B). This efficiency was calculated as the ratio of the DNAzyme shift and maximal FO-SPR shift determined after performing the ligation protocol as explained in Chapter 4[36]. Compared to the standard DNAzyme activity at 55 °C (Figure 6.2B), the synthetic DNAzyme-amps clearly showed a reduced activity at 55 °C, confirmed by a 63.4 % decrease in cleavage efficiency with a SD of 5.0. However, the cleavage activity of the DNAzyme-amps was still significant compared to the control (Figure 6.2B).

Since substrate recognition by the DNAzymes is based on the complementarity with its substrate-binding arms, any modification at this level can influence the DNAzyme behavior[46]. Therefore, it was hypothesized that the reduced DNAzyme-amp activity was related to the shortening of the 5'-substrate arm of the embedded DNAzyme sequence rather than the presence of the amplicon. Because shortening the substrate arm reduces the T_m of the embedded DNAzyme sequence, the DNAzyme-amp activity was evaluated at lower temperatures of 50 and 45 °C in order to improve the DNAzyme-amp activity. Figure 6.2B illustrates the increased DNAzyme-amp

activity based on the efficiency values at both reduced temperatures. Lowering the reaction temperature stabilized the substrate recognition, resulting in faster reaction kinetics, as illustrated in Figure 6.2C by the decrease in half-life values. In order to further support this hypothesis, a synthetic variant of the standard DNAzyme with a 5'-shortened substrate arm (Table S6.1) was evaluated in the same reference conditions and compared to the standard DNAzyme and a control. Figure S6.1 demonstrates a similar reduction in cleavage activity as in Figure 6.2B, supporting the hypothesis formulated above.

Based on these results, it was shown that the DNAzyme-amps could reach the same activity levels as the standard DNAzymes, but at lower temperatures due to the shortening of one of the substrate arms. Therefore, the surface activity of the DNAzyme-amps proved to be independent of amplicon extensions ≤ 115 nt, similar to the solution-based PCR-amplified DNAzyme-amp activity previously reported[27]. This makes the FO-SPR DNAzyme-amp activity suitable for real-time PCR applications[43], however, careful screening of reaction conditions to combine PCR amplification of the DNAzyme-amps with their FO-SPR cleavage activity is required as described in following section.

6.3.3. Screening reaction conditions towards combining PCR amplification with FO-SPR activity of DNAzyme-amplicons

DNAzymes have been reported to reach higher reaction rates at Mg^{2+} concentrations of 10 – 100 mM[23,47,48], while PCR reactions are characterized by lower concentrations of Mg^{2+}, typically between 3 - 6 mM[43]. In addition, DNA hybridization plays an important role for binding targets or substrates in PCR and DNAzyme reactions, respectively. Therefore, other parameters such as temperature, PCR mix composition, and monovalent salt concentrations need to be considered when combining both reaction mechanisms. Due to the multitude of factors at play and their effect on both reactions, a design of experiments (DOE) approach was followed and implemented with the JMP statistical software. Two individual I-optimal response surface experimental designs were created[49]: (i) one for the activity of the DNAzyme-amps on the FO-SPR sensor surface (based on the protocol in Section 6.3.2) and (ii) one for PCR amplification of the DNAzyme-amps with qPCR, using fluorescent DNAzyme substrates and MCR-2 primer pair 1. MCR-

Table 6.1: *DOEs used for selecting reaction conditions, towards combining and optimizing both the PCR-amplification of DNAzyme-amps and their subsequent FO-SPR cleavage activity*

	Design levels	
Factors	**DOE 1:** **DNAzyme-amp activity with FO-SPR**	**DOE 2:** **PCR amplification with qPCR**
Reaction/annealing temperature	45 – 55 °C	45 – 55 °C
Mg^{2+} concentration	7 – 20 mM	5 – 20 mM
Added KCl concentration	0 – 100 mM	0 – 50 mM
FP concentration	/	6 – 24 nM
Response variables[a]	Cleavage efficiency (Maximize) Half-life (Minimize) Wash ratio (Minimize)	Cq value (Minimize)

[a] Optimization criterion or desirability is given in parentheses (Max- or Minimization).

2 is a resistance gene that encodes for a phosphoethanolamine transferase enzyme, adding positively charged carbohydrates to the outer bacterial membranes and reducing their affinity towards last-resort antibiotics, such as colistin[50]. Table 6.1 summarizes both experimental designs. More details can be found in the Supplementary Information. The experimental data were analyzed by (i) determining the significant factor effects (Table S6.2 and Table S6.4), (ii) generating second-order regression models, and (iii) validating the second-order regression models.

Based on the two designs, prediction formulas were determined for every response variable (Table S6.3 and Table S6.5). These formulas show how the response variables behave as a function of the different factors

(Figure S6.2). By combining the obtained prediction formulas with the optimization criteria for the response variables (max- or minimization, Table 6.1), the JMP software predicted optimal reaction conditions to enable one-step PCR amplification and FO-SPR cleavage activity of the DNAzyme-amps (Figure S6.2). When rounded to the nearest integer, these optimal reaction conditions were 46 °C annealing/reaction temperature, 12 mM Mg^{2+}, 0 mM added KCl and 24 nM FP in 1× Takara PCR mix. In order to confirm the feasibility of the predicted optimal reaction conditions, both the FO-SPR DNAzyme-amp activity and PCR amplification with qPCR were performed individually at the optimal reaction conditions. When comparing the FO-SPR surface activity of the DNAzyme-amps and a control at the optimal reaction conditions with the activity at the reference conditions at 45 °C (Section 6.3.2), similar results were observed with DNAzyme-amps showing a cleavage efficiency of 90.5 % with a SD of 1.6 and a half-life of 2.46 min with a SD of 0.06. No significant results were observed for the control. On the other hand, the PCR amplification with qPCR resulted in a Cq of 23.4 cycles with a SD of 0.1 for 40 pg/µL of MCR-2 plasmids (or 2.6×10^7 gene copies, the typical higher range for qPCR experiments[43]). Comparison of the Cq_{sample} with a non-target control Cq_{NTC} value resulted in a significant difference ΔCq of 11.6 cycles with a SD of 0.5.

These results show the potential of the primers to detect the MCR-2 gene successfully and confirm the feasibility of performing both FO-SPR DNAzyme-amp activity and PCR amplification in the same reaction conditions. However, based on the ΔCq value obtained with qPCR, the theoretical achievable dynamic range of these primers, in case of 100 % PCR efficiency, would be only three orders of magnitude[43]. This is rather limited in terms of qPCR[51] and NAzyme-based PCR[27]. Further improvement of the dynamic range would be most relevant towards the lower target concentrations, as the MCR-2 plasmid concentration tested above is rather high for qPCR assays. Therefore, in order to obtain an increased ΔCq value and hence improve the dynamic range of the assay, we focused in the following section on increasing the Cq_{NTC} value by improving the specificity of the qPCR reaction.

6.3.4. PCR specificity improvement and establishment of MCR-2 calibration curve with qPCR

Improving qPCR specificity when using the same primer pair can be obtained by fine-tuning its T-profile. Therefore, from a 3-step T-profile (tested in previous section, Supplementary Information), we switched to a PCR profile with two successive phases, denoted as phase 1 and 2, with each phase consisting of a 2-step T-profile. More specific: (i) phase 1 contained 15 cycles annealing/extension at a higher temperature (range selected based on the T_m of the primers, Supplementary Information) and (ii) phase 2 contained 60 cycles annealing/extension at 46 °C, each followed by a denaturation step. As such, by sustaining higher reaction temperatures in phase 1, potential primer-dimers could be minimized due to the higher stringency for the specific primer binding, while focusing on the PCR amplification of the DNAzyme-amps. In contrast, phase 2 focused on triggering the cleavage activity of the embedded DNAzymes by setting the annealing/extension temperature to 46 °C, however still enabling PCR to take place by using the exact same optimized reaction conditions selected in previous section.

When the 2-step qPCR T-profile was tested with the MCR-2 primer pair 1, no improvement in specificity was observed (data not shown). Therefore, MCR-2 primer pair 2 was introduced (Table S6.1), aiming at a different region of the MCR-2 gene. Moreover, the FP complementarity was increased by 5 nt due to an increased overlap with the DNAzyme complement and extension of the FP. This second primer pair was tested with the 2-step qPCR T-profile for 40 pg/µL of MCR-2 plasmids and a NTC, while varying the higher annealing/extension temperature in phase 1 between 60 – 69 °C. As shown in Figure 6.3A, the improved specificity was obtained with the second primer pair, using an annealing/extension temperature of 60 °C in phase 1, compared to the 2-step results obtained with the primer pair 1. The $Cq_{40\ pg/\mu L\ MCR\text{-}2}$ value decreased (2 cycles with a SD of 0.2), while the Cq_{NTC} value increased more significantly (9 cycles with a SD of 3.7), resulting in an enhanced ΔCq value of > 9 cycles. Moreover, based on the data presented in Figure S6.3, illustrating that the elevated annealing/extension temperature improved the ΔCq value at the cost of increasing Cq_{sample} values, we selected 63 °C as it was the highest

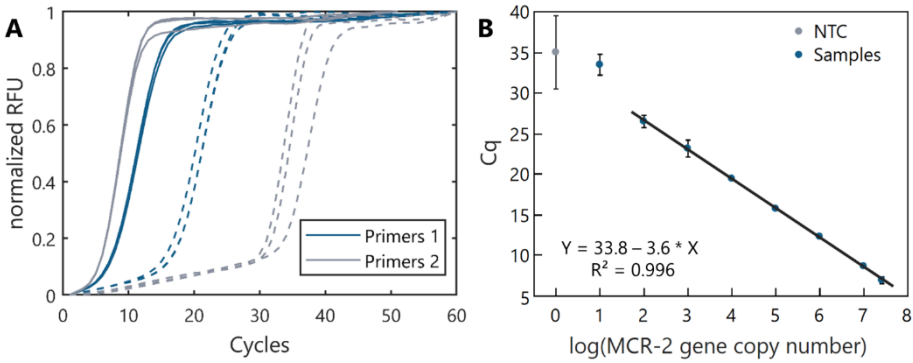

Figure 6.3: *Comparison of primer pairs and reference calibration curve on qPCR.* ***A)*** *Relative position of the $Cq_{samples}$ (solid lines) and the Cq_{NTC} (dashed lines) illustrates the specificity improvement of the MCR-2 primer pair 2 (grey) compared to MCR-2 primer pair 1 (blue). All signals were obtained with the 2-step T-profile with the annealing/extension T at 60 °C in phase 1.* ***B)*** *MCR-2 gene concentrations were measured with qPCR in a range of 10^1 - 10^7 copy numbers and the starting value of 2.6×10^7. The NTC is positioned at 10^0 for comparison. Only the linear points (10^2 - 10^7 copy numbers) were fitted. All signals were obtained with the 2-step T-profile and the annealing/extension temperature at 63 °C in phase 1. For both A) and B), fluorescence was only measured in phase 2 and presented cycle numbers exclude the 15 cycles of phase 1. Error bars represent one standard deviation (n = 3).*

temperature improving specificity without causing a significant increase of the Cq_{sample} value.

The established 2-step T-profile and primer pair 2 were then used to generate a calibration curve with qPCR, which will serve as a reference for the final DNAzyme-based FO-PCR assay. Starting from a MCR-2 plasmid concentration of 2.6×10^7 copy numbers, a 10-fold dilution series was prepared in a range of $10^1 – 10^7$ copy numbers. Figure 6.3B illustrates the different Cq_{sample} values in function of the logarithmic MCR-2 gene copy numbers. The Cq_{sample} values can be distinguished from the NTC down to an experimental LOD of 10^2 copy numbers and a clear linear trend can be observed ($R^2 = 0.996$). Based on the slope of the calibration curve, a PCR efficiency of 89.6 % was calculated, close to the optimal range of 90 – 110 %[43].

These results proved the potential of the second primer pair to be used in combination with the 2-step T-profile for specific MCR-2 gene detection. Compared to Todd *et al.*, similar fluorescence results were obtained, illustrating the universal aspect of PCR-amplified DNAzyme signal

generation[27]. The slightly larger dynamic range in their work (1 order of magnitude) might be related to the different target, primer pair design or reaction conditions, which in our system were optimized towards combining the PCR-amplification of DNAzyme-amps with surface cleavage activity mediated by DNAzyme-amps.

6.3.5. DNAzyme-based FO-PCR assay for MCR-2 detection

In order to establish the final DNAzyme-based FO-PCR assay, we needed to further upscale the PCR reaction to the volume that allows full submersion of the FO-SPR sensors in standard 0.1 mL PCR tubes. The effect of upscaling on the Cq values and PCR specificity was first validated with qPCR by increasing the reaction volume from 25 to 100 µL, while using the optimized reaction conditions and the 2-step T-profile described in previous section. Both PCR reaction mixture and target concentrations were kept the same, resulting in a 4× increase of the copy number. NTCs were included for comparison and specificity determination.

Figure 6.4A (left and middle bars) shows that upscaling of the reaction volume without any modification did not result in any meaningful signal generation. The samples and NTC signals coincided, both having much

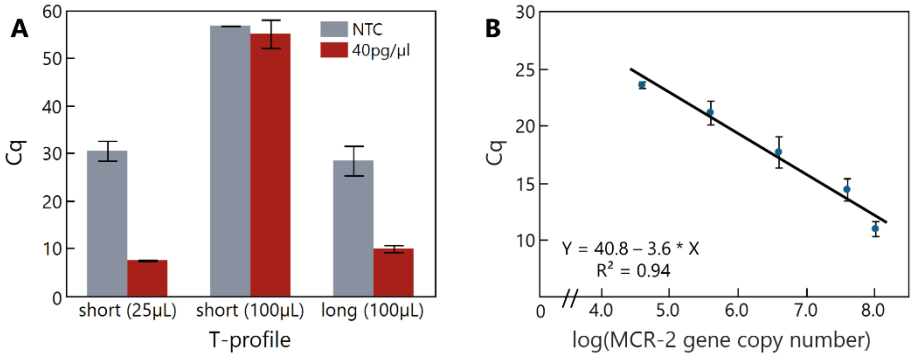

Figure 6.4: *PCR upscaling and calibration curve on FO-SPR setup.* ***A)*** *qPCR results show the loss of specificity in case the PCR reaction is scaled up without any adaptation of the T-profile. Prolonging some of the T-profile steps restored the initial specificity. Fluorescence was only measured in phase 2 and presented cycle numbers exclude the 15 cycles of phase 1.* ***B)*** *MCR-2 gene concentrations were measured in a range of 10^4 – 10^8 copy numbers. Only the linear points (10^4-10^8 copy numbers) were fitted. All signals were obtained with the 2-step T-profile and the annealing/extension temperature at 63 °C in phase 1. Presented cycle numbers exclude the 15 cycles of phase 1, according to the qPCR data. Error bars represent one standard deviation (n ≥ 3).*

higher Cq values than usually accepted. Based on the hypothesis that a bigger volume needs more time to reach the required temperatures when heating/cooling down, we adapted the 2-step T-profile by prolonging the different incubation times. Therefore, both in phase 1 and 2, the annealing/extension step was set to 1 min and the denaturation step to 15 s. As seen in Figure 6.4A (right bars), this adapted T-profile resulted in similar qPCR results as obtained with the initial volumes.

Next, the adapted 2-step T-profile was combined with FO-SPR sensors, prepared as described in Section 6.3.2, to detect different MCR-2 gene concentrations (starting at 4×10^7 copy, 10-fold dilution) based on surface cleavage activity of DNAzyme-amps. This resulted in an experimental LOD of 4×10^5 copy numbers or 6.6 fM with a linear trend between $10^5 – 10^8$ copy numbers (R^2 = 0.94) and PCR efficiency of 89.6 %. (Figure 6.4B). Compared to the qPCR results (previous section), the PCR efficiency remained the same based on the identical slopes of the calibration curves. This was in line with the results in Figure 6.4A where adapting the T-profile allowed for an efficient PCR amplification in larger reactions volumes. On the other hand, the intercept of the FO-PCR calibration curve was clearly positioned higher, indicating increased Cq_{sample} values for all concentrations. It was hypothesized that the delay in signal generation could be linked to the larger reaction volume and surface immobilized DNAzyme substrates compared to the solution-based qPCR.

Finally, the specificity of this approach was demonstrated by its potential to discriminate MCR-2 gene detection from other MCR genes, namely MCR-1. As seen in Figure 6.5, when the FO-SPR sensors were incubated with 5.7×10^7 MCR-1 plasmids, the obtained signal was comparable to the NTC. Furthermore, the obtained LOD improved our previous DNAzyme-based assay with > 5 orders of magnitude[36]. This is well within the range of most sensitive assays (1 µM - 0.1 fM) realized on this type of setup, using NA amplification and AuNPs[34,35,38,52,53].

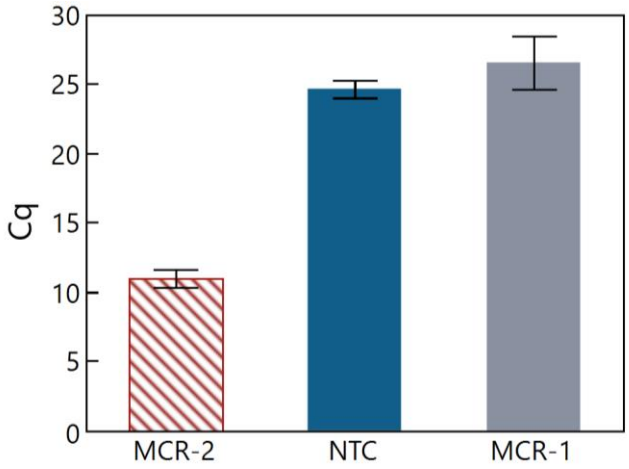

Figure 6.5: *Comparison with another antimicrobial resistance gene. Both a NTC and another antimicrobial resistance gene MCR-1 were tested to assure specificity of the assay. MCR-2 and MCR-1 concentrations were 40 pg/µL. Quantification cycles of the NTC and MCR-1 gene are similar and both significant different compared to the MCR-2 gene. Error bars represent one standard deviation (n ≥ 3).*

6.4. Conclusions

We presented an innovative, generic FO-PCR sensor concept, using a DNAzyme-based primer design that can be utilized for detection of virtually any NA sequence in a real-time manner. The SPR technology makes the concept more suitable to be used in opaque matrices such as blood, stool and wastewater, without the background interference currently plaguing the fluorescent readout methods. Next to the DNAzyme-based colorimetric readout systems, the presented FO-PCR assay is a unique alternative, independent of fluorescent labels. Moreover, most colorimetric assays are multistep endpoint assays (post-PCR), since the H_2O_2-assisted color reactions are not compatible with PCR[18,19,25,54]. Therefore, real-time PCR applications cannot be established, and post-PCR operations increase the risk of contaminations. In addition, the ultrasensitive systems often need extra sequence modifications[21,25] or primer addition steps[55,56] to realize the lower LODs.

Our assay incorporated the DNAzyme-complement in the FP targeting the gene of interest, which resulted in the generation of amplicons harboring the DNAzyme sequence. The DNAzyme-amp surface cleavage activity was proven and shown to be feasible despite the longer sequence

length (149 nt). Further optimization in PCR buffer conditions enabled to obtain similar FO-SPR shifts and kinetics as the standard 10-23 DNAzyme. Next, the PCR-based DNAzyme amplification and subsequent signal generation were integrated and validated using a standard qPCR system. Subsequently, the validated assay was upscaled to a volume of 100 µL and implemented on FO-SPR sensors for NA detection, based on the solid-phase cleavage of DNAzyme substrates. We demonstrated sensitive detection of the MCR-2 gene down to an experimental LOD of 6.6 fM or 4×10^5 copy numbers, using a single step for readout in a timeframe comparable with other fluorescent alternative systems (< 2 hours). In addition, we could successfully discriminate between the MCR-1 and -2 genes, illustrating the superior specificity of the system. Furthermore, the assay was monitored in real-time in a closed system, thereby simplifying handling procedures and eliminating cross-contamination.

In conclusion, this FO-PCR assay provides a universally applicable method for real-time detection of NAs, driven by solid-phase, DNAzyme cleavage activity. Because the DNAzyme complement was embedded in the FP, the DNAzyme substrate could remain the same while changing the target of interest. Additionally, only few other NAzyme-based SPR systems have been reported for the detection of metals[57], proteins[58], miRNA[59] and drugs[60], but none using optical fibers. The current system holds promise to realize such small molecule detection in the future by incorporating aptazymes or protein-DNA conjugates as capture moieties. Moreover, further research into downscaling of the reaction volume and integration of the FO-SPR sensors on chip holds promise to reduce both the assay time and the required reagents. The presented work has opened multiple avenues for development of integrated diagnostics for food and environmental monitoring, and infectious diseases, amongst other applications.

6.5. Supplementary Information

6.5.1. Materials and methods

6.5.1.1. Nucleic acid sequences

Table S6.1: *Overview of the NA sequences used in this study. All sequences are presented in 5' – 3' direction, and different regions are depicted as following: (i) sequence parts that bind with the DNAzyme are in bold, (ii) sequences forming the DNAzyme complement are underlined, and (iii) the 10-23 core DNAzyme is italicized. DNAzyme and substrate sequences are based on Bone et al. (2014)*[61].

Sequence name	**Length (nt)**	**Sequence (5' - 3')**
FO oligo	33	HS-TTTTTTTTTTGAGGGATTATAGTAT**CAGCACAA**
AuNP oligo	23	Phos-**CC**rG**rUCACCAACCG**TTTTTTTTTT-SH
Ligation template	24	TTGGTGACGGTTGTGCTGATACTA
Standard DNAzyme	35	*CGGTTGGTGAGGCTAGCTACAACGAGGTTGTGCTG*
Shortened DNAzyme	33	*GTTGGTGAGGCTAGCTACAACGAGGTTGTGCTG*
DNAzyme-amplicon	149	GTAGCATGATGAGCATATCTTTGCCATTATTGGCGCTGA CATAGTCATCTAGCCCGACAAGCATACCGACATCACGG CATTCGTTATAGGGATTGGTGTTACAGATGGTATTGTT*G GTTGGTGAGGCTAGCTACAACGAGGTTGTGCTG*
Forward primer 1	47	CAGCACAACCTCGTTGTAGCTAGCCTCACCAACCAACAA TACCATCT
Reverse primer 1	21	GTAGCATGATGAGCATATCTT
Forward primer 2	50	CAGCACAACCTCGTTGTAGCTAGCCTCACCAACCACTCA TCAATGCCTAT
Reverse primer 2	21	CGTAGTTCGCTTCATGCGTTT
Fluorescent DNAzyme substrate	21	/56-FAM/**CAGCACAACC**rG**rUCACCAACCG**/3IABkFQ/

For the primer pair selection, first the most interesting locations in the MCR-2 gene were identified for the FP, looking at positions showing the greatest overlap with the DNAzyme sequence by means of the OligoAnalyzer Tool of IDT[62]. Thereafter, primer pairs were defined with the Primerquest Tool from IDT[63], adapting the reaction conditions to the optimized conditions selected in this chapter, using default primer criteria, looking for an amplicon size between 100-200 nt and indicating the locations of interest for the FP to start. Final primer pair selection was based on the amplicon length and specificity, using the NCBI databases and their BLAST® services[64,65]. For the two primer pairs mentioned in Table S6.1, the T_m's were obtained through the OligoAnalyzer Tool: (i) FP_1 and RP_1 had a T_m of 75.9 and 61.7 °C respectively and (ii) FP_2 and RP_2 had a T_m of 76.7 and 67.0 °C respectively.

6.5.1.2. Experimental design and data analysis

In order to combine surface cleavage activity and PCR amplification of the DNAzyme-amps, reaction conditions optimizing both processes had to be identified (Section 6.5.2). Therefore, DOE was used and two individual I-optimal designs were constructed. For the cleavage activity by the DNAzyme-amps on the FO-SPR sensor surface (design 1, Table 6.1), measurements were based on the 4-step protocol described in Section 6.2.4: (i) establishment of a reference baseline, (ii) incubation with the DNAzyme-amps, (iii) inactivation of the surface cleavage activity by washing, and (iv) establishment of a second reference baseline. In step 2, the influence of the different factors was studied by replacing the 1× DNAzyme reaction buffer by: (i) a 1× Takara PCR buffer, based on Chapter 3[38], (ii) 25 nM DNAzyme-amps, and (iii) variable concentrations of KCl and $MgCl_2$, while varying the reaction temperature. The factor levels to be tested were defined by an I-optimal split-plot design, constructed using the JMP 14 software (SAS Institute Inc., Cary) with following response variables: (i) cleavage efficiency, (ii) half-life and (iii) wash ratio. The cleavage efficiency and half-life were defined above (Section 6.3.2). The wash ratio is the fraction of AuNPs that only detached from the FO-sensor surface after washing. This wash ratio is calculated as the ratio of (i) the FO-SPR shift only due to the washing step (step 3, Figure 6.2) and (ii) the total DNAzyme-amp shift as defined in Section 6.3.2.

For the PCR amplification tested on qPCR (design 2, Table 6.1), one additional factor was considered, namely the FP concentration. The PCR reactions were performed in a final volume of 25 µL containing: (i) 1× Takara mix, (ii) 480 nM RP, (iii) 200 nM DNAzyme substrate, (iv) 40 pg/µL of MCR-2 plasmids and (v) variable concentrations of KCl, $MgCl_2$ and FP. All conditions were tested with a 3-step PCR T-profile on qPCR consisting of: 35 s polymerase activation followed by 60 cycles, each of 5 s at 95 °C, 30 s at different annealing temperatures and 30 s at 72 °C. The factor level combinations to be tested were defined by a completely randomized I-optimal design and the response variable Cq value was analyzed with the JMP software. Finally, the prediction formulas resulting from the obtained models were combined in the profiler feature of JMP to select the optimal reaction conditions.

6.5.2. Results and discussion

6.5.2.1. Influence of the substrate arms on surface DNAzyme cleavage activity

In Section 6.3.2, it was hypothesized that the reduced DNAzyme-amp activity (Figure 6.2) was related to the shortening of the 5'-substrate arm of the embedded DNAzyme sequence (Table S6.1) rather than the presence of the amplicon. In order to support this hypothesis, a synthetic variant of the standard DNAzyme with a 5'-shortened substrate arm (less two nucleotides, Table S6.1) was evaluated in the same reference conditions and compared to the standard DNAzyme and a control. Figure S6.1A illustrates the FO-SPR shifts and shows that reducing the 5' substrate arm decreased the cleavage efficiency by 71.4 % with a SD of 5.5 (Figure S6.1B). This can be explained by the fact that reducing one of the substrate arms affected the overall T_m of the DNAzyme, resulting in slower kinetics in case the reaction conditions remain the same (Figure S6.1C). These results support the finding in Section 6.3.2 that the initial reduced cleavage activity of the DNAzyme-amps was mainly caused by the shortening of the 5' substrate arm, rather than the presence of the PCR amplicon.

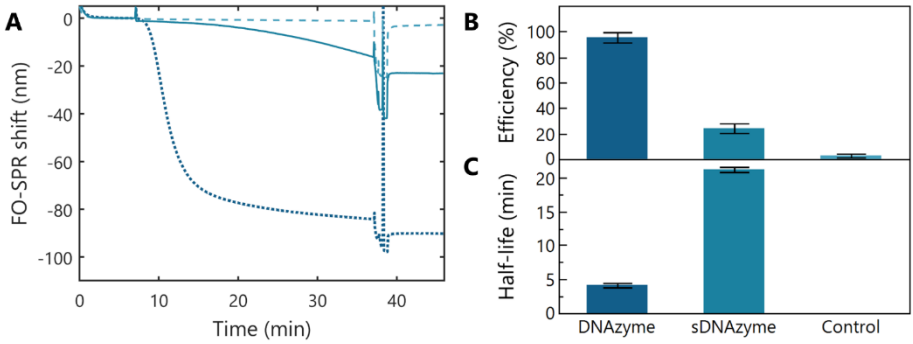

Figure S6.1: *Comparison of shortened DNAzyme with standard DNAzyme activity.* ***A)*** *Real-time FO-SPR shifts for the standard DNAzyme (dotted line) and the shortened DNAzyme (solid line) at 55 °C. Experiments were performed as described in Section 6.2.4 of the main manuscript at 55 °C, while replacing the synthetic DNAzyme-amp with 25 nM shortened DNAzyme. A control (e.g. without any DNAzyme, dashed line) is presented for comparison.* ***B)*** *Quantification of the reduced activity of the shortened DNAzyme by defining cleavage efficiency and* ***C)*** *half-life for both the standard and shortened DNAzyme (DNAzyme and sDNAzyme respectively). Error bars represent one standard deviation (n = 3).*

6.5.2.2. Design of experiment for screening DNAzyme-amplicon activity and PCR reaction conditions

Since the goal is to develop a single-step FO-PCR assay, both DNAzyme-amp cleavage activity and PCR amplification need to take place at the same reaction conditions. Both reactions and their output are based on DNA hybridization, which is affected by multiple factors, such as reaction temperature and mono- and divalent salt concentrations. Moreover, it is known that both reactions work best at opposite Mg^{2+} concentrations (high versus low), complicating the search for suitable conditions at which both reactions can take place. Due to this complication, two I-optimal experimental designs were set up. After analyzing the resulting data, the two fitted response surface models were combined to identify the suitable conditions.

I-optimal experimental designs have proven to lead to precise predictions of the response variables and to determine the optimal settings of experimental factors[49]. I-optimal experimental designs are especially useful when the influential factors are known, while D-optimal designs are mainly used for screening experiments intended for identifying the influential factors. A D-optimal design was not suitable for our study, because previous research within our group and in the literature already identified

the importance of the factors being considered (Table 6.1). Furthermore, a response surface experimental design was chosen for both our experiments, as all factors being considered are continuous and curvature is anticipated in the response-factor relationships. Both experimental designs were analyzed in the same way by (i) fitting a full second-order model to the data, (ii) determining the significance of the various factor effects, (iii) removing the insignificant factor effects from the model, and (iv) obtaining a final reduced second-order regression model. This way of analysis is called backward model selection and is typical for response surface models[49]. In all data analyses, we rescaled the factors to the [-1,+1] interval.

6.5.2.3. Prediction of FO-SPR DNAzyme-amplicon cleavage activity

The design for the DNAzyme-amp activity with FO-SPR was an I-optimal split-plot design generated with JMP. The responses were the cleavage efficiency, half-life and wash ratio. A split-plot design was defined because the FO-SPR setup can deal with two samples (i.e., factor level combinations) at the same time, subjected to the technical constraint that the reaction temperatures of both samples have to be the same. Therefore, the reaction temperature was defined as hard-to-change factor or whole-plot factor when creating the I-optimal split-plot design for the first experiment. Due to the split-plot nature of the experiment, the second-order regression models for cleavage efficiency, half-life and wash ratio were estimated with generalized least squares estimation instead of ordinary least squares estimation[49]. Using the JMP software, regression models for every response were generated and reduced by dropping the insignificant factor effects based on the F-tests for all main effects, interaction effects and quadratic effects. Table S6.2 shows all the remaining significant factor effects for the different responses. Furthermore, the significance and quality of the models were evaluated using analysis of variance (ANOVA) and goodness of fit parameters. The ANOVA showed that, for all three models, there is a significant relation between the factors and the responses ($P \leq 0.005$). The different model fits had adjusted R^2-values of 0.71, 0.99 and 0.92 for the cleavage efficiency, half-life and wash ratio, respectively. The resulting estimates of the factor effects are presented in Table S6.2 and resulting prediction formulas in Table S6.3.

Table S6.2: *Parameter estimates, standard errors and t-test results*

Cleavage efficiency

Term	Estimate	Std Error	DFDen	t Ratio	Prob>|t|
Intercept	0.7258729	0.045525	11.98	15.94	<.0001*
Mg (mM)(7,20)	0.26128	0.035839	11.8	7.29	<.0001*
KCl (mM)(0,100)	0.0798181	0.03415	11.71	2.34	0.0381*
Annealing T (°C) (45,55)	-0.177452	0.027646	5.978	-6.42	0.0007*
Mg (mM)*Mg (mM)	-0.218407	0.062508	11.24	-3.49	0.0049*

Half-life

Term	Estimate	Std Error	DFDen	t Ratio	Prob>|t|
Intercept	6.2544701	0.289742	6.803	21.59	<.0001*
Mg (mM)(7,20)	-8.818327	0.402081	4.302	-21.93	<.0001*
KCl (mM)(0,100)	1.2141641	0.255967	3.865	4.74	0.0098*
Annealing T (°C)(45,55)	9.0591744	0.492319	6.263	18.40	<.0001*
Mg (mM)*Mg (mM)	5.0923934	0.338967	2.955	15.02	0.0007*
Mg (mM)*KCl (mM)	-1.082437	0.32304	5.443	-3.35	0.0178*
Mg (mM)*Annealing T (°C)	-2.924377	0.580962	3.965	-5.03	0.0075*
Annealing T (°C)*Annealing T (°C)	5.9633582	0.487557	7.727	12.23	<.0001*

Wash ratio

Term	Estimate	Std Error	DFDen	t Ratio	Prob>|t|
Intercept	0.0594267	0.027236	7.208	2.18	0.0644
Mg (mM)(7,20)	0.0044837	0.018408	5.196	0.24	0.8169
KCl (mM)(0,100)	-0.02782	0.021726	6.111	-1.28	0.2468
Annealing T (°C)(45,55)	0.1221368	0.023289	5.967	5.24	0.0020*
Mg (mM)*Mg (mM)	0.0873503	0.030278	5.216	2.88	0.0327*
Mg (mM)*KCl (mM)	-0.135463	0.025959	6.758	-5.22	0.0014*
Mg (mM)*Annealing T (°C)	-0.073953	0.022323	4.835	-3.31	0.0223*
Annealing T (°C)*Annealing T (°C)	0.09307	0.034577	5.978	2.69	0.0361*

Table S6.3: *Resulting prediction formulas for the different response variables*

Response variable	**Prediction formulas with factors rescaled between [-1,1]**							
	$Y = \beta_0 + \beta_1 * X_{Annealing\ T} + \beta_2 * X_{Mg2+} + \beta_3 * X_{KCl} + \beta_{12} * X_{Annealing\ T} * X_{Mg2+} + \beta_{13} * X_{Annealing\ T} * X_{KCl} + \beta_{23} * X_{Mg2+} * X_{KCl} + \beta_{11} * X^2_{Annealing\ T} + \beta_{22} * X^2_{Mg2+} + \beta_{33} * X^2_{KCl}$.							
	β0	**β1**	**β2**	**β3**	**β12**	**β23**	**β11**	**β22**
Cleavage efficiency	0.73	-0.18	0.26	0.08	/	/	/	-0.22
Half-life	6.25	9.06	-8.82	1.21	-2.92	-1.08	5.96	5.09
Wash ratio	0.06	0.12	0.004	-0.03	-0.07	-0.14	0.09	0.09

6.5.2.4. Prediction of PCR-based DNAzyme-amplicon amplification

The experimental design for the Cq response with qPCR was a completely randomized I-optimal design generated with JMP, using ordinary least squares estimation to estimate the second-order regression model. All conditions were tested in one qPCR run and all test combinations of the I-optimal design were duplicated without any MCR-2 plasmids (NTC) in order to assure the specificity of the qPCR responses. The Cq_{sample} values used to generate the regression model were all lower than the corresponding Cq_{NTC} values. Table S6.5 shows all the remaining significant factor effects for the response in decreasing order of importance. Furthermore, the ANOVA showed that there is a significant relation between the factors and the response (P = 0.0001), while the adjusted R^2 value is 0.87. The resulting factor effect estimates in our final model are presented in Table S6.4 and resulting prediction formulas in Table S6.5.

Table S6.4: *Parameter estimates, standard errors and t-test results*

Cq value				
Term	**Estimate**	**Std Error**	**t Ratio**	**Prob>|t|**
Intercept	22.869769	0.492854	46.40	<.0001*
Mg (mM)*FP (nM)	2.428569	0.355203	6.84	<.0001*
Annealing T (°C)*FP (nM)	1.4913133	0.355649	4.19	0.0018*
KCl (mM)(0,50)	1.4636287	0.369145	3.96	0.0027*
Mg (mM)*KCl (mM)	1.6334952	0.449129	3.64	0.0046*
Annealing T (°C)(45,55)	-1.052698	0.31535	-3.34	0.0075*
Mg (mM)*Mg (mM)	1.8906937	0.586094	3.23	0.0091*
Annealing T (°C)*Annealing T (°C)	1.8684573	0.605594	3.09	0.0115*
FP (nM)(6,24)	-0.433426	0.32167	-1.35	0.2076
Mg (mM)(5,20)	-0.206949	0.324838	-0.64	0.5384

Table S6.5: *Resulting prediction formulas for the different response variables*

	Prediction formulas with factors rescaled between [-1,1]									
	$Y = \beta_0 + \beta_1 * X_{Annealing\ T} + \beta_2 * X_{Mg2+} + \beta_3 * X_{KCl} + \beta_4 * X_{FP\ conc} + \beta_{12} * X_{Annealing\ T} * X_{Mg2+} + \beta_{13} * X_{Annealing\ T} * X_{KCl} + \beta_{14} * X_{Annealing\ T} * X_{FP\ conc} + \beta_{23} * X_{Mg2+} * X_{KCl} + \beta_{24} * X_{Mg2+} * X_{FP\ conc} + \beta_{34} * X_{KCl} * X_{FP\ conc} + \beta_{11} * X^2{}_{Annealing\ T} + \beta_{22} * X^2{}_{Mg2+} + \beta_{33} * X^2{}_{KCl} + \beta_{44} * X^2_{FP\ conc}$									
Response	**β_0**	**β_1**	**β_2**	**β_3**	**β_4**	**β_{14}**	**β_{23}**	**β_{24}**	**β_{11}**	**β_{22}**
Cq	22.87	-1.05	-0.21	1.46	-0.43	1.49	1.63	2.43	1.87	1.89

6.5.2.5. Joint optimization of FO-SPR DNAzyme-amp activity and the PCR amplification with qPCR

Starting from the final regression models for the response variables corresponding to the FO-SPR DNAzyme-amp activity and the PCR amplification with qPCR, suitable process conditions were determined using JMP's prediction profiler tool. The joint optimization guarantees the most suitable conditions to combine both reactions in a one-step assay. Figure S6.2 shows the prediction profiler, in which every predicted response is plotted as function of the different factors (solid black lines). In addition, the right most column of the prediction profiler defines the goals to achieve for every

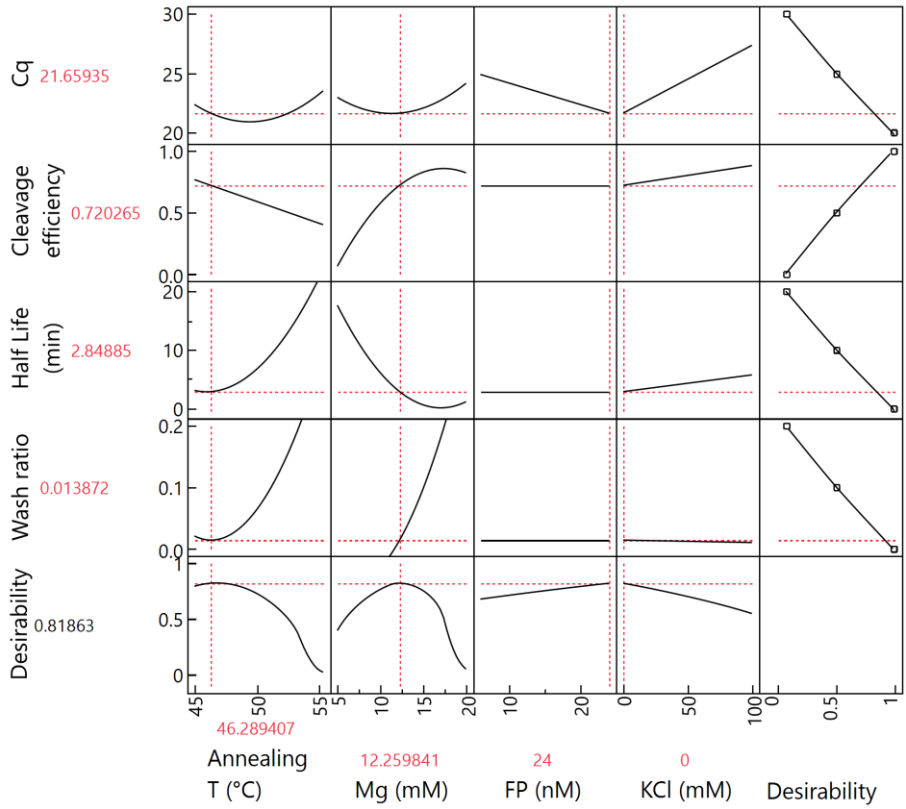

Figure S6.2: *Response prediction profiler for the selection of the optimal reaction conditions. Predicted responses are represented as a function of the different factors (solid black lines). In addition, the desirability functions are visualized in the right most column. The bottom panel visualizes the overall desirability as a function of the factor levels. Different predictions are made when manually changing one of the factor levels (dragging the red dashed lines to the left or right). The factor levels in red maximize the overall desirability. When rounded, these optimal factor levels equal 46 °C, 12 mM Mg^{2+}, 24 nM FP and 0 mM KCl.*

response separately by means of a desirability function. For instance, the Cq value has to be minimized, while cleavage efficiency should be maximized. Through the joint desirability (measured on a scale from 0 to 1) in the bottom panels of Figure S6.2, the extent to which all targets are achieved simultaneously is visualized. When defining the overall desirability, all response variables were given the same importance.

Predicted Cq values, half-life values and wash ratios were defined to be minimized as this is equivalent to getting fast, real-time response curves and minimal chance of AuNPs getting released only after the wash step. In contrast, the cleavage efficiency was to be maximized, assuring maximal signal generation in the selected conditions. Further, maximizing the overall desirability resulted in the factor levels presented in Figure S6.2. The selected optimal conditions were rounded to 46 °C reaction/annealing T, 12 mM Mg^{2+}, 24 nM FP and 0 mM KCl concentration. These optimal conditions were used in all subsequent experiments.

6.5.2.6. PCR specificity improvement and selection annealing temperature primer pair 2 with qPCR

In the previous section, the reaction conditions were jointly optimized for the combination of PCR amplification of the DNAzyme-amps and the subsequent FO-SPR DNAzyme-amp activity. For both the PCR amplification with qPCR and the FO-SPR DNAzyme-amp activity, confirmatory tests were performed in triple to verify the feasibility and the optimality of the settings identified in Figure S6.2. However, the specificity of primer pair 1 in the qPCR experiments was rather restricted and therefore two consecutive 2-step qPCR T-profiles were introduced, while varying the annealing/extension temperature. Quantification of the specificity was done by comparing the Cq values for 40 pg/µL of MCR-2 plasmids and a NTC. Figure S6.3 only illustrates the original 3-step PCR profile, used in the second experimental design, compared to the two-phase PCR profile, with the annealing/extension at 60 °C in phase 1 (shaded bars). No improvement in specificity was observed for primer pair 1.

Next, primer pair 2 was proposed, which aimed at a different region of the MCR-2 gene. This second primer pair was also tested with the two-phase PCR profile, with 2-step T-profiles in each phase, while varying the annealing/extension temperature between 60 – 69 °C based on the T_m of the primer pair. Figure S6.3 illustrates that elevated annealing/extension

temperature improved the ΔCq value, but this at the cost of increased Cq_{sample} values. Therefore, 63 °C was selected, as it was the highest temperature that improved specificity without causing a significant increase in the Cq_{sample} value.

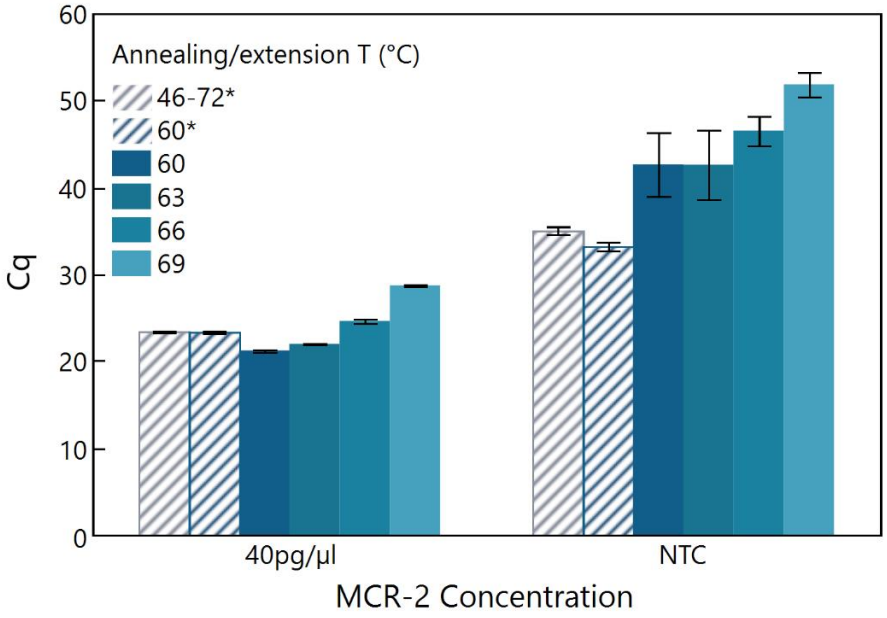

***Figure S6.3**: Comparison of different annealing/extension temperatures for primer pair 2. All qPCR results of primer pair 2 used the two- phase PCR profile, with 2-step PCR T-profile in each phase, as described in Section 6.2.5, while varying the annealing/extension temperature in phase 1 (solid bars). Both the results obtained with the original 3-step PCR profile (grey shaded) and the two-phase PCR profile (blue shaded) for primer pair 1 (*) are presented for comparison. The specificity of the PCR reaction eventually improved by using primer pair 2 in combination with the two-phase PCR profile. Fluorescence was measured during the annealing step for the 3-step PCR profile or during the annealing/extension step of phase 2 for the two-phase PCR profile. To compare the 3-step PCR profile and the two-phase PCR profile, the cycles of phase 1 and 2 were added up to obtain the total Cq values in the histogram. Error bars represent one standard deviation (n ≥ 3).*

6.6. References

1. Dwivedi, S. *et al.* Diseases and Molecular Diagnostics: A Step Closer to Precision Medicine. *Indian J. Clin. Biochem.* **32**, 374–398 (2017).
2. Higuchi, R., Dollinger, G., Walsh, P. S. & Griffith, R. Simultaneous Amplification and Detection of Specific DNA Sequences. *Bio/Technology* **10**, 413–417 (1992).
3. Notomi, T. *et al.* Loop-mediated isothermal amplification of DNA. *Nucleic Acids Res.* **28**, E63 (2000).
4. Liu, Z., Yao, C., Wang, Y. & Yang, C. A G-quadruplex DNAzyme-based LAMP biosensing platform for a novel colorimetric detection of Listeria monocytogenes. *Anal. Methods* **10**, 848–854 (2018).
5. Piepenburg, O., Williams, C. H., Stemple, D. L. & Armes, N. A. DNA Detection Using Recombination Proteins. *PLoS Biol.* **4**, e204 (2006).
6. Lobato, I. M. & O'Sullivan, C. K. Recombinase polymerase amplification: Basics, applications and recent advances. *TrAC Trends Anal. Chem.* **98**, 19–35 (2018).
7. Peng, H. *et al.* DNAzyme-Mediated Assays for Amplified Detection of Nucleic Acids and Proteins. *Anal. Chem.* **90**, 190–207 (2018).
8. Kasprowicz, A., Stokowa-Sołtys, K., Jeżowska-Bojczuk, M., Wrzesiński, J. & Ciesiołka, J. Characterization of Highly Efficient RNA-Cleaving DNAzymes that Function at Acidic pH with No Divalent Metal-Ion Cofactors. *ChemistryOpen* **6**, 46–56 (2017).
9. Nesbitt, S. M., Erlacher, H. A. & Fedor, M. J. The internal equilibrium of the hairpin ribozyme: temperature, ion and pH effects. *J. Mol. Biol.* **286**, 1009–1024 (1999).
10. Travascio, P., Li, Y. & Sen, D. DNA-enhanced peroxidase activity of a DNA aptamer-hemin complex. *Chem. Biol.* **5**, 505–517 (1998).
11. Ida, J. *et al.* G-Quadruplexes as An Alternative Recognition Element in Disease-Related Target Sensing. *Molecules* **24**, 1079 (2019).
12. Golub, E., Freeman, R., Niazov, A. & Willner, I. Hemin/G-quadruplexes as DNAzymes for the fluorescent detection of DNA, aptamer–thrombin complexes, and probing the activity of glucose oxidase. *Analyst* **136**, 4397 (2011).
13. Pelossof, G., Tel-Vered, R., Elbaz, J. & Willner, I. Amplified Biosensing Using the Horseradish Peroxidase-Mimicking DNAzyme as an Electrocatalyst. *Anal. Chem.* **82**, 4396–4402 (2010).
14. Pavlov, V. *et al.* Amplified Chemiluminescence Surface Detection of DNA and Telomerase Activity Using Catalytic Nucleic Acid Labels. *Anal. Chem.* **76**, 2152–2156 (2004).
15. Xia, H., Li, L., Yin, Z., Hou, X. & Zhu, J.-J. Biobar-Coded Gold Nanoparticles and DNAzyme-Based Dual Signal Amplification Strategy for Ultrasensitive Detection of Protein by Electrochemiluminescence. *ACS Appl. Mater. Interfaces* **7**, 696–703 (2015).
16. Xiao, Y. *et al.* Catalytic Beacons for the Detection of DNA and Telomerase Activity. *J. Am. Chem. Soc.* **126**, 7430–7431 (2004).
17. Du, Y. *et al.* G-Quadruplex-based DNAzyme for colorimetric detection of cocaine: Using magnetic nanoparticles as the separation and amplification element. *Analyst* **136**, 493–497 (2011).
18. Luo, R. *et al.* A colorimetric assay method for invA gene of Salmonella using DNAzyme probe self-assembled gold nanoparticles as single tag. *Sensors Actuators B Chem.* **198**, 87–93 (2014).
19. Seok, Y., Byun, J.-Y., Mun, H. & Kim, M.-G. Colorimetric detection of PCR products of DNA from pathogenic bacterial targets based on a simultaneously amplified DNAzyme. *Microchim. Acta* **181**, 1965–1971 (2014).

20. Wang, C. *et al.* Colorimetric biosensor based on a DNAzyme primer and its application in logic gate operations for DNA screening. *Anal. Chim. Acta* **987**, 111–117 (2017).
21. Kim, S. U. *et al.* Colorimetric molecular diagnosis of the HIV gag gene using DNAzyme and a complementary DNA-extended primer. *Analyst* **143**, 695–699 (2018).
22. Breaker, R. R. & Joyce, G. F. A DNA enzyme that cleaves RNA. *Chem. Biol.* **1**, 223–229 (1994).
23. Santoro, S. W. & Joyce, G. F. A general purpose RNA-cleaving DNA enzyme. *Proc. Natl. Acad. Sci.* **94**, 4262–4266 (1997).
24. Zhang, T. *et al.* Ultrasensitive Detection of Pb 2+ Based on a DNAzyme and Digital PCR. *J. Anal. Methods Chem.* **2019**, 1–6 (2019).
25. Cheglakov, Z., Weizmann, Y., Beissenhirtz, M. K. & Willner, I. Ultrasensitive detection of DNA by the PCR-Induced generation of DNAzymes: The DNAzyme primer approach. *Chem. Commun.* 3205 (2006). doi:10.1039/b605205c
26. Xu, J. *et al.* Engineering a DNA-cleaving DNAzyme and PCR into a simple sensor for zinc ion detection. *Anal. Bioanal. Chem.* **406**, 3025–3029 (2014).
27. Todd, A. V, Fuery, C. J., Impey, H. L., Applegate, T. L. & Haughton, M. A. DzyNA-PCR: use of DNAzymes to detect and quantify nucleic acid sequences in a real-time fluorescent format. *Clin. Chem.* **46**, 625–30 (2000).
28. Holland, P. M., Abramson, R. D., Watson, R. & Gelfand, D. H. Detection of specific polymerase chain reaction product by utilizing the 5'----3' exonuclease activity of Thermus aquaticus DNA polymerase. *Proc. Natl. Acad. Sci.* **88**, 7276–7280 (1991).
29. Homola, J. Surface Plasmon Resonance Sensors for Detection of Chemical and Biological Species. *Chem. Rev.* **108**, 462–493 (2008).
30. Oliverio, M., Perotto, S., Messina, G. C., Lovato, L. & De Angelis, F. Chemical Functionalization of Plasmonic Surface Biosensors: A Tutorial Review on Issues, Strategies, and Costs. *ACS Appl. Mater. Interfaces* **9**, 29394–29411 (2017).
31. Caucheteur, C., Guo, T. & Albert, J. Review of plasmonic fiber optic biochemical sensors: improving the limit of detection. *Anal. Bioanal. Chem.* **407**, 3883–3897 (2015).
32. Pollet, J. *et al.* Fiber optic SPR biosensing of DNA hybridization and DNA–protein interactions. *Biosens. Bioelectron.* **25**, 864–869 (2009).
33. Bedford, E. E., Spadavecchia, J., Pradier, C.-M. & Gu, F. X. Surface Plasmon Resonance Biosensors Incorporating Gold Nanoparticles. *Macromol. Biosci.* **12**, 724–739 (2012).
34. Pollet, J., Janssen, K. P. F., Knez, K. & Lammertyn, J. Real-time monitoring of solid-phase PCR using fiber-optic SPR. *Small* **7**, 1003–1006 (2011).
35. Knez, K., Spasic, D., Delport, F. & Lammertyn, J. Real-time ligation chain reaction for DNA quantification and identification on the FO-SPR. *Biosens. Bioelectron.* **67**, 394–399 (2015).
36. Peeters, B., Daems, D., Van der Donck, T., Delport, F. & Lammertyn, J. Real-Time FO-SPR Monitoring of Solid-Phase DNAzyme Cleavage Activity for Cutting-Edge Biosensing. *ACS Appl. Mater. Interfaces* **11**, 6759–6768 (2019).
37. Lu, J. *et al.* Fiber optic-SPR platform for fast and sensitive infliximab detection in serum of inflammatory bowel disease patients. *Biosens. Bioelectron.* **79**, 173–179 (2016).
38. Daems, D. *et al.* Identification and Quantification of Celery Allergens Using Fiber Optic Surface Plasmon Resonance PCR. *Sensors* **17**, 1754 (2017).
39. Xavier, B. B. *et al.* Identification of a novel plasmid-mediated colistin-resistance gene, mcr-2 , in Escherichia coli , Belgium, June 2016. *Eurosurveillance* **21**, 30280 (2016).
40. Liu, Y.-Y. *et al.* Emergence of plasmid-mediated colistin resistance mechanism MCR-1 in animals and human beings in China: a microbiological and molecular biological

study. *Lancet Infect. Dis.* **16**, 161–168 (2016).
41. Hurst, S. J., Lytton-Jean, A. K. R. & Mirkin, C. A. Maximizing DNA Loading on a Range of Gold Nanoparticle Sizes. *Anal. Chem.* **78**, 8313–8318 (2006).
42. Luu-The, V., Paquet, N., Calvo, E. & Cumps, J. Improved real-time RT-PCR method for high-throughput measurements using second derivative calculation and double correction. *Biotechniques* **38**, 287–293 (2005).
43. Life technologies (Thermo Fisher Scientific). *Real-time PCR handbook*. (2012).
44. Bustin, S. A. *et al.* The MIQE Guidelines: Minimum Information for Publication of Quantitative Real-Time PCR Experiments. *Clin. Chem.* **55**, 611–622 (2009).
45. Schlosser, K. & Li, Y. Biologically Inspired Synthetic Enzymes Made from DNA. *Chem. Biol.* **16**, 311–322 (2009).
46. Cairns, M. J. Optimisation of the 10-23 DNAzyme-substrate pairing interactions enhanced RNA cleavage activity at purine-cytosine target sites. *Nucleic Acids Res.* **31**, 2883–2889 (2003).
47. Mokany, E., Bone, S. M., Young, P. E., Doan, T. B. & Todd, A. V. MNAzymes, a Versatile New Class of Nucleic Acid Enzymes That Can Function as Biosensors and Molecular Switches. *J. Am. Chem. Soc.* **132**, 1051–1059 (2010).
48. Baum, D. A. & Silverman, S. K. Deoxyribozymes: useful DNA catalysts in vitro and in vivo. *Cell. Mol. Life Sci.* **65**, 2156–2174 (2008).
49. Goos, P. & Jones, B. *Optimal Design of Experiments*. (John Wiley & Sons, Ltd, 2011). doi:10.1002/9781119974017
50. Bardet, L. & Rolain, J.-M. Development of New Tools to Detect Colistin-Resistance among Enterobacteriaceae Strains. *Can. J. Infect. Dis. Med. Microbiol.* **2018**, 1–25 (2018).
51. Heid, C. A., Stevens, J., Livak, K. J. & Williams, P. M. Real time quantitative PCR. *Genome Res.* **6**, 986–994 (1996).
52. Knez, K. *et al.* Spherical Nucleic Acid Enhanced FO-SPR DNA Melting for Detection of Mutations in Legionella pneumophila. *Anal. Chem.* **85**, 1734–1742 (2013).
53. Daems, D., Knez, K., Delport, F., Spasic, D. & Lammertyn, J. Real-time PCR melting analysis with fiber optic SPR enables multiplex DNA identification of bacteria. *Analyst* **141**, 1906–1911 (2016).
54. Liu, Z. *et al.* Development of DNAzyme-based PCR signal cascade amplification for visual detection of Listeria monocytogenes in food. *Anal. Biochem.* **553**, 7–11 (2018).
55. Du, F. & Tang, Z. Colorimetric Detection of PCR Product with DNAzymes Induced by 5′-Nuclease Activity of DNA Polymerases. *ChemBioChem* **12**, 43–46 (2011).
56. HU, Z., ZHOU, Y., XIE, X., JIANG, R. & LI, N. Two-stage Nicking Enzyme Signal Amplification Combined with DNAzyme Amplification for the Detection of Bone Morphogenetic Protein 6 mRNA. *Anal. Sci.* **30**, 1039–1044 (2014).
57. Pelossof, G., Tel-Vered, R. & Willner, I. Amplified Surface Plasmon Resonance and Electrochemical Detection of Pb 2+ Ions Using the Pb 2+ -Dependent DNAzyme and Hemin/G-Quadruplex as a Label. *Anal. Chem.* **84**, 3703–3709 (2012).
58. Chen, Y. & Corn, R. M. DNAzyme Footprinting: Detecting Protein–Aptamer Complexation on Surfaces by Blocking DNAzyme Cleavage Activity. *J. Am. Chem. Soc.* **135**, 2072–2075 (2013).
59. Li, X. *et al.* A novel surface plasmon resonance biosensor for enzyme-free and highly sensitive detection of microRNA based on multi component nucleic acid enzyme (MNAzyme)-mediated catalyzed hairpin assembly. *Biosens. Bioelectron.* **80**, 98–104 (2016).
60. Li, H., Chang, J., Hou, T. & Li, F. HRP-Mimicking DNAzyme-Catalyzed in Situ Generation of Polyaniline To Assist Signal Amplification for Ultrasensitive Surface Plasmon

Resonance Biosensing. *Anal. Chem.* **89**, 673–680 (2017).
61. Bone, S. M. *et al.* DNA-only Cascade: A Universal Tool for Signal Amplification, Enhancing the Detection of Target Analytes. *Anal. Chem.* **86**, 9106–9113 (2014).
62. IDT. OligoAnalyzer Tool.
63. IDT. Primequest Tool. Available at: https://eu.idtdna.com/Primerquest/Home/Index.
64. Altschul, S. F., Gish, W., Miller, W., Myers, E. W. & Lipman, D. J. Basic local alignment search tool. *J. Mol. Biol.* **215**, 403–410 (1990).
65. Agarwala, R. *et al.* Database resources of the National Center for Biotechnology Information. *Nucleic Acids Res.* **46**, D8–D13 (2018).

Chapter 7

General conclusions and perspectives

7.1. General conclusions

The genetic information contained in the DNA of all organisms makes the detection and analysis of DNA molecules keystones in disease screening and early diagnosis, food quality assurance, and environmental monitoring. However, the majority of DNA analyses are still restricted to conventional laboratory techniques such as PCR, relying on bulky equipment, trained personnel and large batches of samples. Biosensor technology has offered an alternative by developing more user-friendly, time-efficient and affordable devices. Among biosensors, FO-SPR is of interest due to its advantageous features such as user-friendliness, real-time measurement and fast analysis. However, concerning NA-analysis FO-SPR assays are mainly based on classical hybridization strategies. Ultrasensitive detection (low pM to fM range) has remained challenging. These challenges go back to the means of signal generation and amplification, where alternative methods have not been fully explored. Upcoming fields such as DNA nanotechnology have created opportunities in this respect by discovering new functional molecules such as DNAzymes, with promising features supporting biosensor development. DNA nanotechnology is yet far from mature and solid-phase DNAzyme strategies have been concentrating on metal ion detection. NA and protein applications are rare and demand more advanced design and implementation of current DNAzyme-based strategies.

In this framework, **the main objective of this dissertation was to design innovative NA-based biosensing strategies using a FO-SPR platform for the sensitive and specific detection of NAs.** This main objective was translated in following sub-objectives:

- **The design of a FO-PCR melting assay** with the aim of quantifying and differentiating DNA molecules with closely related sequences. The assay is explored for the detection of celery DNA as a proof-of-concept for the food industry and evaluated in cleaning water samples, spiked with known concentrations of celery DNA
- **The design of a FO-SPR biosensing concept sensitive to surface-based catalytic cleavage activity of DNAzymes** with the aim of evaluating the feasibility of this cleavage activity in future universal solid-phase diagnostics.

- **The design of a DNAzyme-based FO-PCR assay** with the aim of real-time and ultrasensitive DNA detection by combining NA amplification strategies and DNAzymes. The assay is explored for the detection of an antimicrobial resistance gene in *E. Coli* as a proof-of-concept for health care and livestock applications.

In **Chapter 2**, the reader was first introduced to the concepts of functional DNA nanotechnology in relation to biosensing. Following the basic principles and physics background of SPR was explained and examples of different SPR configurations were discussed, including our in-house developed FO-SPR platform. Finally, classical DNA functionalization techniques of the gold surface were listed, enabling state-of-the-art DNA-based signal amplification strategies.

ELISA and qPCR are the golden standards for the detection of food allergens. Unfortunately, their use is mostly restricted to sophisticated laboratory environments. Furthermore, cross-reactivity with related species makes accurate detection more challenging. In this context, the first sub-objective of this dissertation was formulated and addressed in **Chapter 3.** A FO-PCR-MA was designed for the detection and differentiation of closely related DNA molecules. FO-SPR sensor functionalization with capture probes enabled binding of the PCR amplified ssDNA targets, which increased the hybridization of AuNP labels with every cycle and enabled target detection. Subsequent HRM after each PCR cycle caused the AuNP labels to be released at the specific T_m of the target, providing a way to differentiate among different sequences. As a proof-of-concept, the design was validated for the celery *Mtd* gene after in-house selection of an optimal gene region referred to as *Mtd 3*. Accurate detection was obtained between 1 pM and down to a LOD of 0.1 fM. The FO-PCR-MA was benchmarked against a classical qPCR assay followed by HRM. The performance of the FO-PCR-MA was slightly improved in terms of dynamic range with one order of magnitude and estimation of the different T_m was similar. Moreover, by including the HRM step in each cycle, the FO-PCR-MA improved the time-to-result with ~25 min. Finally, cleaning water samples spiked with celery DNA were analyzed and benchmarked with excellent accordance between the reference qPCR/HRM and the FO-SPR-MA, confirmed by an ICC of 0.94. These results proved that FO-SPR is suitable for the ultrasensitive detection of NAs and has great

potential as next generation diagnostic test based on its fast, cost-effective and automated aspects.

Next to classical PCR, the upcoming field of DNA nanotechnology has been introducing several concepts, such as DNAzymes, which take DNA far beyond the classical hybridization strategies. In turn, new functional DNA molecules and their potential applications ask for innovative ways of implementation. In **Chapter 4**, the first step was taken to address the second sub-objective of this dissertation. A ligation strategy was presented, enabling the creation of AuNP-labelled DNAzyme substrates on the surface of the FO-SPR sensor. Smart sequence design in combination with the high specificity of the ligase eliminated the formation of non-labelled substrates. This way potential interference with future one-step DNAzyme-based signal generation was minimized. Optimization of the ligation reaction was obtained by screening and selecting the ligation temperature and template concentration, affecting the AuNP density on the sensor surface. Optimal values were 55 °C and 100 nM, causing the FO-SPR sensor surface to be saturated with AuNPs at a density of 666 particles/μm^2 with a SD of 56. Furthermore, the associated real-time FO-SPR shifts were characterized with a 10-fold increase in value compared to usual measured SPR-shifts, having the potential to increase the dynamic range. The quality of the ligation strategy was confirmed by its high specificity and efficiency with an average value of 90.3 % with a SD of 1.4. As such, an innovative surface labeling strategy was developed with great potential to be translated to other solid-phase systems and to study surface confined DNAzyme catalytic cleavage activity.

After establishing the FO-SPR sensor with AuNP-labelled substrates in previous chapter, the second sub-objective was further addressed in **Chapter 5**. Real-time monitoring of DNAzyme cleavage activity and its suitability for biosensing applications were studied. Different DNAzyme concentrations ranging from 3 to 100 nM could be detected by logarithmic transformation of the reaction's half-life values. From 25 nM DNAzyme onward, signal generation efficiencies exceeded 95 % within the incubation time of 30 min, based on the optimal ligation shifts obtained in Chapter 4. Once the cleavage activity could be monitored, the FO-SPR sensor was further adapted towards potential biosensing applications such as NA

detection. Control over the DNAzyme activity was realized by a small excess (1.4:1) of inhibitor strand, temporarily blocking the DNAzyme. Due to a built-in loop structure of the inhibitor strand, target-triggered strand displacement enabled specific, DNAzyme-based detection of ssDNA down to a theoretical LOD of 1.4 nM. Overall, these results confirmed the suitability of our FO-SPR sensor design to monitor DNAzyme catalytic activity, which in a controlled way has the potential of a universal DNA biosensor.

Although Chapter 5 illustrated successful detection of ssDNA using a DNAzyme-based FO-SPR assay, ultrasensitive detection down to the lower pM - fM range was not obtained. The latter is however crucial for early disease diagnosis. In addition, the integration of PCR amplification into DNAzyme-based systems has been limited mainly to end-point detection due to PCR-incompatible signal generation. Therefore in **Chapter 6**, the final sub-objective of this dissertation was addressed. The amplification strength of PCR was translated into the design of a FO-PCR assay, boosting the DNAzyme signal generation introduced in Chapter 5. DNAzymes were integrated into the PCR scheme by extending the forward primer with a complementary DNAzyme sequence. Resulting DNAzyme-amps were proven to be compatible with the AuNP-labelled FO-SPR sensors. Moreover, after optimizing the reaction temperature, the obtained signal generation and kinetics were comparable to the ones of a regular DNAzyme. Therefore, the DNAzyme-amps proved to be independent of amplicon extensions ≤ 115 nt, as observed in solution. Further, PCR-based DNAzyme amplification and subsequent substrate cleavage were verified on a conventional qPCR system. As a proof-of-concept, the assay was designed for the detection of the antimicrobial resistance gene MCR-2. Once verified, upscaling of the FO-PCR assay to standard FO-SPR reaction volumes (100 µL) was proven. Finally, a calibration curve was established using the FO-SPR sensors and enabling a LOD down to 6.6 fM. As such, PCR-amplified DNAzyme-amplicons enabled a generic assay for ultrasensitive NA detection, avoiding fluorescence and post-PCR processing while maintaining the real-time aspect.

In conclusion, creative FO-SPR sensor designs were presented in this dissertation to study and establish innovative NA-based strategies for the sensitive and specific detection of NA targets. While the introduction of DNAzyme technology has been exploited in terms of signal amplification,

stability and universal sensor design, the FO-SPR platform was exploited for its real-time, user-friendly and fast analysis. As such, three different NA-based strategies were developed: (i) a FO-PCR-MA, enabling ultrasensitive (fM) NA detection with high-resolution distinction of closely related sequences, (ii) a DNAzyme-based FO-SPR assay, establishing surface DNAzyme activity and universal NA detection (nM) and (iii) a DNAzyme-based FO-PCR assay, improving the NA sensitivity (fM) of the DNAzyme-based approach, while maintaining the universal aspect. Proof-of-concept applications showed their potential for both food quality and healthcare. Despite the significant progress demonstrated in previous chapters, the work is yet unfinished and future research should be performed to further improve and extend the technology.

7.2. Future perspectives

Whereas different NA-based strategies were explored in this dissertation on a FO-SPR platform for the first time, the dissertation forms the basis for further development and improvement of the presented work. In particular, the introduction of DNAzymes opened the way for new FO-SPR opportunities and applications. These include, for example, expanding the variety in target molecules, further improving the control of surface functionalization, downscaling the FO-SPR technology and integration in new amplification cascades. Some of these applications and opportunities are discussed in more detail as potential future work in the following sections.

7.2.1. Expanding the range of target molecules

Due to the DNA nature of the signal generation and amplification systems introduced in this dissertation, target detection has been limited to NA detection. However, both Chapter 5 and 6 suggest the universal character of the NA-based strategies, combined with the AuNP-labelled FO-SPR sensor design, by illustrating the detection of two different target sequences. We believe that by only adapting the target recognition system, linked to the DNAzyme-based FO-SPR sensor, the range of target molecules could be extended to proteins and small molecules. The FO-SPR platform already proved its capacity to detect a variety of these target molecules[1–4], but requiring thorough optimization at the surface interface for each individual bioassay.

A first approach to broaden the range towards proteins and small molecules would be the introduction of aptamers[5,6] in the proposed NA strategies. For example, the internal loop structure of the DNAzyme-inhibitor strand complex, introduced in Chapter 5, could harbor an aptamer sequence instead of a target complementary sequence. The strand displacement action would be exchanged for target recognition by the aptamer and its associated conformational change, releasing the temporarily blocked DNAzyme sequence (Figure 7.1). This approach could be of interest in the search for protein-free assays, and protein detection for which no two aptamers are available to construct a classical 'sandwich' assay. Aptamers with specific affinities should be selected and additional aspects such as buffer compatibility (e.g. pH, ionic strength, etc.) should be considered. The buffer plays an important role in the appropriate folding of aptamers[7], which might differ from the conditions for optimal DNAzyme activity. As both aptamers and DNAzymes are selected through SELEX, buffer incompatibility might be circumvented by performing the selection of both molecules in the same buffer.

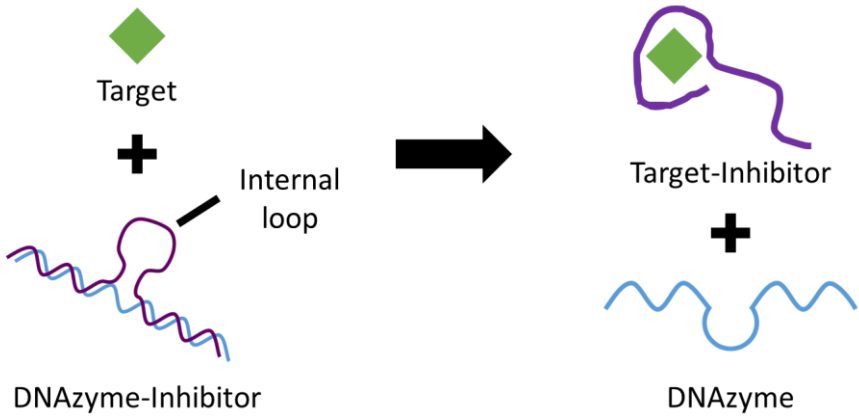

Figure 7.1: *Expanding applications beyond NA detection. The inhibitor strand can act as aptamer towards a protein or small molecule of interest.*

MNAzymes offer a second interesting approach to further improve the universal aspect of the FO-SPR sensor design[8]. By splitting up the catalytic core and addition of the sensor arms, MNAzymes enable straightforward sequence exchanges at the target level without affecting the MNAzyme core or substrate sequences. A good starting point for the implementation of this

generic aspect of MNAzymes would be splitting up the DNAzyme used in Chapters 5 and 6 and extending both parts with a specific sensor arm to form two partzymes (Figure 7.2A). Some preliminary data on this topic was obtained by extending the split catalytic core with sensor arms, complementary to an ATP aptamer[8]. In Figure 7.2A, the activity of the ATP MNAzyme was compared to the one of its equivalent DNAzyme, resulting in DNAzyme shifts of 21.5 nm for 100 nM DNAzyme concentration. In presence of 100 nM ATP aptamer, active MNAzymes were formed and their cleavage activity could be distinguished from the NTC (absence of the ATP aptamer). The MNAzyme efficiency was significantly lower compared to the DNAzyme activity and only resulted in MNAzyme shifts of 2.44 nm.

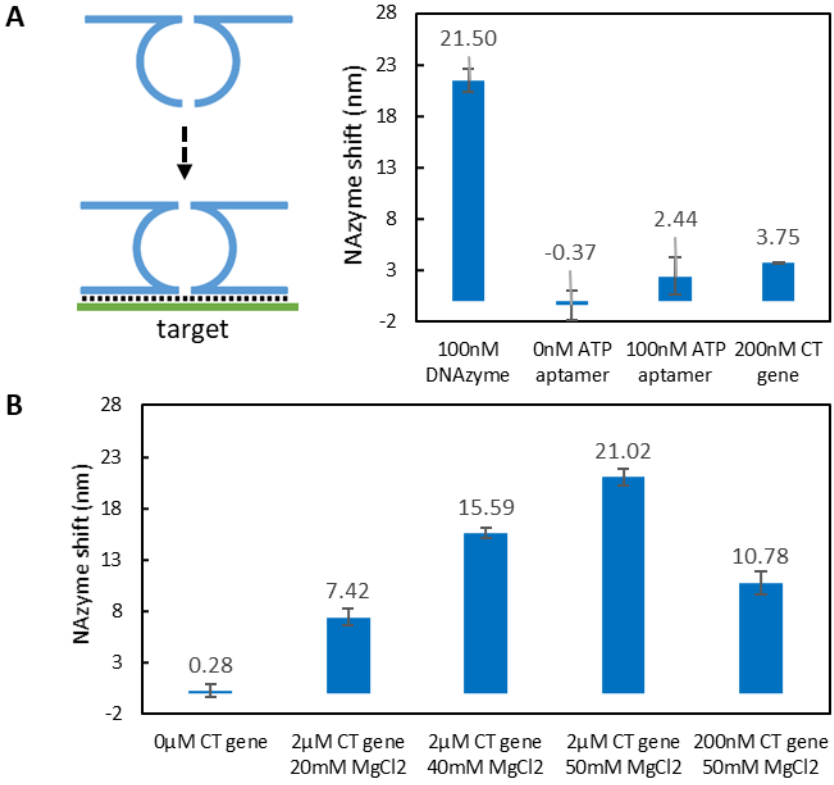

Figure 7.2: *Comparison DNAzyme versus MNAzyme activity.* ***A)*** *A standard DNAzyme was split in 2 and provided with 2 sensor arms able to bind a target of interest. Two targets were selected: (i) an ATP aptamer and (ii) a gene region of Chlamidia trachomatis (CT). Reactions were performed at 55 °C* ***B)*** *Reaction conditions were adapted for the MNAzyme targeting the CT gene. Reaction were performed at 53 °C and $MgCl_2$ concentration were varied between 20 and 50 mM.*

A similar MNAzyme shift of 3.75 nm was obtained for a second MNAzyme and target sequence, corresponding to a specific gene region of *Chlamidia trachomatis* (CT gene)[9]. This illustrated already the generic aspect of MNAzymes, while highlighting the need for further optimization. The MNAzyme shifts increased 2 - 3 fold in value by slightly lowering the temperature and increasing the Mg^{2+} concentrations to 40 and 50 mM (Figure 7.2B). Mainly changing the Mg^{2+} concentration seemed to play a crucial role in improving the MNAzyme activity. It was hypothesized that this could be related to the overall size of the MNAzymes, affecting the interaction with the surface immobilized substrate. Compared to a standard DNAzyme molecule (35 nt), the MNAzyme has a more substantial DNA structure (121 nt), which suggests an overall higher negative charge coming from the DNA backbone. Higher ionic strengths might be needed to counteract the corresponding electrostatic repulsions. Profound optimization of the reaction conditions as described in Chapter 6 for the DNAzyme-amp activity should be considered next. Since the MNAzymes are similar in size compared to the DNAzyme-amps (149 nt), obtaining efficient MNAzyme-based FO-SPR sensors in the near future is promising.

Finally, a more advanced way to expand the range of targets is by selecting new DNAzymes for which the target of interest also acts as cofactor of the catalytic core. This mechanism has been applied from the start for DNAzyme-based metal ion sensors, which all use the metal ion of interest as cofactor[10]. Non-metal cofactors have been reported less frequently but would be of an even greater interest to further simplify more complex systems, introducing additional inhibitor strands or aptamers for target-controlled catalytic activity. Ali *et al.* selected a ligand-responsive DNAzyme in crude extracellular matrix (CEM) of *E. coli*, which made the DNAzyme only responsive to this particular CEM (Figure 7.3)[11]. Identification of the exact nature of the target was beyond the scope of the paper, but preliminary data suggested a protein. The same research group has selected similar ligand-responsive DNAzymes for other bacteria such as *C. difficile* and mammalian cells such as breast cancer cells. For *C. difficile*, the target was identified as the transcription factor TcdC-24, which even turned out to be strain specific. For the mammalian cells, a DNAzyme (AAI2-5) was selected in the cell lysate of the breast cancer cell line MDA-MB-231. The DNAzyme enabled detection

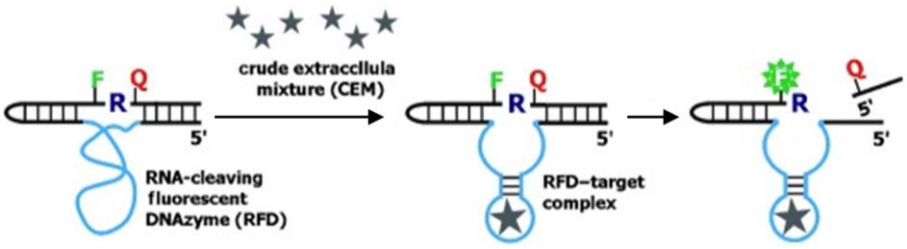

Figure 7.3: *Schematic of a ligand-responsive DNAzymes. Substrate and DNAzyme were coupled into a single strand with built-in fluorophores (F) and quenchers (Q). In presence of the CEM produced by the bacteria, a fluorescent signal proportional to the number of bacteria is produced. Adapted with permission from Ali et al. © (2011) Wiley-VCH Verlag GmbH & Co. KGaA, Weinheim.*

as low as 0.5 µg/mL protein and showed significant lower activity for normal cell lines, other subtypes of breast cancer and other tumor cell lines. So far, main applications used a built-in fluorophore and quencher label for signal generation, which could be replaced by our AuNP-labelled FO-SPR sensor. Further, new ligand-responsive DNAzymes, using the AuNP-labelled substrate, could be selected or the substrates of the ligand-responsive DNAzymes could be immobilized with the ligation strategy designed in Chapter 4. Based on the three approaches mentioned above, the feasibility of detecting proteins or small molecules with the FO-SPR sensor design developed in this dissertation was illustrated. Extending the target repertoire would increase the potential application and could minimize their required optimization steps and costs. Multiple applications of the device would stimulate the use and mass-production of the sensors, further improving the cost-efficiency.

7.2.2. Improving surface functionalization

While most of the chapters in this dissertation focused on signal generation and amplification using NAs, Chapter 4 illustrated the importance of proper surface functionalization, which directly affects the target-bioreceptor interaction. The proposed ligation strategy in Chapter 4 eliminated the presence of non-labelled substrates, minimizing the interference with DNAzyme-based signal generation. However, formation of more than one DNAzyme substrate per AuNP label could not be avoided because of the limited control provided by the DNA SAM covering the sensor surface. Ideal spacing and orientation of the labelled substrate strands could assure direct

contribution to the response signal of every single cleavage event. A potential solution could be found in the subfield of structural DNA nanotechnology, able to build structures with nanoscale precision[12]. Initial insights in this idea were obtained by immobilizing a 3D origami structure with programmable anchor points on the surface of the FO-SPR sensor[13]. The 24-helix bundle was engineered in such a way that immobilization was possible through its lateral surface (LS) or distal end (DE) (Figure 7.4A and B). Tetrahedral structures were used as a reference (Figure 7.4C) and thrombin aptamers were chosen as the bioreceptor to be studied. Comparison between the immobilized DNA origami bundles and tetrahedral structures showed that the LS origami performed best, having the widest linear range and highest signal intensity. Moreover, all DNA structures suggested that

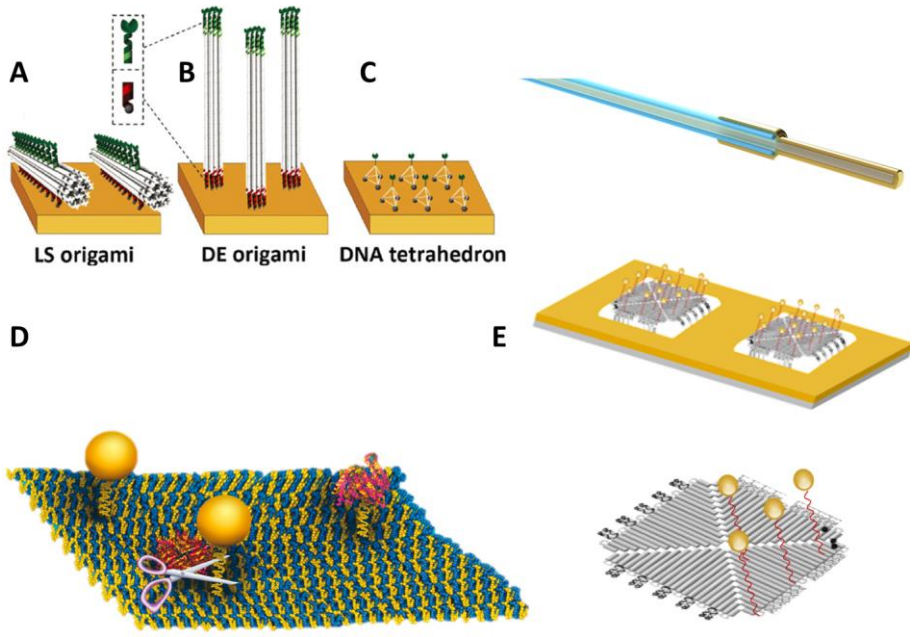

Figure 7.4: *Surface structuring by DNA origami. Schematic of the bioreceptor patterning:* ***A)*** *LS DNA origami,* ***B)*** *DE DNA origami and* ***C)*** *tetrahedral structures as reference. The dark green structures represent the bioreceptors, while the red structures represent the thiol groups for immobilization. In* ***D)*** *the DNA origami tile is illustrated with AuNP labels and a thrombin label. Future research could aim for a functionalization strategy as presented in* ***E).*** *Adapted with permission from Daems et al. © (2018) American Chemical Society; Adapted with permission of Royal Society of Chemistry, from Li et al. © (2016); permission conveyed through Copyright Clearance Center, Inc.*

PEG-backfilling to minimize nonspecific adsorption was unnecessary when immobilizing bioreceptors through DNA structures.

Based on these promising results, future research could focus on the immobilization of origami structures carrying DNAzyme substrates sequences. Li *et al.* reported the use of a DNA origami tile as support of AuNP-labelled DNAzyme substrates (Figure 7.4D)[14]. Labelled substrates were immobilized in the middle and on the side of the origami, illustrating the nanoscale precision. So far, simple hybridization was used for the immobilization and was followed by successful cleave and release events. Similar origami tiles could be immobilized on top of the FO-SPR surface to create local control and more optimized densities of the DNAzyme substrates (Figure 7.4E), enabling few or even a single coupling between the AuNP labels and the surface. Moreover, this type of origami tiles possesses side chains, which could even coordinate aligning of the tiles and further control of the total surface patterning. Optimized surface functionalization could result in improved substrate accessibility, time-to-results and sensitivity of the assay.

7.2.3. Biosensors for point-of-care applications

An effective way to reduce the diagnostic time-to-result and minimize the burden of diseases is making sure that diagnostic tests are readily available for anyone and anywhere. This idea of having diagnostic tests at or near the site of patient care is known as point-of-care testing (POCT)[15,16]. However, the point-of-care can vary from the patient's home to community health posts, a general practitioner's office, peripheral or primary laboratories and the hospital[17]. The latter two would fall within the scope of the DNAzyme-based FO-SPR assays as presented in this dissertation, while being implemented on the user-friendly bench-top device. In contrast, home testing, community health posts or general practitioner's offices ask for even more advanced devices, certainly when considering developing countries[18,19]. Due to the huge potential of this POCT-concept in resource limiting settings, the World Health Organization (WHO) defined specific guidelines, gathered under the acronym 'ASSURED' (Affordable, Sensitive, Specific, User-friendly, Rapid and robust, Equipment-free and Delivered)[18,20]. Although all the work presented in this dissertation was performed in the lab and on a FO-SPR bench-top device, the obtained insights are still valuable for ongoing research, such as POCT. Moreover, both the FO-SPR as the DNA-

based technologies have some interesting characteristics, which could benefit the design of robust and portable FO-SPR POCT devices, as illustrated in following paragraphs.

7.2.3.1. Isothermal signal amplification

Further modifications at the level of the DNAzyme-based amplification strategies could bring the FO-SPR technology closer to some POCT applications. DNAzymes are characterized by their isothermal aspect, avoiding the need for sophisticated thermocyclers to shuttle between different reaction temperatures[21]. In addition, establishing surface cleavage activity at room temperature would avoid extensive heating, further improving the simplicity and cost-efficiency required by every POCT application. As DNAzymes rely on simple hybridization for substrate recognition, adapting their substrate arms can be exploited to fine-tune the reaction temperature. Based on Ven *et al.* the substrate arms of the DNAzyme used in Chapters 5 were shortened[22] and some preliminary data was obtained. Different concentrations of the shortened DNAzyme were incubated with AuNP-labelled FO-SPR sensors, functionalized with the ligation strategy introduced in Chapter 4. Compared to the DNAzyme working at 55 °C (Chapter 5), similar DNAzyme efficiencies were obtained in identical buffer conditions but at room temperature (23 °C) (Figure 7.5A). Moreover, logarithmic transformation of the half-life values resulted in a linear trend across the same DNAzyme concentration range (1 – 100 nM) as

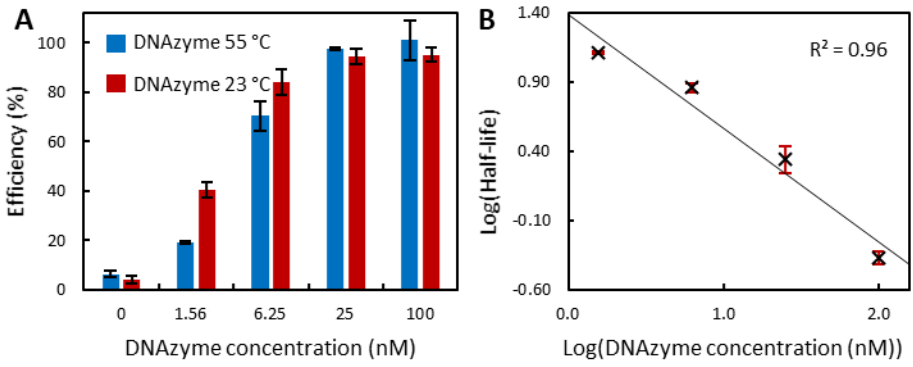

Figure 7.5: *Surface DNAzyme cleavage at room temperature.* ***A)*** *Comparison of the DNAzyme efficiency at 55 and 23 °C for DNAzyme concentrations of 0, 1.56, 6.25 and 100 nM and* ***B)*** *Linear calibration curve of the logarithmic half-life values. Error bars represent one standard deviation (n = 3).*

reported in Chapter 5 (Figure 7.5B). These results suggest that future DNAzyme-based FO-SPR assays can be designed at room temperature, further supporting their potential for more simplified and cost-effective sensing applications. However, future tests should reveal if the catalytic activity at room temperature can be coupled to a specific target and an alternative amplification system for PCR to assure ultrasensitive detection. Most interestingly in terms of POCT would be the coupling with isothermal, protein-free amplification cascades, which multiply the DNAzyme sequence itself. Avoiding Abs and protein enzymes could further increase the stability and improve the cost of bioassays, as has been indicated in the introduction of this dissertation. These amplification systems could be based on CHA (Chapter 2), which uses a triggering strand to sequentially open up two hairpins to form, for example, a MNAzyme together. The triggering strand gets recycled and keeps on triggering MNAzyme assembly as long as hairpins are available[23]. Performing this CHA in presence of the FO-SPR sensor would result in amplified cleavage activity at the surface, increasing the signal. As such, a DNA-only FO-SPR sensor could be developed for the sensitive detection of NAs.

7.2.3.2. Portable FO-SPR sensors

Next to biological improvements, technical improvements such as further miniaturization of the device are also promising. Initial efforts focused on the miniaturization of prism-based systems due to their superior sensitivity (Chapter 2). However, also in terms of miniaturization the FO-SPR technology benefits from its simple optical alignment and light coupling compared to prism-based formats, therefore requiring a minimal number of optical components. Considering the circumstances in developing countries and applications in the field, POCT prefers portable devices, which are extremely user-friendly, robust and cost-effective. In this context, smartphones can come in handy and seem to be quite compatible with the FO-SPR technology[24]. Few concrete designs have been reported[25], but clearly illustrate the potential concept in which the LED flash and the phone camera can be exploited as light source and detector (Figure 7.6A). Proof-of-concept assays were developed for the specific detection of IgG and established LODs of 47.4 nM[25] and 130 nM[26], respectively. The former was compared to a miniaturized prism-based setup, which turned out to have a similar

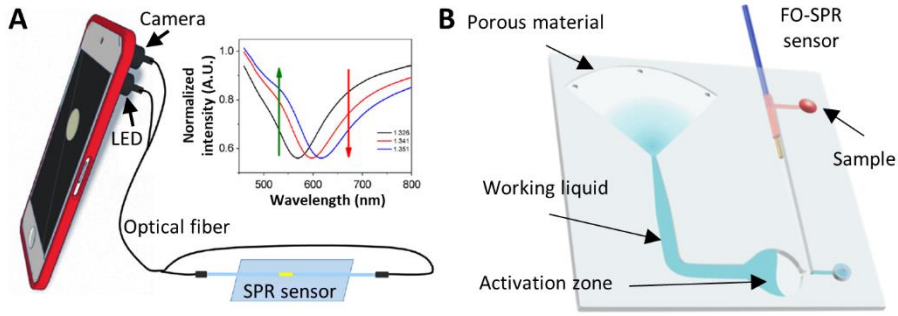

Figure 7.6: *Towards portable FO-SPR sensors.* ***A)*** *Overview of FO-SPR device using the LED flashlight and camera of the smartphone to create and read out the signal,* ***B)*** *Schematic of the FO-SPR SIMPLE chip, which could be further developed towards integration with smartphones. Adapted from Liu et al. (2018) and Dal Dosso (2018).*

sensitivity but was ± 1000 times less cost-effective. Furthermore, some preliminary results were obtained within our lab, illustrating the integration of the FO-SPR sensors into a microfluidic 'SIMPLE' chip (Figure 7.6B)[27,28]. This self-powered pumping system uses a working liquid in combination with a porous material, such as filter paper, to manipulate samples and reagents. The working liquid and other reagents are strictly kept apart through the pre-cut microfluidic network, only transferring the driving pressures. Activation of the chip is achieved by pressing the activation zone with a fingertip, bringing the working fluid in contact with the filter paper and creating a suction force on the samples and/or reagents. In addition, the SIMPLE chips can be produced in low-cost plastic materials and are suitable for mass-production. All advantages summed up, designing a disposable FO-SPR SIMPLE cartridge, which fits into a smartphone case providing the necessary optical connections, has great potential to result into an affordable, fast and sensitive POC device.

7.3. References

1. Pollet, J. *et al.* Fast and accurate peanut allergen detection with nanobead enhanced optical fiber SPR biosensor. *Talanta* **83**, 1436–1441 (2011).
2. Knez, K., Spasic, D., Delport, F. & Lammertyn, J. Real-time ligation chain reaction for DNA quantification and identification on the FO-SPR. *Biosens. Bioelectron.* **67**, 394–399 (2015).
3. Lu, J. *et al.* Fiber optic-SPR platform for fast and sensitive infliximab detection in serum of inflammatory bowel disease patients. *Biosens. Bioelectron.* **79**, 173–179 (2016).
4. Daems, D. *et al.* Competitive inhibition assay for the detection of progesterone in dairy milk using a fiber optic SPR biosensor. *Anal. Chim. Acta* **950**, 1–6 (2017).
5. Song, K.-M., Lee, S. & Ban, C. Aptamers and Their Biological Applications. *Sensors* **12**, 612–631 (2012).
6. Zhang, Y., Lai, B. S. & Juhas, M. Recent advances in aptamer discovery and applications. *Molecules* **24**, (2019).
7. Hianik, T., Ostatná, V., Sonlajtnerova, M. & Grman, I. Influence of ionic strength, pH and aptamer configuration for binding affinity to thrombin. *Bioelectrochemistry* **70**, 127–133 (2007).
8. Mokany, E., Bone, S. M., Young, P. E., Doan, T. B. & Todd, A. V. MNAzymes, a Versatile New Class of Nucleic Acid Enzymes That Can Function as Biosensors and Molecular Switches. *J. Am. Chem. Soc.* **132**, 1051–1059 (2010).
9. Hasick, N. J., Ramadas, R. & Todd, A. V. Subzymes: Regulating DNAzymes for point of care nucleic acid sensing. *Sensors Actuators B Chem.* **297**, 126704 (2019).
10. Zhang, X.-B., Kong, R.-M. & Lu, Y. Metal Ion Sensors Based on DNAzymes and Related DNA Molecules. *Annu. Rev. Anal. Chem.* **4**, 105–128 (2011).
11. Ali, M. M., Aguirre, S. D., Lazim, H. & Li, Y. Fluorogenic DNAzyme Probes as Bacterial Indicators. *Angew. Chemie Int. Ed.* **50**, 3751–3754 (2011).
12. Liu, Y., Kumar, S. & Taylor, R. E. Mix-and-match nanobiosensor design: Logical and spatial programming of biosensors using self-assembled DNA nanostructures. *Wiley Interdiscip. Rev. Nanomedicine Nanobiotechnology* **10**, e1518 (2018).
13. Daems, D. *et al.* Three-Dimensional DNA Origami as Programmable Anchoring Points for Bioreceptors in Fiber Optic Surface Plasmon Resonance Biosensing. *ACS Appl. Mater. Interfaces* **10**, 23539–23547 (2018).
14. Li, F. *et al.* A DNAzyme-mediated logic gate for programming molecular capture and release on DNA origami. *Chem. Commun.* **52**, 8369–8372 (2016).
15. Price, C. P. Clinical review Regular review Point of care testing. *BMJ* **322**, 1285–1288 (2001).
16. Larsson, A., Greig-Pylypczuk, R. & Huisman, A. The state of point-of-care testing: a european perspective. *Ups. J. Med. Sci.* **120**, 1–10 (2015).
17. Ansumana, R., Jacobsen, K. H., Bockarie, M. J. & Stenger, D. A. Point-of-care tests: where is the point? *Lancet Infect. Dis.* **14**, 922–923 (2014).
18. Mabey, D., Peeling, R. W., Ustianowski, A. & Perkins, M. D. Diagnostics for the developing world. *Nat. Rev. Microbiol.* **2**, 231–240 (2004).
19. Drain, P. K. *et al.* Diagnostic point-of-care tests in resource-limited settings. *Lancet Infect. Dis.* **14**, 239–249 (2014).
20. Wu, G. & Zaman, M. H. Low-cost tools for diagnosing and monitoring HIV infection in low-resource settings. *Bull. World Health Organ.* **90**, 914–920 (2012).
21. Craw, P. & Balachandran, W. Isothermal nucleic acid amplification technologies for point-of-care diagnostics: a critical review. *Lab Chip* **12**, 2469 (2012).

22. Ven, K., Safdar, S., Dillen, A., Lammertyn, J. & Spasic, D. Re-engineering 10–23 core DNA- and MNAzymes for applications at standard room temperature. *Anal. Bioanal. Chem.* **411**, 205–215 (2019).
23. Chen, J. *et al.* Enzyme-free amplified detection of microRNA using target-catalyzed hairpin assembly and magnesium ion-dependent deoxyribozyme. *Sci. China Chem.* **58**, 1906–1911 (2015).
24. Bremer, K. & Roth, B. Fibre optic surface plasmon resonance sensor system designed for smartphones. *Opt. Express* **23**, 17179 (2015).
25. Liu, Y. *et al.* Surface Plasmon Resonance Biosensor Based on Smart Phone Platforms. *Sci. Rep.* **5**, 12864 (2015).
26. Liu, Q., Yuan, H., Liu, Y. & Wang, J. Real-time biodetection using a smartphone-based dual-color surface plasmon resonance sensor. *J. Biomed. Opt.* **23**, 1 (2018).
27. Kokalj, T., Park, Y., Vencelj, M., Jenko, M. & Lee, L. P. Self-powered Imbibing Microfluidic Pump by Liquid Encapsulation: SIMPLE. *Lab Chip* **14**, 4329–4333 (2014).
28. Dal Dosso, F. DEVELOPMENT OF A SELF-POWERED MICROFLUIDIC PLATFORM FOR LAB-ON-A-CHIP APPLICATIONS. (KU Leuven, 2018).

Publications

Articles in international reviewed journals

Daems, D., **Peeters, B.**, Delport, F., Remans, T., Lammertyn, J. and Spasic, D., Identification and Quantification of Celery Allergens Using Fiber Optic Surface Plasmon Resonance PCR. *Sensors* 17, 1754 (2017).

Peeters, B., Daems, D., Van der Donck, T., Delport, F. & Lammertyn, J. Real-Time FO-SPR Monitoring of Solid-Phase DNAzyme Cleavage Activity for Cutting-Edge Biosensing. *ACS Appl. Mater. Interfaces* 11, 6759–6768 (2019).

Peeters, B.*, Safdar, S.*, Daems, D., Goos, P., Spasic, D. and Lammertyn, J., Solid-phase PCR-amplified DNAzyme activity for real-time FO-SPR detection of the MCR-2 gene. *Analytical Chemistry*, Submitted.

*Equal authorship

Papers at international scientific conferences

Peeters B., Daems D., Delport F., Lammertyn J., AuNP-labelled FO-SPR sensors to develop innovative DNAzyme-based bioassay concepts. Biosensors 2018. Miami, FL, USA, 12-15 June 2018 (POSTER)

Peeters B., Safdar S., Carlier B., Spasic D., Daems D., Lammertyn J., PCR Amplified DNAzyme-Amplicons for Generic Solid-Phase Antimicrobial Resistance Screening, in 2019 20th Int. Conf. Solid-State Sensors, Actuators Microsystems Eurosensors XXXIII (TRANSDUCERS EUROSENSORS XXXIII), IEEE, 2019, pp. 971–974.

Patents

Daems, D., Delport, F., Lammertyn, J. and **Peeters, B.**, NUCLEIC ACID ENZYME SENSOR, WO/2019/030383, https://patentscope.wipo.int/search/en/detail.jsf?docId=WO2019030383